

HUMAN ORGANOID MODELING OF GASTRIC  
MUCUS LAYER PHYSIOLOGY

by

Katrina Noel Lyon

A dissertation submitted in partial fulfillment  
of the requirements for the degree

of

Doctor of Philosophy

in

Microbiology & Immunology

MONTANA STATE UNIVERSITY  
Bozeman, Montana

December 2024

©COPYRIGHT

by

Katrina Noel Lyon

2024

All Rights Reserved

## DEDICATION

To the mosaic that is all the women I have ever been, the woman I am now, and the countless women I am yet to become.

## ACKNOWLEDGEMENTS

First and foremost, I extend my deepest gratitude to my mentor, Dr. Diane Bimczok, who gave a struggling undergraduate a chance at a new life in research that I never imagined for myself. It was encouragement from Dr. Aga Apple, however, that led me to Diane's door.

Andy Sebrell patiently guided me through the intricacies of organoid culture and endured my steep learning curve. Daily interactions in the lab with Mandi Roe and Marziah Hashimi offered a glimpse into the world of a graduate student and gave me the courage to envision myself in that role. To the rest of my lab mates over the years, your support has been invaluable.

I am profoundly grateful to my committee members—Dr. Rama Bansil, Dr. Doug Kominsky, Dr. Jim Wilking, Dr. Jen Brown, Dr. Susy Kohout, and Dr. Heidi Smith—whose collective expertise shaped a multidisciplinary foundation for my training. A special acknowledgement goes to Dr. Jovanka Voyich, our exemplary department head, whose support and encouragement came in countless forms.

This degree would not have been possible without the support provided by Donna Negaard, Sadie Barac, the VOICE Center, OIE, and Bozeman Counseling Center. I also wish to express appreciation for my families Rosauers and Pizza Campania for their unwavering encouragement and camaraderie.

I would like to thank my friends, whose presence has been a source of strength. I am endlessly grateful to family, for their belief in my ability to do anything I set my mind to. To my partner Dylan—your love and support has been a constant anchor. And finally, Autumn Rohan, thank you for being the sister I never had and always needed.

## TABLE OF CONTENTS

1. INTRODUCTION .....	1
The Human Stomach.....	1
The Gastric Mucus Layer.....	2
The Gastric pH Gradient.....	5
Human Gastric Organoids.....	6
<i>Helicobacter pylori</i> .....	10
Summary of Dissertation Research.....	11
Chapter 2: What is the pH Inside the Organoid Lumen, and Can It Be Profiled with Microelectrodes? .....	12
Chapter 3: What is the Diffusive Behavior of Microparticles Inside the Gastric Organoid Lumen? What Does This Tell Us About the Mucus Rheology? .....	13
Chapter 4: Is Bioengineered Gastric Mucus Biochemically, Structurally, and Functionally Similar to Native Mucus?.....	14
Additional Contributions to Organoid Studies .....	15
Chapter 5: Can Berry Extracts Have Therapeutic Effects on <i>H.</i> <i>pylori</i> -Infected Organoids? .....	15
Chapter 6: Can Organoids Be Generated From the Tissue of Jamaican Fruit Bats to Model SARS-CoV-2 Infection? .....	16
References Cited .....	17
2. PROFILING LUMINAL PH IN THREE-DIMENSIONAL GASTROINTESTINAL ORGANOIDs USING MICROELECTRODES .....	27
Contribution of Authors and Co-Authors .....	27
Manuscript Information .....	28
Abstract .....	29
Introduction.....	29
Protocol .....	32
Preparation of Human Gastric Organoids for pH Profiling .....	33
Unpacking and Calibration of Microelectrodes .....	35
pH Profiling of Human Gastric Organoids .....	36
Motorized Profiling (Optional) .....	38
Cleaning of Electrodes .....	40
Storage of Electrodes .....	40
Methyl Red Injection .....	41
Representative Results .....	42
Discussion .....	46
Supplementary Material.....	49
Acknowledgements.....	53
References Cited .....	54

## TABLE OF CONTENTS CONTINUED

3. MICRORHEOLOGICAL CHARACTERIZATION OF LUMINAL MUCUS IN THREE-DIMENSIONAL HUMAN GASTRIC ORGANIDS .....	59
Contribution of Authors and Co-Authors .....	59
Manuscript Information .....	61
Abstract .....	62
Introduction .....	62
Results & Discussion .....	65
Methods .....	73
Human Tissue Samples .....	73
Organoid Culture .....	74
Alcian Blue Staining .....	74
Particle Microinjection .....	75
Live Confocal Imaging .....	75
Particle Tracking Microrheology .....	75
References Cited .....	77
4. HUMAN GASTRIC ORGANOID-DERIVED MUCUS SHARES KEY PHYSICOCHEMICAL PROPERTIES WITH NATIVE MUCUS .....	82
Contribution of Authors and Co-Authors .....	82
Manuscript Information .....	84
Abstract .....	85
Introduction .....	86
Materials and Methods .....	87
Human Gastric Tissue Samples .....	87
3D Organoid Culture .....	88
2D Monolayer Culture .....	88
Mucus Harvest and Storage .....	89
Lyophilization .....	89
Size Exclusion Chromatography .....	90
Proteomics .....	90
CryoFE-SEM .....	91
Rheometry .....	92
Viscous Fingering Experiments .....	93
Consideration of Biological Variables, Rigor, and Reproducibility and Statistical Analysis .....	94
Results .....	94
Human Gastric Epithelial Monolayers Cultured at the Air-Liquid Interface Produce Apical Mucus .....	94

## TABLE OF CONTENTS CONTINUED

Unbiased Proteomic Analysis of Bioengineered Gastric Mucus Reveals Physiologically Relevant Secretome .....	97
Visualization of Bioengineered Mucus by Cryo-Scanning Electron Microscopy Reveals Heterogeneity and Porosity of Internal Architecture.....	100
Rheometric Frequency Sweeps Confirm Viscoelastic Behavior of Bioengineered Mucus .....	101
Bioengineered Gastric Mucus Enables the Formation of Acid Channels.....	102
Discussion .....	105
Supplementary Materials .....	113
Acknowledgements.....	115
References Cited .....	116
 5. A HIGH-THROUGHPUT METABOLIC MICROARRAY ASSAY REVEALS ANTIBACTERIAL EFFECTS OF BLACK AND RED RASPBERRIES AGAINST <i>HELICOBACTER PYLORI</i> INFECTION .....	125
Contribution of Authors and Co-Authors .....	125
Manuscript Information .....	127
Abstract .....	128
Introduction.....	129
Results.....	131
Analysis of Powders and Extracts of Black and Red Raspberries and Blackberries for Anthocyanin Content and Composition .....	131
Development and Validation of a High-Throughput Assay to Measure <i>H. pylori</i> Growth .....	135
Analysis of the Antibacterial Effects of Black and Red Raspberry and Blackberry Powders and Extracts on <i>H. pylori</i> .....	138
Effect of BRB Extract on Gastric Epithelial Cell Viability in a Human Gastric Organoid Model.....	144
Discussion .....	145
Materials and Methods.....	149
Berry Powders and Preparation of Extracts .....	149
Analysis of Anthocyanin Content .....	150
<i>Helicobacter pylori</i> Strains and Culture Conditions.....	151
High-Throughput <i>Helicobacter pylori</i> Growth Assay.....	151
Data Analysis for Bacterial Growth Assays.....	152
Human Gastric Organoid Culture and Viability Assay .....	152
Statistical Analysis .....	153
Acknowledgements.....	154
Supplementary Materials .....	154

## TABLE OF CONTENTS CONTINUED

References Cited .....	155
6. ANTIVIRAL RESPONSES IN A JAMAICAN FRUIT BAT INTESTINAL ORGANOID MODEL OF SARS-COV-2 INFECTION .....	163
Contribution of Authors and Co-Authors .....	163
Manuscript Information .....	166
Abstract .....	167
Introduction .....	167
Results .....	171
Development and Characterization of JFB Gastrointestinal Organoids .....	171
Infection of Intestinal Organoids from JFBs with SARS-CoV-2 Leads to Replication of Viral Genomes .....	173
Lack of Cytopathic Effect but Increased Growth in SARS-CoV-2- infected JFB Organoids .....	176
SARS-CoV-2 Induces Expression of Type I Interferons and Proinflammatory Cytokines in JFB Organoids .....	176
Impact of SARS-CoV-2 Infection on the JFB Intestinal Epithelial Cell Proteome .....	178
Discussion .....	182
Methods .....	191
Ethics Statement .....	191
Tissue Samples .....	191
Crypt and Gland Isolation .....	191
Maintenance of JFB Organoids .....	192
Optimization of Growth Conditions .....	192
Microscopic Analyses .....	193
Immunofluorescence Staining .....	193
Transepithelial Electrical Resistance .....	194
SARS-CoV-2 Infection of JFB Organoids .....	195
Treatment of JFB Organoids with TLR Agonists and Inactivated Virus .....	195
Quantitative RT-PCR .....	196
Cell Viability and Organoid Growth .....	196
Proteomic Analyses .....	197
Statistical Analyses .....	198
Data Availability .....	198
Acknowledgements .....	199
Supplementary Material .....	200
References Cited .....	206



## TABLE OF CONTENTS CONTINUED

7. CONCLUSION.....	214
Organoid Models: Strengths, Challenges, and Opportunities.....	219
Future Directions .....	221
Using Organoids to Model Acid Secretion .....	222
Enhancing Mucus Production in Organoids .....	223
Final Remarks .....	224
References Cited .....	225
CUMULATIVE REFERENCES CITED.....	233
APPENDICES .....	270
ORGANOID LINES AND TISSUE DONORS .....	271
CULTURE MEDIA .....	275

## LIST OF TABLES

Table	Page
1. Supplemental Table S2.1. Table of Materials. ....	50
2. Supplementary Table 4.1. Proteins shared by or exclusively found in either BGM/NM. ....	113
3. Supplementary Table 4.2. Structures identified by CryoFE-SEM. ....	114
4. Table 5.1. Total concentrations of anthocyanins in black and red raspberry and blackberry powders and extracts determined by LC-MS. ....	133
5. Table 5.2. Anthocyanin composition within powdered berries and berry extracts determined by HPLC-MS. ....	135
6. Supplementary Table S6.1. Composition of culture media for JFB gastrointestinal organoids ....	204
7. Supplementary Table S6.2. Primer and probe sequences ....	205
8. Table A1. All human gastric organoid lines used in Chapter 2 ....	272
9. Table A2. All human gastric organoid lines used in Chapter 3 ....	272
10. Table A3. All human gastric organoid lines used in Chapter 4 ....	273
11. Table B1. Human gastric organoid expansion media components ....	276

## LIST OF FIGURES

Figure	Page
1. Figure 1.1. Overview of Gastric Anatomy.....	2
2. Figure 1.2. Mucosal protective factors. ....	3
3. Figure 1.3. The gastric mucus layer and its mucin glycoproteins.....	4
4. Figure 1.4. Quantitative RT-qPCR analysis of gastric organoids .....	9
5. Figure 1.5. Graphical summary of dissertation research .....	12
6. Figure 2.1. Overview of the pH microprofiling method.....	44
7. Supplemental Figure S2.1. Ion transporter expression in human gastric organoids.....	49
8. Supplemental Figure S2.2. Human gastric organoid with deformed architecture following puncture with the pH microsensor probe.....	50
9. Supplemental Video SV2.1. Unsuccessful profiling attempt in a gastric organoid culture. ....	50
10. Figure 3.1. Alcian blue staining of identifiable acidic mucins .....	66
11. Figure 3.2. Time-lapse microscopy of colloidal probe particles reveals microscale heterogeneities in organoid lumen.....	67
12. Figure 3.3. Mean-square displacements of colloidal probe particles.....	69
13. Figure 3.4. Inverse relationship of $\alpha$ as a function of mucus viscosity.....	70
14. Figure 3.5. Calculated viscoelasticity of all organoids at different time points.....	71
15. Figure 4.1. Gastric epithelial monolayers cultured at the air-liquid interface produce apical mucus.....	96
16. Figure 4.2. Unbiased proteomic analysis of bioengineered gastric mucus reveals physiologically relevant secretome. ....	99
17. Supplemental Figure S4.1. Controls for CryoFE-SEM. ....	114

## LIST OF FIGURES CONTINUED

Figure	Page
18. Figure 5.1. Preparation and anthocyanin content analysis of black raspberries, red raspberries and blackberries .....	132
19. Figure 5.2. Development of a high-throughput metabolic assay to measure <i>H. pylori</i> growth.....	137
20. Figure 5.3. Concentration-dependent growth suppression of <i>H. pylori</i> by metronidazole and black raspberries.....	140
21. Figure 5.4. Growth inhibition of <i>H. pylori</i> by extracts from BRB, RRB, and BB .....	141
22. Figure 5.5. Growth inhibition of <i>H. pylori</i> by lyophilized BRB and BB powder.....	142
23. Figure 5.6. Minimum inhibitory concentrations (MICs) of berry preparations for antibacterial activities against <i>H. pylori</i> .....	144
24. Figure 6.1. Development and culture of gastrointestinal organoids from Jamaican fruit bats .....	174
25. Figure 6.2. Intestinal organoids from Jamaican fruit bats maintain key characteristics of the intestinal epithelium.....	175
26. Figure 6.3. Replication of SARS-CoV-2 in JFB intestinal organoids.....	178
27. Figure 6.4. Increased growth of JFB organoids infected with SARS-CoV-2 .....	181
28. Figure 6.6. Proteome analysis of SARS-CoV-2-infected JFB organoids at 48 h.....	189
29. Supplementary Figure S6.2. Protein sequence alignment of murine and <i>Artibeus jamaicensis</i> growth factors.....	201
30. Supplementary Figure S6.3. Histological analysis of tissue and organoids from JFB stomach and proximal intestine .....	202
31. Supplementary Figure S6.5. Gene expression of JFB organoids following short term TLR stimulation.....	203

## ABSTRACT

The stomach has two major secretory modes of self-defense: acid that facilitates digestion and kills harmful microorganisms, and a sticky, selectively permeable mucus layer that acts as a protective barrier. *Helicobacter pylori*, a pathogen linked to gastric inflammation, ulcers, and cancer, seeks to bypass these defenses to colonize and infect the stomach lining. Human gastric organoids—3D cellular constructs derived from patient tissue—have proven valuable for modeling such diseases *in vitro*. However, the ability of gastric organoid models to accurately replicate these gastric defenses has not been thoroughly examined. In this research, we first developed a novel technique for the measurement of pH inside of organoids using microelectrodes, demonstrating reproducible pH measurement and evidence of a gradient. The pH was alkaline however, indicating a lack of acid secretion in the model. To further investigate the luminal microenvironment, we used particle tracking microrheology and showed that the organoids contain heterogeneously distributed, viscoelastic mucus. As organoids are topologically closed, we next explored a method for culturing the cells as a monolayer at the air-liquid interface, which allowed access to the mucus. This approach enabled the harvesting of milliliter quantities of clean, sterile “bioengineered gastric mucus” (BGM) over several weeks. We found that BGM shared key protective properties with native mucus, including molecular composition, internal architecture, and rheological behavior—all of which contribute to its ability to act as a barrier, maintain structural integrity, and exhibit flow properties essential for defense and maintenance. Proteomic analysis of BGM compared to native human mucus highlighted the impurity of native mucus, underscoring its limitations for functional studies and emphasizing the need for physiologically relevant *in vitro* models. Overall, this research contributes to a more complete biophysical understanding of mucus and acid production by human gastric organoids. These insights enhance the utility of organoid models in gastric physiology studies and may inspire translation of such models toward personalized treatment approaches for gastric disease.

## CHAPTER ONE

## INTRODUCTION

The Bimczok laboratory seeks to uncover the complex interplay between pathogens, mucosal antigen-presenting cells, and epithelial cells. The overall goal of this dissertation research is to explore the relationship between the stomach's two main mechanisms of defense against this pathogen—gastric acid and the mucus layer. The following chapter provides an overview on the gastric pH gradient, mucus layer, organoid models, and infection with *Helicobacter pylori*, an important human pathogen that causes chronic gastritis, peptic ulcer disease, and gastric cancer<sup>1-3</sup>.

The Human Stomach

The human stomach houses one of the most complex offense-defense systems in the human body. The outermost section of the gastric mucosa is the epithelium, which forms a continuous layer of cells that faces the lumen of the stomach. The mucosal surface (Fig. 1A) is patterned with narrow tubular structures called gastric glands, which have four distinct regions from bottom to top: base, neck, isthmus, and pit<sup>4</sup>. While the cells populating each of these regions vary slightly across anatomical regions of the stomach, the isthmus and neck house stem cells that are responsible for the regenerative capacity of the gastric epithelium<sup>5</sup>. The gastric body, its most central and largest section, features pepsinogen-secreting chief cells, HCl-secreting parietal cells, mucus-secreting neck cells, and histamine-secreting enteroendocrine cells (Fig. 1B)<sup>6-9</sup>. The antrum, the transitional region into the duodenum, is decorated with gastrin-secreting enteroendocrine cells and a higher concentration of mucous cells (Fig. 1C)<sup>10</sup>.

Overall, the gastric mucosa serves as a barrier whose primary function is to secrete digestive enzymes and acid while protecting the stomach with its two main secretory defenses—mucus and acid. In its protective state, the mucosa has the ability to sense and react to bacterial perturbation and infection<sup>6</sup>.

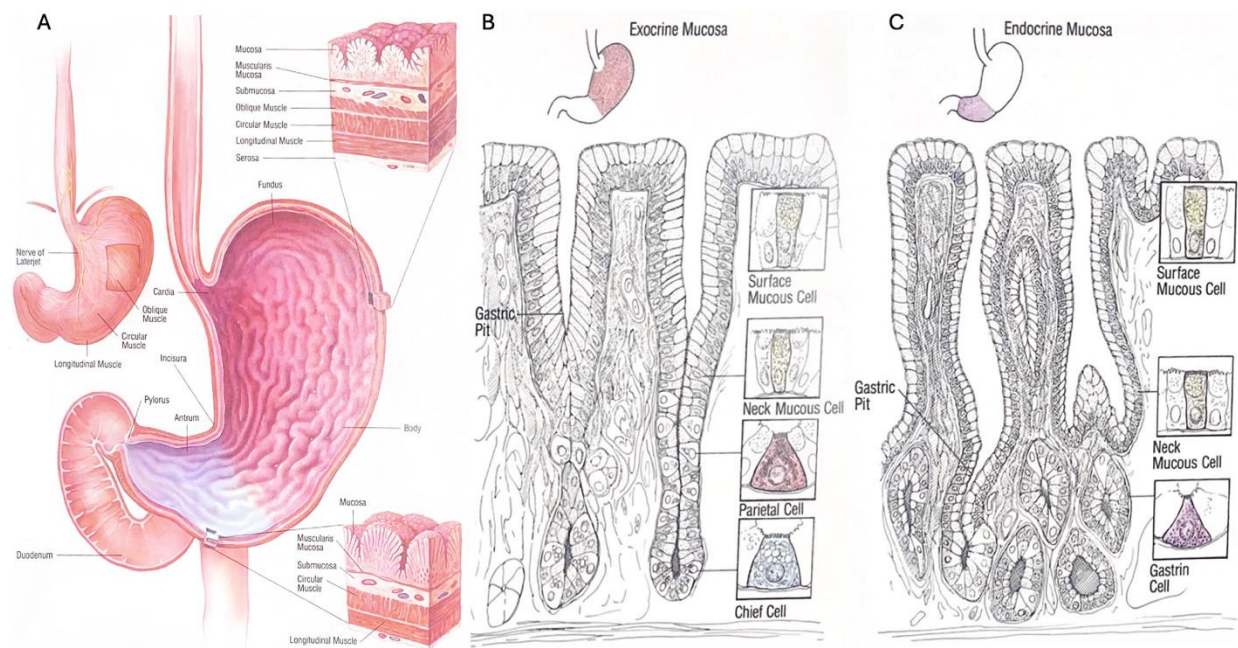


Figure 1.1. Overview of Gastric Anatomy. (A) The anatomy of the stomach. (B) Major cell types in the gastric body. (C) Major cell types in the gastric antrum. Illustrations by Carol Donner<sup>10</sup>.

### The Gastric Mucus Layer

Mucus is a universal and biologically essential hydrogel found at almost every interface between epithelial surfaces and the world, spanning diverse biological classes from mammals to jellyfish<sup>11,12</sup>. Its roles in the body are wide-ranging, from lubrication of the eyes to protection from foreign particles. As a selectively permeable barrier, mucus must balance its ability to trap harmful microbes but continue to allow the transport of drugs to the underlying tissue. In the eyes, mucus is a watery mucin solution designed for lubrication, while in the digestive and

reproductive tracts, it is a stiffer gel that acts as a physical barrier<sup>13</sup>. Conversely, the accumulation of thick and sticky mucus in the respiratory tract can even be obstructive, contributing to diseases like cystic fibrosis<sup>11,14</sup>.

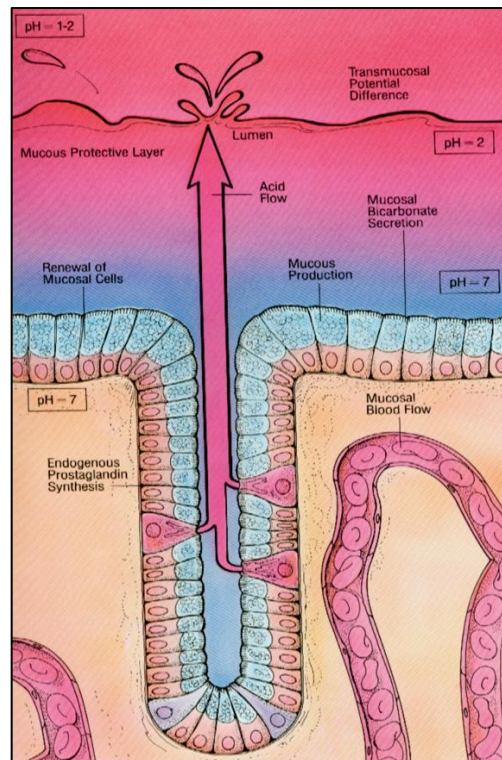


Figure 1.2. Mucosal protective factors. Illustration by Carol Donner<sup>10</sup>.

The gastric mucus layer is a thick, complex fluid that functionally protects the gastric epithelium against acid and bacterial invasion. The physicochemical properties of gastric mucus are known to impact bacterial motility as well as buffer gastric acid<sup>15-18</sup>. The mucus layer demonstrates viscoelastic properties, balancing the material behavior of a viscous liquid that resists flow and an elastic gel that can store energy and return to its original shape after stretching. These properties of the mucus layer are pH dependent, as mucus is a polymer matrix



containing mucins. Gastric mucus is composed of ~95% water, 3% mucins, and other small molecules<sup>19</sup>.

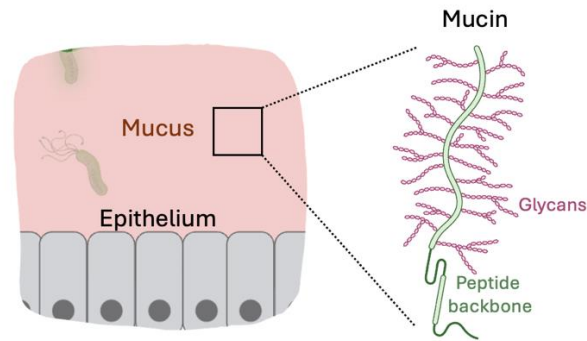


Figure 1.3. The gastric mucus layer and its mucin glycoproteins. Left: The gastric mucus layer. Right: Mucin glycoproteins. Adapted from Wheeler *et al*<sup>20</sup>.

Mucins, the primary viscoelastic components of mucus, are high molecular weight polymeric glycoproteins with peptide backbones and negatively charged glycan chains (Fig. 3)<sup>21</sup>. Their glycosylation patterns are diverse, though often containing sialic acid and sulfated residues, and have been hypothesized to mediate host-pathogen interactions<sup>13,22</sup>. In the stomach, two main mucins dominate: MUC5AC (secreted by surface or pit mucous cells) and MUC6 (secreted by mucous neck cells<sup>19</sup>)<sup>23</sup>.

Despite its critical role as a first line of defense, the physical protective function of gastric mucus has been underexplored by biologists due to its physicochemical complexity and relatively low accessibility for research<sup>24,25</sup>. Methods ranging from animal models to microphysiological systems have been used to study mucus physiology in various systems, but there is an incomplete understanding of the mechanisms by which the gastric mucus layer defends the stomach lining. A complete understanding of gastric mucus is needed as this is the physiological barrier that impedes bacterial motility toward and subsequent infection of the

stomach lining. Notably, the gastric mucus layer would not be effective without its famous and intricate coupling with gastric acid secretion.

### The Gastric pH Gradient

Hydrochloric acid (HCl), secreted mainly by the parietal cells of the gastric body, is essential for digestion and, in theory, killing any harmful microbes ingested with food<sup>26,27</sup>. The secretion of HCl is stimulated by hormones such as histamine and is further regulated by the activity of the gastric  $H^+K^+-ATPase$  pump (commonly known as the proton pump) located in the apical membrane of parietal cells (Figure 4). In exchange for extracellular potassium, this pump releases protons that combine with luminal chloride ions to form HCl<sup>27,28</sup>. Importantly, the stomach lining is shielded from potential damage by its own acidic secretions through the buffering action of gastric mucus<sup>29</sup>.

The 200-300  $\mu m$ -thick gastric mucus layer maintains and buffers the steepest proton gradient in the body—from a pH of around 7 at the epithelium to a pH of about 2 in the lumen (a 100,000-fold difference)<sup>17,30</sup>. We explore the possibility of recapitulating this pH gradient *in vitro* in Chapter 2. Previous research has shown changes in pH influence mucus rheology (the study of its flow and deformation under stress) as well as bacterial motility<sup>16,31,32</sup>. However, it remains unclear how acid is transported across the mucus layer to the lumen without diffusing backward and damaging the underlying host cells. Two main hypotheses regarding how this occurs have been proposed: 1) Protons are sequestered in secreted mucins, move with mucins toward the lumen, and are released as the mucins are degraded by pepsin<sup>33</sup>, and 2) Protons are transported through temporary acid channels in the mucus<sup>30</sup>.

A study by Lewis *et al.* suggested, using mathematical modeling of the first hypothesis, that transmembrane proteins called “sodium hydrogen exchangers” (NHEs) and “anion exchangers” (AEs) could play a key role in maintaining the gastric pH gradient<sup>18</sup>. The authors emphasized the importance of the coupling between gastric proton exchange and bicarbonate secretion, which alone can neutralize pH.

In a hallmark study by Bhaksar *et al.*, the acid channels involved in the second hypothesis were found to occur in porcine gastric mucin (PGM). The authors used a Hele Shaw cell (similar to Chapter 4), in which they flowed HCl through solutions of PGM to reveal these acid channels—called “viscous fingers”<sup>34</sup>. Another study by Johansson *et al.* demonstrated the formation of acid channels in the mucus layer of the rat stomach<sup>35</sup>. These studies were foundational for numerous future studies on viscous fingering as a hydrodynamic phenomenon in gastric mucus. More recently, an experiment performed by Zhang *et al.* demonstrated the tunability of such fingering patterns by modulating the viscosity ratio of two interfacing fluids<sup>36</sup>. Taken together, these studies highlight the influence of pH and rheology on the formation and control of viscous fingering patterns.

To effectively explore the dynamic gastric microenvironment, both gastric acid secretion (Chapter 2) and the mucus barrier (Chapters 3 and 4) must be studied *in vitro*, as they work together to maintain physiological function.

### Human Gastric Organoids

A substantial body of research has been conducted using porcine gastric mucin (PGM) solutions as an analog for the mucus itself. Since PGM is a purified solution of mucin proteins—the functional building blocks of mucus—it lacks the other important components of mucus such

as antimicrobial peptides, lipids, and other small molecules<sup>37</sup>. Alternatively, animal models and immortalized cell lines have been used in mucus research but are severely limited in their ability to mimic human physiology<sup>38</sup>.

A representative system, capable of overcoming the limitations of simpler models, are organoids—*in vitro* engineered tissue constructs that replicate the structure and function of their respective organs. Organoids exhibit remarkable self-organization within a three-dimensional extracellular matrix (often, Matrigel)<sup>39,40</sup>. These models offer significant advantages, including derivation from human stem cells, extended culture longevity, and complex cellular architecture, making them valuable and relevant tools for studying human gastric physiology<sup>38,41</sup>. Overall, organoid technology holds promise for large scale biobanking, personalized medicine, and incorporation into microphysiological systems<sup>38</sup>. While challenges such as batch-to-batch variability, intra-institutional reproducibility, high costs, and ethical considerations remain<sup>42</sup>, progress has been made to optimize these models. Over the past decade, organoids have become widely popular models for the study of gastric development and disease<sup>39,43,44</sup>.

There are two primary methods for generating organoids: using tissue-derived adult stem cells (ASCs) or using human embryonic/induced pluripotent stem cells (iPSCs)<sup>43,45</sup>. Gastric organoids are most commonly generated using adult stem cells to generate primary mucosal cell lines, enabling patient-specific analyses and translational studies<sup>46</sup>. Unlike ASCs, which retain tissue-specific traits, iPSCs require extensive additional instructions to be differentiated into the lineages of interest. While iPSCs are ideal for generating organoids from tissues that are more invasive to sample, ASCs are generally used for gastrointestinal organoid research as they are fast and reliable<sup>47</sup>. The process involves isolating gastric glands from collagenase-digested tissue,

embedding them in Matrigel, and allowing them to self-organize into organoids within 24-48 hours<sup>48,49</sup>. In culture, the Wnt pathway (particularly Wnt3a in conjunction with R-spondin) drives the proliferative and regenerative capacity of these epithelia<sup>43,50-53</sup>, maintaining the organoids in a largely undifferentiated state. Organoids are first cultured in expansion medium with high Wnt levels to promote regeneration, with Lgr5+ stem cells playing a key role in this proliferative stage<sup>54</sup>. When the organoids are ready to be driven toward experimentally desirable phenotypes, they are switched to differentiation medium, which typically involves reducing Wnt3a and adding supplements such as B27<sup>55</sup>.

Our group has used organoids to model the secretory function of gastric epithelial cells in both healthy and disease states, specifically in the context of *Helicobacter pylori* infection. We have investigated whether organoid models could recapitulate the two main defenses of the apical epithelium: mucus production and acid secretion. Our results showed that the organoids produce mucus, which we characterized in terms of its barrier function (Chapters 3 and 4). Previous gastric organoid studies investigating their ability to secrete acid have had mixed results. Bartfeld *et al.* and McCracken *et al.* saw no evidence of the gastric proton pump (expressed by parietal cells) through histological and immunofluorescent staining<sup>56,57</sup>. Conversely, Schumacher *et al.* and Wölffling *et al.* employed various differentiation methods to induce expression of the proton pump in their organoid models, as they confirmed with immunofluorescent staining<sup>55,58</sup>. We therefore explored the organoids' ability to secrete acid—a key feature of the stomach. The organoids demonstrated key features of gastric tissue, including the expression of markers such as MUC5AC, PGC, and ATP4B<sup>48</sup>.

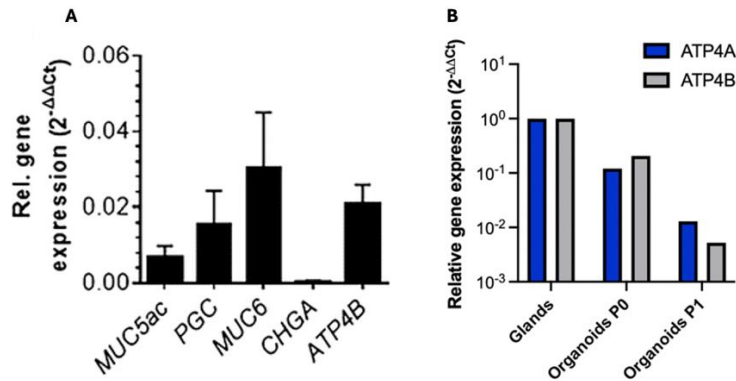


Figure 1.4. Quantitative RT-qPCR analysis of gastric organoids. Performed by A. Sebrell (A) and Jasper Gattiker (B). Samples were analyzed for expression of (A) MUC5AC (mucous neck cells), PGC (pepsinogen C; chief cells), MUC6 (surface mucous cells), CHGA (chromogranin A; enteroendocrine cells), and ATP4B (potassium-transporting ATPase subunit beta; parietal cells)<sup>48</sup>. (B) ATP4A and ATP4B. All data were analyzed by the 2<sup>-ΔΔCt</sup> method, with GAPDH used as a housekeeping gene with cDNA from human gastric tissue used for normalization.

Three-dimensional cell culture is particularly useful for modeling spatial microenvironments and cellular interactions, at times offering a more accurate representation of spatially-dependent physiological processes compared to 2D cultures<sup>38</sup>. However, the lumen of the organoid and its contents have often remained a mystery unexplored. Boccellato *et al.* and Wang *et al.* have developed complimentary methods for the generation of a gastrointestinal mucus layer atop a 2D monolayer at the air-liquid interface (ALI)<sup>37,59</sup>. To address the issue of mucus-producing organoids being topologically closed structures, we adopted these methods to culture gastric epithelial cells at the ALI, which allows for *in vitro* infection experiments while preserving key features of the epithelial barrier—polarized cells, tight junctions, and a mucus layer<sup>37,59</sup>. Upon exploring this method, we found that ALI culture of gastric epithelial cells enabled convenient extraction and analysis of the apical mucus (Chapter 4).

Organoid-based cell culture systems present distinct advantages for modeling the gastric mucosa. While 2D systems offer accessibility and scalability, 3D cultures more accurately mimic

the complexities of tissue architecture and cellular interactions<sup>38</sup>. Both approaches, however, hold vast potential for advancing the modeling of host-pathogen interactions.

### *Helicobacter pylori*

*Helicobacter pylori* (*H. pylori*), the most common gastric invader, is a gram-negative, spiral-shaped, microaerophilic bacterium first identified as a gastric pathogen by Warren and Marshall in 1979<sup>60,61</sup>. The stomach was previously believed to be sterile, lacking microorganisms due to its high acidity<sup>62</sup>. *H. pylori* is typically transmitted via the fecal-oral route, advancing against the pH gradient towards the neutral epithelial layer via chemotaxis<sup>63</sup>. This navigation of *H. pylori* is highly dependent on secreted chemoattractants such as urea, bicarbonate, and specific glycan residues that decorate gastric mucins<sup>62,64,65</sup>. Gastric organoids provide a valuable model for studying the dynamic offense-defense relationship between the gastric mucosa and *H. pylori*.

*H. pylori* employ various virulence factors to overcome the gastric defenses, with flagellar motility and urease secretion being particularly important in its navigation across the gastric mucosa<sup>66</sup>. Their unipolar flagella, driven by a flagellar motor powered by proton motive force, are essential for its colonization<sup>66</sup>. A recent study found that this motility is more effective when paired with the bacterium's body rotation<sup>67,68,69</sup>. Motility is also pH-dependent, as mucins gel below pH 4, resulting in a physical barrier<sup>16</sup>. To counter this, *H. pylori* secretes urease, which hydrolyzes urea into ammonia, raising the local pH to allow itself to swim through the mucus toward the epithelium<sup>70,71</sup>. This gel-to-sol transition has been observed in porcine gastric mucin (PGM), a commonly used model in mucus studies<sup>72</sup>.

*H. pylori* colonizes nearly half of the global population<sup>73,74</sup> and is associated with a range of diseases, including gastritis, peptic ulcer disease, gastric adenocarcinoma, and mucosa-associated lymphoid tissue (MALT) lymphoma<sup>73,75</sup>. In 1994, *H. pylori* was classified as a class I carcinogen by the World Health Organization and continues to be responsible for more than half of all gastric cancer cases<sup>76,77</sup>. Gastric cancer is the fifth most frequent cancer with nearly one million new cases in 2022, and is also the fifth leading cause of cancer-related deaths, claiming almost 700,000 lives annually<sup>78,79</sup>.

In recent years, the increasing prevalence of antibiotic-resistant strains of *H. pylori* has complicated the treatment of *H. pylori* infections, emphasizing the need for alternative therapeutic strategies<sup>80,81</sup>. Treatment of *H. pylori*-associated disease is further complicated by the bacterium's capacity to induce changes in mucin expression, further compromising the stomach's defense mechanisms<sup>82</sup>. Therefore, a deeper understanding of the barrier *H. pylori* overcome to establish infection is critical to the prevention of *H. pylori*-associated gastric disease and the identification of new therapies for restoring mucus integrity.

### Summary of Dissertation Research

The overall hypothesis of this dissertation research is that human gastric organoids are physiologically relevant *in vitro* models for the two key protective mechanisms in the stomach—the mucus barrier and the pH gradient across it. To evaluate this hypothesis, we asked the following questions: 1) What is the pH inside the gastric organoid lumen, and can it be profiled with microelectrodes? 2) What is the diffusive behavior of microparticles inside the gastric organoid lumen, and what does this tell us about the rheology of luminal mucus? 3) Is



bioengineered gastric mucus generated using monolayer ALI cultures biochemically, structurally, and functionally similar to native mucus?

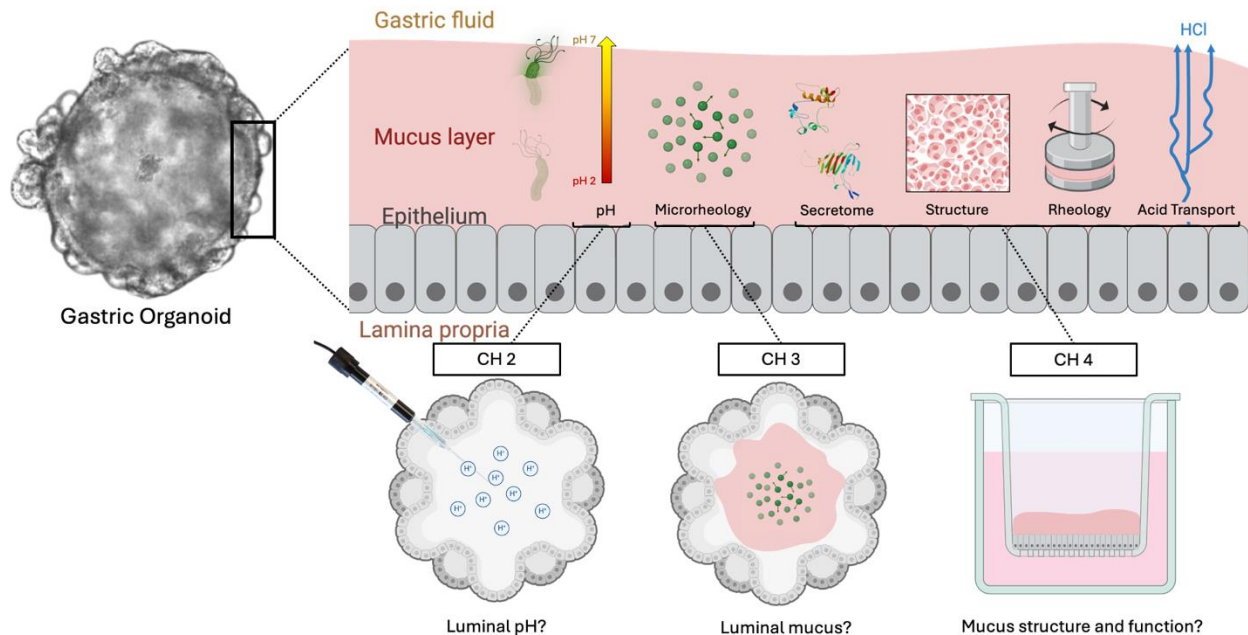


Figure 1.5. Graphical summary of dissertation research. Chapter 2 introduces the development and validation of microelectrode-based intraluminal pH profiling in human gastric organoids. Chapter 3 expands on luminal analysis by employing particle tracking microrheology to characterize the rheological properties of organoid luminal mucus. Chapter 4 compares organoid-derived bioengineered gastric mucus (BGM) to native gastric mucus using advanced biochemical, structural, and mechanical analyses.

## Chapter 2: What is the pH Inside the Organoid Lumen, and Can It Be Profiled with Microelectrodes?

The goal of Chapter 2 was to examine the intraluminal pH of gastric organoids and determine whether they maintain an epithelium-to-lumen pH gradient. As discussed in Chapter 2, traditional methods for measuring pH inside the organoid lumen have involved the use of pH-sensitive dyes or nanoparticles that require pairing with fluorescence microscopy or spectroscopy, leaving potential for imaging bias<sup>83,84</sup>. Our group had previously measured luminal oxygen levels in gastric organoids compared to the surrounding extracellular matrix<sup>48</sup>. We

hypothesized that microelectrode profiling would be a versatile method translatable to the measurement of pH in the organoids. To assess whether this technology could be used to profile intraluminal pH, we developed a reproducible microsensor-based technique to probe the pH inside of the organoid lumen. We used a micromanipulator-controlled microelectrode for intraluminal pH profiling, paired with injection of methyl red (a pH-indicator dye) as a confirmatory test. We demonstrated that, at baseline, the organoids maintained an alkaline luminal microenvironment as well as a microscale pH gradient. To the best of our knowledge, Chapter 2 highlights the first use of microelectrodes for the precise measurement of pH in the organoid intraluminal microenvironment.

### Chapter 3: What is the Diffusive Behavior of Microparticles Inside the Gastric Organoid Lumen? What Does This Tell Us About the Mucus Rheology?

Chapter 3 continues our exploration of the gastric organoid lumen to include the mucus. The goal of this chapter was to determine the diffusive behavior of microparticles about the gastric organoid lumen, thus revealing rheological details of the luminal material. Due to the topologically closed structure of an organoid and subsequently difficult-to-access mucus, it has remained unclear how the mechanical properties of the luminal mucus contribute to its functionality. In a previous study, microscopic visualization of the mucus inside the organoids suggested a heterogeneous distribution<sup>48</sup>. As histological sections can fall victim to artefacts revealed in subsequent immunofluorescence imaging (Chapter 4), we hypothesized that luminal mucus could be analyzed using particle tracking microrheology, a method to quantify microscale rheological behavior<sup>15</sup>. We injected 1  $\mu\text{m}$  fluorescent particles into the organoid lumen, performed time-lapse confocal microscopy, and analyzed their trajectories to characterize the

diffusive behavior of the particles and relate this to the rheological properties of the organoid luminal content. Indeed, we observed that the particles demonstrated a mixture of both diffusive and subdiffusive behavior, indicative of heterogeneous mucus distribution in the organoid lumen<sup>15,85</sup>. Overall, analysis of the viscous and elastic moduli revealed predominantly elastic behavior of the luminal mucus. This chapter provides an overview of particle tracking microrheology as a non-invasive tool for interrogating the rheological properties of organoid mucus, which we explore further in Chapter 4.

#### Chapter 4: Is Bioengineered Gastric Mucus Biochemically, Structurally, and Functionally Similar to Native Mucus?

The goal of Chapter 4 was to evaluate the similarities between native gastric mucus and organoid-derived bioengineered gastric mucus (BGM). While *in vitro* studies have traditionally used purified mucin solutions, mucus from immortalized cell lines, or animal mucus (as demonstrated by earlier research), these models may not fully capture the complexity of *in vivo* human systems<sup>16,86-89</sup>. Access to mucus samples from human patients, however, has also been a critical barrier to mucus research<sup>24,25</sup>. Gastric organoids derived from human patients have the potential to bridge this gap. In the preceding chapters, the mucus in the 3D organoid lumen had been trapped in the lumen, thus limiting our analyses<sup>90</sup>. In Chapter 4, we opened up these organoids by disaggregating them and culturing their cells as a 2D monolayer, enabling access to the mucus at last<sup>37</sup>. Boccellato *et al.* and Wang *et al.* have developed complementary methods for the generation of a gastrointestinal mucus layer atop a 2D monolayer at the air-liquid interface (ALI)<sup>37,59</sup>. Such an *in vitro* barrier, however, had not yet been explored as an analog to native mucus—that which is found *in vivo*. Because organoid-based models provide an alternative for pure mucin and native mucus (which is often contaminated), we hypothesized that BGM would

reveal functional and mechanical similarities to the *in vivo* gastric mucosa<sup>15</sup>. We interrogated the mucus secretome with SEC-MALS and mass spectrometry, the structure with CryoFE-SEM, and the mechanical properties with rheometry and microfluidic experiments. We found that the BGM had similar mucin abundance to the native mucus, as well as similar scaffold/pore structure. Further, we found similar rheological behavior and acid transport phenomena. In this chapter, we demonstrate that it is possible to engineer sterile human gastric mucus *in vitro* for convenient analyses of its structure-function relationship.

### Additional Contributions to Organoid Studies

In addition to the primary foci of my dissertation (Chapters 2-4), I sought to answer two complementary questions in adjacent areas of research that deepened my understanding of both *Helicobacter pylori* infection and organoid culture. These projects provided valuable insights into the management of *H. pylori* infection and the diverse applications of organoid modeling, ultimately enriching my expertise and contributing to the broader scientific context of my work.

#### Chapter 5: Can Berry Extracts Have Therapeutic Effects on *H. pylori*-Infected Organoids?

The goal of Chapter 5 was to assess the therapeutic potential of berry extracts against *H. pylori* infection. Anthocyanins—the phenolic compounds responsible for the coloring of dark berries—have successfully demonstrated chemopreventive, antibacterial, and anti-inflammatory properties<sup>91-93</sup>. We hypothesized that these effects could be replicated *in vitro* using an organoid model of *H. pylori* infection. We assessed the viability and proliferative activity of the organoids in response to this treatment—as uncontrolled proliferation is a hallmark of cancer<sup>94</sup>. We found that the extracts of black raspberries had a bactericidal effect against *H. pylori* infection, but did

not adversely affect proliferation or viability of the gastric organoids<sup>95</sup>. These results suggest that berry preparations have potential as novel antimicrobial agents to combat *H. pylori* infection. The majority of this work was performed during my time as an undergraduate in the Bimczok lab, and enabled me to gain experience with gastric organoid cultures as well as proliferation and viability assays.

#### Chapter 6: Can Organoids Be Generated From the Tissue of Jamaican Fruit Bats to Model SARS-CoV-2 Infection?

The goal of Chapter 6 was to establish an organoid model for SARS-CoV-2 infection in the bat gastrointestinal tract. The COVID-19 pandemic, declared a global health emergency in March 2020, was caused by severe acute respiratory virus-2 (SARS-CoV-2)<sup>96</sup>. This zoonotic virus was hypothesized to have originated in bats<sup>97</sup>. It has been postulated that bats are unusually susceptible to viral infection due to their inability to form a strong gut epithelial barrier<sup>98,99</sup>. We developed gastrointestinal organoids from the tissue of Jamaican fruit bats (JFB) for the study of SARS-CoV-2 infection. For this project, I contributed to the optimization of the culture conditions for the JFB organoids and evaluated their barrier function by growing them in 2D and evaluating their ability to develop transepithelial electrical resistance (TEER). I successfully showed that, indeed, the organoids could demonstrate intact barrier function—a key consideration for viral infection studies. This work—contradicting the previous hypotheses that bats do not have strong gut barriers<sup>98,99</sup>—represents the development and validation of a model that will enable future physiological studies of the Jamaican fruit bat gastrointestinal tract.

### References Cited

- 1 Bravo, D., Hoare, A., Soto, C., Valenzuela, M. A. & Quest, A. F. Helicobacter pylori in human health and disease: Mechanisms for local gastric and systemic effects. *World J Gastroenterol* **24**, 3071-3089 (2018). <https://doi.org/10.3748/wjg.v24.i28.3071>
- 2 Kusters, J. G., Van Vliet, A. H. M. & Kuipers, E. J. Pathogenesis of Helicobacter pylori infection. *Clinical Microbiology Reviews* (2006). <https://doi.org/10.1128/CMR.00054-05>
- 3 Amieva, M. & Peek, R. M., Jr. Pathobiology of Helicobacter pylori-Induced Gastric Cancer. *Gastroenterology* **150**, 64-78 (2016). <https://doi.org/10.1053/j.gastro.2015.09.004>
- 4 Karam, S. M. & Leblond, C. P. Identifying and counting epithelial cell types in the “corpus” of the mouse stomach. *The Anatomical Record* **232**, 231-246 (1992). <https://doi.org/https://doi.org/10.1002/ar.1092320208>
- 5 Kim, T. H. & Shivdasani, R. A. Stomach development, stem cells and disease. *Development* **143**, 554-565 (2016). <https://doi.org/10.1242/dev.124891>
- 6 Xiao, S. & Zhou, L. Gastric Stem Cells: Physiological and Pathological Perspectives. *Front Cell Dev Biol* **8**, 571536 (2020). <https://doi.org/10.3389/fcell.2020.571536>
- 7 Karam, S. M. & Leblond, C. P. Dynamics of epithelial cells in the corpus of the mouse stomach. I. Identification of proliferative cell types and pinpointing of the stem cell. *Anat Rec* **236**, 259-279 (1993). <https://doi.org/10.1002/ar.1092360202>
- 8 Karam, S. M. & Leblond, C. P. Dynamics of epithelial cells in the corpus of the mouse stomach. III. Inward migration of neck cells followed by progressive transformation into zymogenic cells. *Anat Rec* **236**, 297-313 (1993). <https://doi.org/10.1002/ar.1092360204>
- 9 McCracken, K. W. *et al.* Modelling human development and disease in pluripotent stem-cell-derived gastric organoids. *Nature* (2014). <https://doi.org/10.1038/nature13863>
- 10 Arthur J. Atkinson Jr, J. B., Robert M. Craig, James C. Reynolds, Carol Donner. *Peptic Ulcer Disease: Mechanisms & Management*. (The Healthpress Publishing Group, Inc., 1990).

- 11 McShane, A. *et al.* Mucus. *Curr Biol* **31**, R938-R945 (2021).  
<https://doi.org/10.1016/j.cub.2021.06.093>
- 12 Patwa, A. *et al.* Accumulation of nanoparticles in “jellyfish” mucus: a bio-inspired route to decontamination of nano-waste. *Scientific Reports* **5**, 11387 (2015).  
<https://doi.org/10.1038/srep11387>
- 13 Johansson, M. E., Sjoval, H. & Hansson, G. C. The gastrointestinal mucus system in health and disease. *Nat Rev Gastroenterol Hepatol* **10**, 352-361 (2013).  
<https://doi.org/10.1038/nrgastro.2013.35>
- 14 Abdullah, L. H. *et al.* Mucin Production and Hydration Responses to Mucopurulent Materials in Normal versus Cystic Fibrosis Airway Epithelia. *Am J Respir Crit Care Med* **197**, 481-491 (2018). <https://doi.org/10.1164/rccm.201706-1139OC>
- 15 Bansil, R., Celli, J. P., Hardcastle, J. M. & Turner, B. S. The Influence of Mucus Microstructure and Rheology in Helicobacter pylori Infection. *Front Immunol* **4**, 310 (2013). <https://doi.org/10.3389/fimmu.2013.00310>
- 16 Su-Arcaro, C. *et al.* Unraveling the Intertwined Effect of pH on Helicobacter pylori Motility and the Microrheology of the Mucin-Based Medium It Swims in. *Microorganisms* **11** (2023). <https://doi.org/10.3390/microorganisms11112745>
- 17 Bahari, H. M., Ross, I. N. & Turnberg, L. A. Demonstration of a pH gradient across the mucus layer on the surface of human gastric mucosa in vitro. *Gut* **23**, 513-516 (1982).  
<https://doi.org/10.1136/gut.23.6.513>
- 18 Lewis, O. L., Keener, J. P. & Fogelson, A. L. A physics-based model for maintenance of the pH gradient in the gastric mucus layer. *Am J Physiol Gastrointest Liver Physiol* **313**, G599-G612 (2017). <https://doi.org/10.1152/ajpgi.00221.2017>
- 19 Takafumi, I., T., Kazuhiko, I. Protective Effects of Gastric Mucus. *Gastritis and Gastric Cancer* (2011). <https://doi.org/10.5772/23951>
- 20 Wheeler, K. M. *et al.* Mucin glycans attenuate the virulence of Pseudomonas aeruginosa in infection. *Nature Microbiology* **4**, 2146-2154 (2019). <https://doi.org/10.1038/s41564-019-0581-8>

- 21 Reily, C., Stewart, T. J., Renfrow, M. B. & Novak, J. Glycosylation in health and disease. *Nat Rev Nephrol* **15**, 346-366 (2019). <https://doi.org/10.1038/s41581-019-0129-4>
- 22 Cornick, S., Tawiah, A. & Chadee, K. Roles and regulation of the mucus barrier in the gut. *Tissue Barriers* (2015). <https://doi.org/10.4161/21688370.2014.982426>
- 23 Tong, J. & Gu, Q. Expression and Clinical Significance of Mucin Gene in Chronic Rhinosinusitis. *Curr Allergy Asthma Rep* **20**, 63 (2020). <https://doi.org/10.1007/s11882-020-00958-w>
- 24 Parente, I. A., Chiara, L. & Bertoni, S. Exploring the potential of human intestinal organoids: Applications, challenges, and future directions. *Life Sciences* **352**, 122875 (2024). <https://doi.org/https://doi.org/10.1016/j.lfs.2024.122875>
- 25 Izadifar, Z. *et al.* Modeling mucus physiology and pathophysiology in human organs-on-chips. *Adv Drug Deliv Rev* **191**, 114542 (2022). <https://doi.org/10.1016/j.addr.2022.114542>
- 26 Schubert, M. L. Gastric acid secretion. *Curr Opin Gastroenterol* **32**, 452-460 (2016). <https://doi.org/10.1097/mog.0000000000000308>
- 27 Engevik, A. C., Kaji, I. & Goldenring, J. R. The Physiology of the Gastric Parietal Cell. *Physiol Rev* **100**, 573-602 (2020). <https://doi.org/10.1152/physrev.00016.2019>
- 28 Soll, A. H. & Walsh, J. H. Regulation of gastric acid secretion. *Annu Rev Physiol* **41**, 35-53 (1979). <https://doi.org/10.1146/annurev.ph.41.030179.000343>
- 29 Forssell, H. Gastric mucosal defence mechanisms: a brief review. *Scand J Gastroenterol Suppl* **155**, 23-28 (1988). <https://doi.org/10.3109/00365528809096277>
- 30 Allen, A. & Flemström, G. Gastroduodenal mucus bicarbonate barrier: Protection against acid and pepsin. *American Journal of Physiology - Cell Physiology* (2005). <https://doi.org/10.1152/ajpcell.00102.2004>
- 31 Su, C. *et al.* Influence of the viscosity of healthy and diseased human mucins on the motility of *Helicobacter pylori*. *Scientific Reports* **8** (2018). <https://doi.org/10.1038/s41598-018-27732-3>



- 32 Celli, J. P. *et al.* Rheology of Gastric Mucin Exhibits a pH-Dependent Sol–Gel Transition. *Biomacromolecules* **8**, 1580-1586 (2007). <https://doi.org/10.1021/bm0609691>
- 33 Schreiber, S. *et al.* In situ measurement of pH in the secreting canaliculus of the gastric parietal cell and adjacent structures. *Cell and Tissue Research* **329**, 313-320 (2007). <https://doi.org/10.1007/s00441-007-0427-1>
- 34 Bhaskar, K. R. *et al.* Viscous fingering of HCl through gastric mucin. *Nature* **360**, 458-461 (1992). <https://doi.org/10.1038/360458a0>
- 35 Johansson, M., Synnerstad, I. & Holm, L. Acid transport through channels in the mucous layer of rat stomach. *Gastroenterology* **119**, 1297-1304 (2000). <https://doi.org/https://doi.org/10.1053/gast.2000.19455>
- 36 Zhang, Q., Amooie, A., Bazant, M. Z. & Bischofberger, I. Growth morphology and symmetry selection of interfacial instabilities in anisotropic environments. *Soft Matter* **17**, 1202-1209 (2021). <https://doi.org/10.1039/d0sm01706j>
- 37 Boccellato, F. *et al.* Polarised epithelial monolayers of the gastric mucosa reveal insights into mucosal homeostasis and defence against infection. *Gut* **68**, 400-413 (2019). <https://doi.org/10.1136/gutjnl-2017-314540>
- 38 Davies, J. A. in *Organoids and Mini-Organs* (eds Jamie A. Davies & Melanie L. Lawrence) 3-23 (Academic Press, 2018).
- 39 Lancaster, M. A. & Knoblich, J. A. Organogenesis in a dish: modeling development and disease using organoid technologies. *Science* **345**, 1247125 (2014). <https://doi.org/10.1126/science.1247125>
- 40 Simian, M. & Bissell, M. J. Organoids: A historical perspective of thinking in three dimensions. *J Cell Biol* **216**, 31-40 (2017). <https://doi.org/10.1083/jcb.201610056>
- 41 Clevers, H. Modeling Development and Disease with Organoids. *Cell* **165**, 1586-1597 (2016). <https://doi.org/10.1016/j.cell.2016.05.082>
- 42 Davies, J. A. & Lawrence, M. L. in *Organoids and Mini-Organs* (eds Jamie A. Davies & Melanie L. Lawrence) 255-259 (Academic Press, 2018).

- 43 Sato, T. *et al.* Single Lgr5 stem cells build crypt-villus structures in vitro without a mesenchymal niche. *Nature* (2009). <https://doi.org/10.1038/nature07935>
- 44 Dedhia, P. H., Bertaux-Skeirik, N., Zavros, Y. & Spence, J. R. Organoid Models of Human Gastrointestinal Development and Disease. *Gastroenterology* **150**, 1098-1112 (2016). <https://doi.org/10.1053/j.gastro.2015.12.042>
- 45 Jung, P. *et al.* Isolation and in vitro expansion of human colonic stem cells. *Nat Med* **17**, 1225-1227 (2011). <https://doi.org/10.1038/nm.2470>
- 46 VanDussen, K. L. *et al.* Development of an enhanced human gastrointestinal epithelial culture system to facilitate patient-based assays. *Gut* **64**, 911-920 (2015). <https://doi.org/10.1136/gutjnl-2013-306651>
- 47 Seidlitz, T., Koo, B.-K. & Stange, D. E. Gastric organoids—an in vitro model system for the study of gastric development and road to personalized medicine. *Cell Death & Differentiation* **28**, 68-83 (2021). <https://doi.org/10.1038/s41418-020-00662-2>
- 48 Sebrell, T. A. *et al.* Live imaging analysis of human gastric epithelial spheroids reveals spontaneous rupture, rotation and fusion events. *Cell and Tissue Research* **371**, 293-307 (2018). <https://doi.org/10.1007/s00441-017-2726-5>
- 49 Barker, N. *et al.* Lgr5(+ve) stem cells drive self-renewal in the stomach and build long-lived gastric units in vitro. *Cell Stem Cell* **6**, 25-36 (2010). <https://doi.org/10.1016/j.stem.2009.11.013>
- 50 Clevers, H., Loh, K. M. & Nusse, R. Stem cell signaling. An integral program for tissue renewal and regeneration: Wnt signaling and stem cell control. *Science* **346**, 1248012 (2014). <https://doi.org/10.1126/science.1248012>
- 51 Stamos, J. L., Chu, M. L., Enos, M. D., Shah, N. & Weis, W. I. Structural basis of GSK-3 inhibition by N-terminal phosphorylation and by the Wnt receptor LRP6. *Elife* **3**, e01998 (2014). <https://doi.org/10.7554/eLife.01998>
- 52 Sato, T. & Clevers, H. Growing self-organizing mini-guts from a single intestinal stem cell: mechanism and applications. *Science* **340**, 1190-1194 (2013). <https://doi.org/10.1126/science.1234852>

- 53 Sato, T. *et al.* Long-term expansion of epithelial organoids from human colon, adenoma, adenocarcinoma, and Barrett's epithelium. *Gastroenterology* **141**, 1762-1772 (2011). <https://doi.org/10.1053/j.gastro.2011.07.050>
- 54 Leushacke, M. *et al.* Lgr5-expressing chief cells drive epithelial regeneration and cancer in the oxyntic stomach. *Nat Cell Biol* **19**, 774-786 (2017). <https://doi.org/10.1038/ncb3541>
- 55 Wolffling, S. *et al.* EGF and BMPs Govern Differentiation and Patterning in Human Gastric Glands. *Gastroenterology* **161**, 623-636 e616 (2021). <https://doi.org/10.1053/j.gastro.2021.04.062>
- 56 Bartfeld, S. *et al.* In vitro expansion of human gastric epithelial stem cells and their responses to bacterial infection. *Gastroenterology* (2015). <https://doi.org/10.1053/j.gastro.2014.09.042>
- 57 McCracken, K. W. *et al.* Modelling human development and disease in pluripotent stem-cell-derived gastric organoids. *Nature* **516**, 400-404 (2014). <https://doi.org/10.1038/nature13863>
- 58 Schumacher, M. A. *et al.* The use of murine-derived fundic organoids in studies of gastric physiology. *J Physiol* **593**, 1809-1827 (2015). <https://doi.org/10.1113/jphysiol.2014.283028>
- 59 Wang, Y., Kim, R., Sims, C. E. & Allbritton, N. L. Building a Thick Mucus Hydrogel Layer to Improve the Physiological Relevance of In Vitro Primary Colonic Epithelial Models. *Cellular and Molecular Gastroenterology and Hepatology* **8**, 653-655.e655 (2019). <https://doi.org/10.1016/j.jcmgh.2019.07.009>
- 60 Marshall, B. J. & Warren, J. R. Unidentified curved bacilli in the stomach of patients with gastritis and peptic ulceration. *Lancet* **1**, 1311-1315 (1984). [https://doi.org/10.1016/s0140-6736\(84\)91816-6](https://doi.org/10.1016/s0140-6736(84)91816-6)
- 61 Ito, T. *et al.* Helicobacter pylori invades the gastric mucosa and translocates to the gastric lymph nodes. *Lab Invest* **88**, 664-681 (2008). <https://doi.org/10.1038/labinvest.2008.33>

- 62 Yoshiyama, H. & Nakazawa, T. Unique mechanism of *Helicobacter pylori* for colonizing the gastric mucus. *Microbes and Infection* **2**, 55-60 (2000).  
[https://doi.org/https://doi.org/10.1016/S1286-4579\(00\)00285-9](https://doi.org/https://doi.org/10.1016/S1286-4579(00)00285-9)
- 63 Sebrell, T. A. *et al.* A Novel Gastric Spheroid Co-culture Model Reveals Chemokine-Dependent Recruitment of Human Dendritic Cells to the Gastric Epithelium. *Cellular and Molecular Gastroenterology and Hepatology* **8**, 157-171.e153 (2019).  
<https://doi.org/10.1016/j.jcmgh.2019.02.010>
- 64 Gonçalves, I. C. *et al.* Bacteria-targeted biomaterials: Glycan-coated microspheres to bind *Helicobacter pylori*. *Acta Biomaterialia* **33**, 40-50 (2016).  
<https://doi.org/https://doi.org/10.1016/j.actbio.2016.01.029>
- 65 Keilberg, D. & Ottemann, K. M. How *Helicobacter pylori* senses, targets and interacts with the gastric epithelium. *Environmental Microbiology* (2016).  
<https://doi.org/10.1111/1462-2920.13222>
- 66 Nakamura, H. *et al.* Urease plays an important role in the chemotactic motility of *Helicobacter pylori* in a viscous environment. *Infect Immun* **66**, 4832-4837 (1998).  
<https://doi.org/10.1128/IAI.66.10.4832-4837.1998>
- 67 Martínez, L. E. *et al.* *Helicobacter pylori* strains vary cell shape and flagellum number to maintain robust motility in viscous environments. *Molecular Microbiology* (2016).  
<https://doi.org/10.1111/mmi.13218>
- 68 Josenhans, C., Eaton, K. A., Thevenot, T. & Suerbaum, S. Switching of flagellar motility in *Helicobacter pylori* by reversible length variation of a short homopolymeric sequence repeat in *fliP*, a gene encoding a basal body protein. *Infect Immun* **68**, 4598-4603 (2000).  
<https://doi.org/10.1128/IAI.68.8.4598-4603.2000>
- 69 Tan, S. & Berg, D. E. Motility of urease-deficient derivatives of *Helicobacter pylori*. *J Bacteriol* **186**, 885-888 (2004). <https://doi.org/10.1128/JB.186.3.885-888.2004>
- 70 Harris, P. R., Mobley, H. L., Perez-Perez, G. I., Blaser, M. J. & Smith, P. D. *Helicobacter pylori* urease is a potent stimulus of mononuclear phagocyte activation and inflammatory cytokine production. *Gastroenterology* **111**, 419-425 (1996).  
<https://doi.org/10.1053/gast.1996.v111.pm8690207>

- 71 Megraud, F., Neman-Simha, V. & Brugmann, D. Further evidence of the toxic effect of ammonia produced by *Helicobacter pylori* urease on human epithelial cells. *Infect Immun* **60**, 1858-1863 (1992). <https://doi.org/10.1128/iai.60.5.1858-1863.1992>
- 72 Celli, J. P. *et al.* *Helicobacter pylori* moves through mucus by reducing mucin viscoelasticity. *Proc Natl Acad Sci U S A* **106**, 14321-14326 (2009). <https://doi.org/10.1073/pnas.0903438106>
- 73 Venerito, M., Vasapolli, R., Rokkas, T. & Malfertheiner, P. Gastric cancer: epidemiology, prevention, and therapy. *Helicobacter* **23 Suppl 1**, e12518 (2018). <https://doi.org/10.1111/hel.12518>
- 74 Zamani, M. *et al.* Systematic review with meta-analysis: the worldwide prevalence of *Helicobacter pylori* infection. *Aliment Pharmacol Ther* **47**, 868-876 (2018). <https://doi.org/10.1111/apt.14561>
- 75 Roesler, B. M., Rabelo-Goncalves, E. M. & Zeitune, J. M. Virulence Factors of *Helicobacter pylori*: A Review. *Clin Med Insights Gastroenterol* **7**, 9-17 (2014). <https://doi.org/10.4137/CGast.S13760>
- 76 Asaka M, S. A., Sugiyama T, Graham D. in *Helicobacter pylori: Physiology and Genetics* Ch. 40, (ASM Press, 2001).
- 77 Correa, P. & Piazuelo, M. B. *Helicobacter pylori* Infection and Gastric Adenocarcinoma. *US Gastroenterol Hepatol Rev* **7**, 59-64 (2011).
- 78 Bray, F. *et al.* Global cancer statistics 2022: GLOBOCAN estimates of incidence and mortality worldwide for 36 cancers in 185 countries. *CA Cancer J Clin* **74**, 229-263 (2024). <https://doi.org/10.3322/caac.21834>
- 79 Morgan, E. *et al.* The current and future incidence and mortality of gastric cancer in 185 countries, 2020-40: A population-based modelling study. *EClinicalMedicine* **47**, 101404 (2022). <https://doi.org/10.1016/j.eclinm.2022.101404>
- 80 Tshibangu-Kabamba, E. & Yamaoka, Y. *Helicobacter pylori* infection and antibiotic resistance - from biology to clinical implications. *Nat Rev Gastroenterol Hepatol* **18**, 613-629 (2021). <https://doi.org/10.1038/s41575-021-00449-x>

- 81 Smith, S. I. & Yamaoka, Y. Antibiotic Resistance and Therapy for *Helicobacter pylori* Infection. *Antibiotics (Basel)* **12** (2023). <https://doi.org/10.3390/antibiotics12121669>
- 82 Niv, Y. *Helicobacter pylori* and gastric mucin expression: A systematic review and meta-analysis. *World J Gastroenterol* **21**, 9430-9436 (2015). <https://doi.org/10.3748/wjg.v21.i31.9430>
- 83 Lyon, K., Bansil, R. & Bimczok, D. Profiling Luminal pH in Three-Dimensional Gastrointestinal Organoids Using Microelectrodes. *J Vis Exp* (2024). <https://doi.org/10.3791/66900>
- 84 Jewell, M. P., Galyean, A. A., Kirk Harris, J., Zemanick, E. T. & Cash, K. J. Luminescent Nanosensors for Ratiometric Monitoring of Three-Dimensional Oxygen Gradients in Laboratory and Clinical *Pseudomonas aeruginosa* Biofilms. *Appl Environ Microbiol* **85** (2019). <https://doi.org/10.1128/aem.01116-19>
- 85 Mao, Y., Nielsen, P. & Ali, J. Passive and Active Microrheology for Biomedical Systems. *Frontiers in Bioengineering and Biotechnology* **10** (2022). <https://doi.org/10.3389/fbioe.2022.916354>
- 86 Georgiades, P., Pudney, P. D. A., Thornton, D. J. & Waigh, T. A. Particle tracking microrheology of purified gastrointestinal mucins. *Biopolymers* **101**, 366-377 (2014). <https://doi.org/https://doi.org/10.1002/bip.22372>
- 87 Cai, Y. *et al.* SEDDS facilitate cinnamaldehyde crossing the mucus barrier: The perspective of mucus and Caco-2/HT29 co-culture models. *International Journal of Pharmaceutics* **614**, 121461 (2022). <https://doi.org/https://doi.org/10.1016/j.ijpharm.2022.121461>
- 88 Barmapsalou, V. *et al.* Development and validation of a porcine artificial colonic mucus model reflecting the properties of native colonic mucus in pigs. *European Journal of Pharmaceutical Sciences* **181**, 106361 (2023). <https://doi.org/https://doi.org/10.1016/j.ejps.2022.106361>
- 89 Dubbelboer, I. R. *et al.* Gastrointestinal mucus in dog: Physiological characteristics, composition, and structural properties. *Eur J Pharm Biopharm* **173**, 92-102 (2022). <https://doi.org/10.1016/j.ejpb.2022.02.019>

- 90 Hofer, M. & Lutolf, M. P. Engineering organoids. *Nat Rev Mater* **6**, 402-420 (2021). <https://doi.org/10.1038/s41578-021-00279-y>
- 91 Wang, L. S. & Stoner, G. D. Anthocyanins and their role in cancer prevention. *Cancer Lett* **269**, 281-290 (2008). <https://doi.org/10.1016/j.canlet.2008.05.020>
- 92 Samad, M. A., Hashim, S. H., Simarani, K. & Yaacob, J. S. Antibacterial Properties and Effects of Fruit Chilling and Extract Storage on Antioxidant Activity, Total Phenolic and Anthocyanin Content of Four Date Palm (*Phoenix dactylifera*) Cultivars. *Molecules* **21**, 419 (2016). <https://doi.org/10.3390/molecules21040419>
- 93 Marin, L., Miguelez, E. M., Villar, C. J. & Lombo, F. Bioavailability of dietary polyphenols and gut microbiota metabolism: antimicrobial properties. *Biomed Res Int* **2015**, 905215 (2015). <https://doi.org/10.1155/2015/905215>
- 94 Brown, J. S. *et al.* Updating the Definition of Cancer. *Molecular Cancer Research* **21**, 1142-1147 (2023). <https://doi.org/10.1158/1541-7786.MCR-23-0411>
- 95 Goodman, C. *et al.* A High-Throughput Metabolic Microarray Assay Reveals Antibacterial Effects of Black and Red Raspberries and Blackberries against *Helicobacter pylori* Infection. *Antibiotics* **10**, 845-845 (2021). <https://doi.org/10.3390/antibiotics10070845>
- 96 Mallah, S. I. *et al.* COVID-19: breaking down a global health crisis. *Ann Clin Microbiol Antimicrob* **20**, 35 (2021). <https://doi.org/10.1186/s12941-021-00438-7>
- 97 Zhou, H. *et al.* Identification of novel bat coronaviruses sheds light on the evolutionary origins of SARS-CoV-2 and related viruses. *Cell* **184**, 4380-4391 e4314 (2021). <https://doi.org/10.1016/j.cell.2021.06.008>
- 98 Jones, D. N., Ravelomanantsoa, N. A. F., Yeoman, C. J., Plowright, R. K. & Brook, C. E. Do gastrointestinal microbiomes play a role in bats' unique viral hosting capacity? *Trends Microbiol* **30**, 632-642 (2022). <https://doi.org/10.1016/j.tim.2021.12.009>
- 99 Luna, N. *et al.* Characterizing the blood microbiota of omnivorous and frugivorous bats (Chiroptera: Phyllostomidae) in Casanare, eastern Colombia. *PeerJ* **11**, e15169 (2023). <https://doi.org/10.7717/peerj.15169>

CHAPTER TWO

PROFILING LUMINAL PH IN THREE-DIMENSIONAL  
GASTROINTESTINAL ORGANOIDs USING  
MICROELECTRODES

Contribution of Authors and Co-Authors

Manuscript in Chapter 2

Author: Katrina Lyon

Contributions: Designed and performed experiments, analyzed and interpreted data, wrote and revised the manuscript

Co-Author: Rama Bansil

Contributions: Provided microelectrodes and other equipment, interpreted data, revised manuscript

Co-Author: Diane Bimczok

Contributions: Developed the project and designed experiments, analyzed and interpreted data, revised manuscript, provided funding for the project



Manuscript Information

**Katrina Lyon**, Rama Bansil, Diane Bimczok

Journal of Visualized Experiments

Status of Manuscript:

- ☐ Prepared for submission to a peer-reviewed journal
- ☐ Officially submitted to a peer-reviewed journal
- ☐ Accepted by a peer-reviewed journal
- ☒ Published in a peer-reviewed journal

Journal of Visualized Experiments

July 5<sup>th</sup>, 2024

Volume 209

DOI: 10.3791/66900

### Abstract

The optimization and detailed characterization of gastrointestinal organoid models require advanced methods for analyzing their luminal environments. This paper presents a highly reproducible method for the precise measurement of pH within the lumina of 3D human gastric organoids via micromanipulator-controlled microelectrodes. The pH microelectrodes are commercially available and consist of beveled glass tips of 25  $\mu\text{m}$  in diameter. For measurements, the pH microelectrode is advanced into the lumen of an organoid ( $>200 \mu\text{m}$ ) that is suspended in Matrigel, while a reference electrode rests submerged in the surrounding medium in the culture plate.

Using such microelectrodes to profile organoids derived from the human gastric body, we demonstrate that luminal pH is relatively consistent within each culture well at  $\sim 7.7 \pm 0.037$  and that continuous measurements can be obtained for a minimum of 15 min. In some larger organoids, the measurements revealed a pH gradient between the epithelial surface and the lumen, suggesting that pH measurements in organoids can be achieved with high spatial resolution. In a previous study, microelectrodes were successfully used to measure luminal oxygen concentrations in organoids, demonstrating the versatility of this method for organoid analyses. In summary, this protocol describes an important tool for the functional characterization of the complex luminal space within 3D organoids.

### Introduction

Organoids-miniature multicellular structures derived from stem cells-have revolutionized our ability to study human physiology and are starting to replace animal models, even in

regulatory settings<sup>1</sup>. Since the initial description of intestinal organoids by Sato et al. in 2009, organoid technology has become immensely popular<sup>2</sup>. A large number of studies have characterized the cellular composition and function of organoid models in great detail<sup>3-6</sup>. However, the luminal space of these 3D multicellular structures remains largely undefined<sup>7,8</sup>. The lumen is the central cavity of organoids derived from mucosal tissues that is surrounded by the apical portions of polarized epithelial cells. Since cellular secretion and absorption predominantly occur at the apical epithelial surface, the luminal microenvironment of organoids is controlled by these important physiological processes. Currently used organoid models demonstrate variations in cell signaling patterns, overall stemness, metabolite concentration gradients, and environmental conditions<sup>9</sup>. Understanding organoid luminal physiology is therefore necessary for the accurate modeling of organ function and pathology. Unfortunately, the relative inaccessibility of the lumen significantly hinders functional analyses of luminal physiology in 3D organoids<sup>10</sup>.

The ability to examine pH profiles is especially important in the stomach, which is notorious for having the steepest proton gradient in the body, ranging from approximately 1-3 in the lumen, to near neutral at the epithelium<sup>11-13</sup>. There remains a significant gap in our understanding of the microscale maintenance of the gastric pH gradient, and the relevance of organoid models in recapitulating this dynamic milieu across the gastric mucus layer. Traditional approaches for the analysis of organoid pH have involved the use of pH-sensitive dyes, which can be fluorescent or colorimetric indicators. McCracken *et al.* used a luminal injection of SNARF-5F-a ratiometric pH indicator-into organoids to analyze a drop in luminal pH in response to histamine treatment. Such dyes can be incorporated into the culture media, allowing

for real-time, non-invasive monitoring of pH. Not only do pH-sensitive dyes require complex calibration steps that contribute to poor reliability and accuracy with measurements, but such dyes also tend to operate within specific detection ranges that may not be representative of the full pH range within the microenvironment of interest<sup>14,15</sup>. It could be considered reasonable, however, to use indicator dyes for confirmatory experiments. Optical nanosensors that use fluorescent optode-based, pH-sensing approaches have also been developed; however, such sensing techniques require microscopic imaging and are also susceptible to photobleaching, phototoxicity, as well as imaging bias<sup>16,17</sup>. Additionally, Brooks *et al.* have 3D-printed multiwell plates containing microelectrodes on top of which organoids may be plated<sup>18</sup>. This approach, however, does not allow for measurements directly inside the organoid lumen.

Electrode-based pH measurements can achieve improved accuracy compared to other methods, as well as provide real-time pH monitoring. In addition, pH electrodes mounted on micromanipulators allow for superior spatial resolution of pH measurements as the precise location of the electrode tip can be finely controlled. This enables the highest possible flexibility and reproducibility in the analyses of organoid models. The electrodes used here are miniaturized pH microelectrodes that operate based on the diffusion of protons through selective pH glass that surrounds a thin platinum wire. The microelectrode is connected to an external Ag-AgCl reference electrode and then connected to a high-impedance millivolt meter. The electrical potential between the two electrode tips when submerged in the same solution will reflect the pH of the solution<sup>19</sup>. Such microprofiling systems have been used in the metabolic analysis of biofilms<sup>20,21</sup>, planktonic algae<sup>22</sup>, human sputum samples<sup>23</sup>, and even in mesenchymal stem cell spheroids<sup>24</sup>. Both our lab and Murphy *et al.* have previously used micromanipulator-controlled

O<sub>2</sub> microelectrodes to evaluate the oxygen concentrations in the luminal spaces of organoids. Murphy *et al.* paired this method with mathematical modeling to reveal an oxygen gradient within their spheroids. Our group was able to find reduced luminal oxygen levels in tissue-derived gastric organoids compared to the surrounding extracellular matrix<sup>25</sup>.

Here, we provide a detailed method for the manual microelectrode profiling of the luminal pH in spherical gastrointestinal tract organoids that will enable enhanced physiological understanding of their complex luminal microenvironment. We anticipate that this technique will add a new dimension to the exploration of organoid physiology through real-time, high-resolution measurements of pH levels at a microscale. Furthermore, the following protocol could be easily adapted for the analysis of O<sub>2</sub>, N<sub>2</sub>O, H<sub>2</sub>, NO, H<sub>2</sub>S, redox, and temperature in various types of organoid models. Physiological profiling serves as a valuable tool for optimizing organoid culture conditions to better mimic *in vivo* environments, thereby enhancing the relevance and utility of organoid models in biomedical research.

### Protocol

This protocol requires 3D organoids of at least 200 µm in diameter that have a distinct lumen and that are embedded in an artificial extracellular matrix (ECM, e.g., Matrigel). Human gastric tissues for organoid derivation were obtained with approval from the Institutional Review Board of Montana State University and informed consent from patients undergoing upper endoscopy at Bozeman Health (protocol # 2023-48-FCR, to D.B.) or as exempt whole stomach or sleeve gastrectomy specimens from the National Disease Research Interchange (protocol #DB062615-EX). Information about the organoid lines and passage numbers used for this study is provided in Appendix A, and the media composition is listed in Appendix B. Refer to

previously published protocols for the generation and maintenance of gastrointestinal organoid lines<sup>6,26,27</sup>.

#### Preparation of Human Gastric Organoids for pH Profiling

1. Initiate and maintain gastric organoid cultures using standard protocols. Maintain organoids on 24-well plates in 500  $\mu$ L of expansion media per well (Table 2). Passage established organoid lines every 5-7 days, transferring to a 35 mm glass-bottom dish in preparation for pH profiling experiments.  
  
NOTE: Organoid cultures for our experiments are derived from gastric gland preparations, which are obtained from adult tissue as described above. We use a collagenase tissue digestion method to isolate these glands before they are suspended in ECM, as previously described<sup>25,28,29</sup>.
2. From actively growing organoid cultures at passages 1-15, select wells that contain at least 100 organoids (approximately 2 million cells) with diameters between 200 and 700  $\mu$ m for transfer and expansion on 3.5 mm Petri dishes.
3. While preparing organoids for plating (steps 1.4-1.8), allow extracellular matrix (ECM) aliquot(s) to thaw on ice for at least 45 min. Maintain ECM on ice throughout this protocol to prevent gelation. Prewarm cell culture plates by placing them in a 37 °C, 5% CO<sub>2</sub> incubator.
4. Remove the media from the wells and harvest the gastric organoid cultures by pipetting ice-cold PBS onto each ECM droplet and scratching the gel with the tip of a P1000 pipette. Pipette the PBS with the ECM fragments containing organoids into a 15 mL conical tube.

5. Centrifuge the tube at  $200 \times g$  at  $4^{\circ}\text{C}$  for 5 min. ECM fragments containing the organoids will be visible as a layer at the bottom of the tube. Carefully aspirate the supernatant and pipette 350  $\mu\text{L}$  of 0.25% trypsin-EDTA into each tube, mixing gently by pipetting up and down. Incubate the tubes in a  $37^{\circ}\text{C}$  water bath for 2-5 min.
6. Following incubation with trypsin-EDTA, add 600  $\mu\text{L}$  of ice-cold DMEM with penicillin/streptomycin to each tube and vigorously pipette up and down at least 40x. Centrifuge at  $200 \times g$  at  $4^{\circ}\text{C}$  for 5 min. Aspirate the supernatant. To set up cultures for pH measurements, resuspend the cell pellet in ice-cold, liquid ECM at a 1:4 v/v ratio of organoid pellet to ECM for plating.
7. For each sample, plate 40  $\mu\text{L}$  of liquid ECM containing organoids/organoid fragments in a thin horizontal line along the diameter of a 35 mm glass-bottom dish.  
  
NOTE: Dispensing the gel onto the plate in a line instead of a round droplet enables easier access to individual organoids by thinning out the culture.
8. Allow the gel to polymerize for 15-30 min; then, carefully add 2 mL of organoid expansion media to the plate by pipetting along the edge of the well to avoid disturbing the gel.
9. Replace media every other day. Allow 4-8 days for a minimum of 10 organoids to grow to a minimum diameter of 400  $\mu\text{m}$ .
10. To proceed with a pH profiling experiment, ensure that each culture contains at least 10 organoids that meet the following criteria:  $>200 \mu\text{m}$  diameter, healthy appearance (little to no dark material visible within organoids observed with a brightfield microscope), and not overcrowded by other organoids.

### Unpacking and Calibration of Microelectrodes

NOTE: To enable microscale measurements, a separate reference electrode is used in addition to the pH sensor microelectrode rather than using an integrated (and hence bulkier) design. Both pH microelectrode and reference electrode must be stored wet. Do not allow exposure to air for more than 10 min at a time. Determine the appropriate tip size for the application. Here, we used a potentiometric pH microelectrode with a beveled tip diameter of 25  $\mu\text{m}$ .

1. With the microelectrode still in its protection tube, visually inspect the tip for any damage.
2. Connect the reference electrode to the pH electrode cable via the connector. Then, connect the microelectrode to the amplifier and the amplifier to a grounded PC with the software via a USB cable (Figure 2.1A).
3. Fill two 50 mL conical tubes 2/3 with 70% ethanol and deionized  $\text{H}_2\text{O}$  ( $\text{diH}_2\text{O}$ ). Place the microelectrode and the reference electrode in the  $\text{diH}_2\text{O}$  tube, ensuring that both tips appear submerged at least 1 cm in the liquid.

NOTE: Tall beakers can also be used for this and similar steps.

4. Allow the electrodes to equilibrate for  $\sim 10$  min.

NOTE: The procedure can also be paused at this step and resumed later as the electrodes may be stored in  $\text{diH}_2\text{O}$ .

5. While the electrodes are equilibrating, open the software (red icon) on the computer workstation. Under the Settings tab, ensure that the box next to the microelectrode is checked, indicating that it is properly connected and recognized by the software.

Click *Start Experiment* on the top left of the window and enter your desired file name and



destination. In the *Sensor calibration & experiment settings* window, click *Clear all points* to prepare the software for a new calibration.

6. Fill two 50 mL conical tubes 2/3 with pH 4.01 and pH 9.21 calibration buffers. Gently blot the protective tubing and the reference electrode dry with a delicate laboratory wipe.
7. Starting with the electrodes in the pH 4.01 buffer, enter *4.01* as the known pH value. Once the mV reading has stabilized, select *add point*. Confirm that the signal is stable at ~380 mV. After the point has been added, place both electrodes back in diH<sub>2</sub>O to rinse, then blot dry again.
8. Repeat the previous step with the 9.21 buffer and click *add point* when the signal is stable (~83 mV). Check that the microelectrodes respond linearly between pH 4.01 and 9.21; therefore, only a two-point calibration curve is necessary. Ensure that the resulting line between these points has a negative slope of 50-70 mV/pH-unit. Click *Save & use calibration*.

NOTE: You are now ready to begin recording measurements<sup>30</sup>.

### pH Profiling of Human Gastric Organoids

NOTE: The following protocol is described for a right-handed user. CAUTION: Disable all power-saving options on your PC as ongoing measurements will be disrupted if the PC enters sleep mode.

1. Assemble a ring stand with a clamp on the left-hand side of a stereomicroscope to hold the reference electrode. Position a micromanipulator attached to a heavy lab stand on the right side of the microscope (Figure 2.1A).

2. Carefully remove the microelectrode from its protection case by laying it flat on the bench and pulling the case off in a swift, quick motion.

CAUTION: The microelectrodes are incredibly fragile and care should be taken to ensure that the tip does not come into contact with stiff, solid material. For best results, perform measurements on a sturdy benchtop free of equipment that could cause vibration of the bench or unwanted movement of the electrodes

3. Mount the microelectrode on a micromanipulator and arrange the stereoscope and micromanipulator in such a way that the microelectrode may advance toward the culture dish without hitting the objective or other parts of the microscope.
4. Position the culture dish containing the organoids to have adequate visualization of the first organoid that is to be profiled (Figure 2.1B).
5. Lightly secure the reference electrode to the clamp on the ring stand to the left of the stereoscope. Position the reference electrode so that it rests in the medium surrounding the ECM. Take care to ensure that it will not disrupt the organoids as the stage is moved around between measurements.
6. Looking directly at the culture plate (not into the microscope), advance the tip of the microelectrode until it is sufficiently submerged in the media. Under the Data logger tab in the software, click the Start button (single triangle pointing to the right) to begin recording. Ensure that the Calibrated checkbox is selected on the right side of the screen.  
  
NOTE: Allow ~10 s for each reading to stabilize before advancing to the next region.
7. Before entering the ECM, ensure that the electrode tip is visible under the microscope and that it is positioned to advance linearly toward the first organoid of interest. Slowly

advance the electrode into the gel, without making contact with any organoids. Record at least three pH readings and calculate the average.

8. Position the microelectrode so that it is prepared to advance toward the first organoid of interest along the axis perpendicular to the surface. Allow the electrode to make a minor indentation on the epithelial surface without penetrating (Figure 2.1C).

NOTE: This step will also provide insight into whether the organoid will remain in place or whether it may move about more freely in the ECM.

9. With one swift motion, advance the microelectrode into the organoid. If the organoid moves around the microelectrode or moves away, attempt a slightly different angle, or back it up against another organoid or the plastic rim surrounding the coverglass bottom of the dish. Measure the luminal pH (three individual times) of 10 different organoids for each experimental condition. When finished recording measurements, click the square Stop button.

CAUTION: Estimate the diameter of the organoid to decide how far to advance the electrode into the organoid lumen, taking care not to pierce through it. For increased accuracy, measure the diameter with your microscope's camera software, if available.

NOTE: If the tip of the microelectrode becomes noticeably coated with debris following one or multiple measurements, wash the microelectrode in cell dissociation solution, PBS, EtOH, and then diH<sub>2</sub>O before proceeding.

#### Motorized Profiling (Optional)

NOTE: This option requires a micromanipulator that is mounted on a mechanical motor stage, which is ultimately controlled by computer software via a motor controller<sup>31</sup>.

1. Open the Profiling software (brown icon) and start a *new experiment* under the *Profiling* tab.
2. The settings for the z-axis will automatically recognize *Motor* when a motor apparatus is properly connected.

NOTE: Movement in the x and y directions is still controlled manually with this setup.

3. Locate the *Profile interaction tab*<sup>30</sup>. Before hitting *start*, ensure that it is possible to quickly transition to looking at the microscope eyepiece to ensure organoid entry at the desired distance. Go to *Profile settings* and do the following:

- a. Indicate that the *Start distance* is 0  $\mu\text{m}$ .

CAUTION: If the epithelial shell is particularly tough on a given organoid, the organoid may be pushed away or deformed instead of penetrated. If pushing is the case, continue advancing the electrode but note the point at which entry occurs, as the software cannot record this automatically.

- b. Judging the size of the organoid being profiled, indicate an *End distance* that is no more than  $\frac{3}{4}$  way through an organoid's estimated diameter.

NOTE: This particular step is designed to prevent damage to the electrode tip.

- c. Indicate the desired *step size*—100  $\mu\text{m}$  as shown in Figure 2E. Ensure that the minimum step size matches the size of the electrode tip (e.g., 25  $\mu\text{m}$  for a 25  $\mu\text{m}$  pH-25 electrode tip).
- d. Indicate a *safe* position to which the motor will return the electrode tip between profiles.

NOTE: This should be a comfortable height above the sample (outside of the

organoid) where the sensor can be safely moved sideways in the x- and y- directions with the manual micromanipulator. Leave the *Sensor angle* at its default setting.

- e. To allow the electrode to equilibrate, indicate at least 3 s under *Wait before measure(s)*.
- f. Set the *Measure period(s)* to at least 1 s. The measurements over this period will be averaged.

NOTE: If performing measurements in an environment high in electrical noise, it may be helpful to indicate a longer period.

- g. Set the *Delay between(s)* to at least 1 s.
- h. Set the preferred number of *Replicates* to be measured at each depth.
- i. Begin recording measurements by hitting the *Start* button.

#### Cleaning of Electrodes

1. Place the electrode to be cleaned back in its protection tube.
2. Flush the electrodes with diH<sub>2</sub>O after measurements.
3. Flush the electrodes with 70% ethanol for a couple of minutes.
4. Rinse the electrodes with pH 4.01 buffer.
5. Rinse the electrodes once more with diH<sub>2</sub>O before proceeding with measurements.

#### Storage of Electrodes

NOTE: Both electrodes are to be stored at room temperature in a low-activity location, safe from accidental damage.

1. After using the pH microelectrode, carefully slide it horizontally back into its protection tube (sliding along the lab bench for horizontal support).
2. Holding the microelectrode upright (tip pointed upward), gently fill the protection tube with sterile water. Plug the protection tube with the stopper the electrode came with. Ensure that any holes in the protection tube are sealed with electrical tape. Store in a shatter-proof box until the next use.

NOTE: It is recommended to use the original box that the electrodes came in as it will contain protective inserts designed to keep electrodes in place when stored.

3. Store the reference electrode in a beaker or graduated cylinder filled with a 3M KCl solution. Cover the beaker/graduated cylinder with parafilm to prevent evaporation of the solution.

NOTE: If using a graduated cylinder, it is recommended to secure it to the lab bench with tape to prevent accidental movement.

### Methyl Red Injection

NOTE: Methyl red is a colorimetric indicator dye that can be used to validate the microelectrode measurements.

1. Backfill a 2  $\mu$ L glass capillary with sterile mineral oil, load it onto a micromanipulator-controlled nL autoinjector, and subsequently fill it with a solution containing 0.02% methyl red and 150 mM HCl.

NOTE: The solution should appear red/pink while in the capillary due to the acidity of the HCl.

2. Inject organoids of at least 300  $\mu$ m in diameter with 9.2  $\mu$ L of the solution<sup>25</sup>.

3. Capture images or video using a camera adapted to the stereomicroscope (Figure 2.2G).

### Representative Results

Secretion of acid is a crucial function of the human stomach. However, to what extent acid secretion can be modeled in organoids is still a matter of debate<sup>6,32-34</sup>. We therefore developed the protocol detailed above to accurately measure acid production in gastric organoids. Notably, we used unstimulated adult stem cell-derived organoids cultured under standard expansion conditions that had been passaged several times, which led to parietal cell loss<sup>35</sup>. Therefore, the presence of acid-secreting parietal cells and active acid release was not expected in our model system.

For our experiments, we used organoids with diameters between 200  $\mu\text{m}$  and 1,000  $\mu\text{m}$  seeded on glass-bottom dishes. First, we tested two different tip sizes for the microelectrodes-a pH-25 with a tip diameter of 25  $\mu\text{m}$  and a pH-50 with a tip diameter of 50  $\mu\text{m}$ . As shown in Figure 2A, there was no significant difference between measurements obtained with the smaller compared to the larger tips. Interestingly, the baseline pH in the organoids tended to be slightly alkaline at  $\sim\text{pH } 8$ . Using the 25  $\mu\text{m}$  pH-25 tip, we next assessed the variation in luminal pH within different ten organoids maintained on the same culture plate, with three measurements obtained from each organoid (Figure 2B). Within one plate, the luminal pH of individual organoids showed only slight, non-significant variations ( $8.16 \pm 0.12$ ;  $p \geq 0.0445$ -0.99) (Figure 2B). We also compared intraluminal pH measurements within five different organoid lines with passages ranging from 3 to 16 (Figure 2C). Again, we found consistent pH measurements within each culture but significant variability between organoid lines. However, luminal pH generally remained between pH 7.3 and pH 8.2, within one order of magnitude, and there was no apparent

trend for average pH when comparing early to late passage numbers (Figure 2C). We next asked whether the pH of the organoid lumen was directly related to the pH of the organoid expansion media and extracellular matrix (ECM). Comparison between the media, the ECM surrounding the organoids, and the organoid lumen revealed significant differences in pH, with the luminal pH of the organoids lower than that of the ECM, and the ECM pH lower than that of the surrounding organoid expansion media (Figure 2D), suggesting that the luminal pH of the organoids was physiologically relevant rather than directly determined by the culture environment. Across six independent experiments, we measured an average luminal pH that was near neutral at  $7.13 \pm 0.09$ .

A motorized micromanipulator was used to obtain pH measurements of the organoid lumen with greater spatial resolution. This approach is relevant if pH or other gradients within the mucus-filled organoid lumen<sup>29</sup> need to be recorded. Figure 2E shows two representative series of pH measurements in large organoids (>1,000  $\mu\text{m}$  diameter), demonstrating the entry point into each organoid and ending at a depth of  $\sim 800 \mu\text{m}$ . As the two organoids profiled did not have the same diameter, the measurements are not immediately comparable. Regardless, we show evidence of a slight pH gradient of  $\Delta 0.6$  between the epithelial surface and the deeper organoid lumen (Figure 2E). To determine the feasibility of performing pH measurements in the organoids over time, which would enable measurements of treatment responses in real time, we recorded the intraluminal pH inside a representative organoid for approximately 20 min and found that the reading remained highly consistent after an initial adaptation period (Figure 2F). To validate the luminal pH measurements with an independent method, we used a pH-sensitive colorimetric dye (methyl red) that we injected into the organoid lumen using a



micromanipulator-mounted nanoliter autoinjector (Figure 2G). The yellow coloring of the dye confirmed that the organoid lumen had a pH  $>6.2$ , consistent with the microelectrode measurements that showed a near-neutral pH. Overall, these representative results illustrate the feasibility and reproducibility of microelectrode-based pH measurements in organoid cultures.

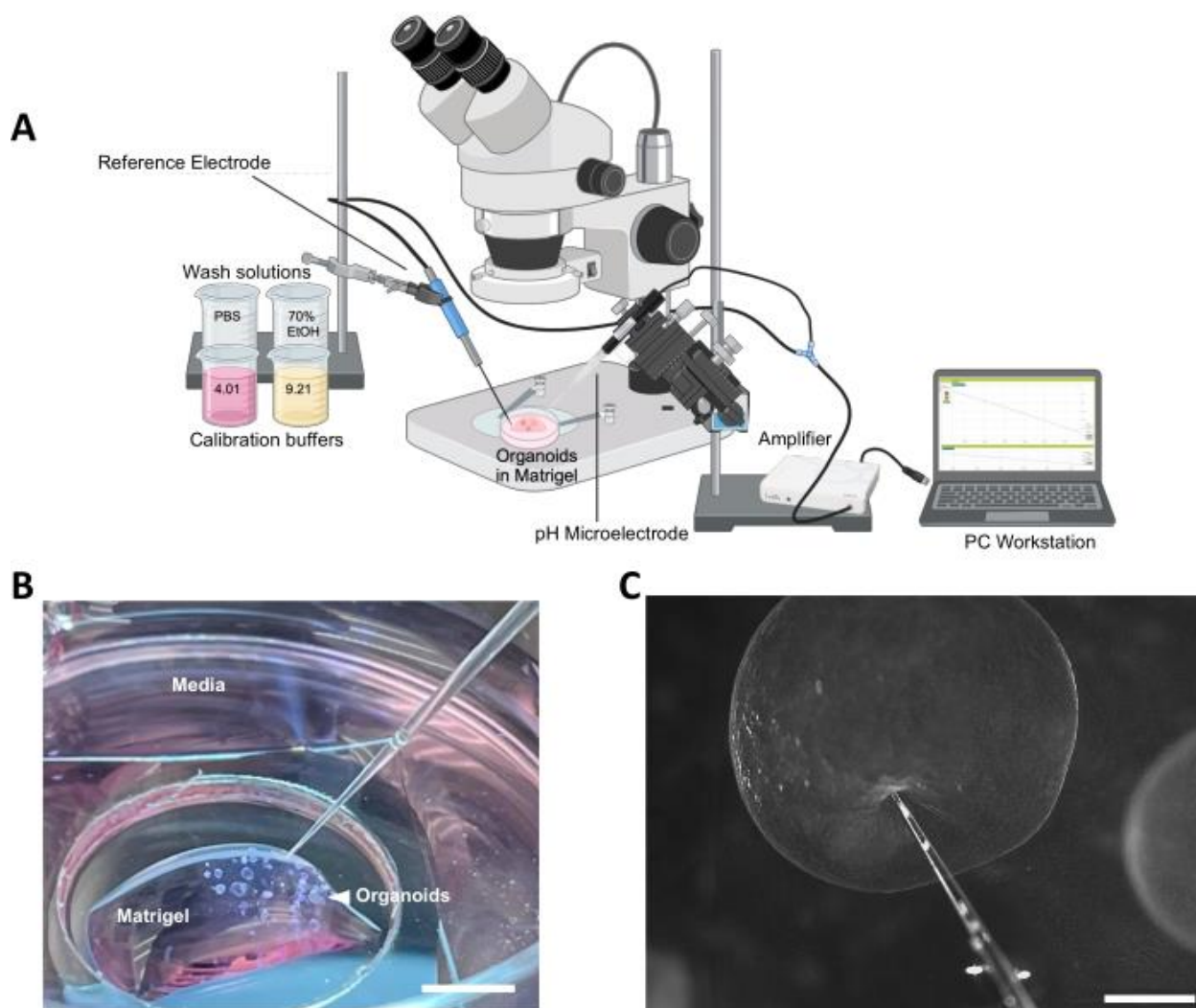


Figure 2.1. Overview of the pH microprofiling method. (A) Schematic diagram of profiling setup. The microelectrode in Figure 1A was taken from the Unisense website<sup>35</sup>. (B) Representative image of organoid culture ready for profiling, surrounding ECM, and surrounding media (scale bar = 5 mm). (C) Example of correct microelectrode positioning in preparation for organoid probing (scale bar = 500  $\mu\text{m}$ ). Abbreviation: ECM = extracellular matrix.

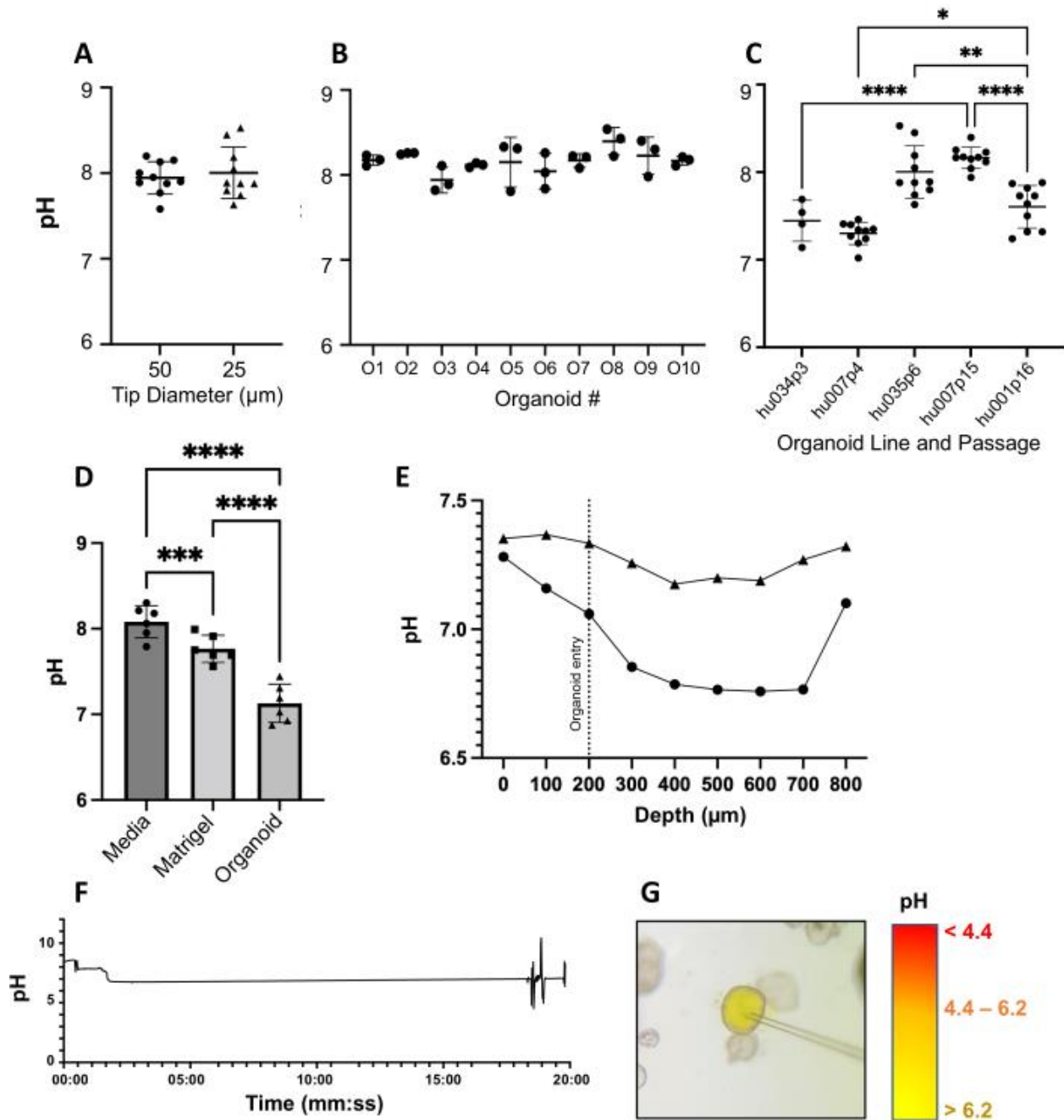


Figure 2.2. Validation of microsensor profiling in human gastric organoids. (A) Comparison of mid-lumen pH measurements using 25  $\mu\text{m}$  (pH-25) and 50  $\mu\text{m}$  (pH-50) microelectrode tips. Data from 10 individual organoids, each from a single representative experiment. (B) Three replicate pH measurements were obtained for 10 individual organoids. One-way ANOVA with multiple comparisons ( $p = 0.1229$ ). (C) pH measurements obtained with a pH-25 electrode are consistent within each of five organoid lines analyzed at different passage numbers; 4-10 organoids measured per line based on size and availability. One-way ANOVA with multiple comparisons ( $p$

< 0.0001). (D) pH measurements within gastric organoids and the surrounding Matrigel and media (n = 6 independent experiments). Measurements obtained by penetrating gastric epithelial organoids with a pH-25. Each data point is the mean of 10 individual pH measurements within a single organoid. One-way ANOVA (p < 0.0001). (E) Epithelial-to-lumen pH profiles of two representative organoids using a motorized micromanipulator. (F) Stability of pH over time (~19.8 min) in one representative organoid. (G) Microinjection of methyl red pH indicator dye and HCl into the gastric organoid lumen.

## Discussion

Limited access to the luminal space of organoids has severely restricted our understanding of the physiological dynamics of this microenvironment. A reliable tool for functional analyses of luminal physiology will expand our ability to leverage organoids as *in vitro* models for physiology, pharmacology, and disease research. Organoids are highly tunable, physiologically relevant models with the added potential to replicate genetic variability within the human population. Existing methods for pH measurement inside the organoid lumen have used pH-sensitive dyes or nanoparticles, methods that often must be coupled with fluorescence microscopy or spectroscopy<sup>15-17</sup>. The described microsensor-based profiling method provides a new route for measuring the intraluminal pH of gastrointestinal organoids with new spatial precision. Our method demonstrates consistent and reliable measurement of gastrointestinal organoid luminal pH, as well as evidence of a pH gradient. In unpublished experiments, we confirmed the expression of *SLC* family genes *SLC4A2* and *26A7*, which are known to be responsible for bicarbonate secretion as well as *SLC9A3*, *9A4*, and *9A8* that are responsible for proton exchange (Supplemental Figure S1)<sup>36-39</sup>. Our studies suggest a predominance of bicarbonate secretion and a lack of parietal cells in our organoids, which may explain the alkalinity.

It is important to ensure that the microelectrodes used are well-suited for organoid microprofiling - this includes selecting the correct tip diameter. We tried both 25  $\mu\text{m}$  and 50  $\mu\text{m}$  tips and obtained similar results (Figure 2A) but decided to move forward with the smaller tip size per the manufacturer's advice since it was expected to be less invasive and provide a higher spatial resolution, as measurements are averaged across the beveled tip area. As a downside, however, smaller tips are more fragile. Organoid size must be considered in determining the desired spatial resolution.

A critical step in the protocol was ensuring the ability to distinguish between the organoid intraluminal pH from the pH in the ECM, and subsequently, in the surrounding culture medium. One would expect a reasonable amount of metabolite flux into and out of the organoids<sup>40</sup>. We expect an organoid's pH to be influenced by its environment and found that the organoids were consistently less alkaline than their surroundings in six independent experiments (Figure 2D). In addition, stability is just as important in profiling as it is during sensor calibration.

Tissue-derived organoids are expected to exhibit a certain degree of donor-to-donor variability, so it is essential to profile any organoid line at baseline before applying any experimental interventions such as drug treatment<sup>41</sup>. We hypothesize that fluctuations in pH within any one organoid culture may be due to local ion gradients at the microscale and the heterogeneous distribution of luminal mucus as determined by immunofluorescence and immunohistochemical staining (Chapter 4). The observed variations in pH between individual organoid lines and passages may be due to individual differences in cell composition and secretory activity of the organoids. We also found that some organoid lines were inherently more difficult to penetrate than others. Similarly, some may lose their structural integrity and collapse

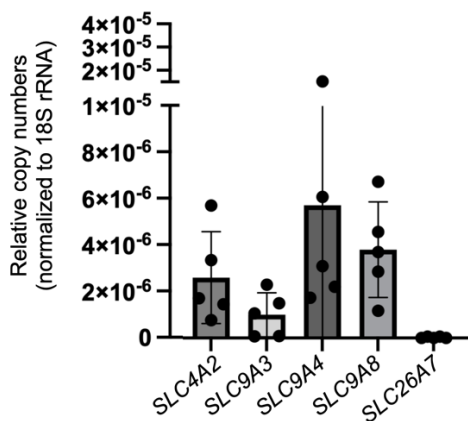
upon electrode entry (Supplemental Figure S2 and Supplemental Video S1). This does not seem to be associated with organoid passage but has been observed most commonly in organoids over ~1.5 mm in diameter. In a previous study, we showed that the mucus inside the organoids was heterogeneously distributed<sup>29</sup>. Because of this heterogeneity, it becomes difficult to determine whether (or the extent to which) mucus distribution has impacted a measurement.

Microsensors are minimally invasive tools that can profile organoid intraluminal physiology with high speed and high spatial resolution. Such sensors also do not disturb chemical gradients and are minimally sensitive to turbulence in the microenvironment of interest. The small design is made possible by separating the sensor electrode from the reference electrode-standard laboratory pH probes combine these two electrodes, leading to a larger size. Optical pH and O<sub>2</sub> nanosensors for intracellular measurements have been developed by the Cash group at the Colorado School of Mines and have been successful in measuring metabolites in both mouse and biofilm models. Because of the heterogeneity in the organoid lumen, however, such sensors may lead to uninterpretable results<sup>17</sup>. McCracken *et al.* analyzed luminal pH in embryonic stem cell-derived gastric organoids by injecting SNARF-5F and visualizing the pH-sensitive dye with real-time confocal microscopy<sup>15</sup>. Notably, measurements reported by McCracken were highly similar to the pH values obtained in our current study (Figure 2B,C). Our technique could perhaps be applied in a monolayer architecture, with more of a vertical setup as in biofilm profiling, though this may pose a risk of damaging the electrodes (44). Future studies also could involve sequential measurements of pH over multiple days to assess changes associated with cell development. Since medium-sized organoids generally recover and heal after probing, one organoid could theoretically be probed multiple times as long as the sterility of the

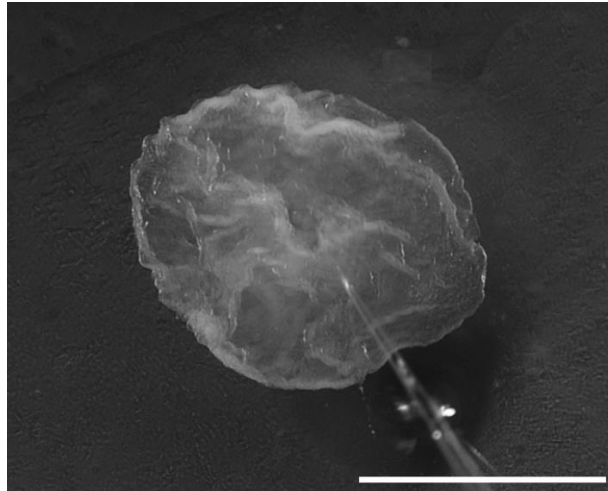
cultures can be maintained. As we refine our understanding of pH dynamics in organoid models, spatial resolution must be a priority for the precise mapping of the complex and historically inaccessible 3D microenvironment within.

In summary, this protocol provides a detailed method for accurate measurements of pH with high spatiotemporal resolution using pH microelectrodes mounted on a micromanipulator and a stereomicroscope. This method was validated with human adult stem cell-derived organoids and is suitable for epithelial organoids of at least 200  $\mu\text{m}$  in diameter that have a distinct lumen. We anticipate that by selecting alternative microelectrodes, this method can be easily adapted to other types of organoids and the measurement of alternative compounds, such as NO or O<sub>2</sub>.

#### Supplementary Material



Supplemental Figure S2.1. Ion transporter expression in human gastric organoids. Relative copy numbers normalized to 18S rRNA.



Supplemental Figure S2.2. Human gastric organoid with deformed architecture following puncture with the pH microsensor probe. Scale bar = 1 mm.

Supplemental Video SV2.1. Unsuccessful profiling attempt in a gastric organoid culture.

The video can be downloaded using the following link:

[https://www.jove.com/files/ftp\\_upload/66900/240229%20Supplemental%20Video%201.zip](https://www.jove.com/files/ftp_upload/66900/240229%20Supplemental%20Video%201.zip)

Supplemental Table S2.1. Table of Materials.

Name	Company	Catalog Number	Comments
3 M KCl	Unisense		
5 mL Wobble-not Serological Pipet, Individually Wrapped, Paper/Plastic, Bag, Sterile	CellTreat	229091B	
10 mL Wobble-not Serological Pipet, Individually Wrapped, Paper/Plastic, Bag, Sterile	CellTreat	229092B	
15 mL Centrifuge Tube - Foam Rack, Sterile	CellTreat	229412	
24 Well Tissue Culture Plate, Sterile	CellTreat	229124	
25 mL Wobble-not Serological Pipet, Individually Wrapped, Paper/Plastic, Bag, Sterile	CellTreat	229093B	
35 mm Dish   No. 1.5 Coverslip   20 mm Glass Diameter   Uncoated	MatTek	P35G-1.5-20-C	

Supplemental Table S2.1 Continued.

Name	Company	Catalog Number	Comments
50 mL Centrifuge Tube - Foam Rack, Sterile	CellTreat	229422	
70% Ethanol	BP82031GAL	BP82031GAL	
70 µm Cell Strainer, Individually Wrapped, Sterile	CellTreat	229483	
1,000 µL Extended Length Low Retention Pipette Tips, Racked, Sterile	CellTreat	229037	
Amphotericin B (Fungizone) Solution	HyClone Laboratories, Inc.	SV30078.01	
Biosafety Cabinet	Nuaire	NU-425-600	Class II Type A/B3
Bovine Serum Albumin	Fisher Bioreagents	BP1605-100	
Cell recovery solution	Corning	354253	Cell dissociation solution
DMEM/F-12 (Advanced DMEM)	Gibco	12-491-015	
Dulbecco's Modification of Eagles Medium (DMEM)	Fisher Scientific	15017CV	
Fetal Bovine Serum	HyClone Laboratories, Inc.	SH30088	
G418 Sulfate	Corning	30-234-CR	
Gentamycin sulfate	IBI Scientific	IB02030	
HEPES, Free Acid	Cytiva	SH30237.01	
HP Pavillion 2-in-1 14" Laptop Intel Core i3	HP	M03840-001	
Hydrochloric acid	Fisher Scientific	A144C-212	
Incubator	Fisher Scientific	11676604	
iPhone 12 camera	Apple		
L-glutamine	Cytiva	SH3003401	
Large Kimberly-Clark Professional Kimtech Science Kimwipes Delicate Task Wipers, 1-Ply	Fisher Scientific	34133	



Supplementary Table S2.1 Continued.

Name	Company	Catalog Number	Comments
M 205 FA Stereomicroscope	Leica		
Matrigel Membrane Matrix 354234	Corning	CB-40234	
MC-1 UniMotor Controller	Unisense		
Methyl red			
MM33 Micromanipulator	Marzhauser Wetzlar	61-42-113-0000	Right handed
MS-15 Motorized Stage	Unisense		
Nanoject-II	Drummond	3-000-204	Nanoliter autoinjector
Penicillin/Streptomycin (10,000 U/ mL)	Gibco	15-140-148	
pH Microelectrodes	Unisense	50-109158, 25-203452, 25-205272, 25-111626, 25-109160	SensorTrace software is not compatible with Apple computers
Reference Electrode	Unisense	REF-RM-001652	SensorTrace software is not compatible with Apple computers
SB 431542	Tocris Bioscience	16-141-0	
Smartphone Camera Adapter	Gosky		
Specifications Laboratory Stand LS	Unisense	LS-009238	
Trypsin-EDTA 0.025%, phenol red	Gibco	25-200-056	
UniAmp	Unisense	11632	
United Biosystems Inc MINI CELL SCRAPERS 200/PK	Fisher	MCS-200	
Y-27632 dihydrochloride	Tocris Bioscience	12-541-0	
μSensor Calibration Kit	Unisense/Mettler Toledo	51-305-070, 51-302-069	pH 4.01 and 9.21, 20 mL packets

### Acknowledgements

The authors would like to acknowledge Dr. Ellen Lauchnor, Dr. Phil Stewart, and Bengisu Kilic for their previous work and assistance with the O<sub>2</sub> microsensors; Andy Sebrell for training in organoid culture and micromanipulation; Lexi Burcham for assistance in organoid culture, media preparation, data recording, and organization; and Dr. Susy Kohout for general advice in electrophysiology. We would like to thank Dr. Heidi Smith for her assistance with imaging and acknowledge the Center for Biofilm Engineering Bioimaging Facility at Montana State University, which is supported by funding from the National Science Foundation MRI Program (2018562), the M.J. Murdock Charitable Trust (202016116), the US Department of Defense (77369LSRIP & W911NF1910288), and by the Montana Nanotechnology Facility (an NNCI member supported by NSF Grant ECCS-2025391).

Special thanks to the entire Unisense team who made this work possible, especially Dr. Andrew Cerskus, Dr. Laura Woods, Dr. Lars Larsen, Dr. Tage Dalsgaard, Dr. Line Daugaard, Dr. Karen Maegaard, and Mette Gammelgaard. Funding for our study was provided by the National Institutes of Health grants R01 GM13140801 (D.B., R.B.) and UL1 TR002319 (K.N.L), and a Research Expansion Award from the Montana State University Office for Research and Economic Development (D.B.). Figure 1A was created with BioRender.

### References Cited

- 1     Zhang, N. *et al.* Tissue Spatial Omics Dissects Organoid Biomimicry. *GEN Biotechnology* **2**, 372-383 (2023). <https://doi.org/10.1089/genbio.2023.0039>
  
- 2     Sato, T. *et al.* Single Lgr5 stem cells build crypt-villus structures in vitro without a mesenchymal niche. *Nature* (2009). <https://doi.org/10.1038/nature07935>
  
- 3     Lancaster, M. A. & Knoblich, J. A. Organogenesis in a dish: modeling development and disease using organoid technologies. *Science* **345**, 1247125 (2014). <https://doi.org/10.1126/science.1247125>
  
- 4     Dutta, D., Heo, I. & Clevers, H. Disease Modeling in Stem Cell-Derived 3D Organoid Systems. *Trends Mol Med* **23**, 393-410 (2017). <https://doi.org/10.1016/j.molmed.2017.02.007>
  
- 5     Achberger, K. *et al.* Merging organoid and organ-on-a-chip technology to generate complex multi-layer tissue models in a human retina-on-a-chip platform. *Elife* **8** (2019). <https://doi.org/10.7554/eLife.46188>
  
- 6     Bartfeld, S. *et al.* In vitro expansion of human gastric epithelial stem cells and their responses to bacterial infection. *Gastroenterology* (2015). <https://doi.org/10.1053/j.gastro.2014.09.042>
  
- 7     Fatehullah, A., Tan, S. H. & Barker, N. Organoids as an in vitro model of human development and disease. *Nat Cell Biol* **18**, 246-254 (2016). <https://doi.org/10.1038/ncb3312>
  
- 8     Clevers, H. Modeling Development and Disease with Organoids. *Cell* **165**, 1586-1597 (2016). <https://doi.org/10.1016/j.cell.2016.05.082>
  
- 9     Davies, J. A. in *Organoids and Mini-Organs* (eds Jamie A. Davies & Melanie L. Lawrence) 3-23 (Academic Press, 2018).
  
- 10    Ambrosini, Y. M. *et al.* Recapitulation of the accessible interface of biopsy-derived canine intestinal organoids to study epithelial-luminal interactions. *PLoS One* **15**, e0231423 (2020). <https://doi.org/10.1371/journal.pone.0231423>

- 11 Williams, S. E. & Turnberg, L. A. Demonstration of a pH gradient across mucus adherent to rabbit gastric mucosa: evidence for a 'mucus-bicarbonate' barrier. *Gut* **22**, 94-96 (1981). <https://doi.org/10.1136/gut.22.2.94>
- 12 Schubert, M. L. Gastric secretion. *Curr Opin Gastroenterol* **20**, 519-525 (2004). <https://doi.org/10.1097/00001574-200411000-00003>
- 13 Celli, J. P. *et al.* Rheology of Gastric Mucin Exhibits a pH-Dependent Sol–Gel Transition. *Biomacromolecules* **8**, 1580-1586 (2007). <https://doi.org/10.1021/bm0609691>
- 14 Takeshita, Y. *et al.* Assessment of pH dependent errors in spectrophotometric pH measurements of seawater. *Marine Chemistry* **223**, 103801 (2020). <https://doi.org/https://doi.org/10.1016/j.marchem.2020.103801>
- 15 McCracken, K. W. *et al.* Wnt/ $\beta$ -catenin promotes gastric fundus specification in mice and humans. *Nature* (2017). <https://doi.org/10.1038/nature21021>
- 16 Larsen, M., Borisov, S. M., Grunwald, B., Klimant, I. & Glud, R. N. A simple and inexpensive high resolution color ratiometric planar optode imaging approach: application to oxygen and pH sensing. *Limnology and Oceanography: Methods* **9**, 348-360 (2011). <https://doi.org/https://doi.org/10.4319/lom.2011.9.348>
- 17 Jewell, M. P., Galyean, A. A., Kirk Harris, J., Zemanick, E. T. & Cash, K. J. Luminescent Nanosensors for Ratiometric Monitoring of Three-Dimensional Oxygen Gradients in Laboratory and Clinical *Pseudomonas aeruginosa* Biofilms. *Appl Environ Microbiol* **85** (2019). <https://doi.org/10.1128/aem.01116-19>
- 18 Brooks, E. L., Hussain, K. K., Kotecha, K., Abdalla, A. & Patel, B. A. Three-Dimensional-Printed Electrochemical Multiwell Plates for Monitoring Food Intolerance from Intestinal Organoids. *ACS Sens* **8**, 712-720 (2023). <https://doi.org/10.1021/acssensors.2c02245>
- 19 Unisense. *pH and reference electrode manual*, <<https://unisense.com/wp-content/uploads/2023/05/2023.05-pH-and-ref-sensor-manual.pdf>> (2023).
- 20 Villahermosa, D., Corzo, A., Garcia-Robledo, E., González, J. M. & Papaspyrou, S. Kinetics of Indigenous Nitrate Reducing Sulfide Oxidizing Activity in Microaerophilic

- Wastewater Biofilms. *PLoS One* **11**, e0149096 (2016).  
<https://doi.org/10.1371/journal.pone.0149096>
- 21 Pabst, B., Pitts, B., Lauchnor, E. & Stewart, P. S. Gel-Entrapped *Staphylococcus aureus* Bacteria as Models of Biofilm Infection Exhibit Growth in Dense Aggregates, Oxygen Limitation, Antibiotic Tolerance, and Heterogeneous Gene Expression. *Antimicrob Agents Chemother* **60**, 6294-6301 (2016). <https://doi.org/10.1128/aac.01336-16>
  - 22 Ploug, H., Stolte, W., Epping, E. H. G. & Jørgensen, B. B. Diffusive boundary layers, photosynthesis, and respiration of the colony-forming plankton algae, *Phaeocystis* sp. *Limnology and Oceanography* **44**, 1949-1958 (1999).  
<https://doi.org/https://doi.org/10.4319/lo.1999.44.8.1949>
  - 23 Kolpen, M. *et al.* Nitrous oxide production in sputum from cystic fibrosis patients with chronic *Pseudomonas aeruginosa* lung infection. *PLoS One* **9**, e84353 (2014).  
<https://doi.org/10.1371/journal.pone.0084353>
  - 24 Murphy, K. C. *et al.* Measurement of oxygen tension within mesenchymal stem cell spheroids. *Journal of The Royal Society Interface* **14**, 20160851 (2017).  
<https://doi.org/10.1098/rsif.2016.0851>
  - 25 Sebrell, T. A. *et al.* A Novel Gastric Spheroid Co-culture Model Reveals Chemokine-Dependent Recruitment of Human Dendritic Cells to the Gastric Epithelium. *Cellular and Molecular Gastroenterology and Hepatology* **8**, 157-171.e153 (2019).  
<https://doi.org/10.1016/j.jcmgh.2019.02.010>
  - 26 Miyoshi, H. & Stappenbeck, T. S. In vitro expansion and genetic modification of gastrointestinal stem cells in spheroid culture. *Nature Protocols* (2013).  
<https://doi.org/10.1038/nprot.2013.153>
  - 27 Takase, Y., Fujishima, K. & Takahashi, T. The 3D Culturing of Organoids from Murine Intestinal Crypts and a Single Stem Cell for Organoid Research. *J Vis Exp* (2023).  
<https://doi.org/10.3791/65219>
  - 28 Cherne, M. D. *et al.* A Synthetic Hydrogel, VitroGel® ORGANOID-3, Improves Immune Cell-Epithelial Interactions in a Tissue Chip Co-Culture Model of Human Gastric Organoids and Dendritic Cells. *Frontiers in Pharmacology* **12** (2021).  
<https://doi.org/10.3389/fphar.2021.707891>

- 29 Sebrell, T. A. *et al.* Live imaging analysis of human gastric epithelial spheroids reveals spontaneous rupture, rotation and fusion events. *Cell and Tissue Research* **371**, 293-307 (2018). <https://doi.org/10.1007/s00441-017-2726-5>
- 30 Unisense. *Sensortrace suite user manual*, <<https://unisense.com/wp-content/uploads/2021/10/SensorTrace-Suite-Manual.pdf>> (2023).
- 31 Unisense. *Microprofiling system user manual*, <<https://unisense.com/wp-content/uploads/2021/09/2023.11-MicroProfiling-System-2.pdf>> (2023).
- 32 Wolffling, S. *et al.* EGF and BMPs Govern Differentiation and Patterning in Human Gastric Glands. *Gastroenterology* **161**, 623-636 e616 (2021). <https://doi.org/10.1053/j.gastro.2021.04.062>
- 33 Boccellato, F. *et al.* Polarised epithelial monolayers of the gastric mucosa reveal insights into mucosal homeostasis and defence against infection. *Gut* **68**, 400-413 (2019). <https://doi.org/10.1136/gutjnl-2017-314540>
- 34 McCracken, K. W. *et al.* Modelling human development and disease in pluripotent stem-cell-derived gastric organoids. *Nature* (2014). <https://doi.org/10.1038/nature13863>
- 35 Unisense. <<https://unisense.com/products/ph-microelectrode/>> (2024).
- 36 Schreiber, S. *et al.* In situ measurement of pH in the secreting canaliculus of the gastric parietal cell and adjacent structures. *Cell and Tissue Research* **329**, 313-320 (2007). <https://doi.org/10.1007/s00441-007-0427-1>
- 37 Xu, H., Li, J., Chen, H., Wang, C. & Ghishan, F. K. NHE8 plays important roles in gastric mucosal protection. *Am J Physiol Gastrointest Liver Physiol* **304**, G257-261 (2013). <https://doi.org/10.1152/ajpgi.00433.2012>
- 38 Gawenis, L. R. *et al.* Impaired gastric acid secretion in mice with a targeted disruption of the NHE4 Na<sup>+</sup>/H<sup>+</sup> exchanger. *J Biol Chem* **280**, 12781-12789 (2005). <https://doi.org/10.1074/jbc.M414118200>

- 39 Lewis, O. L., Keener, J. P. & Fogelson, A. L. A physics-based model for maintenance of the pH gradient in the gastric mucus layer. *Am J Physiol Gastrointest Liver Physiol* **313**, G599-G612 (2017). <https://doi.org/10.1152/ajpgi.00221.2017>
- 40 Okkelman, I. A., Neto, N., Papkovsky, D. B., Monaghan, M. G. & Dmitriev, R. I. A deeper understanding of intestinal organoid metabolism revealed by combining fluorescence lifetime imaging microscopy (FLIM) and extracellular flux analyses. *Redox Biol* **30**, 101420 (2020). <https://doi.org/10.1016/j.redox.2019.101420>
- 41 Pleguezuelos-Manzano, C. *et al.* Establishment and Culture of Human Intestinal Organoids Derived from Adult Stem Cells. *Curr Protoc Immunol* **130**, e106 (2020). <https://doi.org/10.1002/cpim.106>

CHAPTER THREE

MICRORHEOLOGICAL CHARACTERIZATION OF LUMINAL  
MUCUS IN THREE-DIMENSIONAL HUMAN GASTRIC  
ORGANOIDS

Contribution of Authors and Co-Authors

Manuscript in Chapter 3

Author: Barkan Sidar (joint first-authorship)

Contributions: Designed and performed experiments, analyzed and interpreted data

Author: Katrina Lyon (joint first-authorship)

Contributions: Designed and performed experiments, analyzed and interpreted data, wrote and revised the manuscript

Co-Author: Cameron Dudiak

Contributions: Analyzed and interpreted data

Co-Author: Wentian Liao

Contributions: Methodology development and data analysis

Co-Author: Chloe Strupulis

Contributions: Analyzed and interpreted data

Co-Author: Diane Bimczok

Contributions: Analyzed and interpreted data, designed experiments, revised the manuscript, provided funding for the project

Co-Author: James Wilking



Contributions: Developed the project and designed experiments, interpreted data, provided funding for the project, wrote and revised the manuscript

Co-Author: Rama Bansil

Contributions: Developed the project and designed experiments, interpreted data, provided funding for the project, wrote and revised the manuscript

Manuscript Information

Barkan Sidar, **Katrina Lyon**, Cameron Dudiak, Wentian Liao, Chloe Strupulis, Diane Bimeczok, James Wilking, Rama Bansil

Status of Manuscript:

- ☒ Prepared for submission to a peer-reviewed journal
- ☐ Officially submitted to a peer-reviewed journal
- ☐ Accepted by a peer-reviewed journal
- ☐ Published in a peer-reviewed journal

### Abstract

The mucus layer that lines the human stomach is a critical barrier that protects the underlying epithelium from gastric acid and harmful pathogens such as *Helicobacter pylori*. The efficacy of this barrier relies on the structural integrity of the mucus, which is the product of various biochemically and biophysically important features. Human gastric organoids—3D cellular models that resemble the stomach—contain mucus and have been used to investigate gastric disease. Due to the topologically closed structure of an organoid and subsequently difficult-to-access mucus, it remains unclear how the mechanical properties of the luminal mucus contribute to its functionality. Here we used mucin staining and particle-tracking microrheology with 0.5  $\mu\text{m}$  and 1  $\mu\text{m}$  polystyrene particles to characterize the material inside of the organoids. Human gastric organoids showed luminal accumulation of acidic mucin. Live confocal imaging and particle tracking analysis revealed structural heterogeneity of the luminal mucus via two discernible categories of diffusive behavior (i.e., the Brownian motion of particles). The diffusive behavior of the trapped particles suggested elastic gel behavior of the mucus network within the organoid lumen. Taken together, our findings provide new, mechanical insight into the three-dimensional luminal microenvironment within human gastric organoids, and will inform future investigations into the functional relevance of organoid mucus to *in vivo* mucus barriers.

### Introduction

Organoids have significantly improved our ability to study tissue development and disease progression *in vitro* and provide a viable alternative to animal models for pre-clinical drug testing<sup>1-3</sup>. Gastrointestinal organoids are widely used to represent the stomach, small

intestine, and colon in studies of gut health and disease<sup>3-6</sup>. Notably, such organoids are known to produce the protective mucus that lines the gastrointestinal tract<sup>7-9</sup>. Mucus is a viscoelastic material that plays an important role as the body's first barrier from the outside world<sup>10</sup>.

Human gastric organoids (HGOs) generally consist of the apical epithelium facing inwards—naturally separated from the external environment<sup>7,11</sup>. This topologically closed structure of HGOs makes the lumen challenging to analyze. Evaluating the suitability of HGO models for recreating *in vivo* gastric conditions, such as the protective mucus barrier, requires thorough characterization of their luminal composition. The properties and spatial complexity of the lumen are critical for accurately modeling the *in vivo* gastric environment, yet these details are often overlooked, particularly in studies involving the injection of bacteria or fluorescent sensors. Disregard for the spatial arrangement and mechanical behavior of luminal contents can leave room for confounding variables, leading to critical misrepresentations of the organoid internal microenvironment. While fixing and sectioning organoids can reveal a cross-section of the lumen, this process disrupts the natural state and spatial distribution of luminal contents<sup>12</sup>. In contrast, studying intact organoids provides the most comprehensive reflection of their true spatial complexity while minimizes experimental artefacts<sup>13</sup>. We and others have used micromanipulator-controlled microinjection to access the lumen of viable gastric organoids for delivering bacteria or fluorescent tracers<sup>5,9,12,14,15</sup>. Additionally, we have used microelectrodes to measure intraluminal oxygen content<sup>5</sup> and pH<sup>16</sup>. This nondestructive technique is powerful and has enabled real-time observations to be made, including that the organoid lumen maintains microaerophilic conditions and a near-neutral pH. In this study, fluorescent particles were

microinjected into gastric organoids for particle tracking microrheology analysis, enabling the rheological characterization of the mucus within the organoids.

Previous work using microparticle tracking and oscillatory shear rheology have established the micro- and bulk rheological properties of mucus isolated from the stomach and other organs, as well as of several purified mucins from the lung, salivary, gastric, and reproductive systems<sup>17-20</sup>. These studies concluded that mucins and mucus exhibit both viscous and elastic properties, with certain types having the ability to form elastic gels at low pH<sup>21</sup>. Many soft materials exhibit a viscoelastic response to applied shear forces that depends on how liquid-like (viscous) or solid-like (elastic) the material behaves<sup>22</sup>. More specifically, viscosity refers to the ability of a material to dissipate energy and resist flow, and elasticity refers to the ability of a material to store energy and return to its original shape following deformation<sup>23,24</sup>. The extent of each can depend upon the various forces acting on the material. Understanding the rheological behavior of gastric mucus may have physiological relevance to questions such as the response of mucus to shear forces associated with digestion<sup>25</sup> and the transport of food and microorganisms across the mucus barrier<sup>26</sup>.

Previously, we had reported the presence of an optically dense substance in gastric organoids, identified using backscatter light imaging<sup>7</sup>. Based on its increased scattering properties, this substance was classified broadly as luminal material—only hypothesized to be mucus or cell debris as its identity had yet to be confirmed. Organoids have been valuable models for studying infection dynamics and host-pathogen interactions at the apical epithelium, which faces inside the lumen. Explorations of the organoid lumen, particularly in terms of its contents and mechanical properties, have been severely lacking due to challenges posed by its

topologically closed structure, which restricts access for direct analysis. In this manuscript, gastric organoid luminal mucus is characterized followed by real-time visualization of microinjected fluorescent particles into the lumen for particle tracking microrheology. Combined results determined the rheological properties of the mucus inside the organoids. We characterize the mucin content of the organoid lumen and investigate the microrheology of this mucus by performing *in situ* microscopic tracking of micron-sized colloidal particles at various locations within the organoids over time<sup>27</sup>. We employ analytical methods to interrogate the thermally-driven, Brownian motion of the injected particles to extract information about the mechanical properties of the luminal material<sup>28</sup>. We confirm that the mucus secreted by the organoids is viscoelastic, and that the viscoelasticity varies both spatially and temporally, suggesting that gastric organoids can serve as a physiologically relevant model system for investigating the influence of other factors on mucus structure and dynamics<sup>17,24,29,30</sup>.

### Results & Discussion

To confirm the composition of the luminal material, we used the well-known method of histological carbohydrate staining paired with brightfield microscopy. Alcian blue staining indicates the presence of acidic mucin glycoproteins in both the surface epithelia of native gastric tissue and the organoid luminal space, as shown by the microscopy images in Fig. 1<sup>31</sup>. The areas positive for Alcian blue are consistent with the observed distribution of mucin in the gastric mucosa<sup>32</sup>. In another study (Chapter 4), we later used immunohistochemical staining with antibodies against MUC5AC and MUC6, the predominant gastric mucin proteins *in vivo*, to confirm the presence of MUC5AC on the epithelial surface and in the organoid lumen, and MUC6 in the glandular epithelium of both the native tissue and organoid<sup>33</sup>.

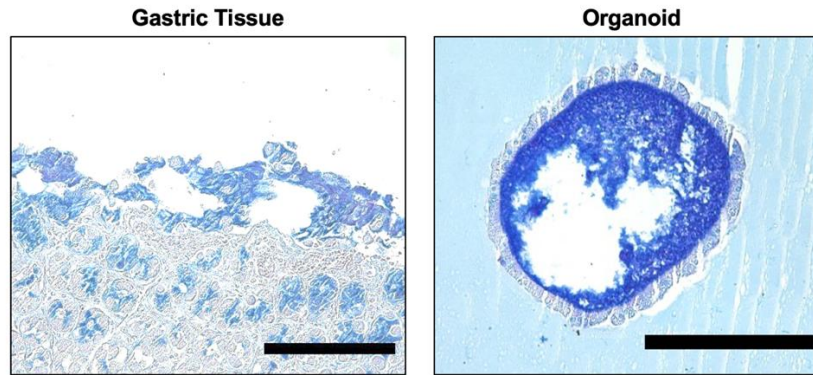


Figure 3.1. Alcian blue staining of identifiable acidic mucins on tissue surface epithelium (left) and in organoid lumen (right). Representative of 3 experiments. Scale bars = 200  $\mu\text{m}$ .

The mechanical properties of gastric mucus, which are essential to its protective function, are known to be pH-dependent<sup>19,21</sup>. Viscoelastic gastric mucin undergoes a transition from a solution at neutral pH to a gel around pH 4<sup>34</sup>. It has also been suggested that the shear-thinning behavior of gastric mucus (such as that which we would observe *in vivo* during digestion) may also be influenced by pH<sup>24,35</sup>. In Chapter 2, to determine the intraluminal pH of the organoids, we injected methyl red into the organoids and observed a rapid color change from red to yellow, indicating a pH > 6.2. We further confirmed these results with more accurate pH measurements using a pH microelectrode, finding that the organoid lumen consistently exhibited a relatively high pH, implying that it lacked acid-secreting cells<sup>16</sup>. This suggests that the mucus within may not behave as a gel that would be strong enough to trap microbes such as *H. pylori*<sup>24</sup>.

In this study we used particle tracking microrheology to probe the viscoelastic properties of the luminal mucus in the gastric organoids. We injected green fluorescently-labeled colloidal polystyrene particles ( $d = 1\ \mu\text{m}$  or  $0.5\ \mu\text{m}$ ) into multiple HGOs ( $n = 10$ ), incubated the organoids for 24 hours, and then imaged the lumen with confocal microscopy. A representative HGO containing these particles is shown in Fig. 2A. We performed two types of time-lapse imaging:

continuous, whole-organoid imaging over three days with images taken every 5 minutes, and intermediate, high-magnification, high frame rate imaging (26 fps for 30 seconds at a fixed z-plane) every 24 hours<sup>7</sup>. Our imaging revealed that the colloidal particles became evenly distributed throughout the organoid lumen, and that HGO integrity was well-maintained (Fig. 2A)– with the exception of occasional rupture events, which have been previously reported<sup>7</sup>. For each high frame-rate series, we used particle tracking image analysis to extract the positional coordinates of individual particles (Fig. 2B) over time and construct individual particle trajectories (Fig. 2C). As the active motion of organoids is limited and slow, particle motion in the organoid lumen is driven primarily by thermal energy<sup>7,36,37</sup>. We found that particle diffusion (or motility) was highly varied within a single HGO–the diffusion of some particles was confined, while that of others was not, as illustrated by the representative trajectories shown in Fig. 2C. This variability indicates that the luminal environment is highly heterogeneous. Similar experiments with smaller colloidal particles ( $d = 0.5 \mu\text{m}$ ) provided further information about the spatial heterogeneity on different length scales.

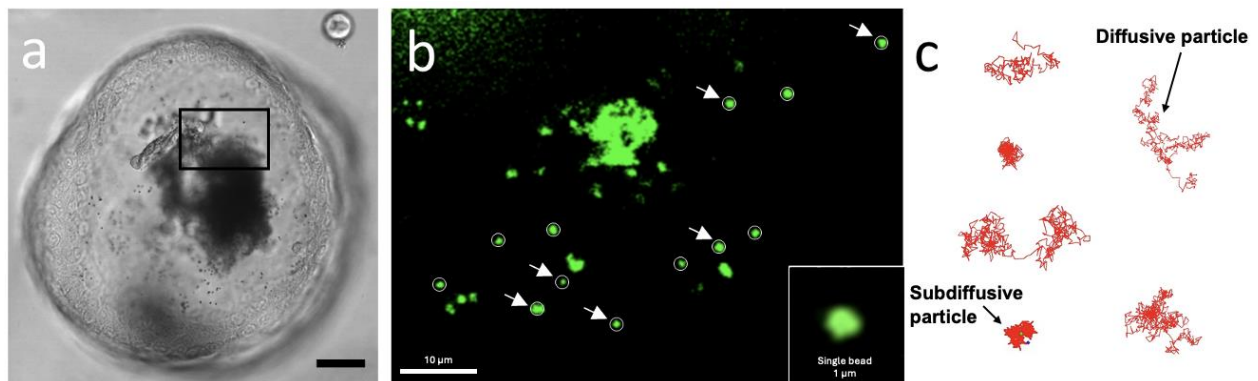


Figure 3.2. Time-lapse microscopy of colloidal probe particles reveals microscale heterogeneities in organoid lumen. (A) Brightfield microscopy image of human gastric organoid containing colloidal microspheres ( $d \approx 1 \mu\text{m}$ ). (B) High magnification fluorescence image of region defined in (A) shows multiple green fluorescent particles. White circles indicate single particles. Inset:



High resolution image of single bead. (C) Individual particle trajectories extracted from 30 second time-lapse videos. Trajectories correspond to particles indicated with arrows in (B).

To quantify particle diffusivity, we calculate the time-dependent mean-squared displacement (MSD),  $\langle \Delta r^2(t) \rangle$  of each particle and then plot these data as a function of time for both 0.5  $\mu\text{m}$  and 1  $\mu\text{m}$  particle experiments (Fig. 3)<sup>27</sup>. For a diffusive particle,  $\langle \Delta r^2(t) \rangle$  should scale as  $t^\alpha$ , with the exponent  $\alpha = 1$  for freely diffusive particles in a viscous liquid, as shown by the data for 1  $\mu\text{m}$  particles diffusing in water (red circles, Fig. 3). Sub-diffusive scaling ( $\alpha < 1$ ) indicates that particle diffusion is confined by the local microenvironment, suggesting more elastic behavior of its surroundings as  $\alpha$  approaches 0. We found that, on average, the larger particles exhibited hindered, more confined diffusion and sampled higher viscosity microenvironments than the smaller particles. To quantify this, we determined the time dependent scaling  $\alpha$  for all particles ( $n = 808$ ) in all HGOs ( $n = 10$ ) and plotted these data as probability distributions  $p(\alpha)$  (bottom, Fig. 3). The resulting distribution is fit well by a log normal distribution, with a mode  $\alpha = 0.13$ , which indicates that most particles within the luminal space were confined in the mucus. By contrast, we also observed a distinct increase in slope that indicates some particles were not trapped by the mucus or had escaped through an opening in the mesh<sup>38</sup>.

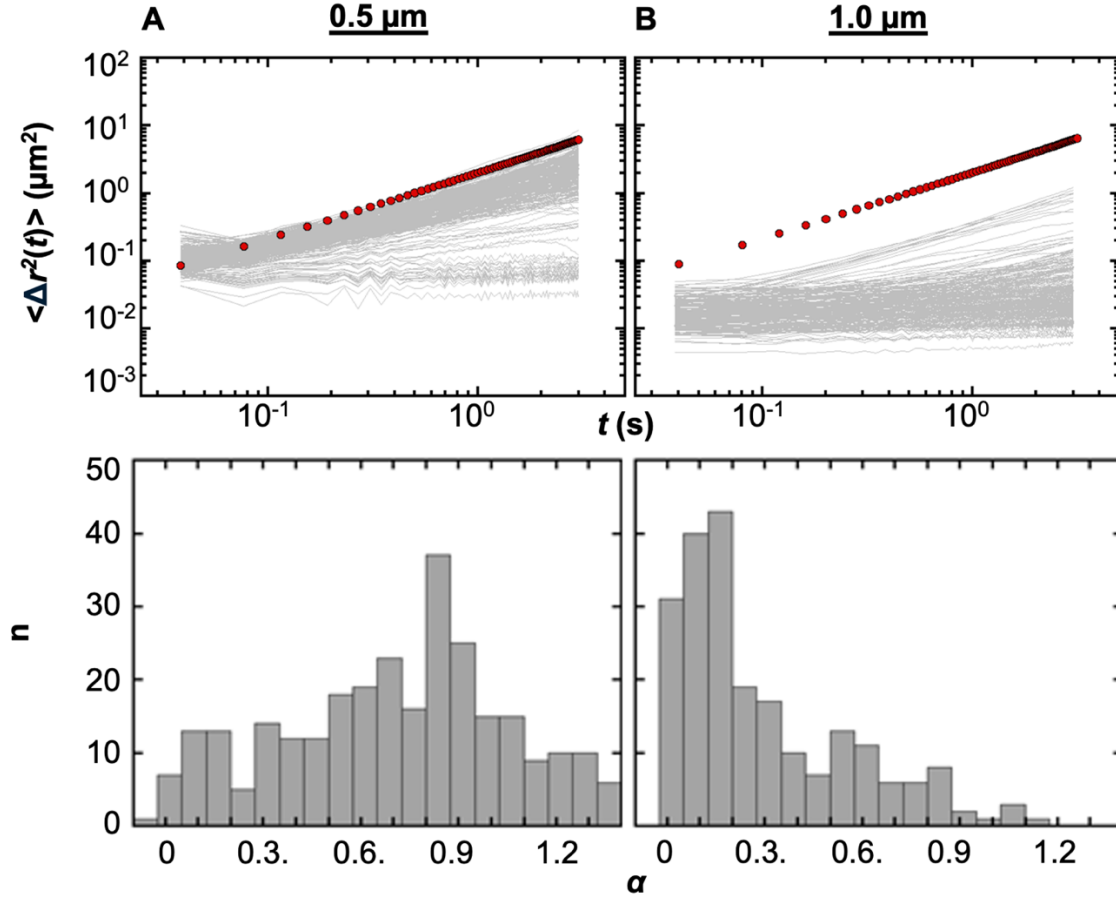


Figure 3.3. Mean-square displacements of colloidal probe particles. Plots of time-dependent mean-squared displacement for individual particles (A)  $d = 1\ \mu\text{m}$ ; (B)  $d = 0.5\ \mu\text{m}$ ). Red circles correspond to average MSD for colloids in water ( $\alpha = 1$ ). Larger particles (A) exhibit more limited diffusion and sample higher viscosity microenvironments than smaller particles (B). Lower panels show distribution of  $\alpha$  for corresponding particle MSDs.

Further, we plotted the viscosity (calculated using the Stokes-Einstein equation) of the mucus as a function of  $\alpha$  to find a negative slope (Fig. 4)<sup>39</sup>. The red symbols represent the smaller  $0.5\ \mu\text{m}$  particles and the black symbols represent the larger  $1\ \mu\text{m}$  particles, with a distinctly broader range of diffusive behavior—beginning with more diffusive at the top left and near complete entrapment as  $\alpha$  nears 0 at the bottom right. We observed that as viscosity is increased, the exponent  $\alpha$  is lower, consistent with the expectation that the particles will

encounter greater hindrance to diffusion in the higher viscosity regions. These results further confirm the spatial heterogeneity of the mucus distributed throughout the organoid lumen. Notably, the larger particles demonstrate this gradient to a greater extent due to their higher likelihood of becoming trapped in the mucus mesh. The smaller  $0.5\ \mu\text{m}$  particles experience mostly free or slightly hindered diffusion in the pores of the viscoelastic polymer whereas the larger  $1\ \mu\text{m}$  particles are mostly trapped in the regions of higher entangled polymers. This suggests that the average size of pores is smaller than  $1\ \mu\text{m}$  but larger than  $0.5\ \mu\text{m}$ .

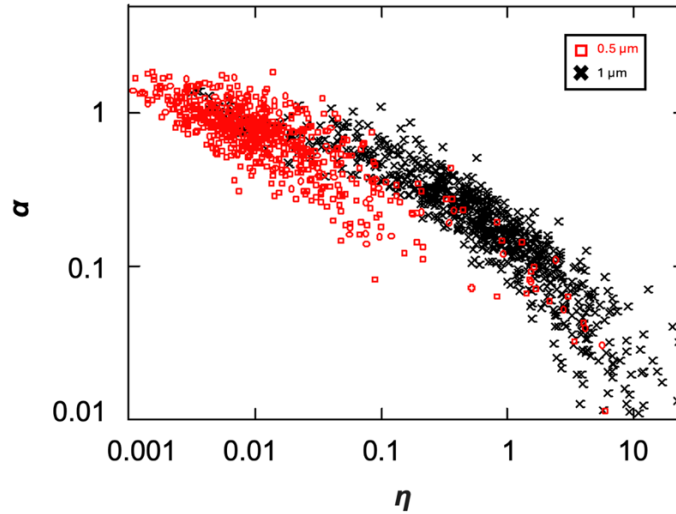


Figure 3.4. Inverse relationship of  $\alpha$  as a function of mucus viscosity. Red symbols represent  $d = 0.5\ \mu\text{m}$  particles, and black symbols represent  $d = 1\ \mu\text{m}$  particles.

Due to the known localization of gastric mucus in the human stomach, one might expect the concentration of mucus to be highest near the epithelium, and lowest near the center of the lumen. However, it is important to consider that such a comparison is limited by the fact that the generally spherical geometry and confinement of an organoid is not a direct reflection of an open tissue section. While we do not know the production rate of mucus as a function of time, one might expect the mucus volume to increase in the luminal space with time. It is more feasible to

quantify mucus production over time using organoid cells in a 2D monolayer culture format, as multiple studies have demonstrated as well as our study in Chapter 4. Taken together, these results indicate that the mucus in the HGOs is highly heterogeneous.

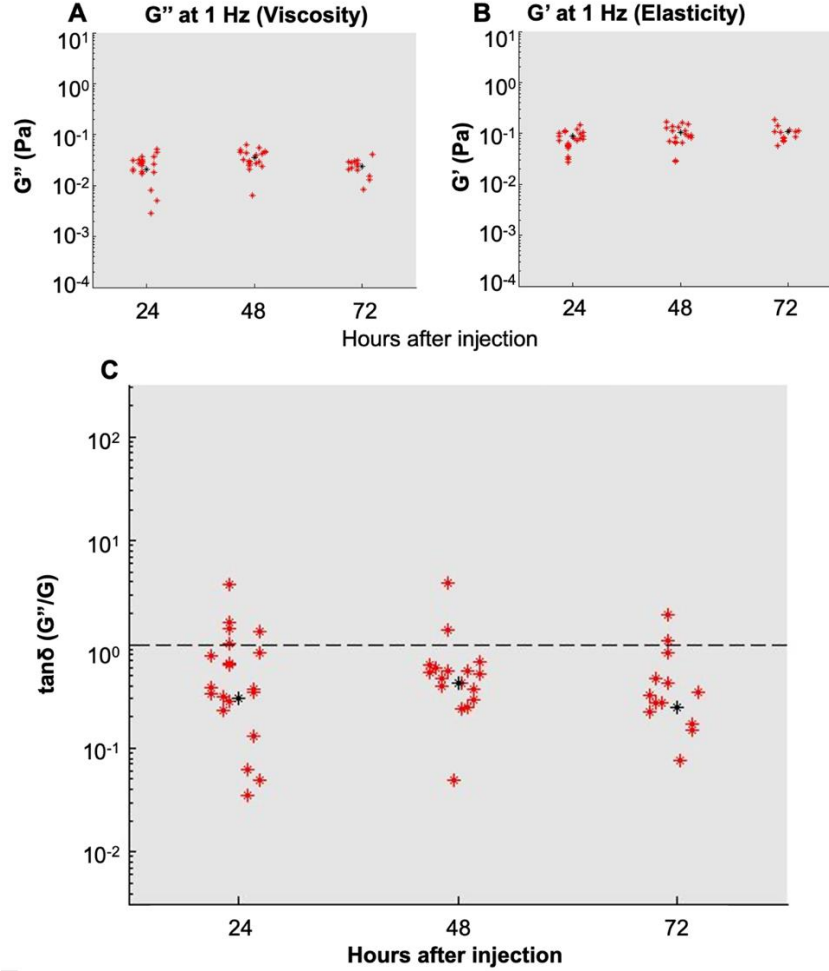


Figure 3.5. Calculated viscoelasticity of all organoids at different time points. (A) Frequency-dependent loss moduli  $G''$  at  $\omega = 1$  Hz. (B) Frequency-dependent storage moduli  $G'$  at  $\omega = 1$  Hz. (C) Ratio of  $G''/G'$  ( $\tan\delta$ ), where  $>1$ : viscous and  $<1$ : elastic.

A strength of particle tracking is that it allows both the calculation of diffusion exponents, and the extraction of the local viscoelastic properties of the mucus<sup>40</sup>. To do this, we ensemble averaged all MSDs from all HGOs and extracted the frequency-dependent elastic and viscous

moduli,  $G'(\omega)$  and  $G''(\omega)$  using a frequency-dependent Stokes-Einstein equation (Fig. 5)<sup>39,41</sup>. These data reveal that the luminal contents are dominantly elastic ( $G' > G''$ ) across all frequencies at all time points. These moduli of the luminal contents, however, are nearly two orders of magnitude lower than those previously reported for gut mucus<sup>42</sup>. Alternatively, bulk rheology (which we perform on organoid mucus in Chapter 4) can provide additional information regarding average mechanical behavior of mucus gels. While microrheology advantageously requires very low sample volume (just a few microliters), the resulting data have the potential to differ. A study by Celli *et al.* found that the viscoelastic moduli of pH 2 (gel) and pH 6 (solution) porcine gastric mucin, obtained by both bulk rheology and particle tracking microrheology, were in agreement in the solution phase but differed in the gel phase<sup>34</sup>. More specifically, the moduli obtained from microrheology in the gel phase were significantly lower than those obtained from bulk rheology. This discrepancy suggested a degree of length-scale dependence of the mucin gel behavior<sup>24</sup>, and is supported by other studies demonstrating greater heterogeneity of mucin at the microscale<sup>43,44</sup>. Future experiments where viscosity is modulated, perhaps by altering the pH of the organoid luminal environment, may additionally be expected to alter the diffusive outcomes<sup>21</sup>.

In our HGO model system, mucus is secreted into the luminal space through the apical surface of gastric epithelial cells. A previous study by our group found that human gastric organoids periodically undergo spontaneous rupture events, during which they expel their luminal contents and then spontaneously re-form<sup>7</sup>. Such behavior must be considered when injecting substances into the lumen—indeed, the organoids used to generate data for this chapter had not purged their luminal contents after injection, as only particles inside of organoids were

taken into consideration. Expelled material continued to be visible, however, in the surrounding extracellular matrix. These data have the potential to be applied to the apical mucus collected from 2D epithelial monolayers cultured at the air-liquid interface, which would be crucial to understanding the impact of the closed confinement of the 3D organoid lumen on the mechanical behavior of the secreted mucus.

To the best of our knowledge, we here present the first *in situ* rheological exploration of any gastrointestinal organoid lumen. We confirm the mucin content of the organoid lumen (Figure 1), as well as spatial heterogeneity of the pore mesh (Figures 2 and 3; more on this in Chapter 4) that particles passively and randomly translocate via Brownian motion. Finally, frequency-dependent storage and loss moduli revealed an elastic predominance of the luminal mucus (Figure 4). Our work demonstrates the minimally-invasive advantage of particle tracking for rheological characterization within the enclosed organoid lumen. Overall, the data described herein provide essential information about the microstructure and rheology of the mucus within the organoid lumen that will inform future investigations into the invasion of the gastric mucus layer by *H. pylori*.

## Methods

### Human Tissue Samples

Human gastric tissue samples for the establishment of organoids were obtained with informed consent and IRB approval from patients undergoing endoscopic biopsy at Bozeman Health Deaconess Hospital (protocol DB050718-FC).

### Organoid Culture

Human gastric organoid cultures were established and maintained as previously described<sup>5,7,16,45,46</sup>. Briefly, gastric glands were isolated by collagenase digestion and seeded into an extracellular matrix, Matrigel (Corning). Polymerized Matrigel was overlaid with L-WRN culture medium (see Appendix A), which contains the supernatants of murine L cells that are known to secrete the growth factors Wnt, Noggin, and R-spondin. Organoid cultures were passaged weekly, and the experiments described herein used organoids in between their third and tenth passages. Organoids for microinjection were prepared on 35 mm glass-bottom plates (MatTek) and allowed to grow for about 5-8 days.

### Alcian Blue Staining

For histological analysis of organoids, culture medium was aspirated, and the Matrigel was overlaid with Histogel<sup>TM</sup> (Epredia HG4000012) which was allowed to polymerize for 15 minutes at room temperature in a biosafety cabinet. A mini cell scraper (Biotium #22003) was then used to transfer the Histogel<sup>TM</sup> into a cassette lined with filter paper. The cassette was submerged in 10% neutral buffered formalin (Richard Allen Scientific, Kalamazoo, MI, USA) overnight, and then transferred to 70% ethanol for at least 24 hours prior to paraffin embedding on a Sakura Tissue-Tek VIP1000 tissue processor/embedding center. Gastric tissue samples were also fixed in formalin and then embedded in paraffin. 5  $\mu$ m sections were then prepared on a Leica 2035 rotary microtome. For staining, slides were deparaffinized with xylene and ethanol in a fume hood. Sections were stained with an Alcian blue-acetic acid solution (pH 2.5, Sigma) for 30 minutes and counterstained with nuclear fast red for 5 minutes. Standard brightfield imaging was performed using a Keyence BZ-X810 microscope.

### Particle Microinjection

A 2  $\mu\text{L}$  glass capillary was backfilled with sterile mineral oil and loaded onto a micromanipulator-controlled Nanoject (Drummond 3-000-204). The capillary was then filled with a  $4.55 \times 10^6$  particle/mL solution of 1  $\mu\text{m}$  Fluoresbrite polystyrene microspheres (Polysciences 17154-10) in PBS. These particles are negatively charged with residual sulfate-ester groups. 9.2 nL of the particle solution was injected into each organoid with a diameter of at least 300  $\mu\text{m}$  ( $n=10$ ). The organoids were then incubated at 37  $^{\circ}\text{C}$ , 5%  $\text{CO}_2$  for 24 hours prior to imaging to allow equilibration of the system.

### Live Confocal Imaging

Organoids on 35 mm plates were imaged on a Leica SP5 confocal laser scanning microscope on a heated stage with an environmental control chamber (37  $^{\circ}\text{C}$ , 5%  $\text{CO}_2$ ; Life Imaging Services). A 20x (0.70 NA) objective and additional 4x optical zoom were used for particle tracking, capturing an average of  $15 \pm 5$  trackable particles in 30 second videos at 26 frames per second. For the long-term time lapse imaging, 25 organoids were imaged over 72 hours at 5 minute intervals<sup>7,21</sup>.

### Particle Tracking Microrheology

Videos were analyzed in MATLAB v7.9.0 using a particle tracking routine which finds the center of intensity for each bead using a polynomial Gaussian fit<sup>47</sup>. Videos and trajectories were inspected to ensure that motion was purely random and no drift was present. Parameters within the particle tracking software were adjusted to only track singlets of particles, as doublets, triplets, and larger bead aggregates do not diffuse in the same way singlets do. Using the trajectory data for each bead, the time dependent mean square displacement was calculated:



$$\text{MSD}(t) = \langle |\mathbf{x}(t) - \mathbf{x}_0|^2 \rangle = \frac{1}{N} \sum_{i=1}^N |\mathbf{x}^i(t) - \mathbf{x}^i(0)|^2.$$

in which  $N$  = total number of particles to be averaged,  $\mathbf{x}^i(0)$  = initial particle reference position, and  $\mathbf{x}^i(t)$  =  $i$ th particle position at time  $t$ .

An exponential model was fit to each tracked MSD profile and power constant  $\alpha$  was recorded:

$$\text{MSD}(t) \approx \beta t^\alpha.$$

in which  $\alpha$  = exponential slope of the MSD profile. In the instance  $\alpha \approx 1.00$ , linear regression was conducted to determine the average slope of  $\text{MSD}(t)$  and subsequently used to calculate the diffusion coefficient using the generalized Stokes-Einstein equation (GSE).  $\tilde{G}(s)$  was calculated by taking the unilateral Laplace transform of  $\text{MSD}(t)$  for each bead using the GSE. Allowing  $s = i\omega$ , we obtained frequency-dependent storage (elastic) ( $G'$ ) and loss (viscous) ( $G''$ ) moduli<sup>39</sup>.

### References Cited

- 1     Bartfeld, S. *et al.* In vitro expansion of human gastric epithelial stem cells and their responses to bacterial infection. *Gastroenterology* (2015).  
<https://doi.org/10.1053/j.gastro.2014.09.042>
  
- 2     Sato, T. *et al.* Long-term expansion of epithelial organoids from human colon, adenoma, adenocarcinoma, and Barrett's epithelium. *Gastroenterology* **141**, 1762-1772 (2011).  
<https://doi.org/10.1053/j.gastro.2011.07.050>
  
- 3     Clevers, H. Modeling Development and Disease with Organoids. *Cell* **165**, 1586-1597 (2016). <https://doi.org/10.1016/j.cell.2016.05.082>
  
- 4     Boccellato, F. *et al.* Polarised epithelial monolayers of the gastric mucosa reveal insights into mucosal homeostasis and defence against infection. *Gut* **68**, 400-413 (2019).  
<https://doi.org/10.1136/gutjnl-2017-314540>
  
- 5     Sebrell, T. A. *et al.* A Novel Gastric Spheroid Co-culture Model Reveals Chemokine-Dependent Recruitment of Human Dendritic Cells to the Gastric Epithelium. *Cellular and Molecular Gastroenterology and Hepatology* **8**, 157-171.e153 (2019).  
<https://doi.org/10.1016/j.jcmgh.2019.02.010>
  
- 6     Seidlitz, T. *et al.* Human gastric cancer modelling using organoids. *Gut* **68**, 207-217 (2019). <https://doi.org/10.1136/gutjnl-2017-314549>
  
- 7     Sebrell, T. A. *et al.* Live imaging analysis of human gastric epithelial spheroids reveals spontaneous rupture, rotation and fusion events. *Cell and Tissue Research* **371**, 293-307 (2018). <https://doi.org/10.1007/s00441-017-2726-5>
  
- 8     Wang, Y., Kim, R., Sims, C. E. & Allbritton, N. L. Building a Thick Mucus Hydrogel Layer to Improve the Physiological Relevance of In Vitro Primary Colonic Epithelial Models. *Cellular and Molecular Gastroenterology and Hepatology* **8**, 653-655.e655 (2019). <https://doi.org/10.1016/j.jcmgh.2019.07.009>
  
- 9     Bartfeld, S. *et al.* In vitro expansion of human gastric epithelial stem cells and their responses to bacterial infection. *Gastroenterology* **148**, 126-136 (2015).  
<https://doi.org/10.1053/j.gastro.2014.09.042>

- 10 McShane, A. *et al.* Mucus. *Curr Biol* **31**, R938-R945 (2021).  
<https://doi.org/10.1016/j.cub.2021.06.093>
- 11 VanDussen, K. L. *et al.* Development of an enhanced human gastrointestinal epithelial culture system to facilitate patient-based assays. *Gut* **64**, 911-920 (2015).  
<https://doi.org/10.1136/gutjnl-2013-306651>
- 12 Schumacher, M. A. *et al.* The use of murine-derived fundic organoids in studies of gastric physiology. *J Physiol* **593**, 1809-1827 (2015).  
<https://doi.org/10.1113/jphysiol.2014.283028>
- 13 Hof, L. *et al.* Long-term live imaging and multiscale analysis identify heterogeneity and core principles of epithelial organoid morphogenesis. *BMC Biology* **19**, 37 (2021).  
<https://doi.org/10.1186/s12915-021-00958-w>
- 14 Bertaux-Skeirik, N. *et al.* CD44 plays a functional role in *Helicobacter pylori*-induced epithelial cell proliferation. *PLoS Pathog* **11**, e1004663 (2015).  
<https://doi.org/10.1371/journal.ppat.1004663>
- 15 Sebrell, T. A. *et al.* Live imaging analysis of human gastric epithelial spheroids reveals spontaneous rupture, rotation and fusion events. *Cell and tissue research* **371**, 293-307 (2018). <https://doi.org/10.1007/s00441-017-2726-5>
- 16 Lyon, K., Bansil, R. & Bimczok, D. Profiling Luminal pH in Three-Dimensional Gastrointestinal Organoids Using Microelectrodes. *J Vis Exp* (2024).  
<https://doi.org/10.3791/66900>
- 17 Bansil, R., Hardcastle, J. M. & Constantino, M. A. Microrheology of Mucin: Tracking Particles and *Helicobacter Pylori* Bacteria. *Épitőanyag* **67**, 150-154 (2015).  
<https://doi.org/10.14382/epitoanyag-jsbcm.2015.25>
- 18 Georgiades, P., Pudney, P. D. A., Thornton, D. J. & Waigh, T. A. Particle tracking microrheology of purified gastrointestinal mucins. *Biopolymers* **101**, 366-377 (2014).  
<https://doi.org/10.1002/bip.22372>
- 19 Su, C. *et al.* Influence of the viscosity of healthy and diseased human mucins on the motility of *Helicobacter pylori*. *Scientific Reports* **8** (2018).  
<https://doi.org/10.1038/s41598-018-27732-3>

- 20 Mao, Y., Nielsen, P. & Ali, J. Passive and Active Microrheology for Biomedical Systems. *Frontiers in Bioengineering and Biotechnology* **10** (2022). <https://doi.org/10.3389/fbioe.2022.916354>
- 21 Su-Arcaro, C. *et al.* Unraveling the Intertwined Effect of pH on *Helicobacter pylori* Motility and the Microrheology of the Mucin-Based Medium It Swims in. *Microorganisms* **11** (2023). <https://doi.org/10.3390/microorganisms11112745>
- 22 Winter, H. H. & Jackson, J. in *Rheological Fundamentals of Polymer Processing* (eds J. A. Covas *et al.*) 61-92 (Springer Netherlands, 1995).
- 23 Fruchart, M., Scheibner, C. & Vitelli, V. Odd Viscosity and Odd Elasticity. *Annual Review of Condensed Matter Physics* **14**, 471-510 (2023). <https://doi.org/https://doi.org/10.1146/annurev-conmatphys-040821-125506>
- 24 Bansil, R., Celli, J. P., Hardcastle, J. M. & Turner, B. S. The Influence of Mucus Microstructure and Rheology in *Helicobacter pylori* Infection. *Front Immunol* **4**, 310 (2013). <https://doi.org/10.3389/fimmu.2013.00310>
- 25 Zhong, C. & Langrish, T. A comparison of different physical stomach models and an analysis of shear stresses and strains in these system. *Food Research International* **135**, 109296 (2020). <https://doi.org/https://doi.org/10.1016/j.foodres.2020.109296>
- 26 Celli, J. P. *et al.* *Helicobacter pylori* moves through mucus by reducing mucin viscoelasticity. *Proc Natl Acad Sci U S A* **106**, 14321-14326 (2009). <https://doi.org/10.1073/pnas.0903438106>
- 27 Mason, T. G., Ganesan, K., van Zanten, J. H., Wirtz, D. & Kuo, S. C. Particle Tracking Microrheology of Complex Fluids. *Physical Review Letters* **79**, 3282-3285 (1997). <https://doi.org/10.1103/PhysRevLett.79.3282>
- 28 Moschakis, T. Microrheology and particle tracking in food gels and emulsions. *Current Opinion in Colloid & Interface Science* **18**, 311-323 (2013). <https://doi.org/https://doi.org/10.1016/j.cocis.2013.04.011>
- 29 Boegh, M., Foged, C., Müllertz, A. & Mørck Nielsen, H. Mucosal drug delivery: barriers, in vitro models and formulation strategies. *Journal of Drug Delivery Science and*

- Technology* **23**, 383-391 (2013). [https://doi.org/https://doi.org/10.1016/S1773-2247\(13\)50055-4](https://doi.org/https://doi.org/10.1016/S1773-2247(13)50055-4)
- 30 Williams, S. E. & Turnberg, L. A. Demonstration of a pH gradient across mucus adherent to rabbit gastric mucosa: evidence for a 'mucus-bicarbonate' barrier. *Gut* **22**, 94-96 (1981). <https://doi.org/10.1136/gut.22.2.94>
  - 31 Dong, W., Matsuno, Y. K. & Kameyama, A. A procedure for Alcian blue staining of mucins on polyvinylidene difluoride membranes. *Anal Chem* **84**, 8461-8466 (2012). <https://doi.org/10.1021/ac301678z>
  - 32 Magalhães, A. *et al.* Muc5ac gastric mucin glycosylation is shaped by FUT2 activity and functionally impacts *Helicobacter pylori* binding. *Scientific Reports* **6**, 25575 (2016). <https://doi.org/10.1038/srep25575>
  - 33 Nordman, H. *et al.* Gastric MUC5AC and MUC6 are large oligomeric mucins that differ in size, glycosylation and tissue distribution. *Biochem J* **364**, 191-200 (2002). <https://doi.org/10.1042/bj3640191>
  - 34 Celli, J. P. *et al.* Rheology of Gastric Mucin Exhibits a pH-Dependent Sol–Gel Transition. *Biomacromolecules* **8**, 1580-1586 (2007). <https://doi.org/10.1021/bm0609691>
  - 35 Ahmad, M., Ritzoulis, C. & Chen, J. Shear and extensional rheological characterisation of mucin solutions. *Colloids and Surfaces B: Biointerfaces* **171**, 614-621 (2018). <https://doi.org/https://doi.org/10.1016/j.colsurfb.2018.07.075>
  - 36 Burada, P. S., Hänggi, P., Marchesoni, F., Schmid, G. & Talkner, P. Diffusion in Confined Geometries. *ChemPhysChem* **10**, 45-54 (2009). <https://doi.org/https://doi.org/10.1002/cphc.200800526>
  - 37 Tallapragada, N. P. *et al.* Inflation-collapse dynamics drive patterning and morphogenesis in intestinal organoids. *Cell Stem Cell* **28**, 1516-1532.e1514 (2021). <https://doi.org/https://doi.org/10.1016/j.stem.2021.04.002>
  - 38 Kapanidis, A. N., Uphoff, S. & Stracy, M. Understanding Protein Mobility in Bacteria by Tracking Single Molecules. *J Mol Biol* **430**, 4443-4455 (2018). <https://doi.org/10.1016/j.jmb.2018.05.002>

- 39 Mason, T. G. Estimating the viscoelastic moduli of complex fluids using the generalized Stokes–Einstein equation. *Rheologica Acta* **39**, 371-378 (2000).  
<https://doi.org/10.1007/s003970000094>
- 40 Weihs, D., Mason, T. G. & Teitell, M. A. Bio-microrheology: a frontier in microrheology. *Biophys J* **91**, 4296-4305 (2006). <https://doi.org/10.1529/biophysj.106.081109>
- 41 Vicsek, T., Czirók, A., Ben-Jacob, E., Cohen, I. I. & Shochet, O. Novel type of phase transition in a system of self-driven particles. *Phys Rev Lett* **75**, 1226-1229 (1995).  
<https://doi.org/10.1103/PhysRevLett.75.1226>
- 42 Lai, S. K., Wang, Y. Y., Wirtz, D. & Hanes, J. Micro- and macrorheology of mucus. *Adv Drug Deliv Rev* **61**, 86-100 (2009). <https://doi.org/10.1016/j.addr.2008.09.012>
- 43 Celli, J. *et al.* Viscoelastic Properties and Dynamics of Porcine Gastric Mucin. *Biomacromolecules* **6**, 1329-1333 (2005). <https://doi.org/10.1021/bm0493990>
- 44 Lieleg, O., Vladescu, I. & Ribbeck, K. Characterization of Particle Translocation through Mucin Hydrogels. *Biophysical Journal* **98**, 1782-1789 (2010).  
<https://doi.org/https://doi.org/10.1016/j.bpj.2010.01.012>
- 45 Goodman, C. *et al.* A High-Throughput Metabolic Microarray Assay Reveals Antibacterial Effects of Black and Red Raspberries and Blackberries against *Helicobacter pylori* Infection. *Antibiotics* **10**, 845-845 (2021).  
<https://doi.org/10.3390/antibiotics10070845>
- 46 Cherne, M. D. *et al.* A Synthetic Hydrogel, VitroGel® ORGANOID-3, Improves Immune Cell-Epithelial Interactions in a Tissue Chip Co-Culture Model of Human Gastric Organoids and Dendritic Cells. *Frontiers in Pharmacology* **12** (2021).  
<https://doi.org/10.3389/fphar.2021.707891>
- 47 Rogers, S. S., Waigh, T. A., Zhao, X. & Lu, J. R. Precise particle tracking against a complicated background: polynomial fitting with Gaussian weight. *Phys Biol* **4**, 220-227 (2007). <https://doi.org/10.1088/1478-3975/4/3/008>

CHAPTER FOUR

HUMAN GASTRIC ORGANOID-DERIVED MUCUS SHARES  
KEY PHYSICOCHEMICAL PROPERTIES WITH NATIVE  
MUCUS

Contribution of Authors and Co-Authors

Manuscript in Chapter 4

Author: Katrina Lyon

Contributions: Designed and performed experiments, analyzed and interpreted data, wrote and revised the manuscript

Co-Author: Barkan Sidar

Contributions: Designed and performed experiments, analyzed and interpreted data, revised the manuscript

Co-Author: Chloe Strupulis

Contributions: Performed experiments, analyzed data, revised manuscript

Co-Author: Alexis Burcham

Contributions: Performed experiments, analyzed and interpreted data, revised manuscript

Co-Author: Luke Domanico

Contributions: Developed the project and designed experiments

Co-Author: Richard Helm

Contributions: Designed and performed experiments, analyzed data, wrote and revised manuscript

Co-Author: Bret Davis

Contributions: Performed experiments, interpreted data

Co-Author: Jennifer Brown

Contributions: Performed experiments, provided resources, analyzed and interpreted data, revised manuscript

Co-Author: James Wilking

Contributions: Developed the project and designed experiments, analyzed and interpreted data, revised manuscript, provided funding for the project

Co-Author: Rama Bansil

Contributions: Developed the project and designed experiments, analyzed and interpreted data, revised manuscript, provided funding for the project

Co-Author: Diane Bimczok

Contributions: Developed the project and designed experiments, analyzed and interpreted data, revised manuscript, provided funding for the project



Manuscript Information

**Katrina Lyon**, Barkan Sidar, Chloe Strupulis, Alexis Burcham, Luke Domanico, Richard Helm, Bret Davis, Jennifer Brown, James Wilking, Rama Bansil, Diane Bimczok

Status of Manuscript:

- ☒ Prepared for submission to a peer-reviewed journal
- ☐ Officially submitted to a peer-reviewed journal
- ☐ Accepted by a peer-reviewed journal
- ☐ Published in a peer-reviewed journal

Abstract

The gastric mucus layer plays a crucial role in homeostasis by providing lubrication and acting as a shield to protect the gastric epithelium from mechanical and chemical damage and food-borne pathogens. The protective barrier function of this mucus is the result of a combination of physical and chemical features such as hydration, viscoelasticity, and acid buffering. Gastric mucus research has been limited by the poor accessibility of native human mucus samples and the abundance of contaminants in these samples. Both 3D organoid models and 2D organoid-derived monolayers have been used to explore the gastric mucosal immune response to *H. pylori* infection, yet few have taken the step back to determine whether the apical mucus contains these functional features. Therefore, a more well-rounded understanding of the structure and function of this mucus layer is of high clinical importance. Here, we used organoid-derived epithelial models cultured at the air-liquid interface (ALI) to generate and harvest clean and sterile gastric mucus, termed bioengineered gastric mucus (BGM), from the apical compartments. This BGM was compared to mucus samples collected from human stomach samples. We used proteomics and CryoFE-SEM to characterize biochemical and structural similarities between the BGM and native mucus, finding porous structures consistent with the literature. Moreover, rheological measurements confirmed the viscoelastic nature of the BGM. Lastly, we used a miniaturized Hele Shaw cell filled with BGM to recapitulate an acid transport phenomenon (“viscous fingering”) hypothesized to occur *in vivo*. Collectively, these findings indicate that our BGM is a sterile, physiologically relevant, and accessible alternative to native gastric mucus for *in vitro* studies. This mucus model has the potential to serve as a valuable tool

for the development of mucus-enhancing therapies, transmucosal drug delivery studies, or for patient-specific investigations into mucosal defects.

### Introduction

The gastric mucus layer is a complex hydrogel that protects the stomach lining from gastric acid and invasion of pathogens such as *Helicobacter pylori*<sup>1</sup>. The internal architecture and viscoelastic properties of mucus are considered essential for its function as a protective barrier<sup>2,3</sup>. Mucus is composed of about 95% water, and the remaining 5% consists of electrolytes, lipids, IgA, DNA, salts, trefoil factor peptides, and most importantly, mucins<sup>1</sup>. Mucin glycoproteins are the functional building blocks of mucus, although pure mucin cannot fully recapitulate the properties of mucus as it lacks a number of its components<sup>4</sup>. Gastric mucus has been difficult to study due to its complex and dynamic physicochemical properties, such as viscoelasticity. In several recent studies, researchers have explored new *in vitro* models for studying mucus, such as organoid and organ-on-a-chip models<sup>5,6</sup>. To date, however, most studies on gastric mucus have been performed with animal mucus or purified mucin, and access to healthy human mucus samples is a critical barrier to many research groups<sup>5,7-9</sup>.

Human gastric organoids have been used as *in vitro* models of gastrointestinal homeostasis and disease, particularly in the context of *H. pylori* infection<sup>10,11</sup>. While the topologically closed structure of 3D organoids is useful for studying the luminal microenvironment, the mucus within remains relatively inaccessible for functional studies<sup>12</sup>. To advance the field of mucus biology, there is a great need *in vitro* mucus layer models that enable greater accessibility for interrogation into its properties, and recapitulate the heterogeneity and functionality found *in vitro*<sup>5,13,14</sup>.

Inspired by previous studies with organoid-derived 2D monolayers, we have leveraged the ability of gastric organoids cultured as 2D monolayers at the air-liquid interface (ALI) to secrete sterile mucus that can be harvested for functional analyses<sup>13,14</sup>. The primary goals of this study were to 1) determine whether the bioengineered gastric mucus (BGM) matches that of native mucus on a biochemical level, and 2) evaluate the efficacy of BGM as a protective barrier by characterizing the biophysical properties of BGM. We first validated our culture model by quantifying mucus production in the monolayer cultures, and subsequently analyzed the structural and functional similarities to native mucus using mass spectrometry, size-exclusion chromatography, cryo-scanning electron microscopy (cryo-SEM), rheometry, and acid transport analysis. Our work suggests that our BGM recapitulates the structural complexity and viscoelasticity of native gastric mucus that are essential to its role as the stomach's first line of defense. This work aims to provide a foundation for future biophysical and biomedical research investigating the dynamics of *H. pylori* infection at the gastric mucosa.

## Materials and Methods

### Human Gastric Tissue Samples

Human gastric tissue samples for the generation of organoid cultures were obtained with informed consent and IRB approval from patients undergoing endoscopy and biopsy at Bozeman Health Deaconess Hospital (protocol 2023-48-FCR). Alternatively, de-identified sleeve gastrectomy samples or whole stomachs collected post-mortem from transplant donors were provided by the National Disease Research Interchange (protocol DB062615-EX) and used for both organoid establishment and mucus collection. Information about tissue samples used in this chapter can be found in Appendix A.

### 3D Organoid Culture

Human gastric organoid cultures were established and maintained as previously described<sup>15-17</sup>. Briefly, gastric glands were isolated by collagenase digestion and seeded into Matrigel (Corning). Polymerized Matrigel was overlaid with L-WRN culture medium containing the supernatants of murine L cells that secrete the growth factors Wnt3a, noggin, and R-spondin 3<sup>18</sup>. The composition of the L-WRN culture medium is listed in Appendix B<sup>15</sup>. Organoid cultures were passaged weekly and are used between passages 2 and 15.

### 2D Monolayer Culture

Transwell permeable supports with PET membranes (surface area: 0.33 cm<sup>2</sup>; pore diameter: 0.4 μm; Corning, 3470) were coated with 15 μg/cm<sup>2</sup> rat tail collagen I (Corning, 354236) for 1 hour at room temperature<sup>13,14</sup>. After aspirating off the remaining collagen, the basolateral chambers were then filled with 600 μL L-WRN culture medium and incubated for at least one hour at 37°C 5% CO<sup>2</sup>. Human gastric organoids (cultured as described above) were expanded, harvested, and trypsinized for 10 minutes in a 37°C water bath<sup>14</sup>. The resulting organoid fragments were mechanically dissociated as previously described, and pipetted through a 70 μm cell strainer to eliminate cell clusters<sup>16</sup>. The filtrate was centrifuged at 400 x g for 5 minutes and the resulting cell pellet was resuspended in L-WRN. A minimum of 2.0 x 10<sup>5</sup> cells were seeded onto each insert, agitated gently for 5 minutes, and incubated undisturbed at 37°C 5% CO<sup>2</sup> for at least 24 hours. Every other day, media was replenished and transepithelial electrical resistance (TEER) was measured using an EndOhm Chamber attachment to an EVOM 2 epithelial volttohmmeter (World Precision Instruments) (Fig. 1E). Once a transepithelial electrical resistance (TEER) of at least 200 Ω\*cm<sup>2</sup> was reached, apical medium was removed to begin

culture at the air-liquid interface (ALI)—a process termed “airlifting”. Cells were then left undisturbed until there was visible production of at least 50  $\mu$ L apical mucus for collection (Fig. 1C,D). Our gastric epithelial cells typically form confluent monolayers within one week, and mucus production was observed within one week of airlifting.

### Mucus Harvest and Storage

Bioengineered mucus (BGM) was harvested off the apical epithelium at either biweekly or weekly intervals using either forceps or a wide-bore pipette and transferred to a microcentrifuge tube. The wet weight of the mucus harvested from each well was recorded. Samples were then either used immediately for experiments, frozen at  $-20^{\circ}\text{C}$ , or frozen at  $-80^{\circ}\text{C}$  for long-term storage. For all experiments, BGM and native mucus (NM) samples were used fresh to preserve their natural state as much as possible<sup>19</sup>, with experiments to measure dry weight of secreted mucus over time being the one exception. Porcine gastric mucin (PGM), prepared as previously described<sup>20</sup>, was lyophilized and rehydrated at a concentration of 10 mg/mL experiments<sup>21</sup>.

### Lyophilization

BGM samples were first flash-frozen in liquid nitrogen and stored on dry ice for a minimum of 30 minutes prior to lyophilization for at least 48 h with a FreeZone<sup>TM</sup> benchtop freeze dryer (Labconco<sup>TM</sup> 700202000). The dry weight of each sample was recorded for quantification of dry mass and water content. Lyophilized BGM samples were only used in the determination of dry mass in Figure 1.

### Size Exclusion Chromatography

Samples for size exclusion chromatography (SEC) were prepared by dissolving 50  $\mu\text{L}$  of mucin in 150  $\mu\text{L}$  of buffer, followed by filtration through a 0.45  $\mu\text{m}$  syringe filter. The buffer comprised 0.001 M  $\text{Na}_2\text{HPO}_4$ , 0.001 M EDTA, 0.1% (w/v)  $\text{NaN}_3$ , and 0.03 M NaCl. Samples labeled 220908 hu007, 220914 hu007, and 220923 hu007 were diluted with a 1:1 factor. A volume of 20  $\mu\text{L}$  from each sample was then loaded onto a YMC Diol-300 SEC column at a flow rate of 1 mL/min. Molecular weight determination and concentration measurements were conducted using multi-angle light scattering (MALS) and refractive index (RI) detection, respectively, through in-line Wyatt Detectors. All data sets were analyzed using Astra 8 software and normalized against commercial PEG and PEO standards from Wyatt.

### Proteomics

Cysteine disulfide bonds were reduced using 4.5 mM dithiothreitol (DTT) and incubation at 37°C for one hour. Free sulfhydryl groups were alkylated with 10 mM iodoacetamide (IAA) at room temperature for 30 min in the dark, then unreacted IAA was quenched with 10 mM DTT. Protein was precipitated by the addition of *o*-phosphoric acid to 1.2% (v/v) and 1 mL methanol followed by overnight incubation at -80°C. Precipitated protein was loaded onto a micro S-Trap (Protifi) by centrifugation at room temperature for 1 minute at 1,000 x g and washed extensively with methanol. Samples were digested using 2  $\mu\text{g}$ . Pierce Trypsin Protease, MS grade (ThermoFisher Scientific) in 50 mM triethylammonium bicarbonate (pH 8.5) at 37°C overnight. Peptides were recovered by sequential washings of the S-Trap (25  $\mu\text{L}$  solvent A, 25  $\mu\text{L}$  50:50 solvent A: solvent B, 25  $\mu\text{L}$  solvent B). Excess acetonitrile was removed by vacuum centrifugation and peptide concentrations were determined using a nano-UV/Vis spectrometer

(DeNovix) to measure the absorbance at 215 nm. (Solvents A and B are the same as solvents A and B used for the chromatography.) The processed samples were analyzed by LCMS on a Bruker MALDI-2 Mass Spectrometer (timsTOF Pro/flex) equipped with a Vanquish Neo UPLC unit. The gradient used LCMS-grade water with 0.01% formic acid as solvent A and 80% acetonitrile with 0.01% formic acid as solvent B. The column used was a  $\mu$ PACTM HPLC column (ThermoFisher Scientific, catalog number COL-NANO200G1B), and the flow rate was 8  $\mu$ L/min. The run was 95 minutes long. The starting percentage of solvent B was 2%. The final percentage of solvent B was 98%..

#### CryoFE-SEM

Cryo-Field Emission Scanning Electron Microscopy (cryo-SEM) was performed at the Imaging and Chemical Analysis Laboratory (ICAL) at Montana State University. Approximately 50  $\mu$ L of mucus (or BGM) were transferred from atop the ALI culture directly onto a gold-coated (Emitech K575X) silicon wafer, flash-frozen in liquid nitrogen, and manually fractured very quickly using a flathead screwdriver before critical point drying and imaging on a Zeiss SUPRA 55VP Field Emission Scanning Electron Microscope. In order to ensure that the least-contaminated and most representative portion of the native mucus sample was used, the clearest portion of the mucus was removed from the tube with forceps, leaving behind any contaminating blood or gastric juice. Images were acquired at -140°C with a cathode-luminescence detector at an accelerating voltage of 2.00 kV. Image analysis was performed using ImageJ<sup>22</sup>.

For image analysis, images were converted to grayscale, contrast-enhanced, and thresholded appropriately. Pores were next identified by the “Analyze Particles” function of the ImageJ software. The outputs were visually inspected to ensure successful pore identification and



to make manual corrections where needed, such as in the case of debris resulting in false pore identification. A minimum of 10 pores per image were analyzed for their diameter and area. Native mucus from three tissue donors and BGM samples from three different organoid lines were analyzed. Information about the samples used is provided in Appendix A. The sizing criteria used for defining the structural features of the mucus are summarized in Supplementary Table 1.

### Rheometry

For rheological measurements, all mucus samples were equilibrated to room temperature. Storage (elastic,  $G'$ ) and loss (viscous,  $G''$ ) moduli—parameters used to describe the extent of solid- and liquid-like behavior, respectively—were measured via the following series of rheometric tests: 1) flow sweeps to obtain viscosity as a function of shear rate, 2) amplitude sweeps to determine the linear viscoelastic region in which subsequent measurements are performed, and 3) frequency sweeps to determine the viscoelastic moduli<sup>23,24</sup>. All tests were performed using an AR-G2 rheometer with a 20 mm parallel plate geometry (TA Instruments)<sup>25,26</sup>. An initial flow sweep was performed to obtain steady shear viscosity as a function of shear stress. Next, an amplitude sweep was performed in a range starting just before the point where the viscosity began to drop off in the flow sweep. The amplitude sweeps were performed at a constant frequency of 1 Hz with oscillatory shear stress of increasing amplitude was performed to determine the linear viscoelastic region (LVR) for each sample. The LVR was determined by identifying the region in which the  $G'$  and  $G''$  plateau because they are undisturbed by the oscillatory strain<sup>27</sup>. A value of applied stress within this linear regime was

then used for subsequent frequency sweeps of the samples with the predetermined optimal amplitude. Samples were allowed to recover for 10 minutes in between tests<sup>27</sup>.

### Viscous Fingering Experiments

A modified Hele-Shaw cell design, kindly provided by Dr. Irmgard Bischofberger (Massachusetts Institute of Technology), was used to assess the capacity of BGM to support viscous fingers<sup>28,29</sup>. A 13 or 25  $\mu\text{m}$  spacer (Precision Brand, 44105 and 44110) was sandwiched by two rectangular pieces of borosilicate (McMaster; 75x25x2.2mm)—the top of which had a hole drilled into it with a 0.5 mm diamond drill bit—and glued by epoxy. A heat gun was used to remove the syringe parts aside from the blunt needle, which was secured into the top hole with epoxy to create the inlet. For visualization of acid flow, hydrochloric acid was combined with Brilliant Blue dye (Coomassie® 190343). The dye was first dissolved in hot water at a concentration of 50 mg/mL, then added to an equal volume of 0.02 M HCl. The resulting dye was 25 mg/mL with 0.01 M HCl. BGM, PGM, or NM samples were adjusted to pH 6 and loaded into the inlet by hand with a Teflon 1 mL syringe and 23-gauge needle (McMaster). L-WRN cell culture medium was used as a control. Flow of the blue-dyed acid through the Hele Shaw cell was initiated through pharmaceutical tubing (SCI BB518-12, I.D. 0.31 mm, O.D. 0.64 mm) and maintained by a syringe pump (New Era Pump Systems, Inc., Farmingdale, NY, USA) with a 1 mL syringe. We began with initial acid flow rates ranging from 2-5  $\mu\text{L}/\text{min}$  and reduced as the flow rate to 1  $\mu\text{L}/\text{min}$  after finger formation was observed<sup>28</sup>. Videos were recorded using an iPad Pro (6th generation) camera at a resolution of 3840 x 2160 pixels and a frame rate of 30 fps. All experiments were performed at room temperature.

### Consideration of Biological Variables, Rigor, and Reproducibility and Statistical Analysis

Tissue samples were obtained from donors of any sex or ethnicity and within an age range of 18-70. The tissue donor information for each experiment can be found in Appendix A. Each experiment was repeated three or more times with different organoid lines or native mucus samples.

All data were analyzed using GraphPad Prism version 10.2.3 (San Diego, CA, USA). Data are presented as the mean  $\pm$  SD. Student's *t* tests and one-way ANOVA with Dunnett's multiple comparisons tests were used to assess statistical significance.  $P \leq 0.05$  was considered to indicate a statistically significant difference.

## Results

### Human Gastric Epithelial Monolayers Cultured at the Air-Liquid Interface Produce Apical Mucus

Using backscatter light confocal imaging, we previously showed that human gastric organoids secrete a dense substance that accumulates in the organoid lumen over time and that is released upon organoid rupture<sup>30</sup>. We here used immunofluorescence staining to confirm that tissue-derived organoids from the human gastric body cultured under expansion conditions produce MUC5AC and MUC6, the major mucins produced in the gastric mucosa (Fig 1A,B). To produce BGM for functional experiments, 3D organoids were expanded and subsequently disaggregated to generate 2D gastric epithelial monolayers<sup>14</sup>. The monolayers were then maintained in submerged culture until they reached confluence and developed a transepithelial electrical resistance of  $>200 \Omega\text{cm}^2$  (TEER). The cultures then were airlifted to promote mucus secretion and accumulation at the ALI (Fig. 1C-E), as described by Boccellato *et al.* and Wang *et*

*al.*<sup>13,14</sup>. Apical mucus was collected every 2-7 days (Fig. 1F,G), and volume and dry weight were determined. On average, monolayers produced  $50 \pm 27$   $\mu$ L mucus per well every 2 days, with an average dry weight of  $39 \pm 21$  mg/mL, which corresponds to a water content of approximately 96%, similar to reported values for gastric mucus<sup>4</sup> (Fig. 1F). In comparison, the average dry mass of five native mucus (NM) samples that we obtained from surgically excised or post-mortem human stomach samples was 123.91 mg/mL, possibly due to the presence of contaminants, which were commonly visible (Fig. 1G). Size exclusion chromatography with multi-angle light scattering (SEC-MALS) revealed molecular weight distributions of BGM and NM that were not statistically different, both samples showing high and low molecular weight components (Fig. 1H,I). Interestingly, porcine gastric mucin contained similar sized large molecular weight compounds as the BGM and NM, but completely lacked low molecular weight compounds. Overall, these data confirmed that human gastric organoids, when cultured as monolayers at the ALI, can produce a mucus layer that can be continuously harvested for functional analyses and has enhanced complexity compared to PGM.

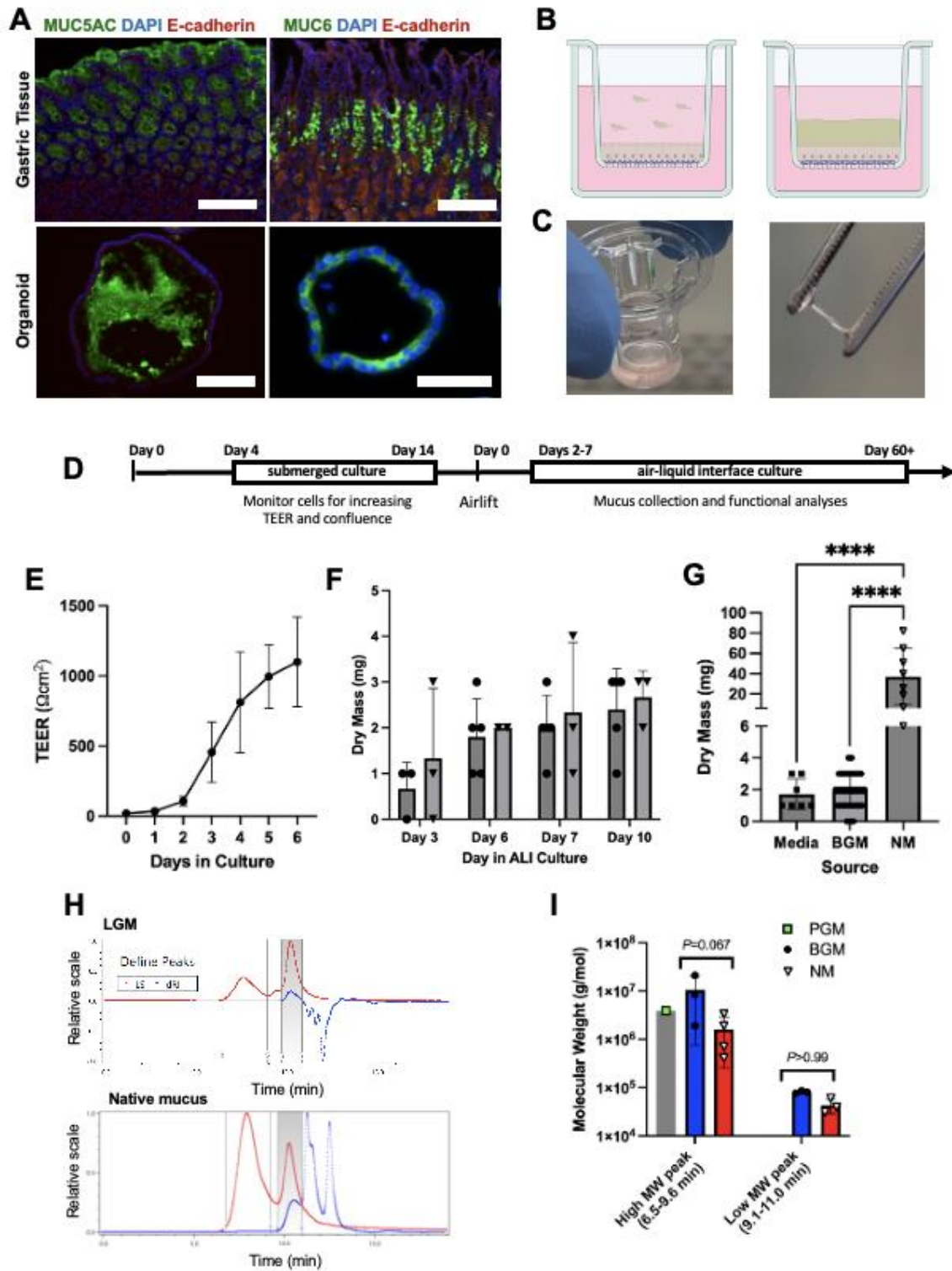


Figure 4.1. Gastric epithelial monolayers cultured at the air-liquid interface produce apical mucus. (A) Immunofluorescent labeling of MUC5AC (green) in human gastric tissue (top left) and in organoid lumen (bottom left). MUC6 (green) on the glandular epithelium of tissue (top

right) and on the outer edges of the organoid lumen (bottom right). Scale bars correspond to 200  $\mu\text{m}$ . Representative of three experiments. (B) Schematic diagram of Transwell 2D culture conditions: submerged (left) and air-liquid interface (right). (C) Clear, viscoelastic mucus on the Transwell insert (left) and removed from the apical epithelium (right). (D) Timeline for 2D culture conditions, mucus collection, and functional analyses. (E) Time-dependent development of transepithelial electrical resistance (TEER) of one representative experiment ( $n=4$ ). Dotted line indicates TEER threshold for airlift at  $y=200 \Omega\text{cm}^2$ . (F) Bioengineered mucus (BGM) dry mass collected per well, every other day (representative of 2 experiments). (G) Average dry mass yield per well in a media control ( $n=7$ ), BGM ( $n=56$ ), and native mucus (NM;  $n=8$ ). (H) Chromatograms of BGM (top) and NM (bottom) showing the differential refractive indices (dRI) in blue and the light scattering (LS) signal in red. (I) Molecular weights of a porcine gastric mucin (PGM) control, BGM, and NM determined by size-exclusion chromatography paired with multi-angle light-scattering (SEC-MALS).

#### Proteomic Analysis of Bioengineered Gastric Mucus Reveals Physiologically Relevant Secretome

Having developed a method for generating gastric mucus on organoid-derived ALI cultures, our next goal was to determine the biochemical composition of these samples and to compare them to native mucus. A non-biased mass spectrometry approach was also used for this analysis. Overall, a total of 1,493 proteins were identified in native human gastric mucus from a total of four individuals, whereas only 144 proteins were found in BGM ( $n=3$ ), with 72 present in both samples (Fig. 2A). A scatterplot comparing the total mean intensity of proteins found in both native mucus and BGM demonstrates no significant correlation between the two samples (Fig. 2B). Interestingly, some of the most prevalent proteins in BGM were intracellular cytoskeletal proteins such as keratins, cytokeratins, and microfilament proteins (Fig. 2C). MUC5AC, MUC1 and MUC6 all were among the top 35 identified proteins in BGM. In native mucus, MUC5AC was found to be the most abundant protein, with other highly expressed proteins also including intracellular proteins such as actin and myosin. Blood proteins such as hemoglobin, indicative of blood contamination, and antibody heavy and light chains, indicative of physiological antibody secretion into the gastric mucus, also were detected in the native

mucus. Overall, the majority of the 1,493 proteins detected in the native mucus samples were intracellular proteins, suggesting significant contamination with cellular debris. Further information regarding the unique proteins found in either NM or BGM can be found in Supplementary Table 1.

Comparison between the BGM and NM revealed a high variability in the abundance of specific mucins between samples, but no significant difference in the abundance of MUC5AC, MUC1, or MUC6 in BGM and native mucus (Fig. 2D). Other commonly recognized gastric mucus components were also identified. Both BGM and native mucus contained TFF2, lipase, gastrin, and gastrin, but TFF1, pepsin, and L-fucosidase were exclusively detected in the native mucus samples (Fig. 2E). These data confirm the identity of the BGM and demonstrate its relative purity compared to native mucus from patient stomachs.

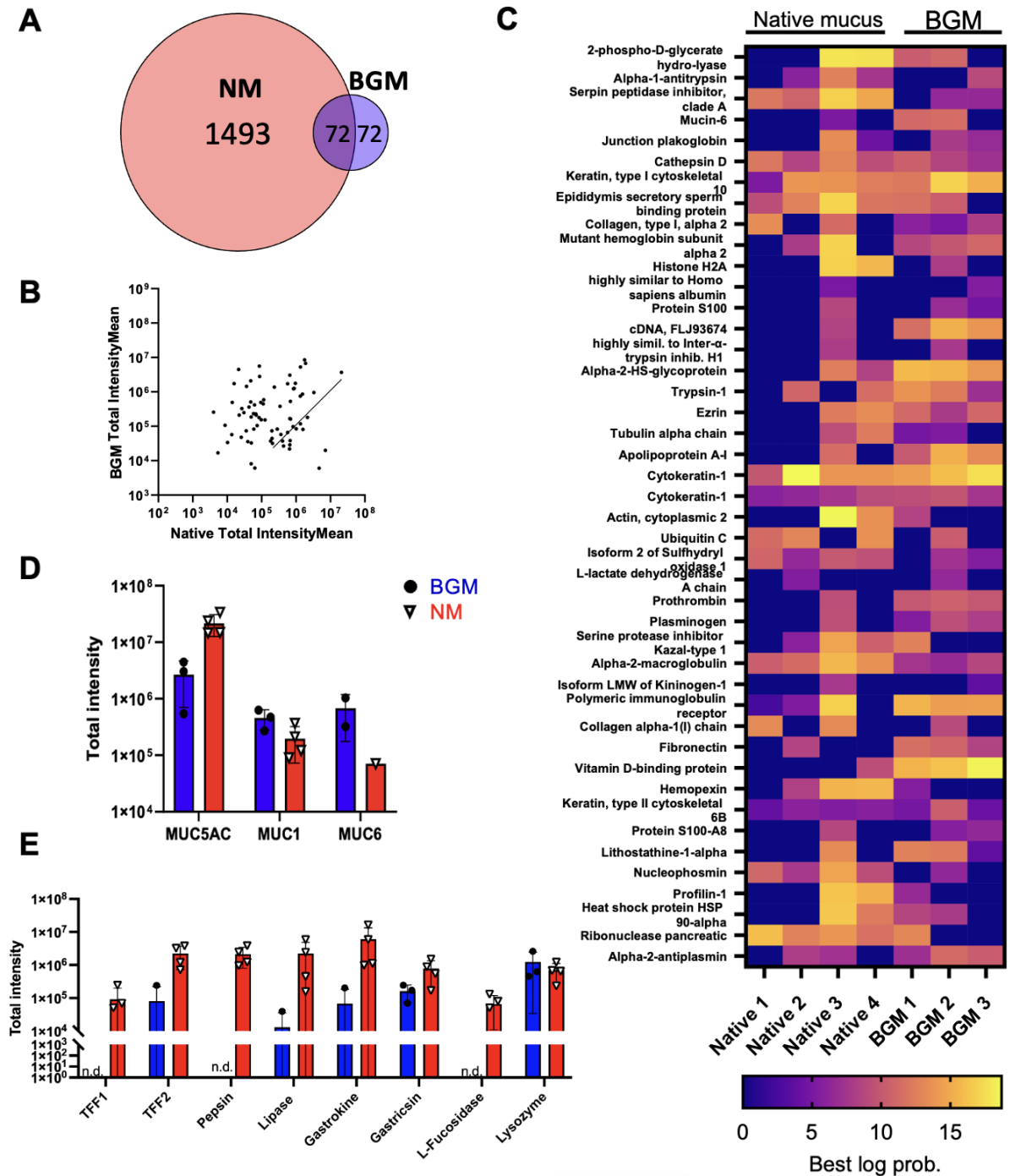


Figure 4.2. Proteomic analysis of bioengineered gastric mucus reveals physiologically relevant secretome. (A) Unique protein identification overlap between NM and BGM, acquired by mass spectrometry. (B) Mass spectrometry analysis of proteins in native mucus (NM; n=4) and bioengineered gastric mucus (BGM; n=3), expressed as total intensity mean. (C) Heatmap showing relative expression of the top 44 identified proteins. Data from n=4 NM and n=3 BGM



samples. (D) Relative abundance of gastric mucins MUC5AC, 1, and 6 in BGM (blue) and NM (red). (E) Relative abundance of other relevant gastric proteins in BGM (blue) and NM (red).

### Visualization of Bioengineered Mucus by Cryo-Scanning Electron Microscopy Reveals Heterogeneity and Porosity of Internal Architecture

Previous studies on native mucus harvested from dog and pig stomach have shown that, at the microscale level, gastric mucus has a honeycomb structure with circular pores of about 4  $\mu\text{m}$  in diameter<sup>22,31</sup>. To assess the structure of BGM and to compare BGM to native human gastric mucus, we used cryo-field emission scanning electron microscopy (Cryo-SEM). As shown in Fig. 3A, both native mucus and BGM had similar, smooth surface patterns that were continuous aside from the fracture lines. Fracturing of the samples immediately prior to imaging exposed similar cross-sections with honeycomb-like scaffolds ranging from 5 to 300  $\mu\text{m}^2$  (Fig. 3A, Supplementary Table 1). The pores in BGM and native mucus were similarly sized, with an average pore area of 2.4  $\mu\text{m}^2$  in BGM and 3.5  $\mu\text{m}^2$  in NM (Fig. 3B). Using digital image analysis, we found no significant differences between the areas of these pores in BGM and NM (Fig. 3B). Finally, to confirm that the microscopic structures observed were not also present in tissue culture media, we imaged apical fluid from blank Transwell® inserts<sup>32</sup> and L-WRN cell culture medium<sup>33</sup> (Supplementary Figure 1). Those controls had morphologies clearly distinct from those of the mucus samples in that they lacked both rounded pore structures and the pseudo-hexagonal geometries of the honeycomb scaffolds seen in BGM and NM. These data confirm the internal architecture of our BGM to be consistent with NM as well as other types of mucus when visualized with CryoFE-SEM<sup>22,31,34</sup>.

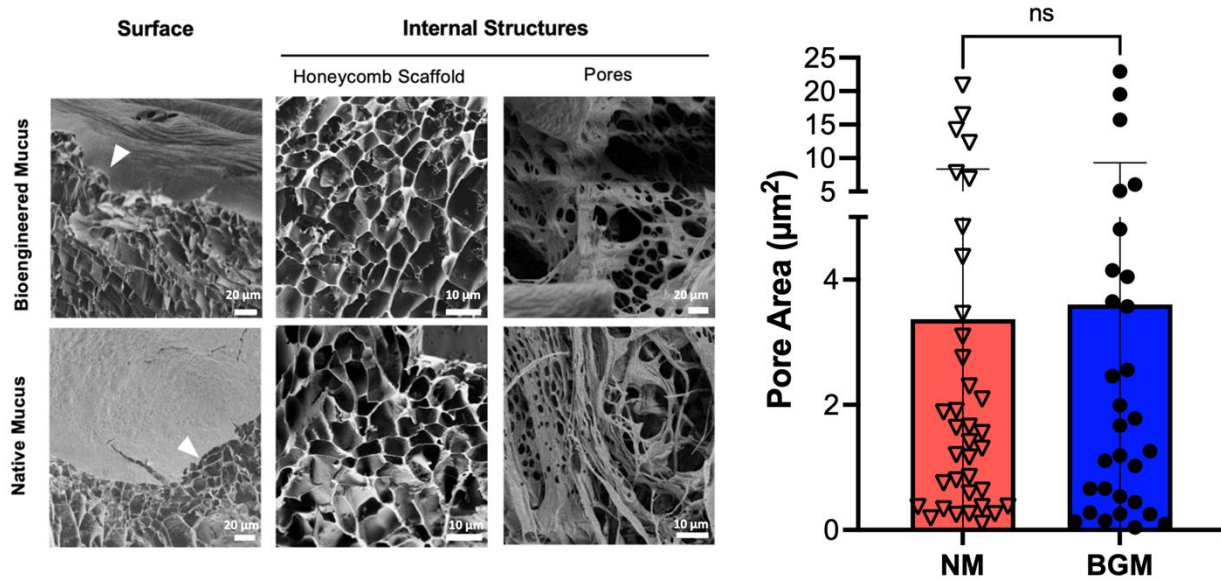


Figure 4.3. Visualization of bioengineered gastric mucus by cryo-scanning electron microscopy. (A) Electron micrographs showing frozen surfaces of BGM (top left) and NM (bottom left) with fractures (arrows) to expose internal architecture (scale bar = 20  $\mu\text{m}$ ). Electron micrographs of internal honeycomb scaffold in BGM (top middle) and NM (bottom middle) (scale bar = 10  $\mu\text{m}$ ). Pores in BGM (top right; scale bar = 20  $\mu\text{m}$ ) and NM (bottom right; scale bar = 10  $\mu\text{m}$ ). (B) Pore mesh area for NM ( $n=10$  pores from 1 biological replicate) and BGM (pooled measurements of  $n=10$  random pores each from 3 biological replicates); Student's  $t$  test: ns. Pores were measured by ImageJ using thresholding and automatic object detection followed by manual correction.

#### Rheometric Frequency Sweeps Confirm Viscoelastic Behavior of Bioengineered Mucus

For rheological characterization of the mucus samples, we measured the steady shear viscosity and frequency-dependent loss and storage moduli of BGM and NM samples using an AR-G2 rheometer with a 20 mm parallel plate geometry (Fig. 4A,B). NM (average viscosity  $2.96 \times 10^{-2} \pm 0.05$  Pa.s) demonstrated far more viscous behavior than BGM (average viscosity  $1.01 \pm 0.85$  Pa.s). For comparison, the viscosity of water at 20  $^{\circ}\text{C}$  is only 0.001 Pa.s<sup>35</sup>. The BGM and NM had similar trends in their frequency-dependent elastic moduli with only slight differences in relaxation time (Fig. 4B). The slopes of the elastic moduli for NM and BGM, respectively, were 0.3285 ( $p=0.0008$ ) and 0.4353 ( $p=0.0040$ ). The slopes of the viscous moduli, similarly, were

0.08349 ( $p=0.0072$ ) and 0.09155 ( $p=0.0293$ ). The values for  $\tan \delta$ —the ratio of viscous to elastic moduli—demonstrated that the NM and BGM both had predominantly elastic behavior (Fig. 4C). This elastic predominance supports the rheological behavior of the organoid luminal mucus from Chapter 3.

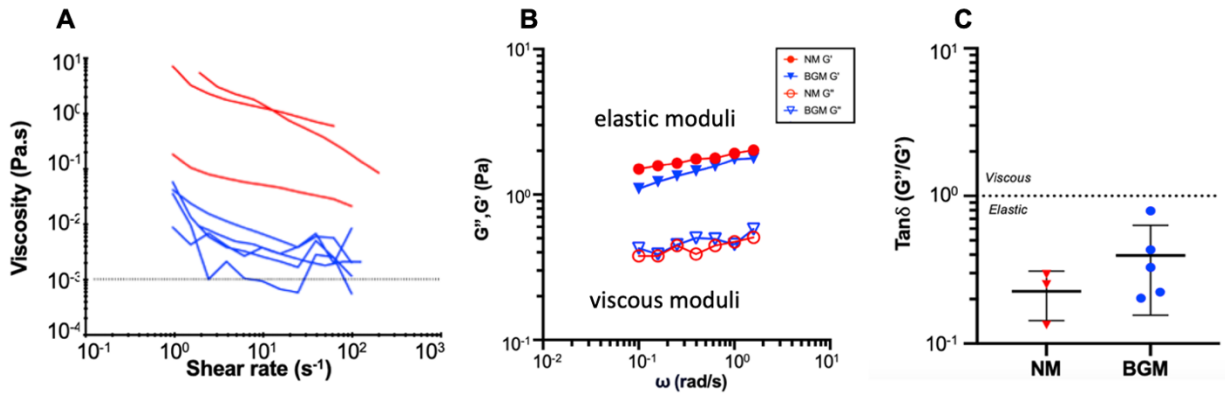


Figure 4.4. Rheological comparison of bioengineered and native gastric mucus. (A) Steady shear viscosity as a function of shear rate for bioengineered gastric mucus (BGM; blue;  $n=5$ ) and native mucus (NM; red;  $n=3$ ). Dotted line represents the viscosity of water (10<sup>-3</sup> Pa.s) as reported by Lai *et al.*<sup>35</sup> (B) Frequency-dependent elastic (storage,  $G'$ ) and viscous (loss,  $G''$ ) moduli of NM (red) and BGM (blue) ( $n=1$ ). Representative of 3 independent experiments. (C) Ratios of viscous to elastic moduli of NM (red;  $n=3$ ) and BGM (blue;  $n=5$ ) ( $>1$ : predominantly viscous behavior,  $<1$ : predominantly elastic behavior). Each point represents the average of  $\tan \delta$  over 0.1-1.5 rad/s, for each independent experiment. All frequency sweep data were performed within the linear viscoelastic region.

### Bioengineered Gastric Mucus Enables the Formation of Acid Channels

One major theory for the transport of protons across the gastric mucus layer is through the development of viscous fingers, which are finger-like instabilities occur at the interface of two fluids<sup>21,28,36</sup>. We initiated flow of hydrochloric acid (pH 2) into mucus solutions (pH 6-8) at 2  $\mu\text{L}/\text{min}$  using a syringe pump (Fig. 5A). We tested the flow of acid through purified PGM at 10 mg/mL and observed the formation of long, thin fingers that branched from one another (Fig. 5G). In native mucus, the acid formed thicker but still distinct fingers, with some visible tip

splitting<sup>37</sup>, until they reached the far edge of the cell (Fig. 5F). We observed that our BGM produced a viscous fingering pattern that expanded radially from the inlet (Fig. 5C) before spreading distally (Fig. 5B). Some of the fingers observed here also demonstrated tip-splitting (Fig. 5B). A phenomenon referred to as “shielding” was also observed, in which mucin gelation occurs quickly upon contact with the acid and a sudden burst of acid is observed after a period of pressure buildup as a result of gelation stopping the flow (Fig. 5D)<sup>37,38</sup>. Flow of acid through the apical fluid collected from a blank Transwell® produced no such structures and the patterning observed represented a standard parabolic laminar flow throughout the experiment (Fig. 5E)<sup>39</sup>. In summary, both our BGM and NM demonstrate characteristic viscous fingering patterning that has been described in other studies of native mucus<sup>21,28,36</sup>.

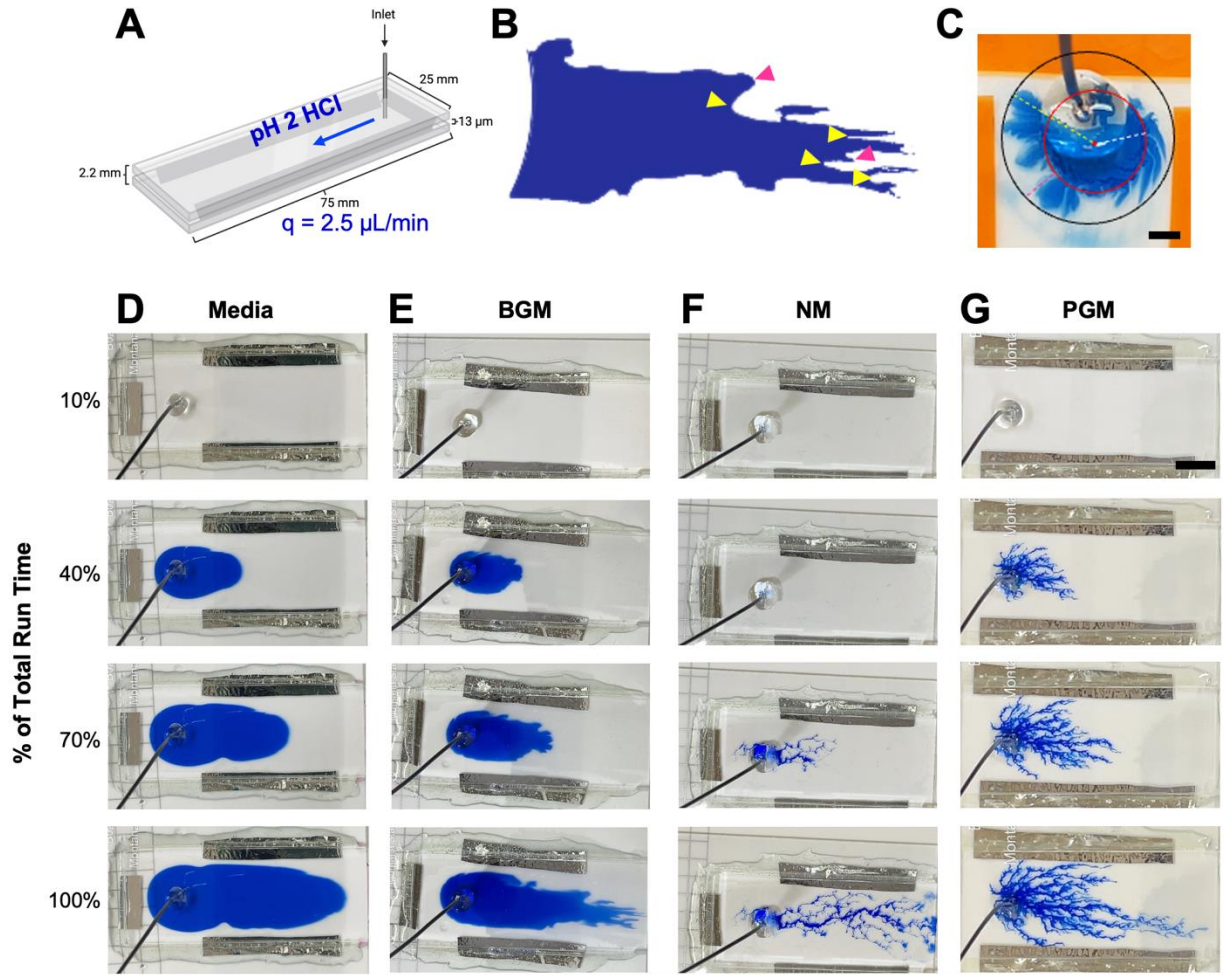


Figure 4.5. Bioengineered gastric mucus enables formation of viscous fingers typical of mucus gels. (A) Miniaturized Hele Shaw cell design. (B) Example of viscous fingering (yellow arrows) and shielding phenomena (pink arrows) in HCl flow through bioengineered gastric mucus (BGM) in a Hele Shaw cell ( $t=13\text{m}36\text{s}$ ,  $z=13\mu\text{m}$ ,  $q=2.5\mu\text{L}/\text{min}$ ). (C) Radial viscous fingering in a Hele Shaw cell ( $z=25\mu\text{m}$ ). The circles demonstrating length scales indicate: compact invasion radius ( $r_d$ ; red), outer pattern radius ( $r_o$ ; black), and outer finger length ( $r_f$ ; yellow). (D-F) Miniaturized Hele Shaw cells ( $z=13\mu\text{m}$ ) were filled with (D) media, (E) BGM, (F) native mucus (NM), or (G) 15 mg/mL porcine gastric mucin (PGM). 0.2M HCl solution at pH 2.0 stained with blue dye was injected into the inlet at  $q=2\mu\text{L}/\text{min}$  and was allowed to flow until the point of drainage. One representative experiment of two to three independent runs for each material is shown.

## Discussion

To prevent and treat *H. pylori*-related disease, it is crucial to understand the role of the stomach's first line of defense against bacterial pathogenesis: the gastric mucus layer. It has previously been shown that human gastric organoid-derived monolayers cultured at the air-liquid interface (ALI) produce mucus and serve as excellent models for *H. pylori* infection<sup>13,40</sup>. Leveraging this *in vitro* mucus layer as a model system for mucus as a biomaterial, however, has been left relatively unexplored. Specifically, the extent to which gastric organoid-derived mucus recapitulates the composition, structure and functionality of native human gastric mucus has remained unclear. To address this issue, we have optimized the collection of this mucus—which we refer to as “bioengineered gastric mucus (BGM)”–for biochemical, structural, and functional characterization in this chapter.

Using immunohistochemistry, we demonstrate expression of MUC5AC and MUC6 in both the native human gastric tissue and in our 3D organoids, similar to the Alcian blue staining for acidic mucins from Chapter 3 (Fig. 1A). We went on to optimize the 2D culture of these organoid cells to maintain BGM production over several months, though the quality of this BGM and barrier integrity (through TEER measurements or transepithelial permeability assays) must be confirmed throughout this timeline. Additionally, the patient-specific nature of organoid models could be leveraged in this 2D monolayer format to address possible predisposition of individual patients toward mucosal defects or susceptibility to mucus-related disease. The cellular composition and differentiation of gastric organoids can be adjusted by altering their culture conditions<sup>13,40</sup>. For example, gastric organoid cultures may be driven toward MUC5AC-producing foveolar cells by supplementing the media with epidermal growth factor (EGF), or

toward a MUC6-dominant phenotype by removing EGF and adding bone morphogenic protein (BMP)<sup>40</sup>. The physiological concentration of mucin (both MUC5AC and MUC6) in native gastric mucus is reported to be around 20 mg/mL in humans<sup>41</sup>. In studies on PGM, concentrations ranging from 15 mg/mL to 30 mg/mL have been used, which still makes up only about 3% of the native mucus<sup>8,42</sup>. In dry weight analysis, the organoid-derived BGM samples averaged ~40 mg/mL, which we would expect given the relative concentration of mucin and other materials in mucus compared to water<sup>1</sup>.

Using mass spectrometry, we confirmed that both BGM and NM contained the three major gastric mucins—MUC5AC, MUC6 (secreted), and MUC1 (membrane-bound). MUC5AC, secreted by foveolar cells, forms the surface of the gastric mucus layer. Expression of MUC5AC can increase over 50-fold when the gastric mucosa is inflamed, and conversely, is reduced in carcinogenesis<sup>43,44</sup>. MUC6 on the other hand, whose expression is restricted to the glandular mucosa, tends to be overexpressed in gastric malignancy<sup>43,45</sup>. These two predominant mucins make up the gastric mucus layer in the anticipated regions, as our data in Figure 1A support<sup>46</sup>. Additionally, these mucins are co-expressed with trefoil factors (TFFs)—MUC5AC with TFF1 and MUC6 with TFF2<sup>40,47</sup>. Given these associations, the presence of TFF2 in BGM was particularly interesting due to its functionally important antimicrobial properties and its propensity to upregulate following gastric mucosal injury, perhaps as a defense mechanism<sup>48-50</sup>. Future studies may explore potential stabilizing effects of TFF2 on the inner adherent mucus layer of the glandular epithelium. A study by Kawakubo *et al.* suggested that the O-linked oligosaccharides on mucin backbones inhibit cholesteryl- $\alpha$ -D-glucopyranoside—a major cell wall component of *H. pylori*<sup>51</sup>. In addition, O-glycans are thought to be responsible for altering

bacterial morphology, which would likely impact motility. Future investigations into the glycosylation patterns of BGM could suggest potential preclinical drug targets for *H. pylori*-associated disease<sup>52-54</sup>. Furthermore, native mucus harvested from patient stomach samples is frequently contaminated with bile, blood, and cellular debris. Our results confirmed that native mucus contained a number of intracellular proteins, including actin, myosin, tubulin and keratin, that were likely cellular debris or proteins derived from blood, such as albumin, prothrombin, and plasminogen. The proteins found in BGM and native mucus do exhibit variation, likely due to different types of contaminants. Fundamentally, however, the samples are still very similar. High detection of cytokeratin in BGM is likely due to cellular material from the epithelial monolayer cultures. Albumin was a protein of high abundance in the BGM (though also present in the NM)—possibly due to contamination with the fetal bovine serum in the cell culture media—which would go on to inform our choice of controls in the electron microscopy described below<sup>33</sup> (Supplementary Table 4.1 and Figure S4.1). Overall, this proteomic analysis was limited by the relatively small number of BGM samples, though a larger scale analysis was beyond the scope of this particular study.

Visualization of the internal structural architecture of the BGM and NM using cryo-SEM showed several key structures that were consistent with those reported in other mucus studies<sup>22,34,55-59</sup>. We therefore assigned the observed structures to three categories: “honeycomb scaffold”, “pores”, and “micropores”, each with distinct characteristics and size parameters (Supplemental Table 1). First, the smooth surface patterning observed is believed to indicate mucus hydration. In some earlier studies, visualization of mucus with electron microscopy led to “drying out” the sample<sup>34</sup>, which we prevented by employing critical point drying—a method that



allows for a more seamless transition from liquid to gas. The honeycomb scaffolds were the largest of the three structures—with a pseudo-hexagonal geometry distinct from the circular pores—and appeared to house the other two. We named this structure based on similar geometries in nature, such as in honeycombs or the eyes of insects, that is mathematically hypothesized to be optimal for material efficiency and structural strength (among other benefits)<sup>60-62</sup>. The pores (also referred to as “mesh size” in the literature) were more circular and uniform. We also noticed a lack of micropores in the albumin and collagen controls, which are far more homogeneous and appear to have mostly sheet- or string-like structures, which are characteristic of albumin and collagen, respectively<sup>32,33</sup>. While honeycombs, pores, and micropores were identified in at least one BGM and one NM sample each, only the BGM from one organoid line (hu007) contained all three. Conversely, there was one native mucus sample in which only pores could be identified. These findings underscore the role of sample variability, which could be caused by patient-specific factors, factors associated with sample collection or preparation, or—for BGM—organoid differentiation state. Overall, our data indicate that the BGM and NM have internal structures similar to those reported in other studies and differ from mucus-free control samples.

Rheological characterization allowed us to assess the viscoelastic properties of our BGM and NM samples. We found a higher steady-shear viscosity, i.e., resistance to deformation, in the NM compared to the BGM. The lower viscosity in BGM may indicate a need for *in vitro* enhancement of viscosity, possibly investigating of the impact of drugs such as tetracycline<sup>63-65</sup>. In both samples, however, the negative slopes reflect the shear-thinning behavior of mucus and other non-Newtonian fluids, as the viscosity decreases with increasing shear rate (Fig. 4A). Shear-thinning is an important property of *in vivo* gastric mucus, particularly in the contexts of

bacterial perturbation<sup>42</sup> and digestive intraluminal flow<sup>66</sup>. *In vitro*, a delicate balance exists between shear forces from media changes and airflow (at the ALI) that might negatively impact mucus viscosity<sup>67</sup>, and mechanical forces such as those involved in cell-cell adhesion that might enhance mucus viscosity for protective purposes<sup>68,69</sup>. The viscoelastic moduli, which we probed using frequency sweeps in the linear viscoelastic region, can span several orders of magnitude in mucus gels<sup>70</sup>. The slopes of the elastic moduli did not differ significantly between the NM and BGM ( $p=0.3019$ ), nor did the slopes of the viscous moduli ( $p=0.8266$ ). These data therefore indicate similar elastic gel behavior in both mucus samples<sup>71</sup>, and are in agreement with previous studies of mucus gels<sup>2,3,70,72</sup>.  $\tan \delta$  is the ratio of viscous to elastic moduli ( $G''/G'$ ) and provides insight into the relative contributions of the viscous ( $G''$ ) and elastic ( $G'$ ) components of a material to its frequency-dependent behavior<sup>73</sup>.  $\tan \delta < 1$  indicated that both the NM and BGM were predominantly elastic, with no significant difference between samples ( $p=0.2209$ ). Notably, the mucus samples used in this study were never homogenized due to the limited availability of samples and the unknown structural damage that homogenization may induce. Native mucus, with all its contaminants, was the most visually heterogeneous. Subsequently, we used a representative portion of the sample (the clear gel) and an appropriately-sized parallel plate geometry that was accommodating of a wider range of sample sizes. Future studies might include less invasive methods for probing the rheological properties of BGM, such as *in situ* piezoelectric sensors built into a culture plate<sup>74</sup>. Due to such limited sample volume, particle tracking microrheology (Chapter 3) may be another feasible solution for *in situ* rheological characterization. More research is necessary to investigate the shear history of mucus gels for the most accurate rheological characterization.

While the precise mechanism by which gastric acid is transported without diffusing back across the mucus layer to the lumen is still unknown, one hypothesis is that acid released under pressure from the gastric pits can form one-way channels toward the lumen<sup>75,76</sup>. These channels are referred to as “viscous fingers”. Viscous fingering (also known as the Saffman-Taylor instability) is a hydrodynamic instability in which a less viscous fluid displaces a more viscous one<sup>38</sup>. The flow of a less viscous fluid through a more viscous one should create a phase separation with two distinct regions: viscous (the displaced fluid) and non-viscous (the displacing fluid). However, when the displaced fluid is not a viscoelastic gel such as mucus, the front remains stable, as seen with culture media in our experiments<sup>77</sup>. A previous study by Bhaksar *et al.* found that injection of HCl into a Hele-Shaw cell loaded with PGM produced viscous fingering patterns<sup>21</sup>. In mucus, viscous fingering is also the result of mucin gelation upon contact with the acid, which creates a barrier to form the channels<sup>36</sup>. To test this with BGM and NM, we injected mucus samples into a miniaturized Hele Shaw cell<sup>28</sup> and introduced acid flow. We found that both BGM and NM supported the formation of viscous fingers, as well as other associated phenomena such as tip-splitting and shielding<sup>28,37,78</sup>. The width of viscous fingers is dependent on the viscosity of the displaced fluid and the resulting interfacial stability. The higher the viscosity ratio of the displaced to the displacing fluid, the thinner the fingers will be<sup>78</sup>. As bulk rheology showed that NM viscosity was higher than that of BGM, this supports the relative finger width we observed in the Hele Shaw experiments, with the pure PGM solution having the smallest fingers.

Interestingly, in all mucus samples, we observed cessation of flow at initial flow rates below 2  $\mu\text{L}/\text{min}$  that were indicative of significant mucus gelation upon slower introduction to

the acid. While the complexity of such hydrodynamic instabilities and the factors involved are beyond the scope of this study, there may exist a relevant trade-off between flow rate and gelation. The characteristics of the fingers are likely to be dependent upon the flow rate of the invading fluid (in this case, acid) into the defending fluid (mucus), and rate by which the interaction between the two occurs will determine the difference between inlet-clogging arrest or uninterrupted flow of acid. Many factors such as flow rate, viscosity ratio, and gelation rate must be considered and some are likely to be intertwined<sup>37</sup>. Overall, our results are in qualitative agreement with the hydrodynamic phenomena reported in other studies<sup>21,28,78</sup>. To our knowledge, we are reporting the first observation of viscous fingering in native as well as organoid-derived human gastric mucus.

The collection of mucus proved to be a significant limitation of this work. Certain cell lines produced a mucus that too viscous to reliably transfer to a tube. Careful aspiration of the apical mucus is also essential to leaving the cell layer undisturbed, so the entirety of the mucus from the cell layer—particularly the portion of the mucus layer that is most adherent to the cells—could never be collected. It is also important to note that the viscoelastic properties of mucus may change once it is extracted from the epithelium. To address these challenges, future research on mucus produced at the ALI might employ more advanced *in situ* techniques for mucus analysis, such as particle tracking (Chapter 3), quantitative immunofluorescence, and optical coherence tomography<sup>6,79-81</sup>. Additionally, the high quality of 3D organoid cultures must be ensured prior to the initiation of submerged monolayer cultures to maximize the mucus yield. Future investigations could explore the effects of secretagogues such as forskolin or prostaglandin E2 on the physical properties of mucus observed through electron microscopy, as

well as their potential to enhance mucus yield<sup>82</sup>. Finally, progress has been made toward optimization of an organoid differentiation protocol for more biorelevant *in vitro* mucus models, but more work remains to be done in selecting for the most experimentally relevant phenotypes<sup>40</sup>.

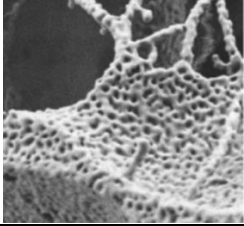
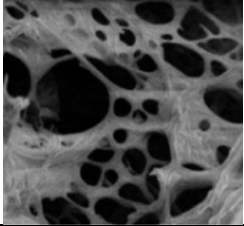
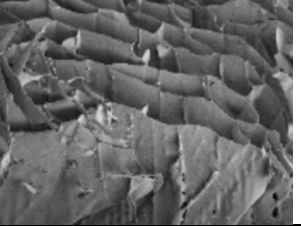
In this study, we have characterized bioengineered gastric mucus (BGM) and have compared it to native gastric mucus (NM) from patient samples. BGM has a similar secretome and viscoelastic gel behavior as NM and sustained viscous fingering patterns typical of mucus gels. BGM has potential, as an *in vitro* mucus layer model, to provide a sterile and accessible mucus for applications in bacterial pathogenesis and drug development studies.

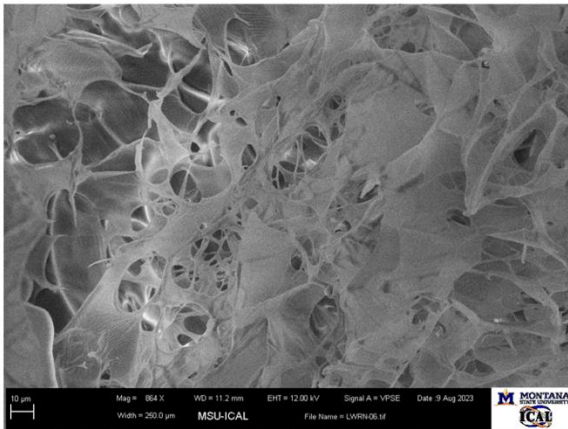
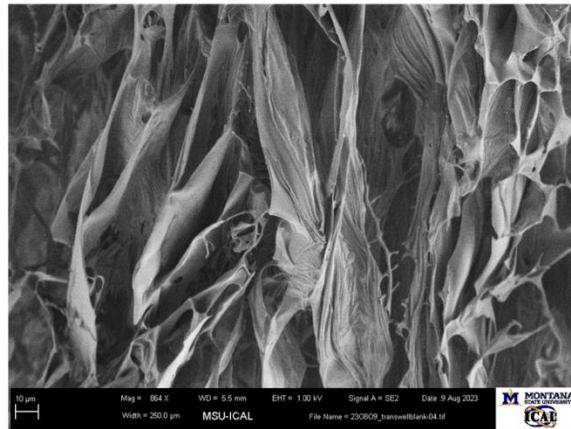
Supplementary Materials

Supplementary Table 4.1. Proteins shared by or exclusively found in either BGM/NM.

BGM	Both	NM
Bovine albumin Contaminant from culture media FBS	Human albumin Blood/plasma contamination	Myosin Cytoskeletal debris
Olfactomedin 4 Gastric stem cell marker	Gastrokinase Mucosal homeostasis/protection	Beta actin Cytoskeletal debris
Alpha-fetoprotein Stem cell/regenerative marker	TFF2 Mucosal protection/repair	Alpha-1-globin Blood contamination
Lactotransferrin Antimicrobial peptide	Lipase Mucosal protection/repair	Aldo-keto-reductase Lipid metabolism/detox
Antithrombin-III Contaminant from culture media FBS	Gastricsin Form of pepsinogen	Alpha-actinin-4 Cytoskeletal debris
Gelsolin (Isoform 4) Actin-modulating protein	Lysozyme Antimicrobial enzyme	Gelsolin (Isoform 2) Actin-modulating protein
Plasminogen Contaminant from culture media FBS		IgGFc-binding protein Pathogen neutralization
Pregnancy zone protein Contaminant from culture media FBS		TFF1 Mucosal surface protection
		Pepsin Chief cell pepsinogen

Supplementary Table 4.2. Structures identified by CryoFE-SEM.

Name	Micropores	Pores	Honeycomb Scaffold
Example			
Area (nm <sup>2</sup> )	1-100	200-12,000	5,000-300,000
Feret's Diameter (nm)	50-500	600-12,000	5,000-100,000
Description	Appear on the flap-like structures between pores and honeycomb scaffolds.	Such pores are also referred to in the literature as “mucus pores”, “mesh space”, and “mesh size”.	In some samples, the honeycomb “flaps” have housed the micropores. Appear as cave-like structures which can complicate automated detection.

**A****B**

Supplemental Figure S4.1. Controls for CryoFE-SEM. (A) L-WRN culture media. (B) L-WRN culture media collected from a blank, collagen-coated Transwell.

Acknowledgements

This project was supported by National Institutes of Health awards R01 GM131408-01 (to D.B., R.B., and J.N.W.), U01 EB029242 (to D.B. and J.N.W.), and TL1 TR002319 (to K.N.L.), an MSU Research Expansion Award (to D.B. and B.S.) and a Kopriva graduate student fellowship (to K.N.L.). We would like to thank Dr. Heidi Smith for her assistance with imaging and acknowledge the Center for Biofilm Engineering Bioimaging Facility at Montana State University, which is supported by funding from the National Science Foundation MRI Program (2018562), the M.J. Murdock Charitable Trust (202016116), the US Department of Defense (77369LSRIP & W911NF1910288), and by the Montana Nanotechnology Facility (an NNCI member supported by NSF Grant ECCS-2025391). We would also like to thank Dr. Farimah Moghimpour for assisting with immunohistochemical staining.



### References Cited

- 1 Takafumi, I., T., Kazuhiko, I. Protective Effects of Gastric Mucus. *Gastritis and Gastric Cancer* (2011). <https://doi.org/10.5772/23951>
- 2 Wagner, C. E. *et al.* Comparison of Physicochemical Properties of Native Mucus and Reconstituted Mucin Gels. *Biomacromolecules* **24**, 628-639 (2023). <https://doi.org/10.1021/acs.biomac.2c01016>
- 3 Bansil, R., Celli, J. P., Hardcastle, J. M. & Turner, B. S. The Influence of Mucus Microstructure and Rheology in *Helicobacter pylori* Infection. *Front Immunol* **4**, 310 (2013). <https://doi.org/10.3389/fimmu.2013.00310>
- 4 Bansil, R. & Turner, B. S. in *Advanced Drug Delivery Reviews* Vol. 124 3-15 (Elsevier B.V., 2018).
- 5 Izadifar, Z. *et al.* Modeling mucus physiology and pathophysiology in human organs-on-chips. *Adv Drug Deliv Rev* **191**, 114542 (2022). <https://doi.org/10.1016/j.addr.2022.114542>
- 6 Cai, P. C. *et al.* Air–liquid intestinal cell culture allows in situ rheological characterization of intestinal mucus. *APL Bioengineering* **8**, 026112 (2024). <https://doi.org/10.1063/5.0187974>
- 7 Derricott, H. *et al.* Developing a 3D intestinal epithelium model for livestock species. *Cell and tissue research* (2019). <https://doi.org/10.1007/s00441-018-2924-9>
- 8 Celli, J. P. *et al.* *Helicobacter pylori* moves through mucus by reducing mucin viscoelasticity. *Proc Natl Acad Sci U S A* **106**, 14321-14326 (2009). <https://doi.org/10.1073/pnas.0903438106>
- 9 Ambrosini, Y. M. *et al.* Recapitulation of the accessible interface of biopsy-derived canine intestinal organoids to study epithelial-luminal interactions. *PLoS One* **15**, e0231423 (2020). <https://doi.org/10.1371/journal.pone.0231423>

- 10 Dedhia, P. H., Bertaux-Skeirik, N., Zavros, Y. & Spence, J. R. Organoid Models of Human Gastrointestinal Development and Disease. *Gastroenterology* **150**, 1098-1112 (2016). <https://doi.org/10.1053/j.gastro.2015.12.042>
- 11 VanDussen, K. L. *et al.* Development of an enhanced human gastrointestinal epithelial culture system to facilitate patient-based assays. *Gut* **64**, 911-920 (2015). <https://doi.org/10.1136/gutjnl-2013-306651>
- 12 Lyon, K., Bansil, R. & Bimczok, D. Profiling Luminal pH in Three-Dimensional Gastrointestinal Organoids Using Microelectrodes. *J Vis Exp* (2024). <https://doi.org/10.3791/66900>
- 13 Boccellato, F. *et al.* Polarised epithelial monolayers of the gastric mucosa reveal insights into mucosal homeostasis and defence against infection. *Gut* **68**, 400-413 (2019). <https://doi.org/10.1136/gutjnl-2017-314540>
- 14 Wang, Y., Kim, R., Sims, C. E. & Allbritton, N. L. Building a Thick Mucus Hydrogel Layer to Improve the Physiological Relevance of In Vitro Primary Colonic Epithelial Models. *Cellular and Molecular Gastroenterology and Hepatology* **8**, 653-655.e655 (2019). <https://doi.org/10.1016/j.jcmgh.2019.07.009>
- 15 Sebrell, T. A. *et al.* Live imaging analysis of human gastric epithelial spheroids reveals spontaneous rupture, rotation and fusion events. *Cell and Tissue Research* **371**, 293-307 (2018). <https://doi.org/10.1007/s00441-017-2726-5>
- 16 Sebrell, T. A. *et al.* A Novel Gastric Spheroid Co-culture Model Reveals Chemokine-Dependent Recruitment of Human Dendritic Cells to the Gastric Epithelium. *Cellular and Molecular Gastroenterology and Hepatology* **8**, 157-171.e153 (2019). <https://doi.org/10.1016/j.jcmgh.2019.02.010>
- 17 Cherne, M. D. *et al.* A Synthetic Hydrogel, VitroGel® ORGANOID-3, Improves Immune Cell-Epithelial Interactions in a Tissue Chip Co-Culture Model of Human Gastric Organoids and Dendritic Cells. *Frontiers in Pharmacology* **12** (2021). <https://doi.org/10.3389/fphar.2021.707891>
- 18 Miyoshi, H. & Stappenbeck, T. S. In vitro expansion and genetic modification of gastrointestinal stem cells in spheroid culture. *Nat Protoc* **8**, 2471-2482 (2013). <https://doi.org/10.1038/nprot.2013.153>

- 19 Bej, R. & Haag, R. Mucus-Inspired Dynamic Hydrogels: Synthesis and Future Perspectives. *Journal of the American Chemical Society* **144**, 20137-20152 (2022). <https://doi.org/10.1021/jacs.1c13547>
- 20 Liao, W. & Aranson, I. S. Viscoelasticity enhances collective motion of bacteria. *PNAS Nexus* **2**, pgad291 (2023). <https://doi.org/10.1093/pnasnexus/pgad291>
- 21 Bhaskar, K. R. *et al.* Viscous fingering of HCl through gastric mucin. *Nature* **360**, 458-461 (1992). <https://doi.org/10.1038/360458a0>
- 22 Dubbelboer, I. R. *et al.* Gastrointestinal mucus in dog: Physiological characteristics, composition, and structural properties. *Eur J Pharm Biopharm* **173**, 92-102 (2022). <https://doi.org/10.1016/j.ejpb.2022.02.019>
- 23 Thim, L., Madsen, F. & Poulsen, S. S. Effect of trefoil factors on the viscoelastic properties of mucus gels. *European Journal of Clinical Investigation* **32**, 519-527 (2002). <https://doi.org/https://doi.org/10.1046/j.1365-2362.2002.01014.x>
- 24 Wykoff, J. A. *et al.* Rapid Viscoelastic Characterization of Airway Mucus Using a Benchtop Rheometer. *J Vis Exp* (2022). <https://doi.org/10.3791/63876>
- 25 Bansil, R., Stanley, E. & LaMont, J. T. Mucin biophysics. *Annu Rev Physiol* **57**, 635-657 (1995). <https://doi.org/10.1146/annurev.ph.57.030195.003223>
- 26 Al-kaby, R. N. *et al.* Rheo-NMR of transient and steady state shear banding under shear startup. *Journal of Rheology* **62**, 1125-1134 (2018). <https://doi.org/10.1122/1.5037594>
- 27 Støvring Mortensen, J., Saaby, L., Harloff-Helleberg, S. & Mørck Nielsen, H. Barrier properties of ex vivo porcine intestinal mucus are highly independent of isolation and storage conditions. *Eur J Pharm Biopharm* **174**, 106-110 (2022). <https://doi.org/10.1016/j.ejpb.2022.03.015>
- 28 Zhang, Q., Amooie, A., Bazant, M. Z. & Bischofberger, I. Growth morphology and symmetry selection of interfacial instabilities in anisotropic environments. *Soft Matter* **17**, 1202-1209 (2021). <https://doi.org/10.1039/d0sm01706j>

- 29 Alqatari, S., Videbæk, T. E., Nagel, S. R., Hosoi, A. & Bischofberger, I. Confined Rayleigh-Taylor instability. *Physical Review Fluids* **7**, 110504 (2022). <https://doi.org/10.1103/PhysRevFluids.7.110504>
- 30 Sebrell, T. A. *et al.* Live imaging analysis of human gastric epithelial spheroids reveals spontaneous rupture, rotation and fusion events. *Cell and tissue research* **371**, 293-307 (2018). <https://doi.org/10.1007/s00441-017-2726-5>
- 31 Barmapsalou, V. *et al.* Development and validation of a porcine artificial colonic mucus model reflecting the properties of native colonic mucus in pigs. *European Journal of Pharmaceutical Sciences* **181**, 106361 (2023). <https://doi.org/https://doi.org/10.1016/j.ejps.2022.106361>
- 32 Farran, A. J. *et al.* Effects of matrix composition, microstructure, and viscoelasticity on the behaviors of vocal fold fibroblasts cultured in three-dimensional hydrogel networks. *Tissue Eng Part A* **16**, 1247-1261 (2010). <https://doi.org/10.1089/ten.tea.2009.0344>
- 33 Li, P.-S. *et al.* A Novel Albumin-Based Tissue Scaffold for Autogenic Tissue Engineering Applications. *Scientific Reports* **4**, 5600 (2014). <https://doi.org/10.1038/srep05600>
- 34 Meziu, E. *et al.* Visualization of the structure of native human pulmonary mucus. *Int J Pharm* **597**, 120238 (2021). <https://doi.org/10.1016/j.ijpharm.2021.120238>
- 35 Lai, S. K., Wang, Y. Y., Wirtz, D. & Hanes, J. Micro- and macrorheology of mucus. *Adv Drug Deliv Rev* **61**, 86-100 (2009). <https://doi.org/10.1016/j.addr.2008.09.012>
- 36 Bunton, P. H., Tullier, M. P., Meiburg, E. & Pojman, J. A. The effect of a crosslinking chemical reaction on pattern formation in viscous fingering of miscible fluids in a Hele-Shaw cell. *Chaos: An Interdisciplinary Journal of Nonlinear Science* **27**, 104614 (2017). <https://doi.org/10.1063/1.5001285>
- 37 Hirano, S., Nagatsu, Y. & Suzuki, R. X. Reversal of effects from gel production in a reacting flow dependent on gel strength. *Physical Review Fluids* **7**, 023201 (2022). <https://doi.org/10.1103/PhysRevFluids.7.023201>
- 38 Singh, A., Singh, Y. & Pandey, K. M. Viscous fingering instabilities in radial Hele-Shaw cell: A review. *Materials Today: Proceedings* **26**, 760-762 (2020). <https://doi.org/https://doi.org/10.1016/j.matpr.2020.01.022>

- 39 Fabricius, J., Manjate, S. & Wall, P. On pressure-driven Hele–Shaw flow of power-law fluids. *Applicable Analysis* **101**, 5107-5137 (2022).  
<https://doi.org/10.1080/00036811.2021.1880570>
- 40 Wolffling, S. *et al.* EGF and BMPs Govern Differentiation and Patterning in Human Gastric Glands. *Gastroenterology* **161**, 623-636 e616 (2021).  
<https://doi.org/10.1053/j.gastro.2021.04.062>
- 41 Kauffman, G. L., Jr. Gastric mucus and bicarbonate secretion in relation to mucosal protection. *J Clin Gastroenterol* **3**, 45-50 (1981).
- 42 Celli, J. P. *et al.* Rheology of Gastric Mucin Exhibits a pH-Dependent Sol–Gel Transition. *Biomacromolecules* **8**, 1580-1586 (2007). <https://doi.org/10.1021/bm0609691>
- 43 Boltin, D. & Niv, Y. Mucins in Gastric Cancer - An Update. *J Gastrointest Dig Syst* **3**, 15519 (2013). <https://doi.org/10.4172/2161-069x.1000123>
- 44 McShane, A. *et al.* Mucus. *Curr Biol* **31**, R938-R945 (2021).  
<https://doi.org/10.1016/j.cub.2021.06.093>
- 45 Marques, T., David, L., Reis, C. & Nogueira, A. Topographic expression of MUC5AC and MUC6 in the gastric mucosa infected by *Helicobacter pylori* and in associated diseases. *Pathology - Research and Practice* **201**, 665-672 (2005).  
<https://doi.org/https://doi.org/10.1016/j.prp.2005.03.007>
- 46 Ho, S. B. *et al.* The adherent gastric mucous layer is composed of alternating layers of MUC5AC and MUC6 mucin proteins. *Digestive Diseases and Sciences* (2004).  
<https://doi.org/10.1023/B:DDAS.0000043371.12671.98>
- 47 Hoffmann, W. Trefoil Factor Family (TFF) Peptides and their Different Roles in the Mucosal Innate Immune Defense and More: An Update. *Curr Med Chem* **28**, 7387-7399 (2021). <https://doi.org/10.2174/0929867328666210215114140>
- 48 Peterson, A. J. *et al.* *Helicobacter pylori* infection promotes methylation and silencing of trefoil factor 2, leading to gastric tumor development in mice and humans. *Gastroenterology* **139**, 2005-2017 (2010). <https://doi.org/10.1053/j.gastro.2010.08.043>

- 49 Jeong, H. J. *et al.* Organoid-Based Human Stomach Micro-Physiological System to Recapitulate the Dynamic Mucosal Defense Mechanism. *Adv Sci (Weinh)* **10**, e2300164 (2023). <https://doi.org/10.1002/advs.202300164>
- 50 Hu, G. Y. *et al.* Expression of TFF2 and Helicobacter pylori infection in carcinogenesis of gastric mucosa. *World J Gastroenterol* **9**, 910-914 (2003). <https://doi.org/10.3748/wjg.v9.i5.910>
- 51 Kawakubo, M. *et al.* Natural antibiotic function of a human gastric mucin against Helicobacter pylori infection. *Science* **305**, 1003-1006 (2004). <https://doi.org/10.1126/science.1099250>
- 52 Agarwal, K. *et al.* Inhibition of mucin-type O-glycosylation through metabolic processing and incorporation of N-thioglycolyl-D-galactosamine peracetate (Ac5GalNTGc). *J Am Chem Soc* **135**, 14189-14197 (2013). <https://doi.org/10.1021/ja405189k>
- 53 Nordman, H. *et al.* Gastric MUC5AC and MUC6 are large oligomeric mucins that differ in size, glycosylation and tissue distribution. *Biochem J* **364**, 191-200 (2002). <https://doi.org/10.1042/bj3640191>
- 54 Rossez, Y. *et al.* Almost all human gastric mucin O-glycans harbor blood group A, B or H antigens and are potential binding sites for Helicobacter pylori. *Glycobiology* **22**, 1193-1206 (2012). <https://doi.org/10.1093/glycob/cws072>
- 55 Kirch, J. *et al.* Optical tweezers reveal relationship between microstructure and nanoparticle penetration of pulmonary mucus. *Proc Natl Acad Sci U S A* **109**, 18355-18360 (2012). <https://doi.org/10.1073/pnas.1214066109>
- 56 Gross, A. *et al.* A foam model highlights the differences of the macro- and microrheology of respiratory horse mucus. *J Mech Behav Biomed Mater* **71**, 216-222 (2017). <https://doi.org/10.1016/j.jmbbm.2017.03.009>
- 57 Boegh, M., Foged, C., Müllertz, A. & Mørck Nielsen, H. Mucosal drug delivery: barriers, in vitro models and formulation strategies. *Journal of Drug Delivery Science and Technology* **23**, 383-391 (2013). [https://doi.org/https://doi.org/10.1016/S1773-2247\(13\)50055-4](https://doi.org/https://doi.org/10.1016/S1773-2247(13)50055-4)

- 58 Nazende, G. T., Akif, E. T. & Marc, S. Inhalable Antibiotic Nanoformulations for the Treatment of *Pseudomonas Aeruginosa* Infection in Cystic Fibrosis – A Review. *Drug Delivery Letters* **4**, 193-207 (2014).  
<https://doi.org/http://dx.doi.org/10.2174/2210303104666140222002101>
- 59 Vukosavljevic, B. *et al.* Tracing molecular and structural changes upon mucolysis with N-acetyl cysteine in human airway mucus. *Int J Pharm* **533**, 373-376 (2017).  
<https://doi.org/10.1016/j.ijpharm.2017.07.022>
- 60 Rätz, T. The silent hexagon: explaining comb structures. *Synthese* **194**, 1703-1724 (2017).  
<https://doi.org/10.1007/s11229-016-1014-3>
- 61 Zhang, Q. *et al.* Bioinspired engineering of honeycomb structure – Using nature to inspire human innovation. *Progress in Materials Science* **74**, 332-400 (2015).  
<https://doi.org/https://doi.org/10.1016/j.pmatsci.2015.05.001>
- 62 Kim, S., Cassidy, J. J., Yang, B., Carthew, R. W. & Hilgenfeldt, S. Hexagonal Patterning of the Insect Compound Eye: Facet Area Variation, Defects, and Disorder. *Biophysical Journal* **111**, 2735-2746 (2016). <https://doi.org/10.1016/j.bpj.2016.11.004>
- 63 Linssen, R. S. N., Ma, J., Bem, R. A. & Rubin, B. K. Rational use of mucoactive medications to treat pediatric airway disease. *Paediatr Respir Rev* **36**, 8-14 (2020).  
<https://doi.org/10.1016/j.prrv.2020.06.007>
- 64 Rubin, B. K. Mucus and Mucins. *Otolaryngologic Clinics of North America* **43**, 27-34 (2010). <https://doi.org/https://doi.org/10.1016/j.otc.2009.11.002>
- 65 Phillips, G. J., James, S. L. & Lethem, M. I. in *Airway Mucus: Basic Mechanisms and Clinical Perspectives* (eds Duncan F. Rogers & Michael I. Lethem) 117-147 (Birkhäuser Basel, 1997).
- 66 O'Farrell, C., Stamatopoulos, K., Simmons, M. & Batchelor, H. In vitro models to evaluate ingestible devices: Present status and current trends. *Advanced Drug Delivery Reviews* **178**, 113924 (2021). <https://doi.org/https://doi.org/10.1016/j.addr.2021.113924>
- 67 Delon, L. C. *et al.* A systematic investigation of the effect of the fluid shear stress on Caco-2 cells towards the optimization of epithelial organ-on-chip models. *Biomaterials* **225**, 119521 (2019). <https://doi.org/https://doi.org/10.1016/j.biomaterials.2019.119521>

- 68 He, H. *et al.* Piezo channels in the intestinal tract. *Frontiers in Physiology* **15** (2024). <https://doi.org/10.3389/fphys.2024.1356317>
- 69 Button, B. & Boucher, R. C. Role of mechanical stress in regulating airway surface hydration and mucus clearance rates. *Respir Physiol Neurobiol* **163**, 189-201 (2008). <https://doi.org/10.1016/j.resp.2008.04.020>
- 70 Jory, M. *et al.* Mucus from human bronchial epithelial cultures: rheology and adhesion across length scales. *Interface Focus* **12**, 20220028 (2022). <https://doi.org/10.1098/rsfs.2022.0028>
- 71 Nnyigide, O. S. & Hyun, K. A comprehensive review of food rheology: analysis of experimental, computational, and machine learning techniques. *Korea-Australia Rheology Journal* **35**, 279-306 (2023). <https://doi.org/10.1007/s13367-023-00075-w>
- 72 MacAdam, A. The effect of gastro-intestinal mucus on drug absorption. *Advanced Drug Delivery Reviews* **11**, 201-220 (1993). [https://doi.org/https://doi.org/10.1016/0169-409X\(93\)90010-2](https://doi.org/https://doi.org/10.1016/0169-409X(93)90010-2)
- 73 Meldrum, O. W. *et al.* Mucin gel assembly is controlled by a collective action of non-mucin proteins, disulfide bridges, Ca<sup>2+</sup>-mediated links, and hydrogen bonding. *Scientific Reports* **8**, 5802 (2018). <https://doi.org/10.1038/s41598-018-24223-3>
- 74 Zhang, J. *et al.* Rapid, autonomous high-throughput characterization of hydrogel rheological properties via automated sensing and physics-guided machine learning. *Applied Materials Today* **30**, 101720 (2023). <https://doi.org/https://doi.org/10.1016/j.apmt.2022.101720>
- 75 Allen, A. & Flemström, G. in *American Journal of Physiology - Cell Physiology* (2005).
- 76 Johansson, M. E., Sjövall, H. & Hansson, G. C. The gastrointestinal mucus system in health and disease. *Nat Rev Gastroenterol Hepatol* **10**, 352-361 (2013). <https://doi.org/10.1038/nrgastro.2013.35>
- 77 Cvetkovic, I. & Milicev, S. Pore-scale viscous fingering as a mechanism for pattern formation – a historical overview, application, and the ways of controlling it. *Advances in Physics: X* **9**, 2370838 (2024). <https://doi.org/10.1080/23746149.2024.2370838>



- 78 Bischofberger, I., Ramachandran, R. & Nagel, S. R. An island of stability in a sea of fingers: emergent global features of the viscous-flow instability. *Soft Matter* **11**, 7428-7432 (2015). <https://doi.org/10.1039/c5sm00943j>
- 79 Huang, H. *et al.* Integrating optical coherence tomography with gravimetric and video analysis (OCT-Gravimetry-Video method) for studying the drying process of polystyrene latex system. *Scientific Reports* **8**, 12962 (2018). <https://doi.org/10.1038/s41598-018-30914-8>
- 80 Pieper, M. *et al.* Intravital imaging of mucus transport in asthmatic mice using microscopic optical coherence tomography. *Am J Physiol Lung Cell Mol Physiol* **323**, L423-l430 (2022). <https://doi.org/10.1152/ajplung.00455.2021>
- 81 Krajina, B. A. *et al.* Dynamic Light Scattering Microrheology Reveals Multiscale Viscoelasticity of Polymer Gels and Precious Biological Materials. *ACS Central Science* **3**, 1294-1303 (2017). <https://doi.org/10.1021/acscentsci.7b00449>
- 82 Zomer-van Ommen, D. D. *et al.* Comparison of ex vivo and in vitro intestinal cystic fibrosis models to measure CFTR-dependent ion channel activity. *J Cyst Fibros* **17**, 316-324 (2018). <https://doi.org/10.1016/j.jcf.2018.02.007>

CHAPTER FIVE

A HIGH-THROUGHPUT METABOLIC MICROARRAY ASSAY  
REVEALS ANTIBACTERIAL EFFECTS OF BLACK AND RED  
RASPBERRIES AGAINST *HELICOBACTER PYLORI*  
INFECTION

Contribution of Authors and Co-Authors

Manuscript in Chapter 5

Author: Candace Goodman

Contributions: Conceptualization and methodology, investigation, formal analysis, original manuscript preparation, manuscript review and editing, funding acquisition

Co-Author: Katrina Lyon

Contributions: Investigation, formal analysis, original manuscript preparation, manuscript review and editing

Co-Author: Aitana Scotto

Contributions: Investigation, manuscript review and editing

Co-Author: Cyra Smith

Contributions: Investigation, manuscript review and editing

Co-Author: Thomas A. Sebrell

Contributions: Investigation, manuscript review and editing

Co-Author: Andrew B. Gentry

Contributions: Investigation, manuscript review and editing

Co-Author: Ganesh Bala

Contributions: Investigation, formal analysis, manuscript review and editing

Co-Author: Gary D. Stoner

Contributions: Conceptualization and methodology, formal analysis, original manuscript preparation, manuscript review and editing, funding acquisition

Co-Author: Diane Bimczok

Contributions: Conceptualization and methodology, investigation, formal analysis, original manuscript preparation, manuscript review and editing, funding acquisition

Manuscript Information

Candace Goodman, **Katrina N. Lyon**, Aitana Scotto, Cyra Smith, Thomas A. Sebrell, Andrew B. Gentry, Ganesh Bala, Gary D. Stoner, Diane Bimczok

Antibiotics

Status of Manuscript:

- ☐ Prepared for submission to a peer-reviewed journal
- ☐ Officially submitted to a peer-reviewed journal
- ☐ Accepted by a peer-reviewed journal
- ☒ Published in a peer-reviewed journal

MDPI

July 12<sup>th</sup>, 2021

Volume 10

DOI: 10.3390/antibiotics10070845

Abstract

*Helicobacter pylori* infection is commonly treated with a combination of antibiotics and proton pump inhibitors. However, since *H. pylori* is becoming increasingly resistant to standard antibiotic regimens, novel treatment strategies are needed. Previous studies have demonstrated that black and red berries may have antibacterial properties. Therefore, we analyzed the antibacterial effects of black and red raspberries and blackberries on *H. pylori*. Freeze-dried powders and organic extracts from black and red raspberries and blackberries were prepared, and high-performance liquid chromatography was used to measure the concentrations of anthocyanins, which are considered the major active ingredients. To monitor antibiotic effects of the berry preparations on *H. pylori*, a high-throughput metabolic growth assay based on the Biolog system was developed and validated with the antibiotic metronidazole. Biocompatibility was analyzed using human gastric organoids. All berry preparations tested had significant bactericidal effects *in vitro*, with MIC90 values ranging from 0.49 to 4.17%. Antimicrobial activity was higher for extracts than powders and appeared to be independent of the anthocyanin concentration. Importantly, human gastric epithelial cell viability was not negatively impacted by black raspberry extract applied at the concentration required for complete bacterial growth inhibition. Our data suggest that black and red raspberry and blackberry extracts may have potential applications in the treatment and prevention of *H. pylori* infection but differ widely in their MICs. Moreover, we demonstrate that the Biolog metabolic assay is suitable for high-throughput antimicrobial susceptibility screening of *H. pylori*.

### Introduction

*Helicobacter pylori* is the major cause of human gastric disease worldwide<sup>1,2</sup>. *H. pylori* is an acid-resistant, Gram-negative bacterium that persistently infects the gastric mucosa of approximately half the world's population, leading to chronic active gastritis<sup>1</sup>. A proportion of infected individuals also develop peptic ulcer disease, autoimmune gastritis or gastric adenocarcinoma, the second leading cause of cancer-related mortality<sup>3</sup>. In spite of decades of active research, no effective vaccine to prevent *H. pylori*-associated illnesses has been developed<sup>4</sup>. Once diagnosed, *H. pylori* infection is generally treated with a combination of antibiotics and proton pump inhibitors. However, increased resistance to two of the standard antibiotics included in *H. pylori* treatment regimens, clarithromycin and metronidazole, has been reported in multiple studies, with resistance rates ranging from 22 to 80%<sup>5,6</sup>. Recently, clarithromycin-resistant *H. pylori* was included in the WHO's high-priority pathogens list for research and development of new antibiotics<sup>7</sup>. Moreover, poor patient compliance with complex medication regimens contributes to decreased treatment success<sup>8,9</sup>. Therefore, eradication rates of *H. pylori* have dropped below 75% in several countries<sup>10,11</sup>. The high failure rate of traditional *H. pylori* therapies points to an urgent need for novel alternative treatments or preventative strategies to combat *H. pylori* infection<sup>12</sup>.

A significant body of research in recent years has shown that natural dietary components, especially plants, contain many bioactive compounds—nutraceuticals—with antibacterial effects<sup>13-15</sup>. Multiple different berries and their products show significant antimicrobial activity in vitro and in vivo, and some promising studies suggesting effectiveness against *H. pylori* have been published. Thus, data by Chatterjee et al.<sup>16</sup> showed significant inhibition of *H. pylori* growth in

the presence of extracts from rasp- berry, strawberry, cranberry, elderberry, blueberry and bilberry. In another recent study, extracts from unripe Korean raspberries and elm tree bark used in combination significantly suppressed *H. pylori* growth both in vitro and in a mouse model<sup>17</sup>. Amongst the multiple bioactive natural compounds, anthocyanins in colored berries of the genus *Rubus* have attracted special attention. Anthocyanins are glycosylated, water-soluble phenolic compounds that are responsible for the red, purple and blue coloring of multiple berry species<sup>14</sup>. Anthocyanins are strong antioxidants that have been used successfully in cancer chemoprevention models<sup>18</sup> and that have been implicated in the antibacterial activities of berry preparations<sup>19,20</sup>. In an in vitro model of *H. pylori* infection, the anthocyanin cyanidin 3-*O*-glucoside significantly decreased *H. pylori*-induced cell death<sup>21</sup>. Since anthocyanin-containing berry products also have proven anti-inflammatory effects and are stable under acidic conditions<sup>22,23</sup>, their potential application in gastric *H. pylori* infection is particularly attractive.

In our study, we developed a high-throughput metabolic assay to screen different black raspberry, red raspberry and blackberry preparations for their ability to prevent *H. pylori* growth in vitro. In addition, a gastric organoid model was used to evaluate the biocompatibility of black raspberry extract. Our results demonstrate that all berry powders and extracts tested caused a significant reduction in *H. pylori* growth in two different strains at concentrations between 0.5 and 3%. An optimum preparation of black raspberry extract used at 0.5% led to complete inhibition of *H. pylori* growth but did not affect the viability of primary gastric epithelial cells. These results suggest that preparations from black and red raspberries and blackberries have potential as novel antimicrobial agents to combat *H. pylori* infection.

## Results

### Analysis of Powders and Extracts of Black and Red Raspberries and Blackberries for Anthocyanin Content and Composition

In order to study the potential antibacterial effects of black raspberry (BRB), red raspberry (RRB) and blackberry (BB) compounds on *H. pylori*, freeze-dried berry powders were purchased from different suppliers or were prepared in our laboratory from fresh-frozen berries. Organic extracts of all berry powders were then prepared using hexane/ethanol extraction. The workflow for sample preparation is shown in Figure 1A, and the different starting materials used are listed in Table 1.

To determine the concentration of anthocyanins, all samples were analyzed by LC–MS for the presence of cyanidin (cyanidin-3-*O*-rutinoside), kuromanin (cyanidin-3-*O*-glucoside) and cyanidin-3-*O*-xylosyrutinoside (Table 1 and Figure 1A,B). Because of overlapping peaks, the cyanidin-3-*O*-xylosyrutinoside may include cyanidin-3-*O*-sambubioside, another phenolic berry compound that has a similar composition and MW as the xylosyl-rutinoside, and that is known to be present in BRB at a low concentration<sup>24</sup>.

Total anthocyanin content (TAC) was calculated by adding up the concentrations of all detected anthocyanins (Figure 1C and Table 1). Overall, large variations in anthocyanin concentrations were observed for berries from different sources and with different processing techniques. Interestingly, lyophilized but otherwise untreated berry powder from RRB and BB contained significantly higher amounts of anthocyanins than the water/ethanol extracts prepared in our laboratory (Figure 1C). This was likely due to an inefficient recovery of anthocyanins in extracts prepared from fresh-frozen berries that were lyophilized in-house (Figure 1D,  $p < 0.001$ ,



Student's *t* test), because anthocyanin recovery was higher if extracts were prepared from commercial berry powders (Figure 1D). Individual data for cyanidin-3-*O*-glucoside, cyanidin-3-*O*-rutinoside, and cyanidin-3-*O*-xylosylrutinoside are presented in Figure 1E and Table 2. Notably, BRB, RRB and BB powders contained similar levels of cyanidin-3-*O*-sambubioside and cyanidin-3-*O*-glucoside, but cyanidin-3-*O*-rutinoside levels were significantly higher in BRBs than in RRBs and BBs, as previously described (Figure 1E,  $p < 0.05$ , mixed model ANOVA).

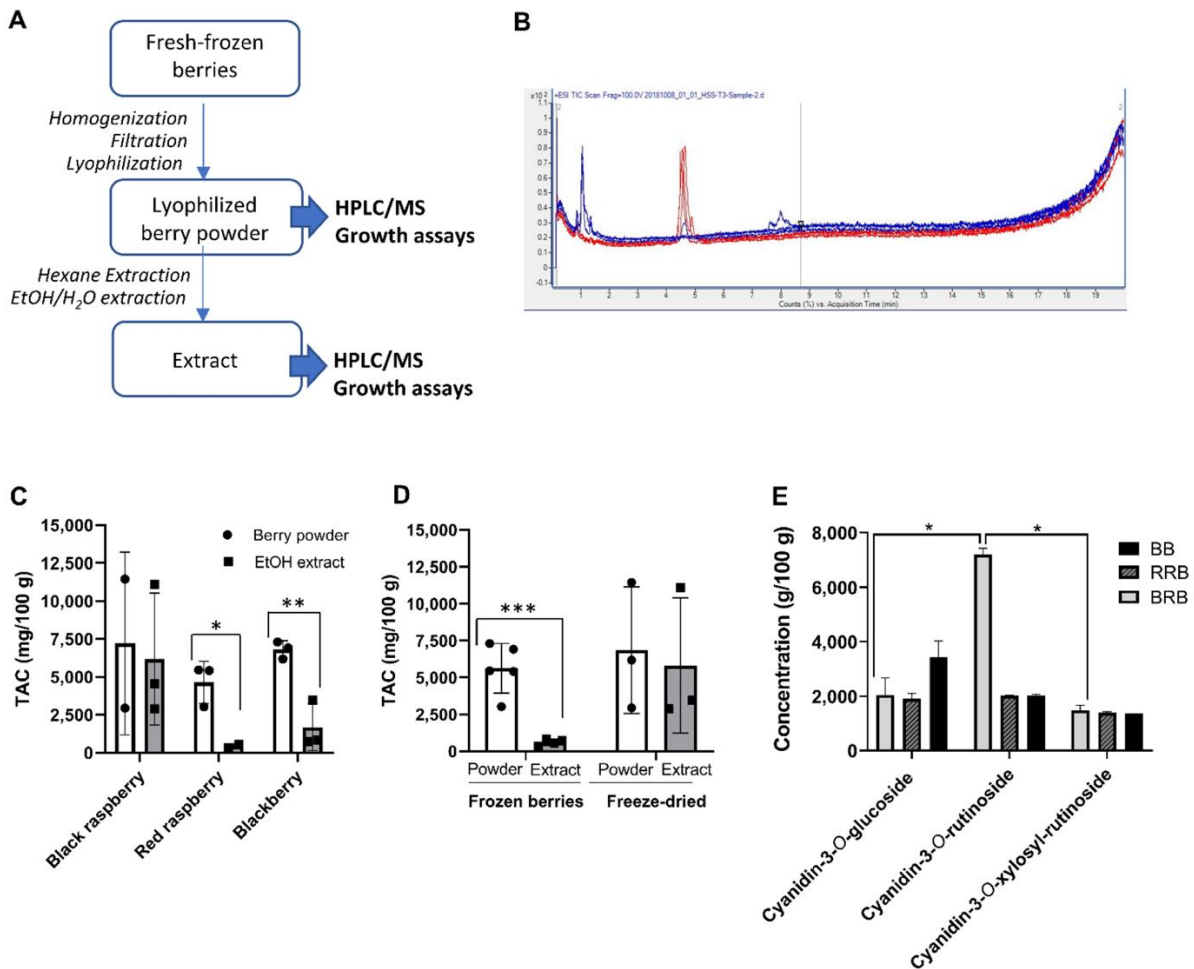


Figure 5.1. Preparation and anthocyanin content analysis of black raspberries, red raspberries and blackberries. (A) Workflow for berry preparation and analysis. (B) Representative LC-MS

spectrum of a berry preparation. Major peaks represent cyanidin-3-*O*-glucoside, cyanidin-3-*O*-rutinoside, and a combination of cyanidin-3-*O*-xylosylrutinoside and cyanidin-3-*O*-sambubioside. (C) Total anthocyanin content (TAC) in suspended powders and ethanol extracts of black raspberries, red raspberries (RRB) and blackberries (BB) determined by LC-MS. Individual data points, mean and SD are shown. (D) TAC in powders and extracts of BRB, RRB and BB purchased as fresh-frozen berries or as freeze-dried berry powder. Pooled data from all berries; individual data points, mean  $\pm$  SD are shown. (E) Concentrations of major anthocyanins in suspended powders of BRB < RRB and BB. Statistically significant differences as determined by (C,D) Student's *t* test (E) or two-way ANOVA are shown as \*  $p < 0.05$ , \*\*  $p < 0.01$ , and \*\*\*  $p < 0.001$ .

Table 5.1. Total concentrations of anthocyanins in black and red raspberry and blackberry powders and extracts determined by LC-MS. \*Absorption assumes all anthocyanins are cyanidin-3-glucoside equivalents (sum of three major cyanidins). BRB: black raspberry; RRB: red raspberry; BB: blackberry; VE: VirginExtracts; BH: BerriHealth; UMN: University of Minnesota; CH: Chile; MX: Mexico; TAC: total anthocyanin content; HPLC-MS: high-performance liquid chromatography/mass spectrometry.

Sample	Source	Country of Origin	Material Type	HPLC-MS *	
				Berry Powder TAC (mg/100 g)	Extract TAC (mg/100 g) *
VE-BRB	VirginExtracts, Foods Super, Bradford, PA, USA	Unknown	Freeze-dried powder	2945	2885
BH-BRB	BerriHealth, Berri Products LLC, Corbett, OR, USA	USA	Freeze-dried powder	11,455	11,109
UMN-BRB	Dr. S. Hecht, University of Minnesota, Minneapolis, MN, USA	USA	Ethanol extract	N/A	4540
USA-RRB	Great Value, Wal-Mart Stores Inc. Bentonville, AR, USA	USA	Whole frozen berries	5424	554

Table 5.1 Continued.

Sample	Source	Country of Origin	Material Type	HPLC-MS *	
				Berry Powder TAC (mg/100 g)	Extract TAC (mg/100 g) *
CH-RRB	Canadian Farms, Small Planet Foods, Inc., Sedro-Woolley, WA, USA	Chile	Whole frozen berries	3027	336
VE-BB	VirginExtracts, Foods Super, Bradford, PA, USA	Unknown	Freeze-dried powder	6175	3465
MX-BB	Western Family Foods Inc., Portland, OR, USA	Mexico	Whole frozen berries	6924	748
CH-BB	Cascadian Farms, Small Planet Foods, Inc., Sedro-Woolley, WA, USA	Chile	Whole frozen berries	7312	847

Table 5.2. Anthocyanin composition within powdered berries and berry extracts determined by HPLC-MS. \*BRB: black raspberry; RRB: red raspberry; BB: blackberry; VE: VirginExtracts; BH: BerriHealth; UMN: University of Minnesota; CH: Chile; MX: Mexico; TAC: total anthocyanin content; HPLC-MS: high-performance liquid chromatography/mass spectrometry.

		HPLC-MS * (mg/100 g)		
Sample		Cyanidin-3- <i>O</i> -glucoside	Cyanidin-3- <i>O</i> -rutinoside	Cyanidin-3- <i>O</i> -xylosylrutinoside
VE-BRB	Powder	1593	7025	1352
	Extract	1537	No data	1348
BH-BRB	Powder	2490	7356	1609
	Extract	2487	7025	1597
UMN-BRB	Powder	No data	No data	No data
	Extract	440	4100	2420
USA-RRB	Powder	1999	1993	1432
	Extract	355	98	101
CH-RRB	Powder	1678	No data	1349
	Extract	267	43	26
VE-BB	Powder	2806	2010	1359
	Extract	2113	No data	1352
MX-BB	Powder	3499	2076	1349
	Extract	564	121	63
CH-BB	Powder	3995	1966	1351
	Extract	748	60	39

#### Development and Validation of a High-Throughput Assay to Measure *H. pylori* Growth

A metabolic bacterial growth assay based on the Biolog system was developed to test a large number of different berry products at different concentrations. This system enables kinetic analysis of microbial growth in a 96-well format based on detection of a redox-sensitive dye by the OmniLog® incubator-reader<sup>25</sup>. Since optimal *H. pylori* growth requires microaerophilic conditions, the 96-well plates were sealed into a plastic sleeve with a CO<sub>2</sub> Gen Compact sachet to reduce oxygen levels. As shown in Figure 2A and the Supplemental Video S1, addition of *H. pylori* bacteria to the plates at different dilutions resulted in a dose-dependent color change over 48 h. Growth curves had a typical appearance, with an exponential growth phase followed by a

plateau phase (Figure 2B). Area under the curve measurements showed significant differences in the growth of *H. pylori* plated at different concentrations, which was confirmed by endpoint measurements at 590 nm in a standard ELISA reader (Figure 2C,D). These results show that *H. pylori* growth can be effectively analyzed in liquid cultures using a high-throughput metabolic growth assay.

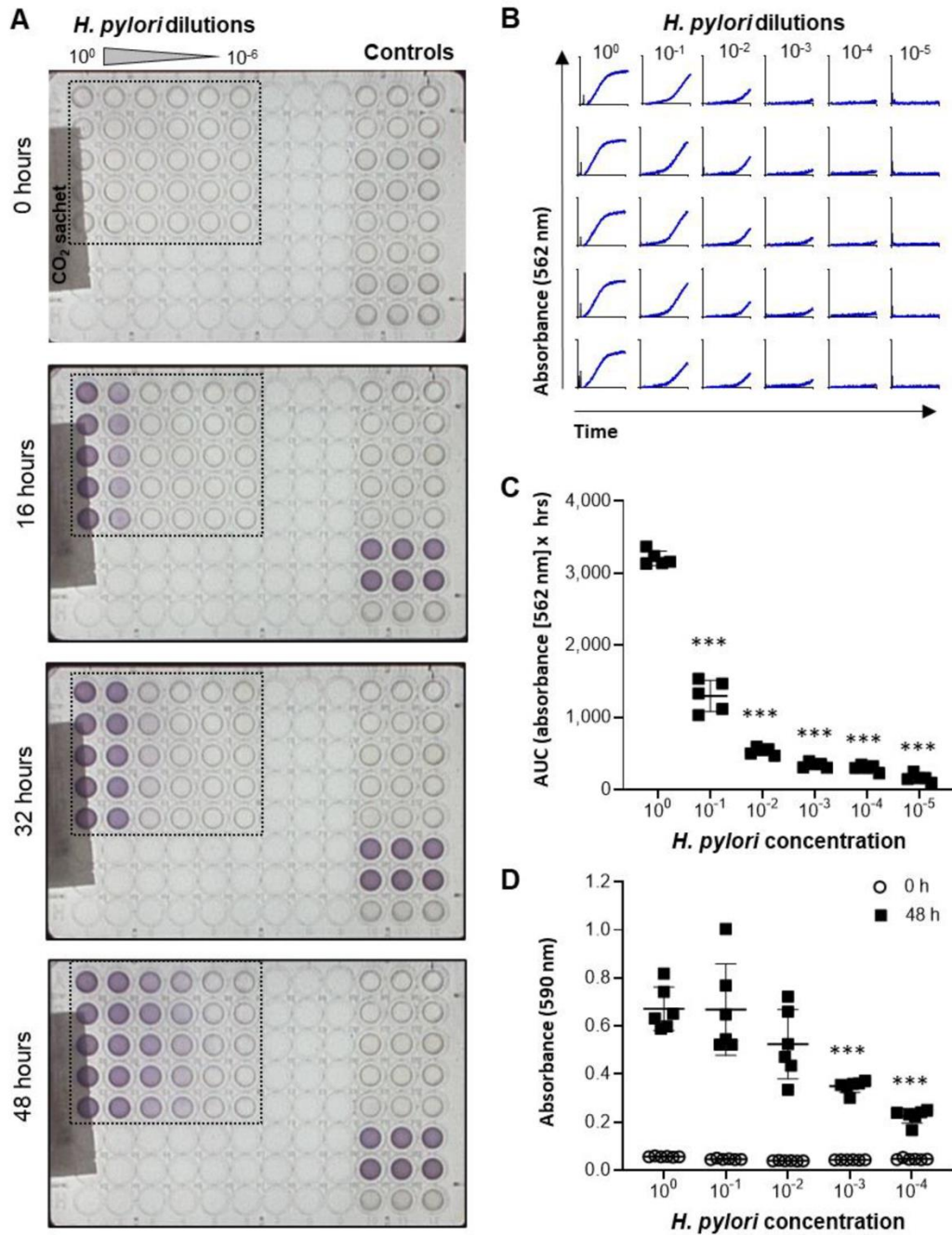


Figure 5.2. Development of a high-throughput metabolic assay to measure *H. pylori* growth. (A) Images of 96-well plates containing various concentrations of *H. pylori* (100 = stock solution used at OD600 = 0.5) obtained by the OmniLog® incubator/reader at different time points after plating the bacteria. (B) Growth curves based on absorbance at 562 nm for the wells outlined in panel A. (C) Area under the curve was determined using GraphPad Prism and shows significant differences in *H. pylori* metabolism between cultures with different initial concentrations of bacteria. (D) Endpoint absorbance (48 h) of an *H. pylori* culture analyzed in a standard 96-well plate reader at 590 nm. Data are representative of n = 4 similar experiments with 5-6 technical

replicates each. Individual datapoints, mean  $\pm$  SD are shown. \*\*\*  $p < 0.01$  compared to undiluted bacteria, one-way ANOVA with Dunnett's multiple comparisons.

#### Analysis of the Antibacterial Effects of Black and Red Raspberry and Blackberry Powders and Extracts on *H. pylori*

The metabolic growth assay was utilized to determine whether anthocyanin-rich berry extracts would inhibit *H. pylori* growth. Metronidazole, a standard antibiotic commonly used in *H. pylori* treatment regimens<sup>26</sup>, was utilized to confirm that the OmniLog® assay successfully detected antimicrobial growth inhibition of *H. pylori*. Metronidazole inhibited *H. pylori* growth in a concentration-dependent manner, with complete growth inhibition achieved at 136  $\mu\text{g/mL}$  (Figure 3A,B). Next, we confirmed that the colored berry extracts did not interfere with dye detection in the OmniLog® assay. As shown in Figure 3C, BRB powder (8%) caused no significant signal over baseline after 48 h, whereas in the presence of both *H. pylori* PMSS1 and the metabolic dye, significant absorbance was measured ( $p \leq 0.001$ ). Absorbance was significantly decreased in the presence of BRB powder. Growth curves over 30 h revealed a concentration-dependent inhibition of *H. pylori* growth at BRB powder concentrations between 0.26% and 4.17% (Figure 3D). Area under the curve (AUC) calculations for the *H. pylori* growth curves similarly showed a significant, concentration-dependent decrease in bacterial growth beginning at 0.26% of berry powder (Figure 3E). To validate the metabolic growth data, 48 h liquid cultures from the growth experiments were re-plated on Brucella agar plates and analyzed for formation of *H. pylori* colonies. Consistent with the results from the metabolic assay, complete growth inhibition was seen at 2.08% and 4.17% of BRB powder, demonstrating strong antibacterial activity of the blackberries on *H. pylori*, whereas colony formation was observed in the absence of BRBs or with lower BRB concentrations (Figure 3E). These results demonstrate

the ability of BRBs to inhibit *H. pylori* growth in vitro and the effectiveness of the OmniLog® assay for evaluating *H. pylori* growth and growth suppression by berry compounds.

As shown in Figure 1 and Tables 1 and 2, the composition of berry preparations was highly variable, depending on berry species, source and processing method. Therefore, the different BRB, RRB and BB whole berry powders and the extracts described above were dissolved/suspended in culture media and then compared for their ability to inhibit the growth of two well-characterized *H. pylori* strains, 60190 and PMSS1, in the OmniLog® microarray assay. All berry preparations tested had significant antibacterial activity (Figures 4 and 5), with complete inhibition of *H. pylori* growth generally achieved at a concentration of about 4%. However, the different berry preparations showed a great variability in their ability to suppress *H. pylori* growth, with significant effects of the specific preparation identified for extracts from BRB and BB for both *H. pylori* strains ( $p \leq 0.001$ ) for the RRB extract and the BRB powders for strain 60190 ( $p \leq 0.05$ ) identified by two-way ANOVA. The UMN BRB extract had the strongest antibacterial activity of all the preparations tested, with an MIC<sub>90</sub> of <0.5%. Conversely, powdered berries generally were less effective than extracts (Figure 5). Both *H. pylori* strains had similar responses to the different berry extracts.



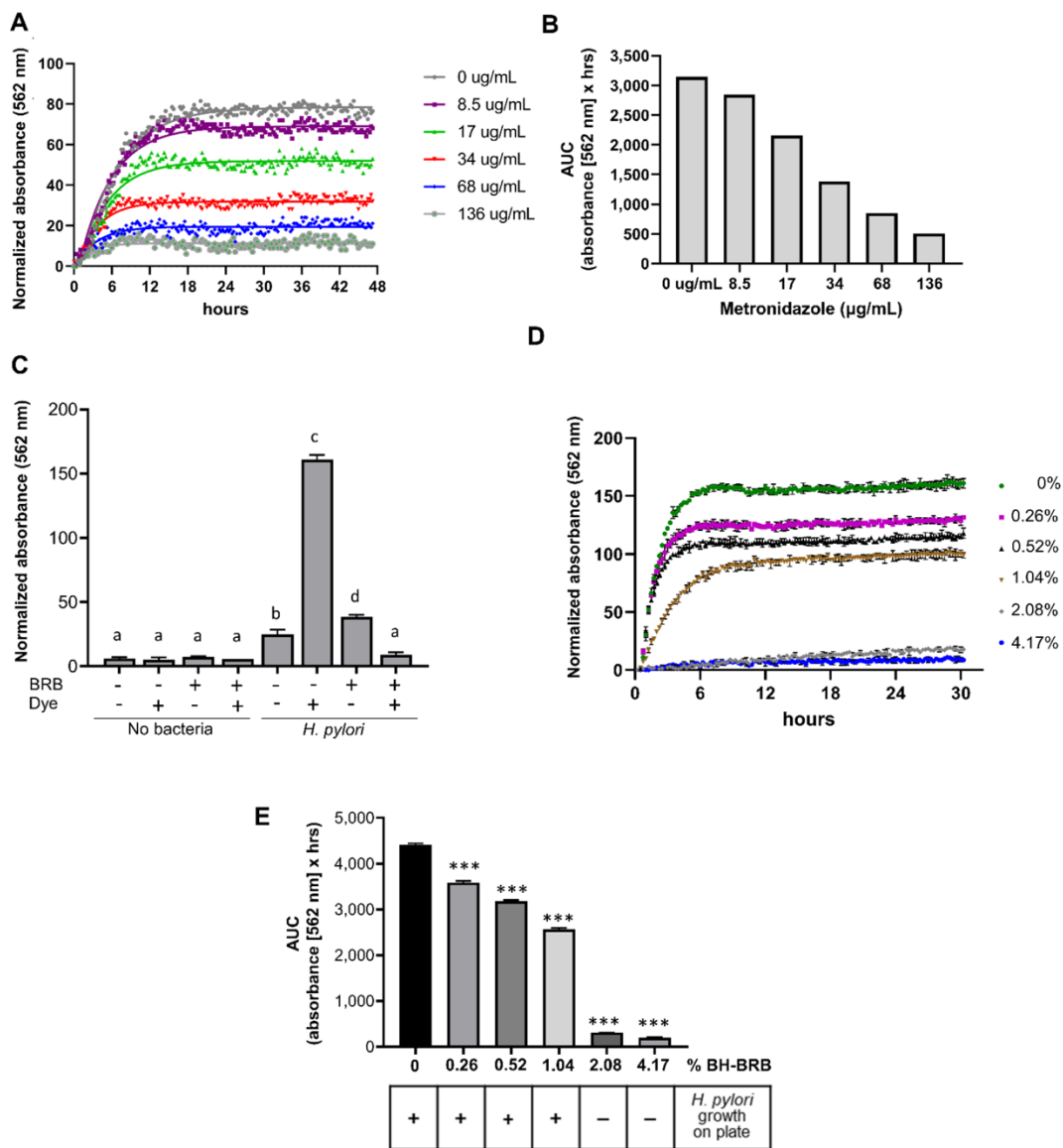


Figure 5.3. Concentration-dependent growth suppression of *H. pylori* by metronidazole and black raspberries measured using the OmniLog<sup>®</sup> assay.

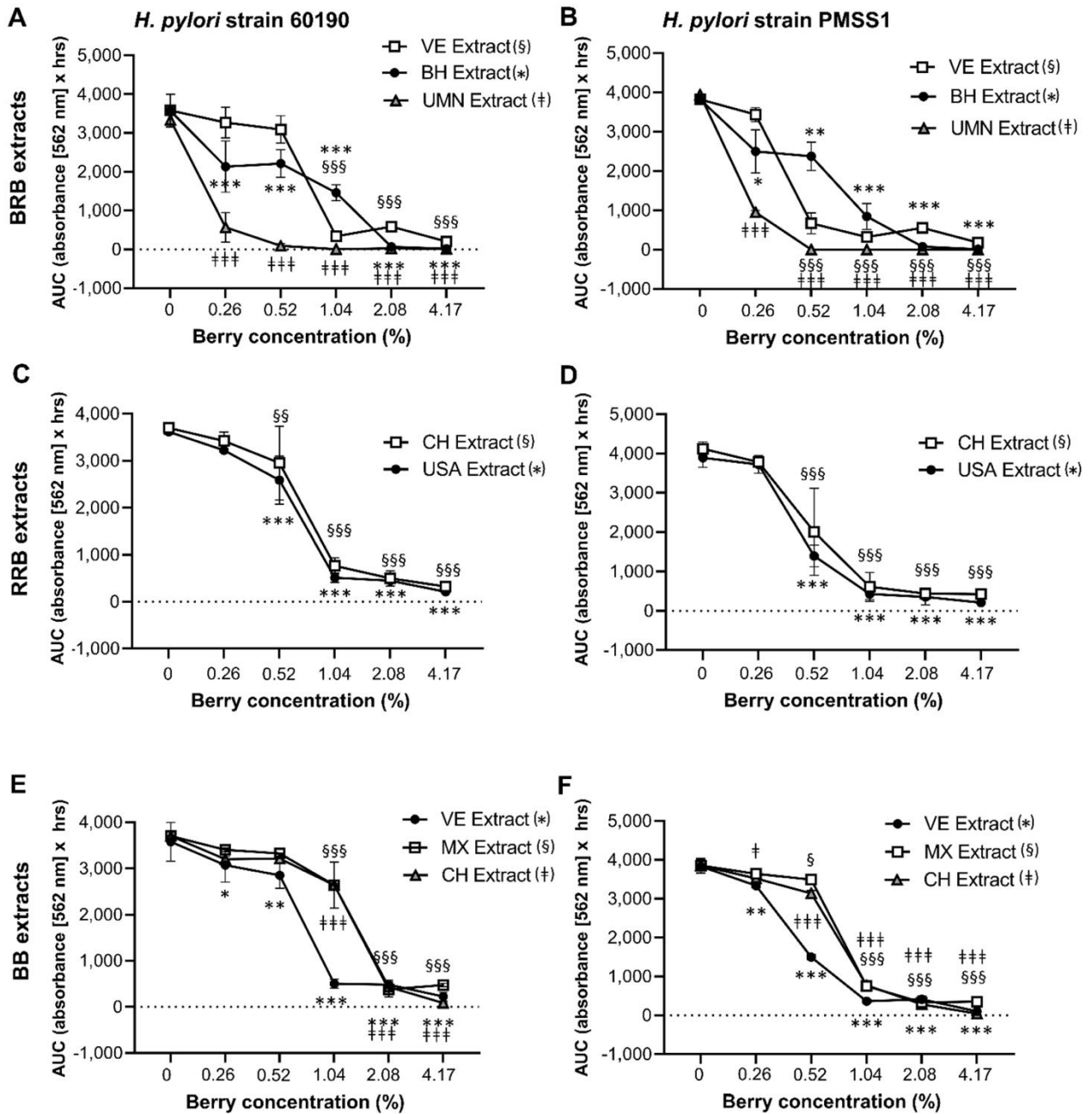


Figure 5.4. Growth inhibition of *H. pylori* by extracts from BRB, RRB, and BB.

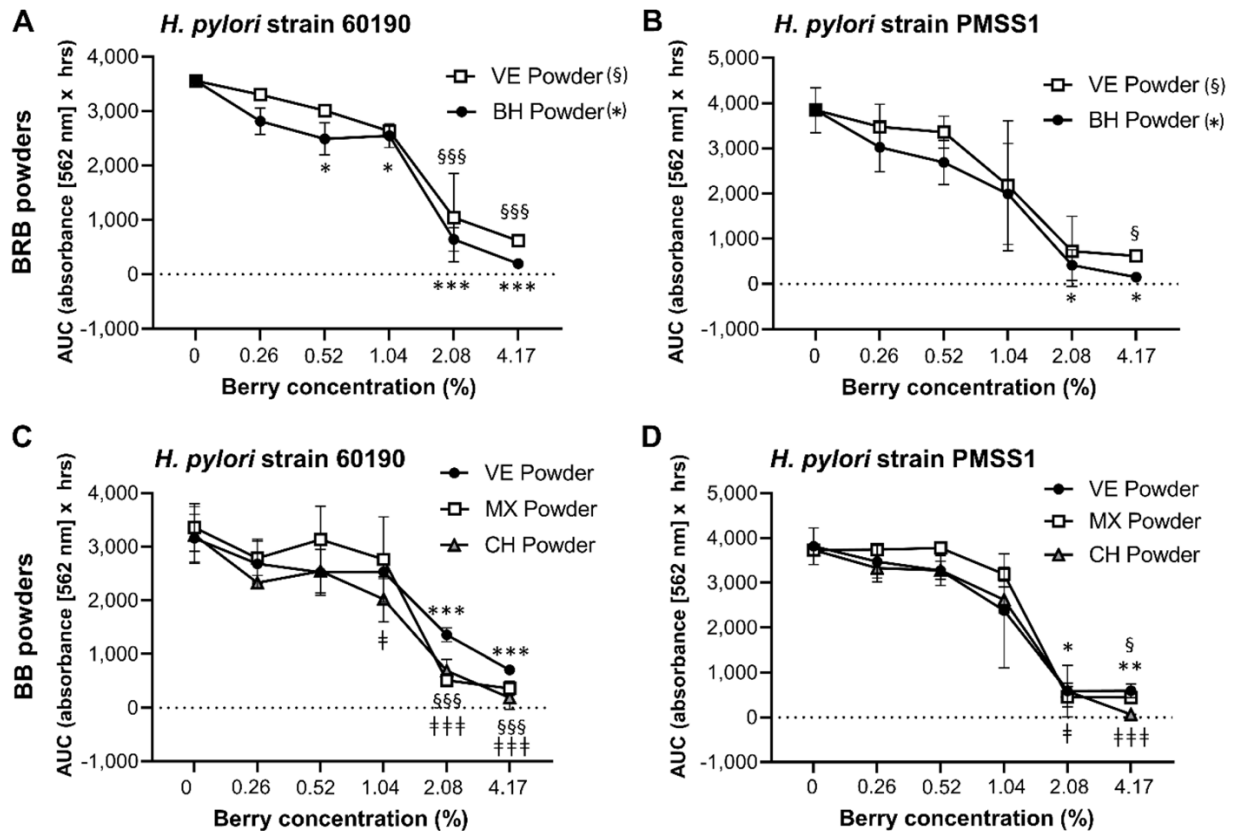


Figure 5.5. Growth inhibition of *H. pylori* by lyophilized BRB and BB powder.

To better understand the large variability in the antibacterial effects of the different berry preparations, the minimum inhibitory concentrations (MICs) required to suppress *H. pylori* growth were analyzed by multifactorial analysis of variance (ANOVA) of (Figure 6A). Overall, berry extracts exhibited a stronger antibacterial response, as evidenced by significantly lower MICs ( $p \leq 0.001$ ). For BRB and BB, the type of berry preparation used (powdered lyophilized powder vs. extract) was responsible for 23% of the variation in MIC. The type of berry (BRB, RRB or BB) and the strain of bacteria also significantly impacted MIC, with BRB associated with lower MICs than BB ( $p = 0.019$ ), and strain PMSS1 impacted MIC, with BRB associated with lower MICs than BB ( $p = 0.019$ ), and strain PMSS1 exhibiting a slightly higher sensitivity

to the antibacterial effects of berries than 60190 ( $p = 0.039$ ). Notably, concentrations of berry products required to achieve antibacterial effects were almost two orders of magnitude higher than those observed for metronidazole (Figure 6B). Surprisingly, no significant relationship between the MIC and the total anthocyanin contents or the concentration of cyanidin-3-O-rutinoside or cyanidin-3-O-xylosylrutinoside was detected based on Pearson's correlation coefficient (Figure 6C,E,F). In contrast, there was a significant positive correlation between cyanidin-3-O-glucoside concentrations and the MICs (Figure 6D,  $p = 0.01$ ,  $R^2 = 0.45$ ), indicating that high concentrations of cyanidin-3-O-glucoside prevented antibacterial activities. These findings suggest that berry components other than the three anthocyanins analyzed contribute to antibacterial activities of BRB, BB and RRB against *H. pylori*.

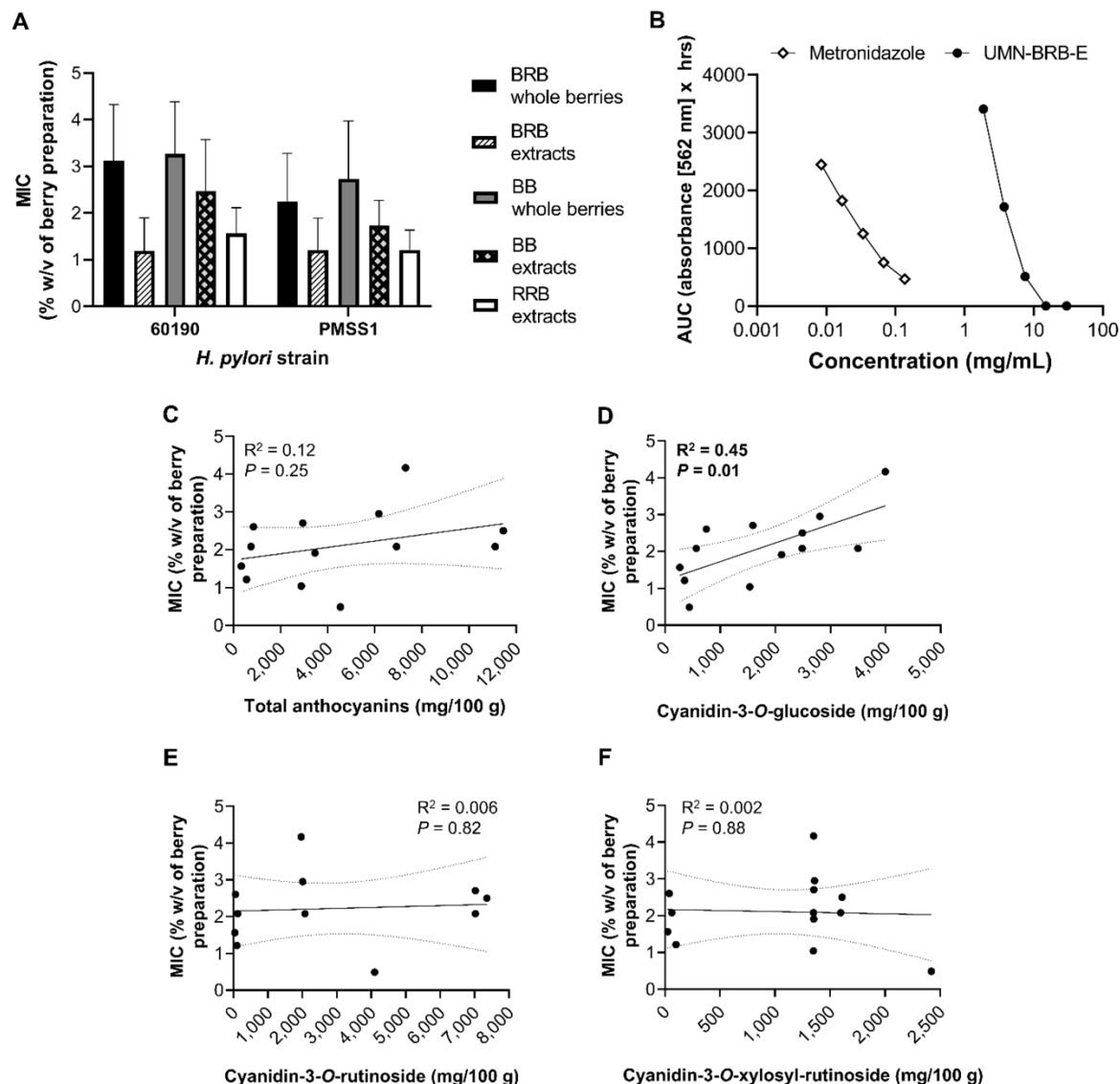


Figure 5.6. Minimum inhibitory concentrations (MICs) of berry preparations for antibacterial activities against *H. pylori*.

#### Effect of BRB Extract on Gastric Epithelial Cell Viability in a Human Gastric Organoid Model

Having shown significant antibacterial effects of multiple different berry preparations against *H. pylori* in vitro, we next sought to confirm that the berries were not toxic to the gastric epithelium, where *H. pylori* bacteria generally reside. Five gastroid lines derived from non-*H.*

*pylori*-infected human gastric biopsies or surgical material were cultured in the presence of UMN-BRB extract, which had the greatest antibacterial activity of all berry preparations tested (Figure 4). As shown in Figure 7, the organoids tolerated the BRB extract over a wide range of concentrations up to 5 mg/mL (0.5%) without any significant impact on organoid viability, as determined by flow cytometric analysis of 7-AAD staining and phase contrast microscopy.

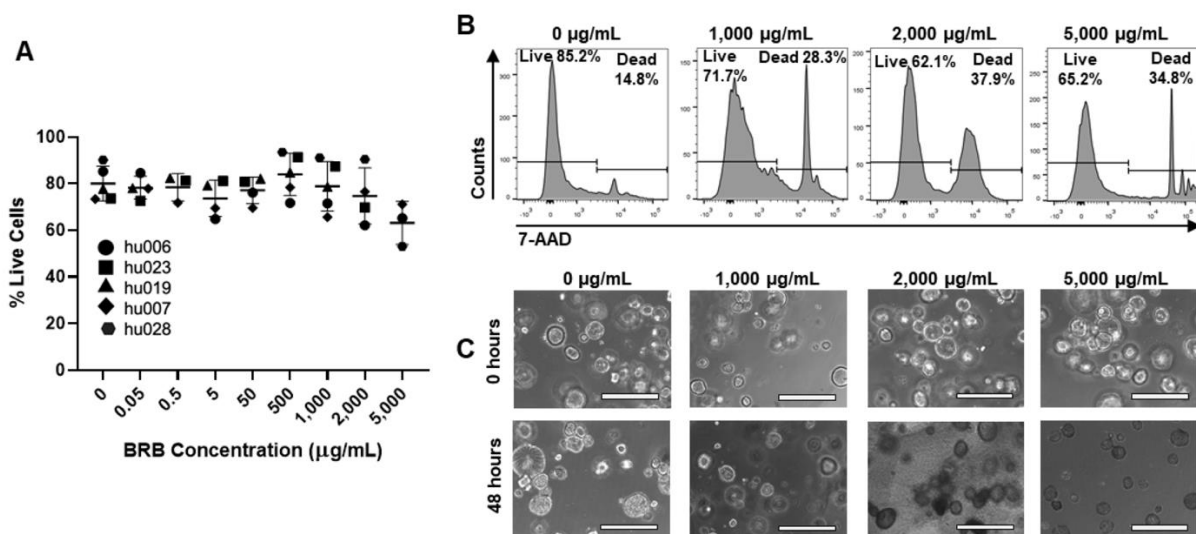


Figure 5.7. Toxicity analysis of BRB extract in primary human gastric epithelial cell cultures.

## Discussion

In this study, significant antimicrobial activity of black and red raspberry and blackberry preparations against *H. pylori* was demonstrated in a high-throughput bacterial growth assay. Interestingly, our analyses showed that both the chemical composition and antimicrobial activity were highly variable depending on berry type, origin and processing method. One major advancement of our study was the development of a high-throughput metabolic microarray assay compatible with the growth requirements of the microaerophilic bacterium *H. pylori*, which enabled us to test a large number of different berry preparations at a wide range of

concentrations. The efficacy of antimicrobial treatments for *H. pylori* is typically still analyzed using the agar dilution or E strip diffusion methods<sup>27-30</sup>, which are work intensive and not easy to scale up. In a previous study, Lee et al. utilized proprietary Biolog Phenotype Microarray plates to evaluate the ability of *H. pylori* to metabolize different carbon sources<sup>31</sup>. Here, Biolog's tetrazolium dye and media were used together with metronidazole and various berry dilutions on standard 96- well plates to dynamically analyze *H. pylori* growth inhibition. By sealing liquid *H. pylori* cultures in transparent, gas-impermeable plastic sleeves with small CO<sub>2</sub> sachets, microaerophilic growth conditions were maintained. Importantly, microarray culture results growth profiles on standard agar plates, as demonstrated by re-culturing *H. pylori* from the microarray plates. The presence of colored berry preparations did not interfere with dye detection, suggesting that our analysis method is suitable for use with other colored natural products as well as a wide range of other chemical compounds.

The metabolic growth assay revealed that black and red raspberries and blackberries have the capacity to block *H. pylori* growth in vitro. Antimicrobial properties of *Rubus* berries have been described in multiple previous studies<sup>15,32-35</sup>. Our analysis of powders and extracts from BRB, RRB and BB from various suppliers and geographical regions revealed that all berry preparations had significant antimicrobial activity against *H. pylori* in vitro, regardless of the *H. pylori* strain used. However, our analyses showed that both the chemical composition and antimicrobial activity (MIC<sub>90</sub>) were highly variable depending on berry type, origin and processing method, corroborating with data from previous studies. Concentrations of active ingredients in *Rubus* berries are known to vary based on geographical location, environmental conditions and berry type<sup>34,36</sup>. In addition, post-harvest processing and storage may affect active

ingredients<sup>37</sup>. Moreover, different bacterial species vary in their susceptibility to the antibacterial effects of berries<sup>38</sup>. One additional consideration that was not tested here is that consumption of berries or berry products can impact other bacteria in the gastrointestinal tract<sup>39</sup>, which in turn might impact *H. pylori* growth<sup>40</sup>. Our data indicate that organic extracts were more potent antimicrobials than powdered berries. Overall, these previous studies and our data indicate that each berry product needs to be carefully tested for specific biological activity and applications prior to use as a nutraceutical. The top-performing preparation in our study was a black raspberry extract from the University of Minnesota (UMB-BRB-E), which achieved complete *H. pylori* growth inhibition at (>90%) at 0.5% (5 mg/mL). This inhibitory concentration is similar to or lower than those of *Rubus* extracts described in other studies<sup>16,32,41</sup>, but several log folds higher than standard antibiotics such as amoxicillin and clarithromycin<sup>42</sup> or the metronidazole used in our study, which completely blocked *H. pylori* growth at 136 µg/mL.

Since anthocyanins are considered the major active ingredients of black and red berries, we hypothesized that anthocyanins would also be responsible for the antibacterial activities observed in our experiments. It was expected that correlation analysis would show a significant inverse relationship between the anthocyanin concentration and the MIC of the berry preparations. Surprisingly, no significant correlation between the concentration of any anthocyanin analyzed in our preparations and increased antibacterial activity was detected, indicating that antimicrobial activity was largely independent of anthocyanins. Anthocyanins exhibit antimicrobial activity against Gram-negative bacteria by causing damage to the cell walls, membranes, and intercellular matrix<sup>43</sup>. Importantly, anthocyanins have been linked to the antimicrobial effects of berry preparations in previous studies<sup>44-46</sup> and are responsible for the



major chemopreventive effects of blackberries and black and red raspberries<sup>18,24,47-49</sup>. However, our correlation analysis suggests that the antibacterial effects against *H. pylori* were independent of anthocyanins and thus must be caused by other active compounds. Indeed, ellagic acid, another polyphenol present in red and black berries, is known to exert antibacterial activity against *H. pylori* as well as other bacteria<sup>17,50,51</sup>. In addition, Lengsfeld *et al.* demonstrated that berry- derived polysaccharides can combat *H. pylori* infection in vivo by preventing bacterial binding to the gastric mucosa<sup>52</sup>. Additional studies have shown antibacterial effects for berry-derived sanguine H-6<sup>35</sup> and rubusoside<sup>53</sup>. Further experiments are needed to identify the raspberry and blackberry compounds that mediate antimicrobial activity against *H. pylori*.

It remains to be tested whether BRB extract can be used to successfully treat *H. pylori* infection in vivo. Berry compounds have been investigated in many studies, and their pharmacokinetics and pharmacodynamics have previously been characterized<sup>50,54</sup>. In our study, human gastric organoids were used as model of primary human gastric epithelial cells to analyze compatibility of BRB extract with gastric epithelial cells, since they closely represent the architecture and cellular complexity of the human gastric mucosa<sup>55,56</sup>. Organoids are three-dimensional long-term cultures of primary cells maintained in a gelatinous extracellular matrix in the presence of specific growth factors. Importantly, exposure of the organoids to BRB did not negatively impact cell viability at the concentrations tested. Moreover, previous animal studies aimed at characterizing the chemopreventive properties of berries have demonstrated that berry products including powdered BRBs are well tolerated at dietary concentrations of up to 10%<sup>57</sup> and that supplementation of the diet with 5% BRB powder, equivalent to 45 g/day in humans<sup>58</sup>, prevented esophageal, oral and colon cancer in rats and colonic polyps in mice<sup>47,59, 60</sup>. In a phase

In a clinical trial, administration of 60 g of BRB powder per day had beneficial effect in colorectal cancer patients with no significant side effects except transient diarrhea or constipation<sup>59</sup>. Other studies have demonstrated that berry extracts have anti-*Helicobacter* activity in animal models. Thus, Park et al.<sup>17</sup> recently showed that extracts prepared from dried, unripened Korean raspberry (*Rubus crataegifolius*) decreased *H. pylori* colonization by about 4 log-fold in a murine model of infection with *H. pylori* strain SS1. Notably, the berry preparation used in the study by Park et al. was highly potent, with an in vitro MIC<sub>90</sub> of 150 µg/mL<sup>17</sup>.

In summary, we have established a high-throughput metabolic growth assay to analyze antimicrobial effects of berry preparations against *H. pylori*. Both freeze-dried powders and ethanol extracts from BRBs, RRBs and BBs obtained from various sources significantly suppressed growth of multiple *H. pylori* strains in vitro. Toxicity studies with human gastric organoids demonstrated good biocompatibility over a wide range of concentrations, including the MIC<sub>90</sub> determined in the growth assay. Together, our findings confirm the potential of berry products as antimicrobial agents but highlight the importance of carefully selecting specific preparations with high antibacterial activity.

## Materials and Methods

### Berry Powders and Preparation of Extracts

Commercially available black raspberry (*Rubus occidentalis*; BRB), blackberry (*Rubus fruticosus*; BB) and red raspberry (*Rubus idaeus*; RRB) samples were either purchased as freeze-dried powders or fresh-frozen whole berries. One additional BRB extract prepared as described in previous studies in Dr. S. Hecht's laboratory at the University of Minnesota was included for comparison<sup>49,59,60</sup>. Suppliers and countries of origin for the berries are listed in Table 1. Fresh-

frozen whole berries were processed into freeze-dried powder using a food processor (Cuisinart® Elemental, Stamford, CT, USA) and lyophilizer (SP VirTis Genesis Pilot Lyophilizer, Warminster, PA, USA) (Figure 1A). Berry powders were either used directly in experiments after mixing the material with IF-10a media plus dye D, both Biolog, Hayward, CA, USA at a final concentration of 0.26–4.17% (w/v; powders) or were processed for hexane/ethanol extraction (extracts). Notably, berry powders contain both water soluble and insoluble materials, so that mixing of the powders with aqueous media results in a colloidal suspension. For hexane/ethanol extraction, nonpolar compounds were extracted using  $3 \times 100$  mL hexane per 10 g powder. Samples were filtered between each extraction, and the hexane filtrate discarded. Anthocyanins and all water-soluble compounds were then extracted using an 80:20 ethanol:water mixture ( $3 \times 100$  mL per 10 g sample). This extract was dried to a syrup under reduced pressure at 30 °C then lyophilized to yield between 1 and 4 g per 20 g powder. All berry preparations were stored in airtight containers at –20 °C until use.

#### Analysis of Anthocyanin Content

Concentrations of major active compounds, i.e., cyanidin-3-*O*-glucoside, cyanidin- 3-*O*-rutinoside, cyanidin-3-*O*-xylosyl-rutinoside and cyanidin-3-sambubioside, for both powder and extract samples were measured by HPLC–MS. The lyophilized samples were mixed with 80:20 (water: sample). The samples were filtered and then injected into an LC– MS system (Agilent 6538 UHD-QTOF equipped with Agilent 1290 infinity UPLC). Upon extracting the chromatograms based on the reported *m/z*, calculations were performed by integrating the peak to obtain the area. Anthocyanin standards were purchased from Extrasynthese S.A.S. (Lyon, France).

### *Helicobacter pylori* Strains and Culture Conditions

Two well-characterized *cagA*<sup>+</sup>, *vacA* *s1/m1* *H. pylori* strains, originally isolated from human patients, were used in our experiments: the reference strain 60190 (kind gift from Dr. G. Perez-Perez, New York University, ATCC #49503<sup>61</sup>), and strain PMSS1 (kind gift from Dr. K. Wilson, Vanderbilt University), which is widely used in murine infection experiments<sup>62</sup>. *H. pylori* strain 60190 was shown to be susceptible to metronidazole, amoxicillin, clarithromycin, levofloxacin, rifampicin and tetracycline, and strain PMSS1 was confirmed to be susceptible to metronidazole, amoxicillin, clarithromycin, and tetracycline in previous studies<sup>63,64</sup>. For the experiments, bacteria were grown at 37 °C under microaerophilic conditions on Brucella agar plates, 5% sheep blood (Becton Dickinson) for 3 days. Colonies were harvested into warm Brucella broth supplemented with 10% FBS and were then cultured in a shaking incubator for a further 18 h period prior to use in the experiments.

### High-Throughput *Helicobacter pylori* Growth Assay

High-throughput bacterial growth assays were performed in 96-well plates using an OmniLog (Biolog, Hayward, CA, USA) plate reader-incubator. Bacterial growth was visualized with a proprietary redox-sensitive tetrazolium dye<sup>25</sup> (dye D, Biolog). Serial dilutions of berry suspensions or extracts (0.26–4.17% w/v) or of metronidazole (8.5–136 µg/mL; Acros Organics, Fair Lawn, NJ, USA) prepared in IF-10a were added to the plates as indicated together with dye D (0.01%) and PM additive (0.05% BSA, 0.01% NaHCO<sub>3</sub> and 0.045% glucose w/v final concentrations). Live *H. pylori* was resuspended in IF-10a (Biolog) to a final OD<sub>600</sub> = 0.5, which corresponds to  $3.4 \times 10^8$  bacteria/mL<sup>65</sup>, and 20 µL of the bacterial suspension were added to the plates together with berry preparations at appropriate dilutions, for a total volume of 120

μL. For analysis, loaded plates were sealed in a gas-impermeable bag with a CO<sub>2</sub> Compact sachet (Oxoid, Nepean, ON, Canada), following the manufacturer's instructions for culturing of microaerophilic bacteria within the OmniLog incubator-reader. Using the bags and sachets was necessary to create microaerophilic conditions, since the OmniLog does not have a controlled CO<sub>2</sub> atmosphere. Plates then were incubated at 37 °C in the OmniLog incubator for 30–48 h. Absorbance values were recorded at 562 nm every 15 min. In some instances, 10-fold serial dilutions of the *H. pylori* cultures were recovered from the plates and were re-streaked on Brucella agar plates to confirm growth and growth suppression.

#### Data Analysis for Bacterial Growth Assays

To analyze *H. pylori* growth inhibition by berry compounds, OmniLog data were exported to Excel using the Biolog Data Converter (version 1.0) and PM Analysis Software (Microbe, version 1.20.02, all Biolog, Hayward, CA, USA). Absorption data for each sample and time point were normalized to baseline by subtracting the average of the first four absorption values from each data point. To quantitate bacterial growth over time, peak area under the curve (AUC; absorbance (562 nm) × h) was determined using GraphPad version 8.3.1 (San Diego, CA, USA). The minimum inhibitory concentration 90 (MIC<sub>90</sub>) of a berry preparation was defined as the concentration at which the AUC values for the growth curves were decreased to ≤10% of the maximum.

#### Human Gastric Organoid Culture and Viability Assay

Human gastric organoid cultures (gastroids) were established and maintained as previously described<sup>66,67</sup>. Briefly, human gastric tissue samples were obtained with informed consent and IRB approval from patients undergoing endoscopy and biopsy at the Bozeman

Health Deaconess Hospital (protocol DB050718-FC). Alternatively, tissue samples from sleeve gastrectomy surgeries were provided by the National Disease Research Interchange (protocol DB062615-EX). None of the donors were positive for active *H. pylori* infection, as determined by rapid urease CLO test (Halyard Health, Alpharetta, GA, USA). Gastric glands were prepared by collagenase digestion and then were plated in Matrigel. Following polymerization, Matrigel was overlaid with L-WRN medium which includes Advanced DMEM/F12 (Gibco by Life Technologies, Grand Island, NY, USA) and 50% supernatant from murine L-WRN cells—which secrete Wnt3a, noggin, and R-spondin 3—and supplemented with 10% FBS (Rocky Mountain Bio, Missoula, MT, USA), 1% L-Glutamine, 10 $\mu$ M Y-27632 (Tocris Biosciences, Bristol, UK), 10  $\mu$ M SB-431542 (Tocris Biosciences, Bristol, UK), and 10 mM HEPES buffer. Black raspberry extract prepared in 90% DMSO and 10% HCl was externally administered to the organoids for a 48 h treatment at 37 °C with 5% CO<sub>2</sub>. Control cultures were treated with dilutions of 90% DMSO/10% HCl alone. To determine cell viability, organoids were harvested by trypsinization, and single- cell suspensions stained with 7-aminoactinomycin D (7-AAD; ThermoFisher Scientific, Waltham, MA, USA) were analyzed on an LSR II flow cytometer (Becton Dickinson).

### Statistical Analysis

Data shown are representative of three or more replicate experiments. For OmniLog assays, 3–6 technical replicates were prepared. All data were analyzed using GraphPad version 8.3.1 (San Diego, CA, USA). Data are shown as the mean  $\pm$  SD. Student's *t* test or a one- or two-way ANOVA with Tukey's or Dunnett's multiple comparisons test were used to determine statistical significance. Differences were considered significant at  $p \leq 0.05$ .

### Acknowledgements

The collaborative support of Bozeman Health Deaconess Hospital for collecting human tissue samples is greatly appreciated. We also would like to thank Stephen Hecht, University of Minnesota, for providing BRB extract.

### Supplementary Materials

The following are available online at <https://www.mdpi.com/article/10.3390/antibiotics10070845/s1>, Video S1: Time lapse series of plate images of the *H. pylori* culture in Figure 2 obtained on the OmniLog™ incubator-reader shows color development consistent with *H. pylori* metabolism and growth over 48 h.

References Cited

- 1     Burucoa, C. & Axon, A. Epidemiology of *Helicobacter pylori* infection. *Helicobacter* **22 Suppl 1** (2017). <https://doi.org/10.1111/hel.12403>
  
- 2     Amieva, M. & Peek, R. M., Jr. Pathobiology of *Helicobacter pylori*-Induced Gastric Cancer. *Gastroenterology* **150**, 64-78 (2016). <https://doi.org/10.1053/j.gastro.2015.09.004>
  
- 3     Fitzmaurice, C. *et al.* Global, regional, and national cancer incidence, mortality, years of life lost, years lived with disability, and disability-adjusted life-years for 32 cancer groups, 1990 to 2015: A Systematic Analysis for the Global Burden of Disease Study Global Burden. *JAMA Oncology* (2017). <https://doi.org/10.1001/jamaoncol.2016.5688>
  
- 4     Blanchard, T. G. & Czinn, S. J. Current Status and Prospects for a *Helicobacter pylori* Vaccine. *Gastroenterol Clin North Am* **44**, 677-689 (2015). <https://doi.org/10.1016/j.gtc.2015.05.013>
  
- 5     O'Connor, A., Liou, J. M., Gisbert, J. P. & O'Morain, C. Review: Treatment of *Helicobacter pylori* Infection 2019. *Helicobacter* **24 Suppl 1**, e12640 (2019). <https://doi.org/10.1111/hel.12640>
  
- 6     Serrano, C. A. *et al.* *Helicobacter pylori*-Clarithromycin Resistance in Symptomatic Pediatric Patients in a High Prevalence Country. *J Pediatr Gastroenterol Nutr* **64**, e56-e60 (2017). <https://doi.org/10.1097/MPG.0000000000001257>
  
- 7     Tacconelli, E. *et al.* Discovery, research, and development of new antibiotics: the WHO priority list of antibiotic-resistant bacteria and tuberculosis. *Lancet Infect Dis* **18**, 318-327 (2018). [https://doi.org/10.1016/S1473-3099\(17\)30753-3](https://doi.org/10.1016/S1473-3099(17)30753-3)
  
- 8     Al-Eidan, F. A., McElroy, J. C., Scott, M. G. & McConnell, J. B. Management of *Helicobacter pylori* eradication--the influence of structured counselling and follow-up. *Br J Clin Pharmacol* **53**, 163-171 (2002). <https://doi.org/10.1046/j.0306-5251.2001.01531.x>
  
- 9     Cutler, A. F. & Schubert, T. T. Patient factors affecting *Helicobacter pylori* eradication with triple therapy. *Am J Gastroenterol* **88**, 505-509 (1993).



- 10 Gatta, L., Vakil, N., Vaira, D. & Scarpignato, C. Global eradication rates for *Helicobacter pylori* infection: systematic review and meta-analysis of sequential therapy. *BMJ* **347**, f4587 (2013). <https://doi.org/10.1136/bmj.f4587>
- 11 Liou, J. M. *et al.* The Primary Resistance of *Helicobacter pylori* in Taiwan after the National Policy to Restrict Antibiotic Consumption and Its Relation to Virulence Factors- A Nationwide Study. *PLoS One* **10**, e0124199 (2015). <https://doi.org/10.1371/journal.pone.0124199>
- 12 Graham, D. Y. Transitioning of *Helicobacter pylori* Therapy from Trial and Error to Antimicrobial Stewardship. *Antibiotics (Basel)* **9** (2020). <https://doi.org/10.3390/antibiotics9100671>
- 13 Puupponen-Pimia, R., Nohynek, L., Alakomi, H. L. & Oksman-Caldentey, K. M. Bioactive berry compounds-novel tools against human pathogens. *Appl Microbiol Biotechnol* **67**, 8-18 (2005). <https://doi.org/10.1007/s00253-004-1817-x>
- 14 Khoo, H. E., Azlan, A., Tang, S. T. & Lim, S. M. Anthocyanidins and anthocyanins: colored pigments as food, pharmaceutical ingredients, and the potential health benefits. *Food Nutr Res* **61**, 1361779 (2017). <https://doi.org/10.1080/16546628.2017.1361779>
- 15 Panda, S. K. *et al.* Antimicrobial, Anthelmintic, and Antiviral Activity of Plants Traditionally Used for Treating Infectious Disease in the Similipal Biosphere Reserve, Odisha, India. *Front Pharmacol* **8**, 658 (2017). <https://doi.org/10.3389/fphar.2017.00658>
- 16 Chatterjee, A., Yasmin, T., Bagchi, D. & Stohs, S. J. Inhibition of *Helicobacter pylori* in vitro by various berry extracts, with enhanced susceptibility to clarithromycin. *Mol Cell Biochem* **265**, 19-26 (2004). <https://doi.org/10.1023/b:mcbi.0000044310.92444.ec>
- 17 Park, J. U. *et al.* Synergistic Effect of *Rubus crataegifolius* and *Ulmus macrocarpa* Against *Helicobacter pylori* Clinical Isolates and Gastritis. *Front Pharmacol* **11**, 4 (2020). <https://doi.org/10.3389/fphar.2020.00004>
- 18 Wang, L. S. & Stoner, G. D. Anthocyanins and their role in cancer prevention. *Cancer Lett* **269**, 281-290 (2008). <https://doi.org/10.1016/j.canlet.2008.05.020>
- 19 Samad, M. A., Hashim, S. H., Simarani, K. & Yaacob, J. S. Antibacterial Properties and Effects of Fruit Chilling and Extract Storage on Antioxidant Activity, Total Phenolic and

- Anthocyanin Content of Four Date Palm (*Phoenix dactylifera*) Cultivars. *Molecules* **21**, 419 (2016). <https://doi.org/10.3390/molecules21040419>
- 20 Marin, L., Miguelez, E. M., Villar, C. J. & Lombo, F. Bioavailability of dietary polyphenols and gut microbiota metabolism: antimicrobial properties. *Biomed Res Int* **2015**, 905215 (2015). <https://doi.org/10.1155/2015/905215>
  - 21 Kim, S. H. *et al.* Cyanidin 3-O-glucoside reduces *Helicobacter pylori* VacA-induced cell death of gastric KATO III cells through inhibition of the SecA pathway. *Int J Med Sci* **11**, 742-747 (2014). <https://doi.org/10.7150/ijms.7167>
  - 22 Markakis, P. *Anthocyanins as Food Colors*. 1 edn, (Elsevier, 2012).
  - 23 Levy, R., Okun, Z. & Shpigelman, A. The Influence of Chemical Structure and the Presence of Ascorbic Acid on Anthocyanins Stability and Spectral Properties in Purified Model Systems. *Foods* **8** (2019). <https://doi.org/10.3390/foods8060207>
  - 24 Tulio, A. Z., Jr. *et al.* Cyanidin 3-rutinoside and cyanidin 3-xylosylrutinoside as primary phenolic antioxidants in black raspberry. *J Agric Food Chem* **56**, 1880-1888 (2008). <https://doi.org/10.1021/jf072313k>
  - 25 Bochner, B. R. Global phenotypic characterization of bacteria. *FEMS Microbiol Rev* **33**, 191-205 (2009). <https://doi.org/10.1111/j.1574-6976.2008.00149.x>
  - 26 Chey, W. D., Leontiadis, G. I., Howden, C. W. & Moss, S. F. ACG Clinical Guideline: Treatment of *Helicobacter pylori* Infection. *Am J Gastroenterol* **112**, 212-239 (2017). <https://doi.org/10.1038/ajg.2016.563>
  - 27 Lee, J. W. *et al.* Favorable outcomes of culture-based *Helicobacter pylori* eradication therapy in a region with high antimicrobial resistance. *Helicobacter* **24**, e12561 (2019). <https://doi.org/10.1111/hel.12561>
  - 28 Tan, B. *et al.* *Helicobacter pylori* Antimicrobial Susceptibility Testing-Guided Salvage Therapy in the USA: A Real Life Experience. *Dig Dis Sci* **63**, 437-445 (2018). <https://doi.org/10.1007/s10620-017-4880-8>

- 29 Biernat, M. M. *et al.* Antimicrobial susceptibility of *Helicobacter pylori* isolates from Lower Silesia, Poland. *Arch Med Sci* **10**, 505-509 (2014).  
<https://doi.org/10.5114/aoms.2013.36917>
- 30 Pastukh, N. *et al.* Antimicrobial susceptibility of *Helicobacter pylori* strains isolated from children in Israel. *J Glob Antimicrob Resist* **12**, 175-178 (2018).  
<https://doi.org/10.1016/j.jgar.2017.10.004>
- 31 Lee, W. C., Goh, K. L., Loke, M. F. & Vadivelu, J. Elucidation of the Metabolic Network of *Helicobacter pylori* J99 and Malaysian Clinical Strains by Phenotype Microarray. *Helicobacter* **22** (2017). <https://doi.org/10.1111/hel.12321>
- 32 Khalifa, H. O., Kamimoto, M., Shimamoto, T. & Shimamoto, T. Antimicrobial Effects of Blueberry, Raspberry, and Strawberry Aqueous Extracts and their Effects on Virulence Gene Expression in *Vibrio cholerae*. *Phytother Res* **29**, 1791-1797 (2015).  
<https://doi.org/10.1002/ptr.5436>
- 33 Strugala, P. *et al.* Biological activity of the methanol and water extracts of the fruits of anthocyanin-rich plants grown in south-west Poland. *Nat Prod Commun* **10**, 467-474 (2015).
- 34 Abu Bakar, M. F., Ismail, N. A., Isha, A. & Mei Ling, A. L. Phytochemical Composition and Biological Activities of Selected Wild Berries (*Rubus moluccanus* L., *R. fraxinifolius* Poir., and *R. alpestris* Blume). *Evid Based Complement Alternat Med* **2016**, 2482930 (2016). <https://doi.org/10.1155/2016/2482930>
- 35 Krauze-Baranowska, M. *et al.* The antimicrobial activity of fruits from some cultivar varieties of *Rubus idaeus* and *Rubus occidentalis*. *Food Funct* **5**, 2536-2541 (2014).  
<https://doi.org/10.1039/c4fo00129j>
- 36 Klesk, K., Qian, M. & Martin, R. R. Aroma extract dilution analysis of cv. Meeker (*Rubus idaeus* L.) red raspberries from Oregon and Washington. *J Agric Food Chem* **52**, 5155-5161 (2004). <https://doi.org/10.1021/jf0498721>
- 37 Hager, T. J., Howard, L. R. & Prior, R. L. Processing and storage effects on monomeric anthocyanins, percent polymeric color, and antioxidant capacity of processed blackberry products. *J Agric Food Chem* **56**, 689-695 (2008). <https://doi.org/10.1021/jf071994g>

- 38 Gurbuz, I. *et al.* Antibacterial, antifungal and enzyme inhibitory effects of selected plants from Turkey. *Pak J Pharm Sci* **34**, 1011-1017 (2021).
- 39 Tian, L. *et al.* Metabolism of anthocyanins and consequent effects on the gut microbiota. *Crit Rev Food Sci Nutr* **59**, 982-991 (2019).  
<https://doi.org/10.1080/10408398.2018.1533517>
- 40 Serrano, C., Harris, P. R., Smith, P. D. & Bimczok, D. Interactions between *H. pylori* and the Gastric Microbiome: Impact on Gastric Homeostasis and Disease. *Curr Opin Physiol* **21**, 57-64 (2021). <https://doi.org/10.1016/j.cophys.2021.04.003>
- 41 Tabarki, S. *et al.* Comparison of Phytochemical Composition and Biological Activities of *Rubus ulmifolius* Extracts Originating from Four Regions of Tunisia. *Chem Biodivers* **14** (2017). <https://doi.org/10.1002/cbdv.201600168>
- 42 Kim, J. M. *et al.* Distribution of antibiotic MICs for *Helicobacter pylori* strains over a 16-year period in patients from Seoul, South Korea. *Antimicrob Agents Chemother* **48**, 4843-4847 (2004). <https://doi.org/10.1128/AAC.48.12.4843-4847.2004>
- 43 Pojer, E., Mattivi, F., Johnson, D. & Stockley, C. S. The Case for Anthocyanin Consumption to Promote Human Health: A Review. *Compr Rev Food Sci Food Saf* **12**, 483-508 (2013). <https://doi.org/10.1111/1541-4337.12024>
- 44 Chen, H. *et al.* Antinociceptive and Antibacterial Properties of Anthocyanins and Flavonols from Fruits of Black and Non-Black Mulberries. *Molecules* **23** (2017).  
<https://doi.org/10.3390/molecules23010004>
- 45 Cerezo, A. B. *et al.* Anthocyanins in Blueberries Grown in Hot Climate Exert Strong Antioxidant Activity and May Be Effective against Urinary Tract Bacteria. *Antioxidants (Basel)* **9** (2020). <https://doi.org/10.3390/antiox9060478>
- 46 Puupponen-Pimia, R. *et al.* Antimicrobial properties of phenolic compounds from berries. *J Appl Microbiol* **90**, 494-507 (2001). <https://doi.org/10.1046/j.1365-2672.2001.01271.x>
- 47 Chen, K. M. *et al.* Effects of Black Raspberry on Dibenzo[a,l]Pyrene Diol Epoxide Induced DNA Adducts, Mutagenesis, and Tumorigenesis in the Mouse Oral Cavity. *Cancer Prev Res (Phila)* **11**, 157-164 (2018). <https://doi.org/10.1158/1940-6207.CAPR-17-0278>

- 48 God, J., Tate, P. L. & Larcom, L. L. Red raspberries have antioxidant effects that play a minor role in the killing of stomach and colon cancer cells. *Nutr Res* **30**, 777-782 (2010). <https://doi.org/10.1016/j.nutres.2010.10.004>
- 49 Peiffer, D. S. *et al.* Chemoprevention of esophageal cancer with black raspberries, their component anthocyanins, and a major anthocyanin metabolite, protocatechuic acid. *Cancer Prev Res (Phila)* **7**, 574-584 (2014). <https://doi.org/10.1158/1940-6207.CAPR-14-0003>
- 50 Ceci, C., Graziani, G., Faraoni, I. & Cacciotti, I. Strategies to improve ellagic acid bioavailability: from natural or semisynthetic derivatives to nanotechnological approaches based on innovative carriers. *Nanotechnology* **31**, 382001 (2020). <https://doi.org/10.1088/1361-6528/ab912c>
- 51 De, R. *et al.* Antimicrobial activity of ellagic acid against *Helicobacter pylori* isolates from India and during infections in mice. *J Antimicrob Chemother* **73**, 1595-1603 (2018). <https://doi.org/10.1093/jac/dky079>
- 52 Lengsfeld, C., Deters, A., Faller, G. & Hensel, A. High molecular weight polysaccharides from black currant seeds inhibit adhesion of *Helicobacter pylori* to human gastric mucosa. *Planta Med* **70**, 620-626 (2004). <https://doi.org/10.1055/s-2004-827184>
- 53 Kim, J. *et al.* Anti-cariogenic Characteristics of Rubusoside. *Biotechnol Bioprocess Eng* **24**, 282-287 (2019). <https://doi.org/10.1007/s12257-018-0408-0>
- 54 Lila, M. A., Burton-Freeman, B., Grace, M. & Kalt, W. Unraveling Anthocyanin Bioavailability for Human Health. *Annu Rev Food Sci Technol* **7**, 375-393 (2016). <https://doi.org/10.1146/annurev-food-041715-033346>
- 55 Blutt, S. E., Crawford, S. E., Ramani, S., Zou, W. Y. & Estes, M. K. Engineered Human Gastrointestinal Cultures to Study the Microbiome and Infectious Diseases. *CMGH* (2018). <https://doi.org/10.1016/j.jcmgh.2017.12.001>
- 56 Hill, D. R. & Spence, J. R. Gastrointestinal Organoids: Understanding the Molecular Basis of the Host-Microbe Interface. *Cell Mol Gastroenterol Hepatol* **3**, 138-149 (2017). <https://doi.org/10.1016/j.jcmgh.2016.11.007>

- 57 Kula, M. & Krauze-Baranowska, M. Rubus occidentalis: The black raspberry--its potential in the prevention of cancer. *Nutr Cancer* **68**, 18-28 (2016). <https://doi.org/10.1080/01635581.2016.1115095>
- 58 Stoner, G. D., Wang, L. S. & Casto, B. C. Laboratory and clinical studies of cancer chemoprevention by antioxidants in berries. *Carcinogenesis* **29**, 1665-1674 (2008). <https://doi.org/10.1093/carcin/bgn142>
- 59 Wang, L. S. *et al.* Anthocyanins in black raspberries prevent esophageal tumors in rats. *Cancer Prev Res (Phila)* **2**, 84-93 (2009). <https://doi.org/10.1158/1940-6207.CAPR-08-0155>
- 60 Peiffer, D. S. *et al.* Dietary Consumption of Black Raspberries or Their Anthocyanin Constituents Alters Innate Immune Cell Trafficking in Esophageal Cancer. *Cancer Immunol Res* **4**, 72-82 (2016). <https://doi.org/10.1158/2326-6066.CIR-15-0091>
- 61 Peek, R. M., Jr. *et al.* Helicobacter pylori strain-specific genotypes and modulation of the gastric epithelial cell cycle. *Cancer Res* **59**, 6124-6131 (1999).
- 62 Dyer, V. *et al.* Genomic features of the Helicobacter pylori strain PMSS1 and its virulence attributes as deduced from its in vivo colonisation patterns. *Mol Microbiol* **110**, 761-776 (2018). <https://doi.org/10.1111/mmi.14123>
- 63 Arnold, I. C. *et al.* Tolerance rather than immunity protects from Helicobacter pylori-induced gastric preneoplasia. *Gastroenterology* **140**, 199-209 (2011). <https://doi.org/10.1053/j.gastro.2010.06.047>
- 64 Sierra, J. C. *et al.* Epidermal growth factor receptor inhibition downregulates Helicobacter pylori-induced epithelial inflammatory responses, DNA damage and gastric carcinogenesis. *Gut* (2018). <https://doi.org/10.1136/gutjnl-2016-312888>
- 65 Bimczok, D. *et al.* Human primary gastric dendritic cells induce a Th1 response to H. pylori. *Mucosal Immunol* **3**, 260-269 (2010). <https://doi.org/10.1038/mi.2010.10>
- 66 Sebrell, T. A. *et al.* Live imaging analysis of human gastric epithelial spheroids reveals spontaneous rupture, rotation and fusion events. *Cell and Tissue Research* **371**, 293-307 (2018). <https://doi.org/10.1007/s00441-017-2726-5>

- 67 Sebrell, T. A. *et al.* A Novel Gastric Spheroid Co-culture Model Reveals Chemokine-Dependent Recruitment of Human Dendritic Cells to the Gastric Epithelium. *Cellular and Molecular Gastroenterology and Hepatology* **8**, 157-171.e153 (2019).  
<https://doi.org/10.1016/j.jcmgh.2019.02.010>

CHAPTER SIX

ANTIVIRAL RESPONSES IN A JAMAICAN FRUIT BAT  
INTESTINAL ORGANOID MODEL OF SARS-COV-2  
INFECTION

Contribution of Authors and Co-Authors

Manuscript in Chapter 6

Author: Marziah Hashimi

Contributions: Conceptualization, methodology, investigation, data analysis, manuscript writing, manuscript editing

Co-Author: T. Andrew Sebrell

Contributions: Methodology, resources

Co-Author: Jodi F. Hedges

Contributions: Investigation, methodology, resources, manuscript revision

Co-Author: Deann Snyder

Contributions: Investigation

Co-Author: Katrina Lyon

Contributions: Investigation, methodology, manuscript writing

Co-Author: Stephanie D. Byrum

Contributions: Investigation, methodology, formal analysis

Co-Author: Samuel G. Mackintosh

Contributions: Investigation, methodology

Co-Author: Dan Crowley



Contributions: Methodology

Co-Author: Michelle D. Cherne

Contributions: Investigation, methodology

Co-Author: David Skwarchuk

Contributions: Investigation

Co-Author: Amanda Robison

Contributions: Investigation

Co-Author: Barkan Sidar

Contributions: Investigation, visualization

Co-Author: Anja Kunze

Contributions: Methodology, investigation, supervision

Co-Author: Emma K. Loveday

Contributions: Resources and methodology

Co-Author: Matthew P. Taylor

Contributions: Resources, methodology, supervision

Co-Author: Connie B. Chang

Contributions: Conceptualization, funding acquisition, project supervision

Co-Author: James N. Wilking

Contributions: Conceptualization and funding acquisition

Co-Author: Seth T. Walk

Contributions: Conceptualization and funding acquisition

Co-Author: Tony Schountz

Contributions: Resources

Co-Author: Mark A. Jutila

Contributions: Conceptualization, funding acquisition, project supervision

Co-Author: Diane Bimczok

Contributions: Conceptualization, funding acquisition, project administration, formal analysis, manuscript writing, manuscript editing

Manuscript Information

Marziah Hashimi, T. Andrew Sebrell, Jodi Hedges, Deann Snyder, **Katrina Lyon**, Michelle D. Cherne, Amanda Robison, Barkan Sidar, Emma Loveday, Connie Chang, James N. Wilking, Seth Walk, Tony Schountz, Mark Jutila, Diane Bimczok

Nature Communications

Status of Manuscript:

- ☐ Prepared for submission to a peer-reviewed journal
- ☐ Officially submitted to a peer-reviewed journal
- ☐ Accepted by a peer-reviewed journal
- ☒ Published in a peer-reviewed journal

Nature

October 28<sup>th</sup>, 2023

Volume 14

DOI: 10.1038/s41467-023042610-x

### Abstract

Bats are natural reservoirs for several zoonotic viruses, potentially due to an enhanced capacity to control viral infection. However, the mechanisms of antiviral responses in bats are poorly defined. Here we established a Jamaican fruit bat (JFB, *Artibeus jamaicensis*) intestinal organoid model of severe acute respiratory syndrome coronavirus-2 (SARS-CoV-2) infection. Upon infection with SARS-CoV-2, increased viral RNA and subgenomic RNA was detected, but no infectious virus was released, indicating that JFB organoids support only limited viral replication but not viral reproduction. SARS-CoV-2 replication was associated with significantly increased gene expression of type I interferons and inflammatory cytokines. Interestingly, SARS-CoV-2 also caused enhanced formation and growth of JFB organoids. Proteomics revealed an increase in inflammatory signaling, cell turnover, cell repair, and SARS-CoV-2 infection pathways. Collectively, our findings suggest that primary JFB intestinal epithelial cells mount successful antiviral interferon responses and that SARS-CoV-2 infection in JFB cells induces protective regenerative pathways.

### Introduction

Bats are considered important natural reservoirs for a variety of emerging zoonotic viruses that cause several illnesses in humans and other mammals<sup>1</sup>, including severe acute respiratory syndrome coronavirus (SARS-CoV), Middle East respiratory syndrome coronavirus (MERS-CoV), Hendra virus, and Nipah virus<sup>2,3,4,5,6</sup>. The COVID-19 pandemic was caused by severe acute respiratory coronavirus-2 (SARS-CoV-2)<sup>7</sup>, which also is thought to have its evolutionary origin in bats. This hypothesis is based on multiple studies that demonstrated a high

level of genetic similarity between SARS-CoV-2 and several bat-borne coronaviruses such as RatG13 (96.1% identity<sup>7</sup>) and BANAL-52 (96.8% identity<sup>8</sup>), which have been detected in bat feces. Studies from a number of different bat species have shown that bat viruses, including coronaviruses, achieve long-term colonization of intestinal tissues without causing apparent disease<sup>9,10,11,12</sup>. In a study by Watanabe *et al.* on wild bats captured in the Philippines<sup>10</sup>, enteric coronaviruses were detected in >50% of the animals, but clinical signs of disease were absent. Similarly, Subudhi *et al.* found that 30% of North American little brown bats harbored coronaviruses in their intestines but did not display any signs of illness<sup>11</sup>. Becker *et al.* describe a similar level of coronavirus infection, 21%, in rectal swabs of vampire bats (*Desmodus rotundus*), with no significant impact on serum proteome composition<sup>13</sup>. Tong *et al.* analyzed rectal swabs and intestinal tissues from asymptomatic fruit bats in Peru and identified a novel influenza A virus, H18N11<sup>12</sup>. In contrast to bats, where gastrointestinal infections with eukaryotic viruses are frequent and are commonly asymptomatic<sup>14</sup>, a similar colonization of the human gut with non-pathogenic eukaryotic viruses has not been reported, pointing to species-specific mechanisms<sup>15</sup>.

Studying coronavirus infection in the GI tracts of bats is difficult, since few institutions maintain bat colonies for *in vivo* infection experiments, and cell lines from the GI tract of bats are not available, limiting *in vitro* analyses<sup>16,17</sup>. Organoid cultures have excellent potential as a model to study the mechanisms of viral infection in bat cells *in vitro*<sup>18,19</sup>, since organoid lines can be derived from multiple species and tissues and can be maintained long term. Organoids are permanent three-dimensional cultures that replicate the physiological and functional characteristics of their tissues of origin and that allow controlled studies of complex primary GI

epithelial tissues *in vitro* <sup>20</sup>. Organoids from various human and murine tissues have been developed from tissue-derived stem cells and have been successfully used to investigate a wide range of disease processes, including viral infections <sup>18, 19, 21, 22</sup>. Importantly, growth conditions for organoids appear similar across multiple species <sup>23</sup>. In a recent study, Chan et al. successfully generated 3-D airway organoids from tracheal epithelial monolayer cultures of cave nectar bats, *Eonycteris spelaea* <sup>24</sup>. Two previous reports describe the generation of intestinal organoid cultures from bat species <sup>25, 26</sup>. Intestinal organoids developed from Chinese horseshoe bats, *Rhinolophus sinicus*, showed susceptibility to SARS-CoV-2, but lacked long-term active proliferation past 4-5 weeks <sup>27</sup>. Intestinal organoids derived from Leschenault's rousette, *Rousettus leschenaultii*, showed susceptibility to *Pteropine* orthoreovirus, but not SARS-CoV-2 <sup>25</sup>. However, neither of these studies evaluated the cellular antiviral mechanisms of bat organoid tissues <sup>25, 27</sup>.

The hypothesis that altered IFN responses in bats compared to other species promote increased viral tolerance is a central paradigm in bat immunology <sup>28, 29, 30</sup>. In Australian black flying foxes (*P. alecto*) and lesser short nosed fruit bats (*C. brachyotis*), a high level of constitutive IFN- $\alpha$  expression was detected <sup>30</sup>, which has led to the concept that an “always on” IFN signaling system in bats can effectively suppress viral replication and prevent disease early on after infection <sup>28, 31</sup>. Increased basal gene expression in bats also was described for several other genes involved in innate viral recognition and response, including IRF1, IRF3 and IRF7 <sup>32</sup> and the ISG oligoadenylate synthase 1 (OAS1) <sup>33</sup>. Conversely, gene expression of type I IFNs in multiple tissues from Egyptian fruit bats (*R. aegyptiacus*) was low at baseline, but was inducible upon viral infection <sup>34</sup>. Other studies have reported dampened activation of stimulator of IFN genes (STING), a nucleic acid sensor involved in the regulation of IFN expression upon viral

infection<sup>35,36</sup>. These reports highlight that the mechanisms of IFN expression, regulation, and signaling appear to be unique to individual bat species, pointing to a need for more detailed analyses.

Jamaican fruit bats (*Artibeus jamaicensis*, JFBs) are thought to be natural carriers of zoonotic pathogens such as rabies virus, West Nile virus and dengue virus<sup>37,38,39,40</sup>. JFBs are New World bats that are among the most common bats in the Americas and often live close to human settlements, so that spillover of zoonotic pathogens may occur. JFBs also are susceptible to experimental infection with Zika virus and MERS-CoV<sup>4,41</sup>. Based on the recently annotated genome<sup>42,43</sup>, JFBs have one interferon (IFN)- $\beta$ , four IFN $\alpha$ , one INF- $\kappa$ , one IFN- $\epsilon$  and four IFN- $\omega$  genes. Multiple interferon regulatory factors (IRFs) have also been identified. Therefore, JFBs are considered a relevant and tractable model system for studies of viral infection and antiviral immunity.

Here we established and characterized gut organoids from JFBs to study the susceptibility and immune response of the JFB intestinal epithelium to SARS-CoV-2 infection. Importantly, our organoid model was developed for a New World bat species, which have generally been underinvestigated<sup>44,45</sup>. We found that JFB intestinal epithelial cells supported modest viral replication that did not result in the release of infectious virions or cytopathic effects. Importantly, the organoids mounted a robust interferon response following exposure with infectious SARS-CoV-2. Proteomics and pathway analysis revealed that the JFB organoid proteome profiles matched profiles found in other SARS-CoV-2 infection studies in human nasal epithelium and multiple cell lines<sup>46,47,48,49,50</sup>. Moreover, SARS-CoV-2 infection activated innate inflammatory and cellular repair responses in the intestinal organoid model.

## Results

### Development and Characterization of JFB Gastrointestinal Organoids

We established JFB gastrointestinal organoid cultures from fresh and cryopreserved stomach and from proximal and distal intestine (Fig. 1a and Supplementary Fig. 1a, b). The microscopic anatomy of the proximal and distal intestinal tissue used for organoid derivation was consistent with that of the small intestine, with prominent villi and few goblet cells (Fig. 1b and Supplementary Fig. 3b). Organoids formed within one day of crypt/gland isolation and were successfully maintained in a simple growth medium containing DMEM and 50% L-WRN-conditioned medium (Supplementary Fig. 1c). The murine noggin, R-spondin, and Wnt3a secreted by the L-WRN cells<sup>1</sup> show protein sequence similarities of 98%, 86%, and 99% with the orthologous JFB proteins, suggesting that these factors would be active in JFB cells (Supplementary Fig. 2).

Established JFB organoids mimicked the epithelial structure of JFB gastrointestinal tissue, with a simple columnar epithelium, a basal nucleus, and a defined luminal space (Fig. 1b, Supplementary Fig. 3a, b). Mucus-secreting goblet cells were more common in organoids derived from distal intestine than those from proximal intestine, similar to the cellular composition of the respective tissues of origins (Fig. 1b, Supplementary Fig. 3a, b). Morphometric analysis with OrganoSeg<sup>2</sup> showed that organoid size varied between different passages, but with no clear trends, and organoid shape also did not change significantly over six consecutive passages (Fig. 1c).

We next performed transcriptional analysis of the organoids to confirm tissue-specific gene expression patterns. The distal and proximal intestinal organoids expressed the intestine-



specific genes *Vill* and *Cdx2* as well as *Ace2*, while the gastric organoids showed increased expression of the chief cell marker pepsinogen C (*Pgc*) (Fig. 1d). For two representative lines of the distal intestine, expression of the intestinal markers *Muc2*, *Vill* and *Cdx2* remained relatively stable over eight passages (Fig. 1e), with a significant increase of villin expression in p7 but no clear trends overall. Expression of *Pgc* and *Ace2* also remained stable (Fig. 1e). While *Pgc* is predominantly expressed in the stomach, expression in the small intestine has been described in humans<sup>3</sup>. Notably, copy numbers for *Ace2* were very low compared to the other targets.

We focused our further analyses on organoids from the intestine as a putative site for SARS-CoV-2 replication. To confirm the identity of the distal intestinal epithelium in our organoid model, we used immunofluorescence staining with cross-reactive antibodies and reagents. The majority of organoids had a typical apical-in conformation, with apical villin expression and strong phalloidin staining of the apical cell portions, indicative of the terminal actin web and microvilli formation (Fig. 2a). All cells also expressed intracellular epithelial cytokeratin. ACE2 expression was detected on the apical cell surface, with some weak basal staining. Transmission electron microscopy (Fig. 2b) confirmed the presence of characteristic microvilli on the apical surface of the epithelial cells, along with electron-dense apical junctional complexes consistent with an enterocyte phenotype. We further characterized the JFB distal intestinal organoids by performing an unbiased proteome analysis using data-independent acquisition (DIA) mass spectrometry. Several key proteins characteristic of small intestinal epithelial cells in other mammals such as villin, E-cadherin, keratin 18 and 19, Na<sup>+</sup>/K<sup>+</sup> ATPase, claudin 18, and a mucin (MUC5AC-like) were detected (Fig. 2c)<sup>4</sup>. Measurement of transepithelial electrical resistance (TEER) across organoid monolayers seeded on Transwell

inserts showed that the gastrointestinal organoids established a physiological epithelial barrier, with the stomach having the highest TEER compared to the intestinal organoids (Fig. 2d).

Collectively, these analyses demonstrate that gastrointestinal organoids from JFBs replicate key features of the gut epithelium.

#### Infection of Intestinal Organoids from JFBs with SARS-CoV-2 Leads to Replication of Viral Genomes

To determine whether the JFB intestine supports SARS-CoV-2 infection, organoids were dissociated and then inoculated with SARS-CoV-2 at MOIs of 0.1, 1 and 10. We selected distal intestinal organoids for these experiments, based on several previous publications that demonstrated SARS-CoV-2 replication in human ileal organoids<sup>5-7</sup>. Quantitative PCR analysis of viral genomes in JFB organoid cell lysates revealed a significant, concentration-dependent increase ( $>1$  log,  $P \leq 0.05$ ) in SARS-CoV-2 gene E RNA at 48 and 72 hours post infection (hpi, Fig. 3a). The SARS-CoV-2 PCR in culture supernatants showed a similar increase at an MOI of 1 at 48 hpi (Fig. 3b). Importantly, significant expression of subgenomic (sg)RNA ( $>2$  log-fold above baseline) for gene E indicating active viral replication in the organoids also was identified<sup>8</sup>, albeit at low levels (Fig. 3c). However, plaque assays performed on the culture supernatants failed to detect the presence of infectious SARS-CoV-2 above baseline values derived from the inoculum, suggesting incomplete or ineffective viral replication or failure to secrete infectious progeny virus (Fig. 3d). Notably, SARS-CoV-2 incubation in medium for 48 h did not impact detection of viral copy numbers by PCR but did reduce the viral titer measured by plaque assay by  $>1$  log-fold, suggesting a loss of infectivity over time (Supplementary Fig. 4). Interestingly, immunofluorescence analysis of SARS-CoV-2 spike protein in infected JFB organoids revealed

only a few positive cells, and these cells were not associated with morphologically intact organoids (Fig. 3e).

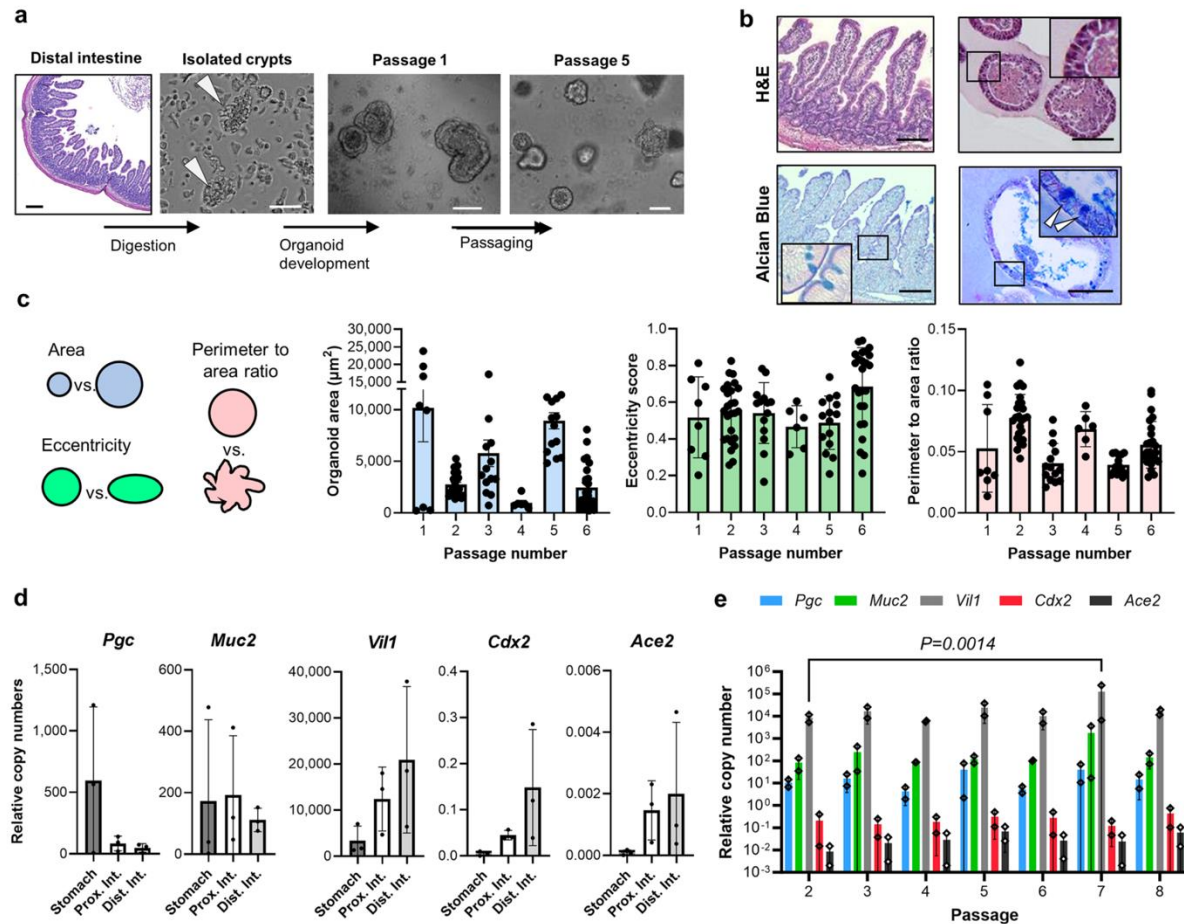


Figure 6.1. Development and culture of gastrointestinal organoids from Jamaican fruit bats. (A) Organoid derivation from Jamaican fruit bat (JFB) distal intestine. Tissue of origin, isolated intestinal crypts and formed organoids, representative of tissues from three bats, are shown. Scale bar: 200  $\mu\text{m}$  for distal intestine, others are 50  $\mu\text{m}$ . (B) Morphology of distal intestinal tissue (left) and distal intestinal organoids (right). Formalin-fixed, paraffin-embedded sections were stained with H&E (top row; bat 001, p2) or Alcian Blue (bottom row; bat 004, p3). High magnification insets show columnar cell shape and morphology of mucus-secreting goblet cells. Bars: 100  $\mu\text{m}$ . Images are representative of 2 organoid lines and tissues. (C) Size and morphology of distal intestinal organoids were analyzed over six consecutive passages using OrganoSeg<sup>2</sup>. Dots: individual organoids (p1: n = 8, p2: n = 26, p3: n=14, p4: n=6, p5: n=15, p6: n=25); bars: mean $\pm$ SD. (D) Tissue-specific gene expression patterns in JFB organoids derived from stomach, proximal and distal intestine. Pooled qRT-PCR data from n = 3 established organoid lines (p2-5) are shown; mean  $\pm$  SD. (E) Gene expression of distal intestinal organoids from two lines (bat004 and 005) was monitored over eight passages. Mean  $\pm$  SD from two

organoid lines with two technical replicates each; data was analyzed using ANOVA with Dunnett's multiple comparison test;  $P = 0.0014$  compared to p2. Source data are provided as a Source Data file.

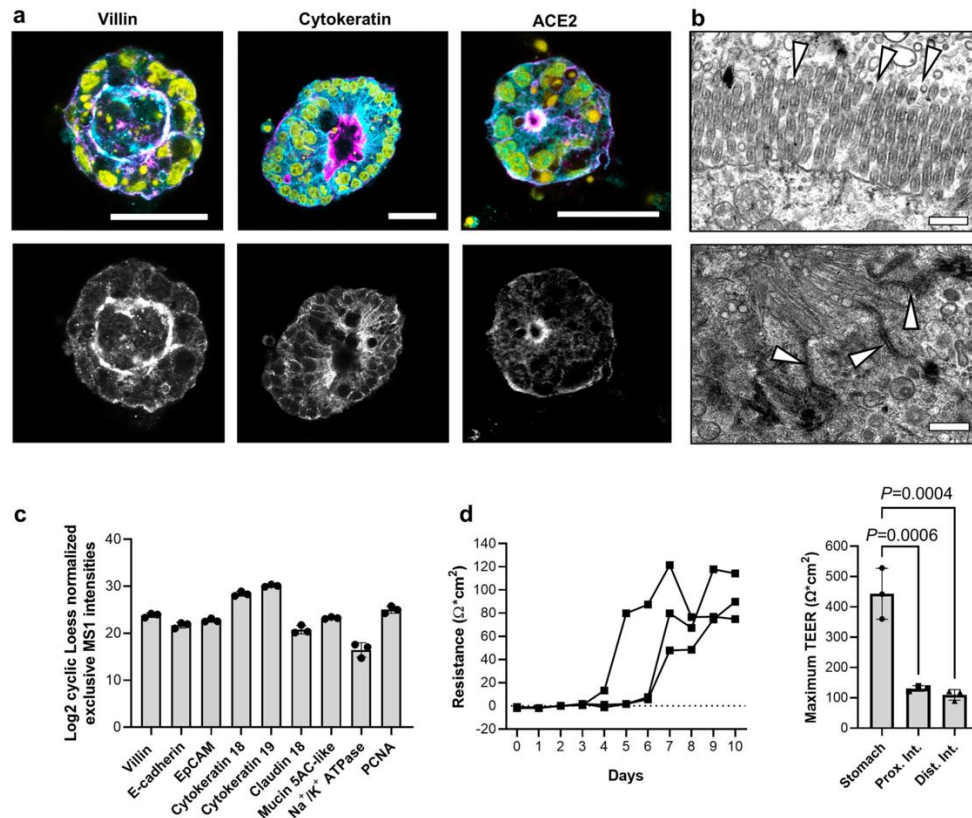


Figure 6.2. Intestinal organoids from Jamaican fruit bats maintain key characteristics of the intestinal epithelium. (A) Expression of intestinal epithelial cell markers and of ACE2 in JFB distal intestinal organoids. Whole mount cultures from three organoid lines (bat003, 004 and 005, all at p2) were stained with cross-reactive antibodies to cytokeratin, villin and ACE2 (cyan), phalloidin-Ax488 (magenta) and DAPI (yellow) and were imaged by confocal microscopy. Representative Z stacks created from 3-5 adjacent images are shown. Bars: 25  $\mu\text{m}$ . (B) Transmission electron microscopy images of JFB intestinal organoids, representative of two independent samples, show apical microvilli (top) and apical junctional complexes (bottom). Bat001, p1, bar = 500 nm. (C) Expression of select intestinal epithelial cell-specific proteins. JFB distal intestinal organoids (bat003, p9,  $n = 3$  technical replicates) were lysed and processed for data-independent acquisition mass spectrometry. Individual datapoints and mean  $\pm$  SD. (D) Transepithelial resistance (TEER) of JFB organoid cells cultured on Transwell inserts for 10 days (bat001, p5). One representative experiment with triplicate wells of distal intestinal organoids (left), and comparative data for the highest TEER achieved by three independent cultures each of gastric, proximal, and distal intestinal organoids are shown (right; individual data, mean  $\pm$  SD); one-way ANOVA with Tukey's post hoc test.

### Lack of Cytopathic Effect but Increased Growth in SARS-CoV-2-infected JFB Organoids

We also evaluated the cell viability of JFB distal intestinal organoids following SARS-CoV-2 infection by measuring caspase-3 activity with NucView®<sup>9</sup> (Fig. 4a). In Vero E6 cells, infection with SARS-CoV-2 induced a strong upregulation of caspase-3, consistent with the well-characterized cytopathic effect of the virus in this cell type. A small number of apoptotic cells were present in all JFB organoid cultures, likely due to physiological cell turnover. However, in contrast to observations in *Rhinolophus sinicus* organoids<sup>10</sup>, SARS-CoV-2 did not appear to have a cytopathic effect in JFB organoids (Fig. 4a,b), since the proportion of apoptotic cells did not change upon infection. Interestingly, SARS-CoV-2 caused a significant increase in organoid size and in the number of organoids that had re-formed from single cells after 48 h of infection (Fig. 4c,d), indicating that viral infection triggered increased cell proliferation in the bat intestinal epithelium.

### SARS-CoV-2 Induces Expression of Type I Interferons and Proinflammatory Cytokines in JFB Organoids

Unique characteristics of the interferon (IFN) system have been linked to the increased viral tolerance observed in many bat species<sup>11</sup>. Therefore, we used quantitative RT-PCR to analyze gene expression of type I interferons and proinflammatory cytokines in JFB distal intestinal organoids following 48 h exposure to SARS-CoV-2. As shown in Fig. 5a, expression of *Ifna* was upregulated at 48 hpi with an MOI of 10, while an MOI of 1 caused significant upregulation of the gene at 72 hpi. Gene expression of *Ifnb* also was significantly increased with both MOIs at 48 hpi and remained elevated with the lower viral dose at 72 hpi (Fig. 5b). Type III IFNs are known to play a role in mucosal antiviral immunity and SARS-CoV-2 infection and

also may have unique functions in bats<sup>12-14</sup>. However, the type III IFN loci in JFBs are poorly annotated<sup>15,16</sup>, and we were unable to generate functional primers based on the published genome. Interestingly, organoid infection with SARS-CoV-2 at an MOI of 1 significantly increased expression of the proinflammatory cytokines *Tnf* and *Il6* at 48 hpi, and *Il6* remained elevated at 72 hpi (Fig. 5c,d). The above data suggest that JFB distal organoids exhibited an antiviral and pro-inflammatory response to SARS-CoV-2 infection.

To determine whether active viral infection was responsible for the observed induction of antiviral and inflammatory genes, or whether gene expression was induced by unspecific activation of pattern recognition receptors, we also treated the JFB organoids with a panel of TLR agonists targeting TLR2, 3, 7, and 9 and with UV-inactivated SARS-CoV-2 for 48 h. Notably, stimulation with TLR2/1 and TLR3 agonists led to increased expression of interferon and inflammatory cytokines 6 h post inoculation (Supplementary Fig. 5). However, no significant upregulation of these genes was observed with any of the stimuli at 48 h (Fig. 5e-h). These observations suggest that active infection with SARS-CoV-2 is required for sustained upregulation of antiviral and inflammatory gene expression.

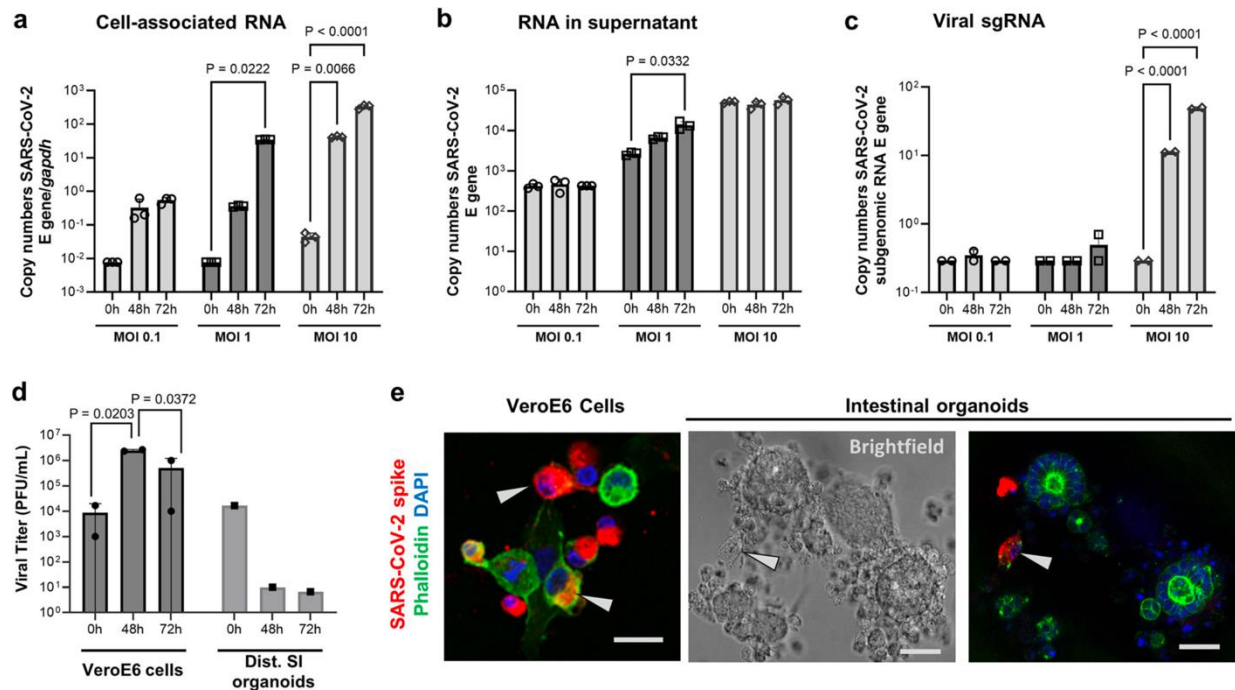


Figure 6.3. Replication of SARS-CoV-2 in JFB intestinal organoids. Dissociated JFB distal intestinal organoids (bat001, p6) were inoculated with SARS-CoV-2 (strain USA-WA1/2020) for 2 h or were mock-treated and then washed and re-embedded in Matrigel. At 48 and 72 h post-infection, RNA was extracted from (A) the organoids and (B) the culture supernatants, and replication of SARS-CoV-2 was analyzed by quantitative real-time PCR (qRT-PCR) for the envelope (E) gene using the standard curve method. Panels show data from one representative out of four independent experiments with  $n = 3$  technical replicates as mean  $\pm$  SD, analyzed by ANOVA with Dunnett's multiple comparisons test. (C) RNA extracted from the organoids was analyzed for viral sgRNA (E gene) using a leader-specific primer. One representative out of three independent experiments with  $n = 2$  technical replicates, mean  $\pm$  SD, analyzed by ANOVA with Dunnett's multiple comparisons test. (D) Supernatants from SARS-CoV-2 infected organoids (pooled from three replicates) or Vero E6 cells (duplicate wells) were analyzed by plaque assay for the presence of infectious SARS-CoV-2; representative of four experiments. e SARS-CoV-2 protein detection in isolated epithelial cells, but not in intact JFB intestinal organoids. Organoids or Vero E6 cells were fixed and permeabilized at 48 h post SARS-CoV-2 infection (MOI 10) and then were stained with DAPI (blue), phalloidin (green) and a monoclonal antibody to SARS-CoV-2 spike protein (red). Arrows point out cells containing SARS-CoV-2 spike protein. Data are representative of three independent experiments. Scale bar = 25  $\mu$ m.

### Impact of SARS-CoV-2 Infection on the JFB Intestinal Epithelial Cell Proteome

A quantitative proteomic workflow based on data-independent acquisition (DIA) mass spectrometry was used to perform a comprehensive analysis of the cellular responses of JFB

organoids to SARS-CoV-2 infection. The DIA analysis of SARS-CoV-2-infected and mock infected enteroids after 48 h yielded a total of 8,321 proteins and protein isoforms, based on protein FASTA files retrieved from the *A. jamaicensis* reference genome<sup>17,18</sup>. Interestingly, all detected proteins were present in both experimental conditions. A comparative analysis of mock-infected and SARS-CoV-2 infected JFB organoids revealed 63 upregulated and 155 downregulated proteins, including isoforms, with a  $\geq 2$ -fold change at  $P \leq 0.05$  (Fig. 6a and Supplementary Data 1). To better understand antiviral responses in the JFB intestine, we next compared the identified proteins to a comprehensive list of human interferon-stimulated genes (ISGs, Supplementary Data 2)<sup>19</sup>. Interestingly, 100 of all identified JFB proteins could tentatively be classified as ISGs. However, only one of the ISG proteins, ribonucleases P/MRP protein subunit POP1 (POP1), was significantly upregulated in response to SARS-CoV-2, while four ISG proteins (ERLEC1, CFB, ARMCX3 and ITIH2) were significantly downregulated (Fig. 6b). Overall, top upregulated proteins, based on fold change in abundance, were hepatocyte growth factor-like protein/macrophage stimulatory protein (HGFL/MST1), CUB domain-containing protein 1-like, acyl-CoA-binding domain-containing protein 5 (ACBD5), ketosamine-3-kinase (KT3K) and insulin-like growth factor 2 mRNA-binding protein 1 (IGF2BP1, Fig. 6c). Top down-regulated proteins included BTB/POZ domain-containing adapter for CUL3-mediated RhoA degradation protein 3 (KCTD10), CSC1-like protein 1 (TMEM63A), nuclear complex protein 3 homologue, histone H2A- $\beta$ , and cell division complex protein 45 homologue (CDC45). Several of these proteins are involved in regulation of cell turnover and posttranslational modifications. We next performed Ingenuity Pathway Analysis (IPA) and Enrichr analysis<sup>20</sup> to assess more complex functional changes induced by SARS-CoV-2. IPA revealed acute phase



response signaling, a key innate pathway triggered by infection and injury, as the most significantly regulated pathway, followed by Apelin liver signaling<sup>21</sup>, which is involved in intestinal inflammation, repair, and wound healing (Fig. 6d). Top regulated cellular functions were cell assembly, organization, maintenance, movement, signaling and morphology (Fig. 6d). These findings suggest that SARS-CoV-2 triggers regenerative response pathways, consistent with the increased organoid size observed in the SARS-CoV-2-infected compared to mock-infected cultures. Similarly, Enrichr identified significant upregulation of pathways associated with cell viability and differentiation, such as PI3/AKT signaling and the longevity regulating pathway, along with signatures associated with intestinal epithelial infection and chemokine signaling when using the human 2021 KEGG pathways database (Fig. 6e). Importantly, Enrichr analysis also found multiple significant matches for protein signatures that were previously found to be upregulated in SARS-CoV-2 infection in Vero E6 cells<sup>22-24</sup>, MA-104 cells<sup>24</sup>, a human hepatocyte line<sup>25</sup>, and human nasal epithelium<sup>26</sup> (Fig. 6f). Overall, the proteomics analysis points to the activation of innate inflammatory and regenerative pathways along with characteristic COVID-19 signatures upon SARS-CoV-2 infection of the JFB intestinal epithelium.

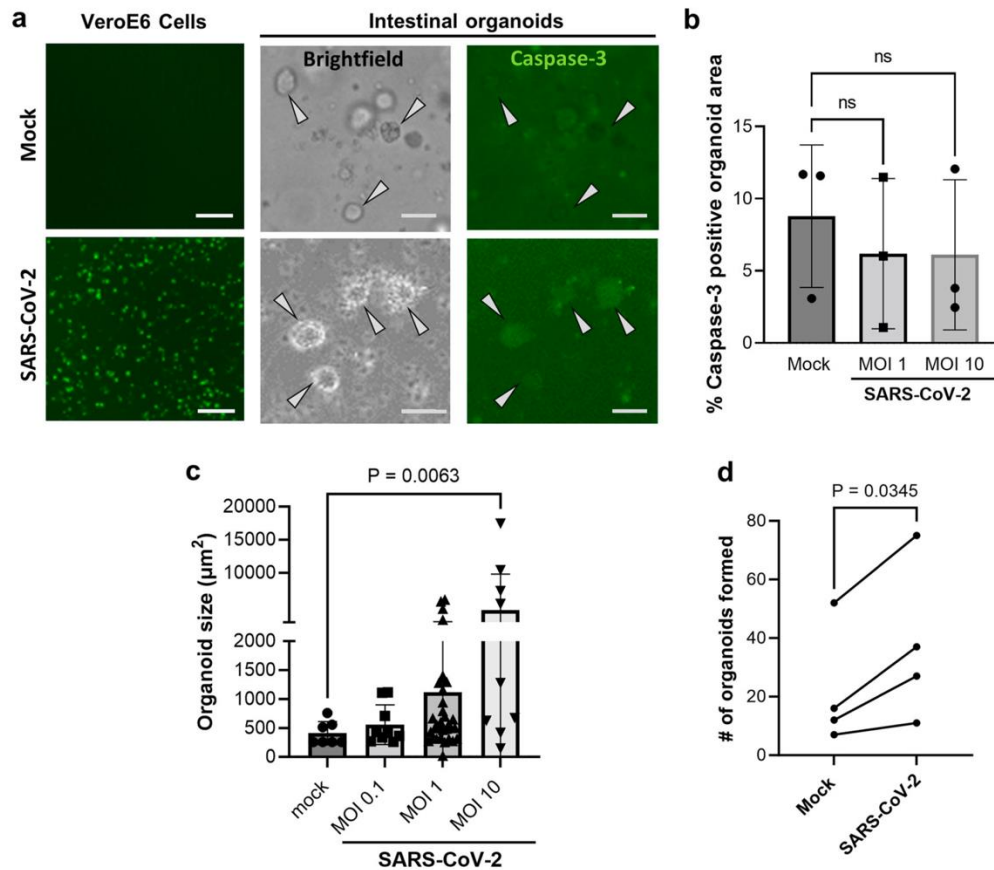


Figure 6.4. Increased growth of JFB organoids infected with SARS-CoV-2. Dissociated JFB distal intestinal organoids or Vero E6 cells were mock-inoculated or were infected with SARS-CoV-2 at an MOI of 1 or 10, as described above, with NucView® 488, a cell membrane-permeable fluorogenic caspase-3 reporter, added to the medium. (A) At 48 h post infection, the cells were imaged using fluorescence and phase contrast (brightfield) microscopy. Bat005, p7, scale bars = 50  $\mu\text{m}$ , representative of four experiments. (B) ImageJ was used to quantitate NucView® fluorescence based on pixel counts in thresholded digital images of manually selected organoids. Individual data points, mean  $\pm$  SD of one representative (bat002, p7) of four independent experiments with three technical replicates is shown, data were analyzed by ANOVA with Tukey's multiple comparison test. (C) Organoid size in SARS-CoV-2-infected organoid cultures after 48 h was determined on brightfield images using ImageJ. Individual data points, mean  $\pm$  SD of one representative experiment (bat001, p6) of five independent experiments with three technical replicates is shown, data were analyzed by ANOVA with Tukey's multiple comparisons test. (D) Number of detected organoids in random brightfield images from mock-infected and SARS-CoV-2 infected JFB organoid cultures (MOI 10, 48 h). Pooled data from four independent experiments (bat001, p6; bat002, p7; bat003, p13; bat005, p5); analyzed using a paired 2-sided Student's t test.

## Discussion

In this study, we established and characterized organoid cultures from the proximal and distal intestine and stomach of JFBs, a frugivorous species of New World bats, which have generally been underrepresented in immunological and virological studies<sup>27,28</sup>. Using this organoid model, we investigated the response of JFB intestinal epithelial cells to infection with SARS-CoV-2. Considering that JFBs are susceptible to MERS-CoV, Zika virus, and rabies virus<sup>29-31</sup>, we evaluated the susceptibility of the JFB distal intestinal organoids to SARS-CoV-2. We found evidence of limited, non-productive infection with induction of antiviral genes. Notably, JFBs are not thought to be natural carriers of SARS-CoV-2 or of related sarbecoviruses, and a recent preprint describing *in vivo* infection experiments in JFBs indicated that SARS-CoV-2 leads to an abortive infection of the intestine without development of clinical disease<sup>32</sup>. Since SARS-CoV-2 is not adapted to JFBs, we assume that no host-specific viral immune evasion mechanisms have evolved, enabling activation of innate response pathways. Considering the vast number and associated genetic diversity of bat species, it is not surprising that SARS-CoV-2 infection experiments in other bat species have yielded conflicting results. In Egyptian fruit bats (*Rousettus aegyptiacus*), transient asymptomatic respiratory tract infection with viral replication in lung and trachea and oral and fecal shedding was achieved upon experimental SARS-CoV-2 inoculation<sup>33</sup>. Conversely, American big brown bats (*Eptesicus fuscus*) appeared resistant to infection with SARS-CoV-2<sup>34</sup>. Two independent studies on Brazilian free-tailed bats (*Tadarida brasiliensis*) by Bosco-Lauth<sup>35</sup> and Hall<sup>36</sup> found variable levels of susceptibility to SARS-CoV-2 infection in the absence of clinical signs. Likewise, intestinal organoids derived from two different bat species responded differently to SARS-CoV-2 infection. Organoids from Chinese

horseshoe bats, where SARS-CoV-2-like virus has been detected<sup>37</sup>, produced infectious SARS-CoV-2 virions at similar levels as human intestinal organoids<sup>10</sup>. In contrast, intestinal organoids from Leschenault's rousette bats (*Rousettus leschenaultii*) failed to support SARS-CoV-2 replication<sup>38</sup>, and airway organoids from cave nectar bats (*Eonycteris spelaea*) allowed ACE2-dependent viral entry, but no productive viral replication<sup>39</sup>. In our hands, the JFB intestinal organoids consistently expressed low levels of ACE2 that could support viral entry. Interestingly, PCR analysis revealed a significant increase in viral and sgRNA in the JFB distal organoids at 48 and 72 hpi, which demonstrates initiation of viral replication in the organoids. SARS-CoV-2 genomes also were significantly increased in organoid culture supernatants, whereas plaque-forming units were detected but did not increase over time. Thus, it remains unclear whether any infectious or non-infectious virions were released. Using immunohistochemistry, we detected SARS-CoV-2 spike protein in individual cells, but not in morphologically intact JFB organoids. This observation may reflect shedding of viable virus-infected cells from the epithelial monolayer, as described for other viral infections<sup>40</sup>. Overall, our data suggest that JFB intestinal organoids support incomplete SARS-CoV-2 infection. A similar limited and incomplete replication of SARS-CoV-2 was also reported in cell lines from several different bat species, even after transduction with human ACE2, in a recent study by Aicher *et al.*<sup>41</sup>. However, the presence of sgRNA and of SARS-CoV-2 protein in some cells suggest that entry and replication of the virus did occur in the JFB organoids. This interpretation is consistent with a study by Yan *et al.* that predicted a moderate ability of SARS-CoV-2 to infect JFB cells based on the protein sequence of the SARS-CoV-2 receptor ACE2<sup>42</sup> and our observations of low ACE-2 gene expression in the JFB organoids. Loss of the furin cleavage site in the WA01 reference strain of

SARS-CoV-2 also may have had an impact on the efficacy of infection<sup>43</sup>. Further experiments are needed to evaluate at which stage of the viral replication cycle SARS-CoV-2 replication stalls in the JFB organoid model and upon *in vivo* infection of JFBs<sup>32</sup>. Notably, many previous studies on viral infection in bats have relied solely on viral nucleic acids to measure infection<sup>34,44-48</sup>. Therefore, it is difficult to assess whether the failure to detect replication-competent virions was unique to our infection model.

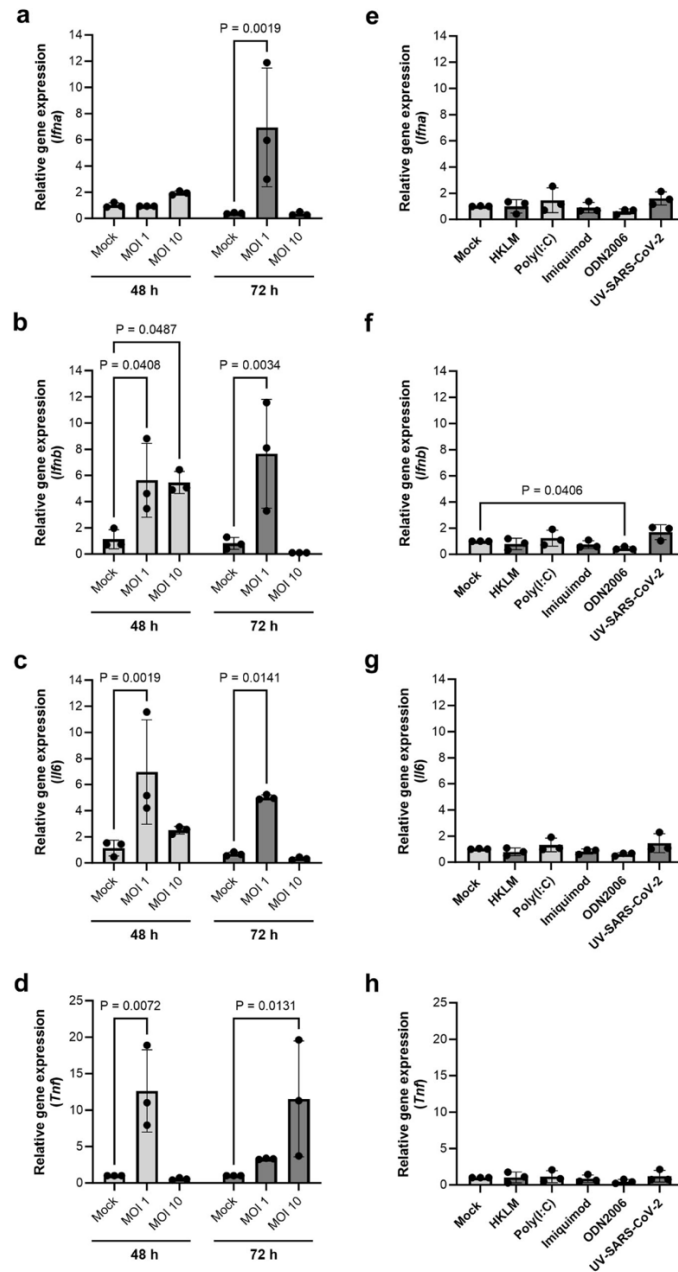


Figure 6.5. JFB distal intestinal organoids express antiviral and pro-inflammatory genes in response to infection with SARS-CoV-2. (A-D) Dissociated JFB distal intestinal organoids (bat001, p6, three replicates) were infected with active SARS-CoV-2 at an MOI of 1 or 10. The unbound virus was washed off, and the cells were re-plated in Matrigel. After 48 or 72 h, the RNA was extracted from the cells to evaluate gene expression via quantitative real-time PCR (qRT-PCR). Data from one representative out of four independent experiments are shown as mean  $\pm$  SD. (E-H) Organoids were treated with UV-inactivated SARS-CoV-2 at 10  $\mu$ g/mL, or with a panel of TLR agonists (TLR2: heat-killed *L. monocytogenes*, HKLM; TLR3: low MW poly I: C; TLR7: imiquimod, TLR9: ODN2006) and then were analyzed by qRT-PCR 48 h after

stimulation. Pooled data from three independent experiments (bat001, p6; bat004, p5; bat003, p5); mean  $\pm$  SD are shown. Graphs show gene expression of (A,E) *Ifna* (IFN- $\alpha$ ), (B,F) *Ifnb* (IFN- $\beta$ ), (C,G) *Il6* (IL-6) and (D,H) *Tnf* (TNF- $\alpha$ ). All data were analyzed using the  $2^{(-\Delta\Delta Ct)}$  method with GAPDH as a housekeeping gene and are expressed as fold change relative to the mock-infected control. ANOVA with Dunnett's multiple comparisons test.

Our results demonstrate that active SARS-CoV-2 virus induced a robust anti-viral immune response, with increased expression of IFN- $\alpha$  and IFN- $\beta$  at 48 h after SARS-CoV-2 infection. This induction of interferons in response to viral infection was surprising, since it has been proposed that the interferon system in bats is constitutively active, based on studies in Australian black flying foxes (*P. alecto*)<sup>11,49</sup>. Conversely, potent interferon responses were detected in serotine bats (*Eptesicus serotinus*) and David's myotis bat cells upon SARS-CoV-2 infection<sup>41</sup>. These observed differences point to species-specific immune system characteristics in bats, consistent with the high level of genetic diversity in the order Chiroptera, which comprises over 1,400 species.

The lack of a cytopathic effect in SARS-CoV-2-infected JFB organoids was an intriguing observation. It has been shown that SARS-CoV-2 causes neither apoptotic nor necrotic cell death in the gastrointestinal tract of infected human patients. Whether SARS-CoV-2 impacts viability of organoid cultures is still a matter of debate. Lamers *et al.*<sup>5</sup> observed increased apoptotic cell death in human enteroids at 60 hpi, and Zhou *et al.*<sup>10</sup> state that both human and horseshoe bat enteroids developed a cytopathic effect after SARS-CoV-2 inoculation. Conversely, studies by Stanifer *et al.*<sup>12</sup> and Zang *et al.*<sup>50</sup> did not describe increased cell death in human SARS-CoV-2 infected enteroids. Data from several studies in bat cells suggest that heightened IFN responses in these cultures may prolong viral infection by limiting pathogen-induced cell death through induction of anti-apoptotic genes including BCL-2 and PMAIP1<sup>48,51</sup>. While we did not detect an

upregulation in anti-apoptotic factors in our proteome screen of SARS-CoV-2-infected JFB organoids, we found a significant upregulation of pathways associated with cell growth and repair, including apelin liver signaling and wound healing signaling. These observations were consistent with the increase in organoid size and organoid formation that we detected by microscopic analysis and indicate activation of growth and repair pathways in response to SARS-CoV-2 infection. Taken together, our findings suggest that bat organoids activate protective repair pathways upon viral infection that may enable the bats to tolerate viral infection in the absence of tissue damage and associated clinical signs.

We used a DIA-based proteomic approach to gain deeper insights into the cellular responses induced in the SARS-CoV-2 infected JFB intestinal epithelium. Notably, only few studies in bats and other non-model organisms have included proteomics<sup>52,53</sup>, although proteomics techniques can be particularly useful in species where few specific reagents are available<sup>54</sup>. We confirmed the identity of the organoids as small intestinal epithelial cells based on expression of key enterocyte markers. Consistent with the increased gene expression of pro-inflammatory cytokines in SARS-CoV-2-infected JFB organoids that we detected, inflammatory pathways including the acute phase response and chemokine signaling also were induced at the protein level. Conversely, although SARS-CoV-2 infection induced expression of type I interferon transcripts in JFB organoids, no significant increase in ISGs was detected on the protein level. This lack of ISG regulation is inconsistent with proteomics results obtained in SARS-CoV-2-infected human Calu-3 cells, which showed a strong induction of the antiviral ISG signature<sup>55</sup>, and may reflect a JFB-specific disconnect between transcriptional activation of interferons and downstream ISGs that warrants further studies. Alternatively, downregulation of



ISG proteins may have been caused by active downregulation of antiviral ISG pathways by SARS-CoV-2 accessory proteins. Importantly, Enrichr analysis also revealed that some of the activated pathways matched those identified by other studies on SARS-CoV-2 infection. Notably, there are several limitations to the proteomics approach undertaken in our study. First, the non-targeted DIA approach may not be sensitive enough to identify strongly regulated targets with a low overall expression level <sup>56</sup>. Second, an annotated proteome of the JFB is currently not available and thus had to be inferred from the genome, which may lead to misidentified proteins. Lastly, pathway analysis was based on human databases, which again may miss JFB-specific signaling pathways.

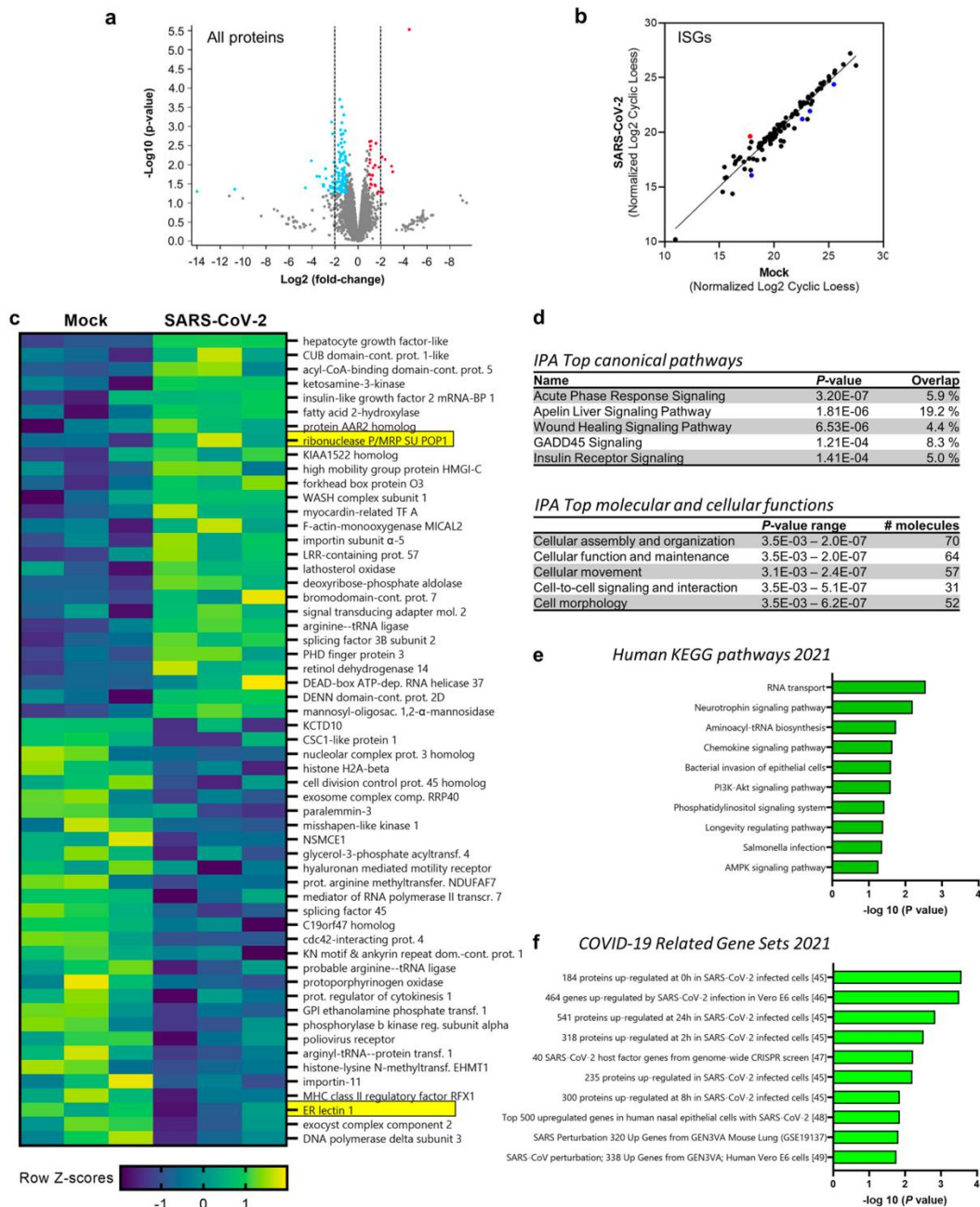


Figure 6.6. Proteome analysis of SARS-CoV-2-infected JFB organoids at 48 h. JFB distal SI organoids (bat003, p9) were infected with SARS-CoV-2 at an MOI of 10 or underwent mock treatment for 48 h and then were lysed and processed for data-independent acquisition (DIA) mass spectrometry. N = 3 replicates from one organoid line were analyzed. Imfit with empirical Bayes smoothing, a linear regression model from the Limma R package, was used with FDR correction for multiple tests. (A) Volcano plot showing all detected proteins and protein isoforms. Proteins with significantly increased or decreased expression ( $\geq 2$ -fold change;  $P \leq 0.05$ ) are shown in red and blue. (B) Expression of interferon-stimulated genes (ISGs), identified based on OhAinle *et al.* (2018)<sup>19</sup>, in mock-infected and SARS-CoV-2 infected JFB organoids. Proteins

with significantly increased or decreased expression ( $\geq 2$ -fold change;  $P \leq 0.05$ ) are shown in red and blue. (C) Heatmap showing relative change (Z-scores) of all 27 significantly upregulated proteins and of the top 30 downregulated proteins ( $P \leq 0.05$ ). Data from triplicate cultures are shown. Protein function was determined using UniProtKB (H. sapiens). Significantly regulated ISGs are highlighted in yellow. (D) IPA analysis showing top regulated canonical signaling pathways (top) and molecular and cellular functions (bottom) activated in SARS-CoV-2 infected JFB organoids. Enrichr pathway analysis using (E) the 2021 human KEGG pathway database and (F) the 2021 COVID-19 related gene sets. Pathways were ranked based on combined score ranking.

Importantly, we successfully validated JFB organoids as an experimental tool and demonstrated that these JFB organoids can be maintained long term without the need for bat specific growth factors. Wnt, noggin and R-spondin are highly conserved in mammalian species, with a high degree of sequence identity between mice and JFBs. The growth requirements for our JFB organoids are consistent with growth conditions previously described for Chinese horseshoe bats<sup>10</sup> and Rousettus bats<sup>38</sup>. Similar culture conditions also have been successfully used to culture intestinal organoids from cat, dog, cow, horse, pig and sheep<sup>57</sup>. We demonstrate that JFB organoids from stomach, proximal and distal intestine recapitulate the histology and morphology of the tissue of origin, with polarized columnar epithelial cells, mucus secretion, development of an intact epithelial barrier and expression of tissue-specific genes and proteins. Thus, we have developed and validated a research tool that will allow experimental analysis of the physiology and function of the gastrointestinal epithelium of Jamaican fruit bats in future studies.

To summarize, we established and characterized JFB gastrointestinal organoids that recapitulated the organ-specific multicellular composition of JFB gastrointestinal tissue. We demonstrated SARS-CoV-2 sgRNA replication at a low efficiency in JFB distal intestinal organoids via qPCR but were unable to detect release of infectious virus. SARS-CoV-2 infection

induced a robust upregulation of interferons and pro-inflammatory genes in the organoid cells. Moreover, SARS-CoV-2 infection of JFB organoids led to increased growth and activation of cellular regeneration and healing pathways, which might contribute to the improved viral tolerance in this bat species.

## Methods

### Ethics Statement

The research presented here complies with all relevant ethical regulations and was approved by the Colorado State University Institutional Animal Care and Use Committee (IACUC) under protocol #1034.

### Tissue Samples

Male and female Jamaican fruit bats (*Artibeus jamaicensis*) aged between one and eight years were maintained as an outbred breeding colony in an AAALAC-accredited facility at Colorado State University (CSU). For organoid derivation, five bats (4 males, bat001, 002, 004 and 005; and 1 female, bat 003) were euthanized by 5% isoflurane in O<sub>2</sub> followed by thoracotomy. The gastrointestinal tracts were harvested in RPMI-1640 medium and were shipped overnight on ice from CSU to Montana State University (MSU).

### Crypt and Gland Isolation

Bat tissues were processed immediately upon arrival or were cryopreserved and then thawed rapidly if needed<sup>58</sup>. To derive organoids, proximal intestinal and distal small intestinal tissues were washed in cold PBS and cut into ~1mm pieces. The minced tissue was incubated in 15 mM EDTA in PBS supplemented with penicillin, streptomycin, and Fungizone (GE

Healthcare Life Sciences) with gentle shaking for 10 min increments until crypts appeared in the supernatant. Large tissues pieces were removed by sedimentation. The supernatant containing the crypts was transferred into a new 50 mL tube and pelleted by centrifugation for 8 min at 150 g. Gastric tissues were digested for one hour at 37° C using a digestion solution containing 5 U/mL collagenase type IV and 0.2 mg/mL DNase (both Sigma-Aldrich), following our published protocols<sup>59,60</sup>. Recovered crypts/glands were resuspended in 10 µl of Matrigel and plated in 96-well plates. After the gel was polymerized, 200 µl of medium (Supplementary Table 1) was added, and the plates were incubated at 37°C with 5% CO<sub>2</sub> for one week.

#### Maintenance of JFB Organoids

For passaging, the Matrigel patties containing organoids were digested for 3 min in TrypLE (Gibco) at 37°C and pipetted up and down 50 times. The digested organoids were harvested by centrifugation for 5 min, 200 g at 4°C, then were resuspended in Matrigel and plated in a 24-well plate. After the gel had polymerized, 500 µl of 50% L-WRN-conditioned medium<sup>1</sup> (Supplementary Table 1) was added and the plate was incubated at 37°C with 5% CO<sub>2</sub>. The medium was changed every other day and the organoids were passaged every 5-7 days. In general, organoids at passages three to ten were used for experiments.

#### Optimization of Growth Conditions

In addition to the basic growth medium, termed L-WRN medium, described above, we also tested a commercially available growth medium, IntestiCult™ (StemCell), a complex medium termed “colonoid medium” described by Tsai *et al.*<sup>58</sup>, and analyzed medium supplementation with a number of different growth factors commonly used in organoid culture protocols (Supplementary Table 1). We prepared a medium with all available growth factors (L-

WRN Plus) and then eliminated one reagent at a time from L-WRN Plus to determine the influence of the reagent on organoid growth. For this assay, the organoids were digested with TrypLE for 3 min and plated in a 96-well plate with the different media. Cell viability and proliferation were measured using the CellTiter-Glo luminescence assay (Promega).

### Microscopic Analyses

Images of organoid cultures were captured using a Keyence BZ-X800 microscope with BZ-X800 Viewer software, v01.02.03.02 or an EVOS FL Auto System (ThermoFisher). Size and morphology of organoids was analyzed using OrganoSeg software<sup>2</sup> and phase contrast images. Measurements were performed on digital images by blinded investigators using ImageJ software. For histological analyses, organoids were recovered from the culture plates and treated with Histogel (ThermoFisher) prior to formalin fixation and paraffin embedding, following standard protocols. Slides were stained with hematoxylin/eosin and with Alcian Blue to visualize mucus production. TEM was performed as previously described for human organoids<sup>59</sup>. Briefly, organoids were fixed in 3% glutaraldehyde, processed for ultrathin sectioning, and then were imaged on a Zeiss LEO 912AB TEM.

### Immunofluorescence Staining

To detect enterocyte markers and ACE2, we used antibodies to epithelial cytokeratin (1 : 50, ThermoFisher, #4545; clone C11), villin (1 : 100, Invitrogen, PIMA516408, clone SP145) and ACE2 (1 : 100, R&D Systems, AF933, goat polyclonal) that have known reactivity across multiple different species. To detect SARS-CoV-2 protein in the organoid cultures, a monoclonal antibody to SARS-CoV-2 (11G10-F8) was generated in house, using a standard hybridoma protocol<sup>61</sup>. Briefly, mice were immunized with 10 µg UV-inactivated SARS-CoV-2 (USA-

WA1/2020)<sup>62</sup> in Titermax adjuvant (Sigma) three times separated by at least two weeks. 11G10-F8 was then generated from a fusion of mouse splenocytes with SP2/0 cells. Mouse sera were screened for reactivity to the virus by ELISA. Clone 11G10-F8 recognizes the RBD region of the S1 subunit of the spike protein, as determined by ELISA, and was used at a concentration of 10 µg/mL. For immunofluorescence analysis, organoids were fixed with 4% PFA, permeabilized with 0.2% Triton X-100, and then treated with blocking buffer (DPBS with 10% FBS, 0.2% Triton X-100, 0.1% BSA, and 0.05% Tween) overnight. After washing, samples were incubated with primary antibody for 2 hours at room temperature. Then the secondary antibodies (anti-rabbit IgG AlexaFluor 555, 1: 50, Southern Biotechnology, #4050-32; goat anti-mouse IgG (H+L) AlexaFluor 594, 1 : 100, Invitrogen, A11005; or rat anti-mouse IgG1 eFluor660, 1 : 100, eBiosciences, 50-112-4348), were added and incubated for 2 hours at room temperature. The nuclei were stained with 5 µM DAPI (MP Biomedicals, 0215757405). Actin filaments were stained with ActinGreen 488 ReadyProbes reagent (Invitrogen, R37110). Stained organoids were imaged on an inverted SP5 Confocal Scanning Laser Microscope or an inverted DMI8 Stellaris (Leica) with LAS X software version 4.5.0 or earlier using a 20x objective (W 2010; Zeiss, Oberkochen, Germany). Z-stacks of 2-11 randomly selected organoids with intact morphology for each experiment and condition were recorded.

### Transepithelial Electrical Resistance

To assess development of barrier function, organoids were dissociated and re-seeded on Transwell inserts (Costar, Corning, 3 µm pore size) coated with collagen I. Transepithelial resistance was measured daily using a Voltohmmeter (EVOM2™, World Precision Instruments) and is expressed as  $\Omega \cdot \text{cm}^2$ .

### SARS-CoV-2 Infection of JFB Organoids

Bat organoids were dissociated by incubation with 350  $\mu$ L TrypLE to expose the apical and basolateral epithelial surface to the virus. Dissociated organoids were transferred to a BSL3 laboratory and then inoculated with SARS-CoV-2 (strain USA-WA1/2020, BEI Resources), at a multiplicity of infection (MOI) of 0.1, 1 and 10 for 2 h at 37°C with frequent gentle agitation. Notably, the SARS-CoV-2 strain used was shown to have a defective furin cleavage site <sup>63</sup>, but readily infected inducible pluripotent stem cell-derived human intestinal organoids in control experiments. Following incubation with the virus, organoids were collected into 500  $\mu$ L DMEM and centrifuged at 200 g for 5 min to wash. Then cells were resuspended in 30  $\mu$ L Matrigel and plated. After 10 min to allow gelation of the Matrigel, medium was added to the organoids. This medium was removed and fresh medium added to eliminate free viral particles. Then the plates were incubated at 37°C for the indicated intervals. Infectious particles in culture supernatants were detected for each time point by plaque assay on Vero E6 cells, as previously described<sup>62</sup>.

### Treatment of JFB Organoids with TLR Agonists and Inactivated Virus

To analyze the transcriptional response of JFB organoids to stimulation with pathogen-associated molecular patterns, organoids were trypsinized and then re-embedded into Matrigel in the presence of the following TLR agonists (Human TLR1-9 agonist kit, InvivoGen): TLR1, Pam3CSK4, 1  $\mu$ g/mL; TLR2, heat-killed *Listeria monocytogenes* ( $10^8$ /mL); TLR3, low molecular weight poly I:C, 10  $\mu$ g/mL; TLR7, imiquimod, 1  $\mu$ g/mL; TLR9, ODN2006, 5  $\mu$ M. Alternatively, organoids were treated with UV-inactivated SARS-CoV-2 <sup>62</sup> (10  $\mu$ g/mL). After 48 h, organoids were lysed in TRI Reagent (Sigma) and processed for RNA isolation and RT-PCR.



### Quantitative RT-PCR

To analyze gene expression and cell-associated viral RNA, RNA was extracted from organoids using the Direct-zol RNA Miniprep-Plus (Zymo Research). The RNA was converted to cDNA using iScript Reverse Transcription Super mix for RT-qPCR (BioRad). Primers for gastric and intestinal epithelial cell-specific genes and cytokines were designed using NCBI primer blast using the JFB genome (*Artibeus jamaicensis*, NCBI:txid9417,) and are listed in Supplementary Table 2. GAPDH was amplified as housekeeping gene in each PCR reaction. For each gene, a standard curve was created, and gene copy numbers for each gene of interest were normalized to the copy numbers of the housekeeping gene, GAPDH. To quantify SARS-CoV-2 in the organoid supernatant, viral RNA was extracted from culture supernatants using the QIA®Amp Viral RNA Mini kit (Qiagen). Viral genomes were then quantified in a single step RT-PCR reaction using primers and a TaqMan probe to the SARS-CoV-2 envelope (E) gene, as previously described <sup>62</sup>, and the Quanta Bio ToughMix Master Mix. In addition, a forward primer to the leader sequence was used together with the reverse primer and probe to detect E gene sgRNA as described by Wölfel *et al.* <sup>8</sup>. An RNA standard curve generated from a T7 *in vitro* transcribed gBlock™ sequence (Integrated DNA Technologies) was used for normalization.

### Cell Viability and Organoid Growth

To measure caspase-3 activity in SARS-CoV-2-infected organoids, NucView488 (Biotium) was added to the medium at 3  $\mu$ M once the organoids were re-plated following incubation with the virus. For measuring caspase-3 activity, the organoids were imaged using Life Technologies EVOS FL Auto system with a 10x objective. The images were analyzed using ImageJ version 1.48V and NucView positive pixels were counted automatically on the

thresholded images. Brightfield images of the organoid cultures were used to measure organoid size for normalization of the NucView data and for assessment of organoid growth.

### Proteomic Analyses

Triplicate samples of distal intestinal organoids were infected with SARS-CoV-2, MOI 10, for 48 h as described above and then were lysed in RIPA lysis buffer (25 mM Tris/Cl, 150 mM NaCl, 1% NP-40, 1% SDS, 1% protease inhibitor) by passing the samples through a 26.5G needle 5 times on ice. Samples were stored at -80° C until they were analyzed at the IDeA National Resource for Quantitative Proteomics. An Orbitrap Exploris 480 was used for data-independent acquisition (DIA) mass spectrometry with a 60 min gradient per sample and gas-phase fractionation to obtain comprehensive proteomic profiles of the organoids. Chromatogram libraries were constructed using Prosit<sup>64</sup>, and proteins were identified and quantified using EncyclopeDIA, based on protein FASTA files retrieved from NCBI RefSeq for the Jamaican fruit bat (BioProject PRJNA673233)<sup>17,18</sup>. The mass spectrometry proteomics data have been deposited to the ProteomeXchange Consortium via the PRIDE<sup>65</sup> partner repository with the dataset identifier PXD036016. False discovery thresholds of 1% were applied. The ProteiNorm app was used to optimize data normalization<sup>66</sup>, and Scaffold DIA version 3.3.1 (Proteome Software, Portland, OR) was used for visualization. The MS2 exclusive intensities were normalized using cyclic loess and linear models for microarray (limma), and lmf with empirical Bayes smoothing was used for the analysis<sup>67</sup>. Proteins with an FDR-adjusted  $P$ -value  $\leq 0.05$  and an absolute fold change  $\geq 2$  were considered significant. Ingenuity Pathway Analysis (Qiagen)<sup>68</sup> and Enrichr<sup>20</sup> with combined score ranking ( $c = \log(p) * z$ , where  $c$  = the combined score,  $P$  = Fisher exact test  $P$ -value, and  $z$  = z-score) were used to identify cellular signaling pathways.

Relevant public databases queried by Enrichr were Human KEGG pathways 2021 (<https://www.kegg.jp/>) and COVID-19 Related Gene Sets 2021<sup>69</sup> (<https://maayanlab.cloud/covid19/>). To analyze the impact of SARS-CoV-2 infection on ISGs, proteins identified in the JFB organoids were compared to a comprehensive list of ISGs<sup>19</sup> using a Python script.

### Statistical Analyses

All data, except the proteome data, were analyzed using GraphPad Prism 9.5.1 or earlier versions and are shown as individual data points with mean  $\pm$  SD. Comparisons between two treatments were made using a 2-tailed Student's *t* test or the Kruskal-Wallis test for data that was not normally distributed, and comparisons between multiple treatments were made using one-or two-way ANOVA with Dunnett's or Tukey's post hoc tests. Each sample was analyzed one time.

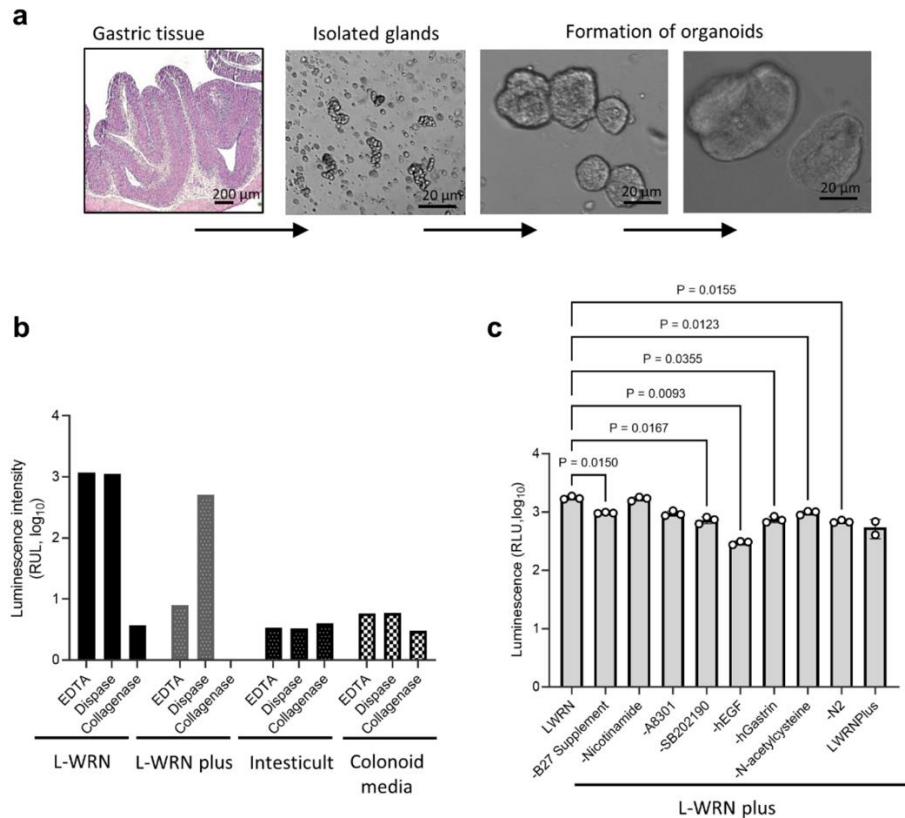
### Data Availability

Source data are provided with this paper. The mass spectrometry proteomics data have been deposited to the ProteomeXchange Consortium via the PRIDE<sup>65</sup> partner repository with under accession code PXD036016. The raw data underlying bar charts and scatter plots that support the findings of this study are provided in the Source Data file and in Figshare under accession code <https://doi.org/10.6084/m9.figshare.23536797><sup>70</sup>. Raw imaging data are available from the corresponding author upon reasonable request. Relevant public databases queried by Enrichr are Human KEGG pathways 2021 (<https://www.kegg.jp/>) and COVID-19 Related Gene Sets 2021 (<https://maayanlab.cloud/covid19/>).

Acknowledgements

Funding from the National Institutes of Health (U01EB029242-02S1 to D.B., C.B.C., M.A.J., S.T.W., and J.N.W.; R21AI169536 to D.B.; and R01AI140442 to T.S.), the Montana State University Office of Research, Economic Development and Graduate Education (D.B., C.B.C.), the Montana Agricultural Experiment Station (D.B., M.A.J.), and the Kopriva Family Foundation (M.H.) is gratefully acknowledged. We greatly appreciate the support of Dr. Aga Rynda-Appl, Evelyn Benson, and Caylee Falvo for help with developing bat-specific experimental methods, B. Tegner Jacobson for preparing a Python script to compare comprehensive protein lists, and Conner Killeen and Travis Van Leeuwen for performing OrganoSeg analyses. We also would like to thank Drs. Raina Plowright, Arinjay Banerjee, Vincent Munster, Emi DeWit, Steve Smith, and Alyssa Evans for helpful discussions about this study. The National Resource for Quantitative Proteomics is supported by NIH grant R24GM137786.

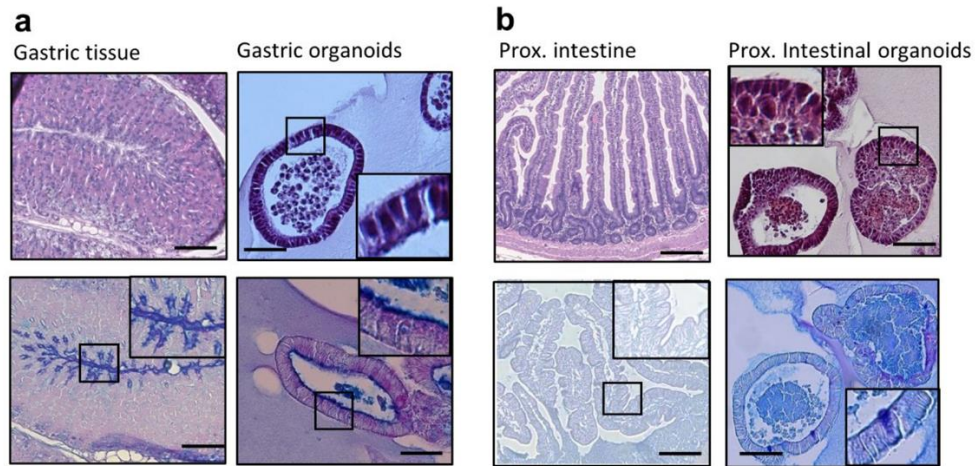
# Supplementary Material



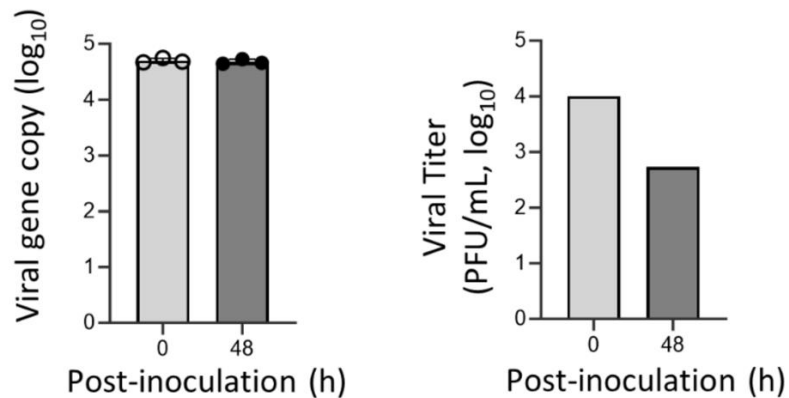
Supplementary Figure S6.1. Development and characterization of gastrointestinal organoids from Jamaican fruit bats. (A) Gastric tissue from a Jamaican fruit bat was incubated for 60 min in collagenase IV solution to isolate glands. The isolated glands were resuspended in Matrigel, seeded in a 96-well plate and cultured with L-WRN media. Organoid formation was observed 24 hours later. (B) JFB distal intestinal tissue was digested in EDTA solution, Dispase® or collagenase to isolate crypts. For Dispase® digestion, the minced tissue was placed in 1-2 mL of Dispase® (Gibco) and incubated on ice for up to 30 min with periodic gentle shaking until crypts appeared in supernatant. The isolated crypts were resuspended in Matrigel, seeded in a 96-well plate and then were overlaid with L-WRN media, L-WRN plus media, IntestiCult™ or colonoid media. After four days, organoid proliferation was analyzed using the CellTiter-Glo Luminescence assay. One representative out of three experiments with n=1 wells per condition. (C) Growth conditions were further optimized by eliminating one additive/growth factor from the L-WRN plus media at a time, n=3 technical replicates, mean  $\pm$  SD, representative of three independent experiments. Data were analyzed using One-way ANOVA with Tukey's multiple comparisons.

Noggin	Mus musculus	MERCPSLGVTLALVVLGLRAAPAGGQHYLHIRPAPSDNLPVLDLIEHPDPIFDPKEDLNELLRSLGGHYDPGFMA
	Artibeus jamaicensis	MDRCPSLGVTLALVVLGLRAAPAGGQHYLHIRPAPSDNLPVLDLIEHPDPIFDPKEDLNELLRSLGGHYDPGFMA *:*****
	Mus musculus	TSPPEDRPGGGGGPAGGAEDLAELDQLLRQPSGAMPSEIKGLEFSEGLAQKKQRLSKKLRRKLQMWLWSQTFCPVLYA
	Artibeus jamaicensis	TSPPEDRPGGGGGPAGGAEDLAELDQLLRQPSGAMPSEIKGLEFSEGLAQKKQRLSKKLRRKLQMWLWSQTFCPVLYA *:*****
	Mus musculus	WNDLGSRFWPRYKVGSCFSKRSCSVPEGMVCKPSKSVHLTVLRWRCQRRGGQRCGWIPYIYQYPIISECKCSC
	Artibeus jamaicensis	WNDLGSRFWPRYKVGSCFSKRSCSVPEGMVCKPSKSVHLTVLRWRCQRRGGQRCGWIPYIYQYPIISECKCSC *:*****
R-spondin	Mus musculus	MRLGLCVVALVLSWTHIAVGSRGTKGKRQRRIISAEQSACAKGCELCSEVNGCLKCSPKLFILLERNDIRQVGVCPLSCP
	Artibeus jamaicensis	MRLGLCVVALVLSWTHIAVGSRGTKGKRQRRIISAEQSACAKGCELCSEVNGCLKCSPKLFILLERNDIRQVGVCPLSCP *:*****
	Mus musculus	PGYFDARNPDMNCKICKIEHCEACFSHNFCTKCQEGLYLHKGRCYACPEGSTAANSTMECGSPAQCEMSEWSPWGPCS
	Artibeus jamaicensis	PGYFDARNPDMNCKICKIEHCEACFSHNFCTKCQESLYLHKGRCYLTCPEGSTAANGTMECSPPOCEMTEWSPWGPCS *:*****
	Mus musculus	KKRKLCGFRKGSEERTRRVLHAPGGDHTTCSDTKETKCTVRRTPCPGQKRRKGQGRRENANRHPARKNSKEPGNSR
	Artibeus jamaicensis	KKKKTGFRKGSEERTRRVLQAPGGDHAVCSDTKETKCTVRRTPCPGQKRRKGQGRRENANRNASKEAGTSGSR *:*****
Wnt3a	Mus musculus	MEPHLLGLLLGLLGGTVLAGYPIWWSLALGQQYTSLSQPLLCSIPGLVPKQLRFRNYIEIMPSVAEGVKLGIEQC
	Artibeus jamaicensis	MEPHLLGLLLGLLGGTVLAGYPIWWSLALGQQYTSLSQPLLCSIPGLVPKQLRFRNYIEIMPSVAEGVKLGIEQC *:*****
	Mus musculus	QHQRGRRWNCCTIDDSLAIFGPVLDKATRESAFVHAIASAGVAFVTRSCAEGTSTICGCDSHHKGPPGEGWKWGCSE
	Artibeus jamaicensis	QHQRGRRWNCCTIDDSLAIFGPVLDKATRESAFVHAIASAGVAFVTRSCAEGTSTICGCDSHHKGPPGEGWKWGCSE *:*****
	Mus musculus	DADFGVLVSREFADARENRPDARSAMNKHNEAGRRTILDHMHKCKCHGLSGSCVKTCTWMAQPDFRAIGDFLKDKYDS
	Artibeus jamaicensis	DADFGVLVSREFADARENRPDARSAMNKHNEAGRRTILDHMHKCKCHGLSGSCVKTCTWMAQPDFRAIGDFLKDKYDS *:*****
	Mus musculus	ASEMVVEKHRESRGWETLRKAYALFKPPTERDLVYVENSFNFCEPNPETGSFGTRDRTCNVTSHGIDGCDLLCCGRGHN
	Artibeus jamaicensis	ASEMVVEKHRESRGWETLRKAYALFKPPTERDLVYVENSFNFCEPNPETGSFGTRDRTCNVTSHGIDGCDLLCCGRGHN *:*****
	Mus musculus	TRTEKRKEKCHCTFWCCYVSCQECTRIYDVHTCK
	Artibeus jamaicensis	TRTEKRKEKCHCTFWCCYVSCQECTRIYDVHTCK *:*****

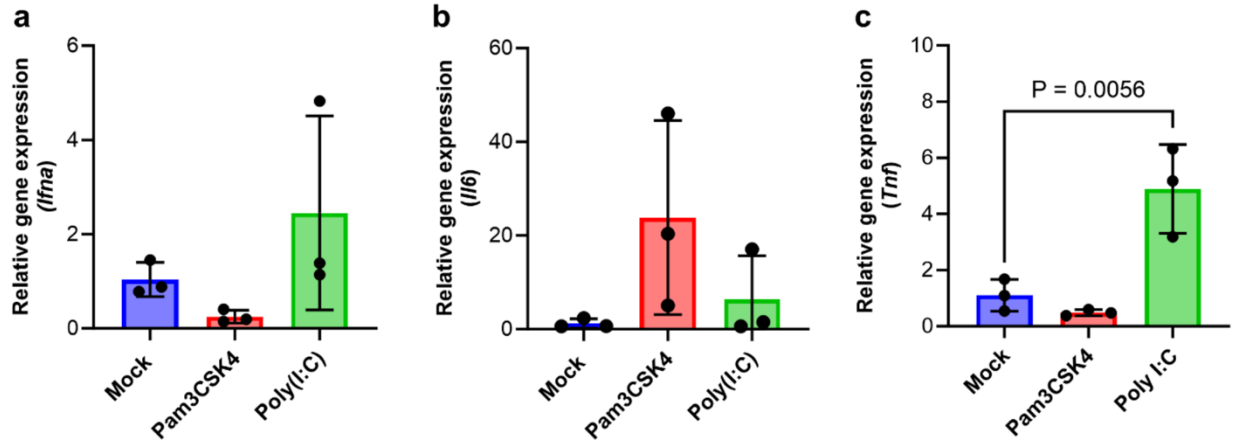
Supplementary Figure S6.2. Protein sequence alignment of murine and *Artibeus jamaicensis* growth factors. Protein sequence alignment of murine and *Artibeus jamaicensis* (taxid:9417) Noggin, R-spondin, and Wnt3a was performed using T-Coffee, a multiple sequence alignment web server 1. Noggin had 98% positive identity with 98% coverage, R-spondin has 86% positive identity and 98% coverage, and Wnt3 had 99% positive identity with 90% coverage. [\*] Same AA; [:] and yellow highlight: conservative AA replacement; [.] and red highlight: semi-conservative AA replacement; space and cyan highlight: non-conservative AA replacement. The gap in the R-spondin sequence is highlighted in dark red.



Supplementary Figure S6.3. Histological analysis of tissue and organoids from JFB stomach and proximal intestine. Morphology of (A) JFB stomach tissue and organoids and (B) proximal intestinal tissue and organoids. Formalin-fixed, paraffin-embedded sections were stained with hematoxylin and eosin (top row) or Alcian Blue to identify mucus (bottom row). High magnification insets show columnar cell shape and morphology of mucus-secreting goblet cells. Representative images out of four tissue samples and organoid lines are shown.



Supplementary Figure S6.4. SARS-CoV-2 loses infectivity in culture medium. SARSCoV-2 was resuspended in medium and at time 0 h and 48 h post infection, the medium was collected, and viral RNA was extracted using QIAmp Viral RNA mini kit (Qiagen). SARS-CoV-2 RNA was measured via quantitative real-time PCR for the E gene (left). Plaque assay was also performed on these supernatants (right). The experiment was performed once, with three technical replicates for the PCR and one well for plaque assays.



Supplementary Figure S6.5. Gene expression of JFB organoids following short term TLR stimulation. Organoids were treated with the TLR2/1 agonist Pam3CSK4 or the TLR3 agonist low MW poly I:C for 6 h and then were analyzed by qRT-PCR for expression of (A) *Ifna*, (B) *Il6*, (C) *Tnf*. Three technical replicates with mean  $\pm$  SD, representative of  $n=6$  (*Ifna*) or  $n=4$  (*Tnf*, *Il6*) independent experiments are shown. Data were analyzed by one-way ANOVA with Dunnett's multiple comparison test.



Supplementary Table S6.1. Composition of culture media for JFB gastrointestinal organoids.

	Concentration	Supplier
<u>L-WRN Media</u>		
Advanced DMEM/F12		Gibco by Life Technology #12-491-015
HEPES	10 mM	Cytiva Hyclone #SH3023701
Pen/Strep	1 %	Cytiva Hyclone #SV30010
L-WRN Conditioned Supernatant	50 %	In house, cells kindly provided by Dr. T. Stappenbeck. ATCC #CRL-3276
ROCK-inhibitor (Y-27632)	10 M	Tocris Bioscience #125410
Amphotericin B	10 $\mu$ M	Fisher Scientific #BP928-250
Gentamycin	1 %	IBI Scientific #IB02030
L-glutamine	1 %	Cytiva # SH30034.01
TGF- $\beta$ inhibitor (SB-431542)	10 $\mu$ M	Tocris Bioscience #161410
FBS	10 %	Atlas Biologicals #F-0500-D
<u>L-WRN Plus Media</u>		
L-WRN Media (as above)		
B27 Supplement	1x	Gibco by Life Technology #A-3582801
Nicotinamide	10 mM	Thermo Scientific #AC128275000
A8301	500 nM	Tocris #2939/10
Human Epidermal Growth Factor (hEGF)	100 ng/mL	Abcam #AB28545850011G
N-acetylcysteine	1 mM	Sigma Aldrich #A9165-5G
<u>IntestiCult™ Media</u>		StemCell Technologies, #06005
<u>Colonoid Media</u>		
Advanced DMEM/F12		Gibco by Life Technology #12-491-015
L-WRN Conditioned Supernatant	50 %	In house, cells kindly provided by Dr. T. Stappenbeck. ATCC #CRL-3276
HEPES	10 mM	Cytiva Hyclone #SH3023701
N2 Supplement	1x	Gibco by Life Technology #17502048
B27 Supplement	1x	Gibco by Life Technology #A3582801
Pen/Strep	1 %	Cytiva Hyclone #SV30010
N-acetylcysteine	2 mM	Sigma Aldrich #A9165-5G
Nicotinamide	10 mM	Thermo Scientific #AC128275000
Human Epidermal Growth Factor (hEGF)	100 ng/mL	Abcam #AB28545850011G

Supplementary Table S6.2. Primer and probe sequences.

<u>Gene Name</u>	<u>Sequence (5'-3')</u>
<u>Stomach</u>	
<i>Pgc</i>	
Forward	CCCCTGAGAGAGTCAAGTGC
Reverse	TGGCACTTCTGAACAGGGTC
<i>MUC5AC</i>	
Forward	AGTGCAGGGCAAATCGTACA
Reverse	AGGCGTCTGCATCGTATGTG
<u>Small Intestine</u>	
<i>Cdx2</i>	
Forward	GCCAAGTGAAAACCAGGACG
Reverse	TCTCGGAGAGCCCCAGG
<i>Vil1</i>	
Forward	CTTGCCTGTGTGGAAGCAAC
Reverse	GGCTGCTCACAGGTACAAC
<i>Muc2</i>	
Forward	GTGGTCGTCTCCTACAACGG
Reverse	ATCCTGCGTGTGTTGTTGTC
<i>Ace2</i>	
Forward	ACTAAGCCAGATGATGGCCG
Reverse	GTAGGAAGGGTTGGTTGGCA
<u>Immune Genes</u>	
<i>Ifna4l</i> and <i>IFNa10l</i>	
Forward	ACAAATGAGAAGGACCGCCT
Reverse	GAAGTGGTTGCCACTGAACG
<i>Ifnb</i>	
Forward	GAGCTACGATGTGCTTCGGT
Reverse	CATCCTGTCCTGGAGGCAAT
<i>Tnf</i>	
Forward	AATTGGCCCTTCACTGGCTC
Reverse	CCCACAGCTTGCTGATTGTC
<i>Il6</i>	
Forward	GACAATGCCAAGGCTATGCAG
Reverse	GTCTTCCTCCACTCGTTCTGG
<u>SARS-CoV-2</u>	
<i>E gene/genomic</i>	
Forward	ACAGGTACGTTAATAGTTAATAGCGT
Reverse	ATATTGCAGCAGTACGCACACA
Probe	FAM-ACACTAGCCATCCTTACTGCGCTTCG-BHQ1
<i>E gene/subgenomic</i>	
Forward	CGATCTCTTGTAGATCTGTTCTC
Reverse	ATATTGCAGCAGTACGCACACA

### References Cited

- 1 Miyoshi, H. & Stappenbeck, T. S. In vitro expansion and genetic modification of gastrointestinal stem cells in spheroid culture. *Nat Protoc* **8**, 2471-2482 (2013). <https://doi.org/10.1038/nprot.2013.153>
- 2 Borten, M. A., Bajikar, S. S., Sasaki, N., Clevers, H. & Janes, K. A. Automated brightfield morphometry of 3D organoid populations by OrganoSeg. *Sci Rep* **8**, 5319 (2018). <https://doi.org/10.1038/s41598-017-18815-8>
- 3 Fagerberg, L. *et al.* Analysis of the human tissue-specific expression by genome-wide integration of transcriptomics and antibody-based proteomics. *Mol Cell Proteomics* **13**, 397-406 (2014). <https://doi.org/10.1074/mcp.M113.035600>
- 4 Kip, A. M. *et al.* Proteomics analysis of human intestinal organoids during hypoxia and reoxygenation as a model to study ischemia-reperfusion injury. *Cell Death Dis* **12**, 95 (2021). <https://doi.org/10.1038/s41419-020-03379-9>
- 5 Lamers, M. M. *et al.* SARS-CoV-2 productively infects human gut enterocytes. *Science* **369**, 50-54 (2020). <https://doi.org/10.1126/science.abc1669>
- 6 Triana, S. *et al.* Single-cell analyses reveal SARS-CoV-2 interference with intrinsic immune response in the human gut. *Mol Syst Biol* **17**, e10232 (2021). <https://doi.org/10.15252/msb.202110232>
- 7 Jang, K. K. *et al.* Variable susceptibility of intestinal organoid-derived monolayers to SARS-CoV-2 infection. *PLoS Biol* **20**, e3001592 (2022). <https://doi.org/10.1371/journal.pbio.3001592>
- 8 Wolfel, R. *et al.* Virological assessment of hospitalized patients with COVID-2019. *Nature* **581**, 465-469 (2020). <https://doi.org/10.1038/s41586-020-2196-x>
- 9 Cen, H., Mao, F., Aronchik, I., Fuentes, R. J. & Firestone, G. L. DEVD-NucView488: a novel class of enzyme substrates for real-time detection of caspase-3 activity in live cells. **22**, 2243-2252 (2008). <https://doi.org/https://doi.org/10.1096/fj.07-099234>

- 10 Zhou, J. *et al.* Infection of bat and human intestinal organoids by SARS-CoV-2. *Nature Medicine* **26**, 1077-1083 (2020). <https://doi.org/10.1038/s41591-020-0912-6>
- 11 Clayton, E. & Munir, M. Fundamental Characteristics of Bat Interferon Systems. *Front Cell Infect Microbiol* **10**, 527921 (2020). <https://doi.org/10.3389/fcimb.2020.527921>
- 12 Stanifer, M. L. *et al.* Critical Role of Type III Interferon in Controlling SARS-CoV-2 Infection in Human Intestinal Epithelial Cells. *Cell Rep* **32**, 107863 (2020). <https://doi.org/10.1016/j.celrep.2020.107863>
- 13 Stanifer, M. L., Guo, C., Doldan, P. & Boulant, S. Importance of Type I and III Interferons at Respiratory and Intestinal Barrier Surfaces. *Front Immunol* **11**, 608645 (2020). <https://doi.org/10.3389/fimmu.2020.608645>
- 14 Zhou, P. *et al.* Type III IFNs in pteropid bats: differential expression patterns provide evidence for distinct roles in antiviral immunity. *J Immunol* **186**, 3138-3147 (2011). <https://doi.org/10.4049/jimmunol.1003115>
- 15 Shaw, T. I. *et al.* Transcriptome sequencing and annotation for the Jamaican fruit bat (*Artibeus jamaicensis*). *PLoS One* **7**, e48472 (2012). <https://doi.org/10.1371/journal.pone.0048472>
- 16 Wang, K. *et al.* Molecular adaptation and convergent evolution of frugivory in Old World and neotropical fruit bats. *Mol Ecol* **29**, 4366-4381 (2020). <https://doi.org/10.1111/mec.15542>
- 17 Searle, B. C. *et al.* Chromatogram libraries improve peptide detection and quantification by data independent acquisition mass spectrometry. *Nat Commun* **9**, 5128 (2018). <https://doi.org/10.1038/s41467-018-07454-w>
- 18 Pruitt, K. D. *et al.* RefSeq: an update on mammalian reference sequences. *Nucleic Acids Res* **42**, D756-763 (2014). <https://doi.org/10.1093/nar/gkt1114>
- 19 OhAinle, M. *et al.* A virus-packageable CRISPR screen identifies host factors mediating interferon inhibition of HIV. *Elife* **7** (2018). <https://doi.org/10.7554/eLife.39823>

- 20 Chen, E. Y. *et al.* Enrichr: interactive and collaborative HTML5 gene list enrichment analysis tool. *BMC Bioinformatics* **14**, 128 (2013). <https://doi.org/10.1186/1471-2105-14-128>
- 21 Wang, X. *et al.* Apelin/APJ system in inflammation. *Int Immunopharmacol* **109**, 108822 (2022). <https://doi.org/10.1016/j.intimp.2022.108822>
- 22 Bouhaddou, M. *et al.* The Global Phosphorylation Landscape of SARS-CoV-2 Infection. *Cell* **182**, 685-712 e619 (2020). <https://doi.org/10.1016/j.cell.2020.06.034>
- 23 Riva, L. *et al.* Discovery of SARS-CoV-2 antiviral drugs through large-scale compound repurposing. *Nature* **586**, 113-119 (2020). <https://doi.org/10.1038/s41586-020-2577-1>
- 24 DeDiego, M. L. *et al.* Severe acute respiratory syndrome coronavirus envelope protein regulates cell stress response and apoptosis. *PLoS Pathog* **7**, e1002315 (2011). <https://doi.org/10.1371/journal.ppat.1002315>
- 25 Baggen, J. *et al.* Genome-wide CRISPR screening identifies TMEM106B as a proviral host factor for SARS-CoV-2. *Nat Genet* **53**, 435-444 (2021). <https://doi.org/10.1038/s41588-021-00805-2>
- 26 Gamage, A. M. *et al.* Infection of human Nasal Epithelial Cells with SARS-CoV-2 and a 382-nt deletion isolate lacking ORF8 reveals similar viral kinetics and host transcriptional profiles. *PLoS Pathog* **16**, e1009130 (2020). <https://doi.org/10.1371/journal.ppat.1009130>
- 27 Crowley, D., Becker, D., Washburne, A. & Plowright, R. Identifying Suspect Bat Reservoirs of Emerging Infections. *Vaccines (Basel)* **8** (2020). <https://doi.org/10.3390/vaccines8020228>
- 28 Cohen, L. E., Fagre, A. C., Chen, B., Carlson, C. J. & Becker, D. J. Coronavirus sampling and surveillance in bats from 1996-2019: a systematic review and meta-analysis. *Nat Microbiol* (2023). <https://doi.org/10.1038/s41564-023-01375-1>
- 29 Malmlov, A. *et al.* Experimental Zika virus infection of Jamaican fruit bats (*Artibeus jamaicensis*) and possible entry of virus into brain via activated microglial cells. *PLoS Negl Trop Dis* **13**, e0007071 (2019). <https://doi.org/10.1371/journal.pntd.0007071>

- 30 Munster, V. J. *et al.* Replication and shedding of MERS-CoV in Jamaican fruit bats (*Artibeus jamaicensis*). *Sci Rep* **6**, 21878 (2016). <https://doi.org/10.1038/srep21878>
- 31 Reid, J. E. & Jackson, A. C. Experimental rabies virus infection in *Artibeus jamaicensis* bats with CVS-24 variants. *J Neurovirol* **7**, 511-517 (2001). <https://doi.org/10.1080/135502801753248097>
- 32 Burke, B. *et al.* Regulatory T Cell-like Response to SARS-CoV-2 in Jamaican Fruit Bats (*Artibeus jamaicensis*) Transduced with Human ACE2. *bioRxiv*, 2023.2002.2013.528205 (2023). <https://doi.org/10.1101/2023.02.13.528205>
- 33 Schlottau, K. *et al.* SARS-CoV-2 in fruit bats, ferrets, pigs, and chickens: an experimental transmission study. *Lancet Microbe* **1**, e218-e225 (2020). [https://doi.org/10.1016/S2666-5247\(20\)30089-6](https://doi.org/10.1016/S2666-5247(20)30089-6)
- 34 Hall, J. S. *et al.* Experimental challenge of a North American bat species, big brown bat (*Eptesicus fuscus*), with SARS-CoV-2. *Transbound Emerg Dis* **68**, 3443-3452 (2021). <https://doi.org/10.1111/tbed.13949>
- 35 Bosco-Lauth, A. M. *et al.* Experimental Infection of Brazilian Free-Tailed Bats (*Tadarida brasiliensis*) with Two Strains of SARS-CoV-2. *Viruses* **14** (2022). <https://doi.org/10.3390/v14081809>
- 36 Hall, J. S. *et al.* Experimental Infection of Mexican Free-Tailed Bats (*Tadarida brasiliensis*) with SARS-CoV-2. *mSphere* **8**, e0026322 (2023). <https://doi.org/10.1128/msphere.00263-22>
- 37 Zhou, P. *et al.* A pneumonia outbreak associated with a new coronavirus of probable bat origin. *Nature* **579**, 270-273 (2020). <https://doi.org/10.1038/s41586-020-2012-7>
- 38 Elbadawy, M. *et al.* Establishment of Intestinal Organoid from *Rousettus leschenaultii* and the Susceptibility to Bat-Associated Viruses, SARS-CoV-2 and Pteropine Orthoreovirus. *Int J Mol Sci* **22** (2021). <https://doi.org/10.3390/ijms221910763>
- 39 Chan, L. L. Y. *et al.* Generation of self-replicating airway organoids from the cave nectar bat *Eonycteris spelaea* as a model system for studying host-pathogen interactions in the bat airway epithelium. *Emerg Microbes Infect* **12**, e2148561 (2023). <https://doi.org/10.1080/22221751.2022.2148561>

- 40 Lin, W. W., Tsay, A. J., Lalime, E. N., Pekosz, A. & Griffin, D. E. Primary differentiated respiratory epithelial cells respond to apical measles virus infection by shedding multinucleated giant cells. *Proc Natl Acad Sci U S A* **118** (2021). <https://doi.org/10.1073/pnas.2013264118>
- 41 Aicher, S. M. *et al.* Species-Specific Molecular Barriers to SARS-CoV-2 Replication in Bat Cells. *J Virol* **96**, e0060822 (2022). <https://doi.org/10.1128/jvi.00608-22>
- 42 Yan, H. *et al.* ACE2 receptor usage reveals variation in susceptibility to SARS-CoV and SARS-CoV-2 infection among bat species. *Nat Ecol Evol* **5**, 600-608 (2021). <https://doi.org/10.1038/s41559-021-01407-1>
- 43 Johnson, B. A. *et al.* Loss of furin cleavage site attenuates SARS-CoV-2 pathogenesis. *Nature* **591**, 293-299 (2021). <https://doi.org/10.1038/s41586-021-03237-4>
- 44 Leroy, E. M. *et al.* Fruit bats as reservoirs of Ebola virus. *Nature* **438**, 575-576 (2005). <https://doi.org/10.1038/438575a>
- 45 Watanabe, S. *et al.* Bat coronaviruses and experimental infection of bats, the Philippines. *Emerging infectious diseases* **16**, 1217-1223 (2010). <https://doi.org/10.3201/eid1608.100208>
- 46 Subudhi, S. *et al.* A persistently infecting coronavirus in hibernating *Myotis lucifugus*, the North American little brown bat. *J Gen Virol* **98**, 2297-2309 (2017). <https://doi.org/10.1099/jgv.0.000898>
- 47 Tong, S. *et al.* New world bats harbor diverse influenza A viruses. *PLoS Pathog* **9**, e1003657 (2013). <https://doi.org/10.1371/journal.ppat.1003657>
- 48 Gerrard, D. L. *et al.* Transcriptomic Signatures of Tacaribe Virus-Infected Jamaican Fruit Bats. *mSphere* **2** (2017). <https://doi.org/10.1128/mSphere.00245-17>
- 49 Schountz, T., Baker, M. L., Butler, J. & Munster, V. Immunological Control of Viral Infections in Bats and the Emergence of Viruses Highly Pathogenic to Humans. *Front Immunol* **8**, 1098 (2017). <https://doi.org/10.3389/fimmu.2017.01098>

- 50 Zang, R. *et al.* TMPRSS2 and TMPRSS4 promote SARS-CoV-2 infection of human small intestinal enterocytes. *Sci Immunol* **5** (2020).  
<https://doi.org/10.1126/sciimmunol.abc3582>
- 51 Brook, C. E. *et al.* Accelerated viral dynamics in bat cell lines, with implications for zoonotic emergence. *Elife* **9** (2020). <https://doi.org/10.7554/eLife.48401>
- 52 Hecht-Höger, A. M. *et al.* Plasma proteomic profiles differ between European and North American myotis bats colonized by *Pseudogymnoascus destructans*. *Mol Ecol* **29**, 1745-1755 (2020). <https://doi.org/10.1111/mec.15437>
- 53 Neely, B. A. *et al.* Surveying the Vampire Bat (*Desmodus rotundus*) Serum Proteome: A Resource for Identifying Immunological Proteins and Detecting Pathogens. *J Proteome Res* **20**, 2547-2559 (2021). <https://doi.org/10.1021/acs.jproteome.0c00995>
- 54 Heck, M. & Neely, B. A. Proteomics in Non-model Organisms: A New Analytical Frontier. *J Proteome Res* **19**, 3595-3606 (2020).  
<https://doi.org/10.1021/acs.jproteome.0c00448>
- 55 Mosbauer, K. *et al.* The Effect of Allicin on the Proteome of SARS-CoV-2 Infected Calu-3 Cells. *Front Microbiol* **12**, 746795 (2021). <https://doi.org/10.3389/fmicb.2021.746795>
- 56 Vidova, V. & Spacil, Z. A review on mass spectrometry-based quantitative proteomics: Targeted and data independent acquisition. *Anal Chim Acta* **964**, 7-23 (2017).  
<https://doi.org/10.1016/j.aca.2017.01.059>
- 57 Powell, R. H. & Behnke, M. S. WRN conditioned media is sufficient for in vitro propagation of intestinal organoids from large farm and small companion animals. *Biol Open* **6**, 698-705 (2017). <https://doi.org/10.1242/bio.021717>
- 58 Tsai, Y. H. *et al.* A Method for Cryogenic Preservation of Human Biopsy Specimens and Subsequent Organoid Culture. *Cell Mol Gastroenterol Hepatol* **6**, 218-222 e217 (2018).  
<https://doi.org/10.1016/j.jcmgh.2018.04.008>
- 59 Sebrell, T. A. *et al.* Live imaging analysis of human gastric epithelial spheroids reveals spontaneous rupture, rotation and fusion events. *Cell and tissue research* **371**, 293-307 (2018). <https://doi.org/10.1007/s00441-017-2726-5>



- 60 Sebrell, T. A. *et al.* A Novel Gastric Spheroid Co-culture Model Reveals Chemokine-Dependent Recruitment of Human Dendritic Cells to the Gastric Epithelium. *Cell Mol Gastroenterol Hepatol* **8**, 157-171 e153 (2019).  
<https://doi.org/10.1016/j.jcmgh.2019.02.010>
- 61 Ridley, R. G. *Antibodies: A Laboratory Manual*. 2009/04/14 edn, Vol. 54 (Cambridge University Press, 1989).
- 62 Loveday, E. K. *et al.* Effect of Inactivation Methods on SARS-CoV-2 Virion Protein and Structure. *Viruses* **13** (2021). <https://doi.org/10.3390/v13040562>
- 63 Hedges, J. F. *et al.* An ADAM17-Neutralizing Antibody Reduces Inflammation and Mortality While Increasing Viral Burden in a COVID-19 Mouse Model. *Front Immunol* **13**, 918881 (2022). <https://doi.org/10.3389/fimmu.2022.918881>
- 64 Gessulat, S. *et al.* Prosit: proteome-wide prediction of peptide tandem mass spectra by deep learning. *Nat Methods* **16**, 509-518 (2019). <https://doi.org/10.1038/s41592-019-0426-7>
- 65 Perez-Riverol, Y. *et al.* The PRIDE database and related tools and resources in 2019: improving support for quantification data. *Nucleic Acids Res* **47**, D442-D450 (2019).  
<https://doi.org/10.1093/nar/gky1106>
- 66 Graw, S. *et al.* proteiNorm - A User-Friendly Tool for Normalization and Analysis of TMT and Label-Free Protein Quantification. *ACS Omega* **5**, 25625-25633 (2020).  
<https://doi.org/10.1021/acsomega.0c02564>
- 67 Ritchie, M. E. *et al.* limma powers differential expression analyses for RNA-sequencing and microarray studies. *Nucleic Acids Res* **43**, e47 (2015).  
<https://doi.org/10.1093/nar/gkv007>
- 68 Kramer, A., Green, J., Pollard, J., Jr. & Tugendreich, S. Causal analysis approaches in Ingenuity Pathway Analysis. *Bioinformatics* **30**, 523-530 (2014).  
<https://doi.org/10.1093/bioinformatics/btt703>
- 69 Kuleshov, M. V. *et al.* The COVID-19 Drug and Gene Set Library. *Patterns (N Y)* **1**, 100090 (2020). <https://doi.org/10.1016/j.patter.2020.100090>

- 70 Bimczok, D. H., Marziah; Sebrell, Thomas; Hedges, Jodi; Snyder, Deann; Lyon, Katrina; et al. . (<https://doi.org/10.6084/m9.figshare.23536797>, 2023).

## CHAPTER SEVEN

## CONCLUSION

This dissertation research described herein sought to explore human gastric organoids as physiologically relevant *in vitro* models for studying two key gastroprotective mechanisms: the mucus barrier and pH gradient across it. To test this hypothesis, we addressed three main questions: 1) What is the pH within the gastric organoid lumen, and can it be characterized with microelectrodes?; 2) What are the biophysical properties of mucus in the organoid lumen; 3) Does bioengineered gastric mucus effectively recapitulate native mucus in its biochemical composition, structure, and protective function?

The stomach's ability to defend itself against damage by invading pathogens and autodigestion is heavily dependent on the coupling of the gastric mucus layer and its associated pH gradient, which work together to form a barrier that shields the gastric epithelium from the outside world<sup>1,2</sup>. The mucus layer functions as a dynamic polymeric matrix that buffers stomach acid and allows the unique one-way transport of protons from the epithelial layer into the lumen<sup>3-5</sup>. Previous *in vitro* studies interrogating the protective nature of this mucus have used pure mucin solutions isolated from pig stomach, or mucus secreted by immortalized cell lines<sup>1,6-8</sup>. More recent studies have demonstrated the apical secretion of airway, colonic, and gastric mucus by organoid-derived epithelial monolayers cultured at the air-liquid interface (ALI)<sup>9-12</sup>. While gastric ALI models have been successfully used to study the gastric immune response to *H. pylori* infection, the specific characteristics of this mucus as a material and its potential as a functional *ex vivo* model of the human gastric mucus layer had yet to be fully explored.

The major findings of this dissertation research are: 1) Micromanipulator-controlled microelectrodes enable accurate measurements of organoid intraluminal pH with high spatiotemporal resolution (Chapter 2). Interestingly, we found that undifferentiated human gastric organoids maintain a neutral to slightly alkaline luminal environment but do maintain a microscale pH gradient, with a more acidic lumen (Chapter 2). 2) Organoid luminal mucus is heterogeneous and viscoelastic (Chapter 3). 3) Organoid-derived bioengineered gastric mucus shares key properties with native mucus: molecular weight distribution, mucin abundance, rheological behavior, and formation of acid channels (Chapter 4).

Chapter 2 highlights the significance of gastric pH and provides a detailed method for pH measurements with enhanced spatial and temporal resolution in 3-D gastric organoids using microelectrodes mounted on a micromanipulator, with a stereomicroscope for visualization<sup>13</sup>. This method, validated with human adult stem cell-derived organoids, is suitable for epithelial organoids of at least 200  $\mu\text{m}$  in diameter that have a distinct lumen. Traditional methods for pH measurement within the organoid lumen have employed pH-sensitive dyes or nanoparticles, generally requiring fluorescence microscopy or spectroscopy for quantification<sup>14-16</sup>. In contrast, our microsensor-based profiling technique offers a novel route for measuring organoid intraluminal pH in real-time and with enhanced spatial precision. This method enables consistent and reliable measurement of luminal pH and reveals a discernible pH gradient. Notably, organoid size must be considered in determining the desired spatial resolution and the scale in which the measurements are to be considered. This is of particular importance if a comparison should ever be made to a mathematical model of the same system<sup>17,18</sup>. We find a relatively alkaline pH within the organoid lumen (Fig. 2.2), as well as low gene expression of proton pump genes *ATP4A* and

*ATP4B* (Fig. 1.4). These findings suggest a predominance of bicarbonate secretion and a profound absence of parietal cells in our organoids, likely explaining their alkalinity. Loss of parietal cell gene expression is commonly seen over time with gastric organoids; it is possible that the steep decline in parietal cells is simply due to carryover from the tissue of origin and lack of a supportive culture medium<sup>19,20</sup>. Wölffling *et al.* have found that organoids require highly specific differentiation conditions to maintain the parietal cell population<sup>12</sup>. Furthermore, one would expect a reasonable amount of metabolite flux into and out of the organoids<sup>21</sup>. We expect an organoid's pH to be influenced by its environment and found that the organoids were consistently less alkaline than their surroundings in six independent experiments. pH fluctuations within individual cultures likely arise from ion gradients at the microscale and the heterogeneous distribution of luminal mucus. Average pH variation between organoid lines of various passages may reflect innate donor differences in cell composition and secretory activity<sup>22</sup>.

In Chapter 3, we began interrogating the material properties of organoid intraluminal mucus. An earlier study from our group applied backscatter light imaging to identify a light-scattering substance within our organoids, which was provisionally classified as “luminal material” due to its undefined composition at the time<sup>18</sup>. In this chapter, we confirmed the presence of mucin in the organoid lumen using Alcian Blue staining of acidic carbohydrates and analyzed the microscale rheological characteristics of the mucus using *in situ* particle tracking microrheology. A strength of particle tracking is that it allows both the calculation of diffusion exponents—which describe how particles move through a material—and the extraction of the local viscoelastic properties of the mucus<sup>23-25</sup>. Using fluorescent green polystyrene microspheres ( $d = 1\ \mu\text{m}$ ) injected into the organoid lumen, we performed confocal imaging over 24-72 hours. Our

findings suggest that the mucus within the organoid lumen is 1) heterogeneously distributed, with particle trajectories revealing both trapped and freely diffusive particles, and 2) exhibits viscoelastic behavior, with two distinct diffusive behaviors. The viscoelastic behavior was determined through ensemble averaging of mean-square displacements and subsequent analysis of the viscous and elastic moduli. Additionally, the calculated ratios of viscous to elastic moduli ( $\tan \delta$ ) revealed that the luminal contents are predominantly elastic ( $G' > G''$ ) across a range of frequencies<sup>1</sup>.

Chapter 4 examines the structure-function relationship of organoid-derived bioengineered gastric mucus (BGM) and evaluates its suitability as a model system for mucus research. Traditionally, purified solutions of porcine gastric mucin have been widely used to study the gastric mucus layer<sup>1,6,8</sup>. Notably, these mucin purification processes are time-consuming and require many steps that have the potential to introduce damage at the protein level, such as ultracentrifugation and dialysis<sup>26</sup>. While mucin proteins are the main viscoelastic components of mucus, they cannot represent the complexity of mucus in its entirety<sup>2</sup>. It has previously been shown that human gastric organoid-derived monolayers cultured at the air-liquid interface (ALI) produce mucus and serve as robust models for *H. pylori* infection<sup>11,12</sup>. Building upon this method, we leveraged ALI cultures for the purpose of analyzing BGM as a biomaterial, comparing its protective properties to those of native mucus samples. Biochemical analyses, including mass spectrometry and size-exclusion chromatography, revealed similarities in mucin abundance and molecular weights. Further structural analysis using cryo-scanning electron microscopy (cryo-SEM) interrogated the internal architecture of BGM and native mucus, revealing structures characteristic of mucous networks<sup>27,28</sup>. Image analysis showed that both

types of mucus appeared highly similar but differed from serum-rich culture medium imaged using the same approach<sup>29,30</sup>. While key features were consistent across samples, we also found that only one sample (hu007 BGM) had all of the characterized structures<sup>31</sup>. Rheological behavior was also assessed via rheometry and microfluidic tests of gelation phenomena using Hele Shaw cells.<sup>32</sup> Both BGM and native mucus were capable of supporting the formation of acid channels at around 2.5  $\mu\text{L}/\text{min}$  in our miniaturized Hele Shaw cell, while slower flow rates caused significant gelation of both types of mucus<sup>33</sup>. Viscous fingering is the result of hydrodynamic instability between two fluids, with the viscosity ratio of the displaced fluid (the mucus) to that of the displacing fluid (the HCl) determining the extent of this instability<sup>34,35</sup>. The patterns by which our BGM and native mucus formed acid channels demonstrated significant qualitative differences in patterning from the control, which involved the flow of acid through cell culture media instead of mucus.

In summary, we have uncovered some previously elusive details of the mostly inaccessible gastric organoid lumen<sup>36</sup>. The insights presented in this dissertation address a crucial gap in our understanding of the biophysical properties of gastric mucus, offering new routes of experimental access to the organoid lumen (Chapters 2 and 3), as well as an improved understanding of luminal mucus as a biomaterial (Chapter 4). This deeper biophysical understanding of organoid luminal dynamics paves the way for a more diverse and increasingly relevant range of biomedical organoid studies. Taken together, our findings suggest that the once inaccessible organoid lumen can now be exposed and interrogated in new ways to address critical questions regarding the relevance of these models in gastric physiology. As organoid

models are central to this dissertation research, the following section provides an overview of the advantages, limitations, and potential of organoid models.

### Organoid Models: Strengths, Challenges, and Opportunities

Over the past decade, there has been a surge in the use of organoids as models for biomedical research, enabling significant advantages over traditionally used animal models and commercial cell lines for studies of human disease. Unlike animal models, which can poorly predict pharmacological toxicity in humans<sup>37</sup>, or immortalized cell lines, which have limited ability to predict responses of *in vivo* tissue<sup>38</sup>, organoids have been praised for offering a closer physiological representation of human tissues in a dish<sup>39,40</sup>. In addition, human organoids consisting of primary epithelial cells can replicate the natural genetic variability among humans, rendering them particularly useful for long-term and/or patient-specific studies. 3D organoids, supported by their extracellular matrix (ECM), boast spatial complexity that more closely mimics *in vivo* architecture and is more representative of cell-cell and cell-ECM interactions<sup>41</sup>. In gastrointestinal research, for example, organoids have demonstrated the remarkable ability to develop mature structures such as intestinal crypts<sup>42-45</sup>. While advanced differentiation protocols can drive organoids toward experimentally desirable phenotypes (such as mucus-producing cells), the absence of such biological instructions can result in spontaneous differentiation depending on the content of the original tissue sample<sup>46,47</sup>. Through differentiation, organoids can be driven toward experimentally relevant phenotypes, thus enhancing their relevance in disease studies as well as drug testing<sup>12</sup>.

Despite their clear utility, organoids that are derived from human tissues are not suitable for every research question, as they present certain challenges that can threaten experimental



reproducibility. Their genetic variability, while useful for personalized medicine, often leads to experimental inconsistencies in which organoids derived from different tissue donors can behave somewhat differently (Fig. 2.2C, 4.2C, 4.3)<sup>22</sup>. For example, we found that organoid pH differed between organoid lines as well as experimental passage, as shown in Chapter 2 (Fig. 2.2C). In Chapter 4, we reported secretome differences among the mucus samples from different donors (n=4) and different organoid lines (n=3) (Fig. 4.2C). Additionally, both native mucus from tissue donors (n=3) and BGM from organoid lines (n=3) showed differences in structural characteristics (Fig. 4.3). It is therefore essential to characterize any organoid line used at baseline before applying any experimental treatments, as we did in Chapter 2. Another more subjective challenge is the emphasis that can be placed on the appearance and size of organoids. While these can be important qualitative indicators of viability and maturity in a culture that drive decision such as when to begin an experimental treatment, we have found that bigger is not always better<sup>13</sup>. In Chapter 2, we profiled the intraluminal pH of organoids ranging from 200-800  $\mu\text{m}$  in diameter—organoids below 200  $\mu\text{m}$  were physically challenging to penetrate, and organoids above 800  $\mu\text{m}$  had a greater tendency to collapse—we hypothesize that this may be due to weakened structural integrity due to size or compromised Matrigel stiffness<sup>48-50</sup>. With that said, an organoid's appearance may give clues about its suitability but should not be the predicting factor of functionality. The typical polarity (apical inside, basolateral outside) of organoids further complicates experiments that require control of and access to the apical epithelium<sup>51</sup>. This polarity can be reversed by removing the organoids from the extracellular matrix, which leads to an exposed luminal surface that facilitates infection studies<sup>36</sup>. Lastly, as organoids may contain a mixture of both differentiated and stem cells, achieving a

physiologically representative cellular composition can be challenging<sup>39</sup>. This can be manipulated through different cocktails of growth factors, though favoring of one phenotype for the sake of disease modeling often comes at the cost of another, such as the differentiation by Wölffling *et al.* into either chief cells or mucous cells, but not both<sup>12,52,53</sup>.

Both the strengths and challenges of organoid technology alike present exciting opportunities for expanding applications in basic and translational research. Organoids can be cultured in both 3D and 2D formats, each with distinct advantages: 3D cultures retain the spatial complexity and cellular interactions of the native tissue, while 2D cultures (particularly in Transwell systems) allow for access to both the basolateral and apical epithelial surfaces and less frequent passaging<sup>11,51</sup>. Our group has leveraged both methods to improve our understanding of gastric self-defense mechanisms such as acid and mucus secretion<sup>13,18,54-56</sup>. The flexibility to transition between 3D and 2D culture (and vice versa) facilitates exciting new tools such as microphysiological systems, where organoids can be integrated with perfusion and multi-organ systems<sup>57</sup>. The minimally invasive derivation of organoids from the stem cells of unique patients holds great translational potential, as they can be biobanked, applied to patient-specific studies<sup>58-60</sup>, with further potential to address data gaps (e.g., racial, gender, etc) in research<sup>61-63</sup>. Ongoing research continues to push the boundaries of what organoid technology is capable of, with the ultimate goal of generating the most physiologically relevant models for human health and disease.

### Future Directions

In this dissertation research, we have evaluated the efficacy of our gastric organoids in modeling the protective mechanisms of the stomach. In Chapter 2, we did not find evidence of

acid secretion in our organoid model. In Chapters 3 and 4, we used both 3D organoids and 2D monolayers to characterize the secreted mucus and assess its relevance to native gastric mucus. However, we have not yet employed differentiation and/or treatment strategies that may improve both of these mechanisms.

### Using Organoids to Model Acid Secretion

Future research into gastric organoid intraluminal pH would include differentiation and subsequent treatment of the organoids to stimulate acid secretion. Parietal cells and their  $H^+K^+$ -ATPase are responsible for most acid secretion into the stomach lumen, but are difficult to maintain in organoid cultures<sup>20,52,53</sup>. While we have observed some evidence of the proton pump in our organoid models, such as gene expression of ATP4B and presence of cells with intracellular canalicular structures<sup>64</sup>, ATP4A/B expression was diminished with increasing organoid passage (Figure 1.4). In Chapter 2, we hypothesized that the alkaline luminal pH was due to a predominance of mucus- and bicarbonate-secreting cells in our organoids. Wölffling *et al.* discovered that bone morphogenic protein (BMP), in the absence of EGF, promotes parietal cell differentiation in human gastric epithelial monolayers<sup>12</sup>. To test this in our organoids, we could optimize a protocol for the differentiation of the organoids by simultaneous supplementation with bone morphogenic protein (BMP) and deprivation of epidermal growth factor (EGF). After a treatment period of about one week, organoids could be fixed, sectioned, and stained for ATP4B, the beta subunit of the  $H^+K^+$ -ATPase. Further functional analysis could include pH measurement of live organoids using the microelectrode-based method described in Chapter 2. Once expression of  $H^+K^+$ -ATPase in our organoid models has been achieved, experiments could be performed to determine whether treatment with histamine (and subsequent

inhibition with omeprazole) would stimulate acid secretion as studies have shown *in vivo*. It is crucial to keep in mind that luminal ionic composition is a dynamic quantity and must be treated as such. Epithelial cell turnover may result in the amount of ion transporters also being just as dynamic.

### Enhancing Mucus Production in Organoids

Future research into organoid mucus could include further optimization of our organoid-based model for the gastric mucus layer. In Chapter 4, we compared the chemical and physical properties of our BGM to the *in vivo* gastric mucus layer. We could further explore pharmacological enhancement of the protective properties of our *in vitro* gastric mucus layer to improve its efficacy as a barrier against *Helicobacter pylori*. For example, rebamipide is a cytoprotective drug that has been reported to increase human gastric mucus secretion by enhancing endogenous prostaglandin production<sup>65,66</sup>. We may also attempt to induce mucus secretion with forskolin, PMA, or prostaglandin E2<sup>67-70</sup>. Upon testing these secretagogues, we would include naproxen—a COX-1/2 inhibitor and previously reported inhibitor of mucus secretion<sup>71</sup>. Upon determining whether mucus secretion by our epithelial cells could be enhanced by these treatments, we could also attempt experiments that we previously performed with the 3D organoids, such as *in situ* the rheological characterization with particle tracking microrheology described in Chapter 3, as mucus collection (Fig. 4.1) has the potential to alter mucus structure and viscoelasticity<sup>72</sup>. Alternatively, viscosity could be analyzed using culture plates equipped with piezoelectric sensors for even less invasive interrogation of the mucus properties<sup>73</sup>. We are particularly interested in the ability of BGM to alter *H. pylori* motility. In preliminary studies, we found that BGM significantly reduced *H. pylori* swimming speed and

track length, but came to realize that this may have been due to the carry-over of antibiotics from the basolateral culture medium into the apically secreted mucus. We did not initially anticipate that this would be a problem, as we found in Chapter 5 that *H. pylori* survives and proliferates in the gastric organoid lumen over several weeks. However, in preliminary experiments showed that even short-term exposure of *H. pylori* (several minutes) was sufficient to significantly reduce motility. Therefore, it will be crucial to optimize culture conditions for a complete transition to antibiotic-free media to enable greater relevance of our bacterial motility studies. Overall, these studies could be combined to learn more about mucus-enhancing treatments that could have cytoprotective effects against *H. pylori* invasion of the gastric epithelium.

### Final Remarks

This dissertation is concluded with a further understanding of the role of epithelial secretions—particularly mucus and acid—play in the gastric organoid lumen. With this research, we have leveraged techniques such as pH microprofiling, particle-tracking microrheology, and 2D air-liquid interface culture to analyze the production of acid and mucus in gastric organoids, going on to assess the suitability of bioengineered gastric mucus as an alternative model to native mucus for future studies. Further multidisciplinary works such as ours will advance organoid technology toward the development of organoid systems that can be used in patient-specific preclinical studies and identify potential drug targets related to these gastroprotective mechanisms.

### References Cited

- 1     Su, C. *et al.* Influence of the viscosity of healthy and diseased human mucins on the motility of *Helicobacter pylori*. *Scientific Reports* 8 (2018).  
<https://doi.org/10.1038/s41598-018-27732-3>
  
- 2     McShane, A. *et al.* Mucus. *Curr Biol* 31, R938-R945 (2021).  
<https://doi.org/10.1016/j.cub.2021.06.093>
  
- 3     Takafumi, I., T., Kazuhiko, I. Protective Effects of Gastric Mucus. *Gastritis and Gastric Cancer* (2011). <https://doi.org/10.5772/23951>
  
- 4     Schreiber, S. *et al.* In situ measurement of pH in the secreting canaliculus of the gastric parietal cell and adjacent structures. *Cell and tissue research* 329, 313-320 (2007).  
<https://doi.org/10.1007/s00441-007-0427-1>
  
- 5     Allen, A. & Flemström, G. Gastroduodenal mucus bicarbonate barrier: Protection against acid and pepsin. *American Journal of Physiology - Cell Physiology* (2005).  
<https://doi.org/10.1152/ajpcell.00102.2004>
  
- 6     Celli, J. P. *et al.* Rheology of Gastric Mucin Exhibits a pH-Dependent Sol–Gel Transition. *Biomacromolecules* 8, 1580-1586 (2007). <https://doi.org/10.1021/bm0609691>
  
- 7     Celli, J. P. *et al.* *Helicobacter pylori* moves through mucus by reducing mucin viscoelasticity. *Proc Natl Acad Sci U S A* 106, 14321-14326 (2009).  
<https://doi.org/10.1073/pnas.0903438106>
  
- 8     Liao, W. & Aranson, I. S. Viscoelasticity enhances collective motion of bacteria. *PNAS Nexus* 2, pgad291 (2023). <https://doi.org/10.1093/pnasnexus/pgad291>
  
- 9     Lin, H. *et al.* Air-Liquid Interface (ALI) culture of human bronchial epithelial cell monolayers as an in vitro model for airway drug transport studies. *Journal of Pharmaceutical Sciences* 96 (2007). <https://doi.org/10.1002/jps.20803>
  
- 10    Wang, Y., Kim, R., Sims, C. E. & Allbritton, N. L. Building a Thick Mucus Hydrogel Layer to Improve the Physiological Relevance of In Vitro Primary Colonic Epithelial

- Models. *Cellular and Molecular Gastroenterology and Hepatology* 8, 653-655.e655 (2019). <https://doi.org/10.1016/j.jcmgh.2019.07.009>
- 11 Boccellato, F. *et al.* Polarised epithelial monolayers of the gastric mucosa reveal insights into mucosal homeostasis and defence against infection. *Gut* 68, 400-413 (2019). <https://doi.org/10.1136/gutjnl-2017-314540>
  - 12 Wolffling, S. *et al.* EGF and BMPs Govern Differentiation and Patterning in Human Gastric Glands. *Gastroenterology* 161, 623-636 e616 (2021). <https://doi.org/10.1053/j.gastro.2021.04.062>
  - 13 Lyon, K., Bansil, R. & Bimczok, D. Profiling Luminal pH in Three-Dimensional Gastrointestinal Organoids Using Microelectrodes. *J Vis Exp* (2024). <https://doi.org/10.3791/66900>
  - 14 Larsen, M., Borisov, S. M., Grunwald, B., Klimant, I. & Glud, R. N. A simple and inexpensive high resolution color ratiometric planar optode imaging approach: application to oxygen and pH sensing. *Limnology and Oceanography: Methods* 9, 348-360 (2011). <https://doi.org/10.4319/lom.2011.9.348>
  - 15 Jewell, M. P., Galyean, A. A., Kirk Harris, J., Zemanick, E. T. & Cash, K. J. Luminescent Nanosensors for Ratiometric Monitoring of Three-Dimensional Oxygen Gradients in Laboratory and Clinical *Pseudomonas aeruginosa* Biofilms. *Appl Environ Microbiol* 85 (2019). <https://doi.org/10.1128/aem.01116-19>
  - 16 McCracken, K. W. *et al.* Wnt/ $\beta$ -catenin promotes gastric fundus specification in mice and humans. *Nature* (2017). <https://doi.org/10.1038/nature21021>
  - 17 Murphy, K. C. *et al.* Measurement of oxygen tension within mesenchymal stem cell spheroids. *Journal of The Royal Society Interface* 14, 20160851 (2017). <https://doi.org/10.1098/rsif.2016.0851>
  - 18 Sebrell, T. A. *et al.* Live imaging analysis of human gastric epithelial spheroids reveals spontaneous rupture, rotation and fusion events. *Cell and Tissue Research* 371, 293-307 (2018). <https://doi.org/10.1007/s00441-017-2726-5>

- 19 Bartfeld, S. *et al.* In vitro expansion of human gastric epithelial stem cells and their responses to bacterial infection. *Gastroenterology* (2015).  
<https://doi.org/10.1053/j.gastro.2014.09.042>
- 20 Schumacher, M. A. *et al.* The use of murine-derived fundic organoids in studies of gastric physiology. *J Physiol* 593, 1809-1827 (2015).  
<https://doi.org/10.1113/jphysiol.2014.283028>
- 21 Okkelman, I. A., Neto, N., Papkovsky, D. B., Monaghan, M. G. & Dmitriev, R. I. A deeper understanding of intestinal organoid metabolism revealed by combining fluorescence lifetime imaging microscopy (FLIM) and extracellular flux analyses. *Redox Biol* 30, 101420 (2020). <https://doi.org/10.1016/j.redox.2019.101420>
- 22 Mohammadi, S. *et al.* Assessing donor-to-donor variability in human intestinal organoid cultures. *Stem Cell Reports* 16, 2364-2378 (2021).  
<https://doi.org/10.1016/j.stemcr.2021.07.016>
- 23 Moschakis, T. Microrheology and particle tracking in food gels and emulsions. *Current Opinion in Colloid & Interface Science* 18, 311-323 (2013).  
<https://doi.org/https://doi.org/10.1016/j.cocis.2013.04.011>
- 24 Mao, Y., Nielsen, P. & Ali, J. Passive and Active Microrheology for Biomedical Systems. *Frontiers in Bioengineering and Biotechnology* 10 (2022).  
<https://doi.org/10.3389/fbioe.2022.916354>
- 25 Georgiades, P., Pudney, P. D. A., Thornton, D. J. & Waigh, T. A. Particle tracking microrheology of purified gastrointestinal mucins. *Biopolymers* 101, 366-377 (2014).  
<https://doi.org/https://doi.org/10.1002/bip.22372>
- 26 Marczynski, M., Rickert, C. A., Fuhrmann, T. & Lieleg, O. An improved, filtration-based process to purify functional mucins from mucosal tissues with high yields. *Separation and Purification Technology* 294, 121209 (2022).  
<https://doi.org/https://doi.org/10.1016/j.seppur.2022.121209>
- 27 Meziu, E. *et al.* Visualization of the structure of native human pulmonary mucus. *Int J Pharm* 597, 120238 (2021). <https://doi.org/10.1016/j.ijpharm.2021.120238>



- 28 Dubbelboer, I. R. *et al.* Gastrointestinal mucus in dog: Physiological characteristics, composition, and structural properties. *Eur J Pharm Biopharm* 173, 92-102 (2022). <https://doi.org/10.1016/j.ejpb.2022.02.019>
- 29 Farran, A. J. *et al.* Effects of matrix composition, microstructure, and viscoelasticity on the behaviors of vocal fold fibroblasts cultured in three-dimensional hydrogel networks. *Tissue Eng Part A* 16, 1247-1261 (2010). <https://doi.org/10.1089/ten.tea.2009.0344>
- 30 Li, P.-S. *et al.* A Novel Albumin-Based Tissue Scaffold for Autogenic Tissue Engineering Applications. *Scientific Reports* 4, 5600 (2014). <https://doi.org/10.1038/srep05600>
- 31 Wen, R. Polymorphisms in mucin genes in the development of gastric cancer. *World Journal of Gastrointestinal Oncology* (2015). <https://doi.org/10.4251/wjgo.v7.i11.328>
- 32 Zhang, Q., Amooie, A., Bazant, M. Z. & Bischofberger, I. Growth morphology and symmetry selection of interfacial instabilities in anisotropic environments. *Soft Matter* 17, 1202-1209 (2021). <https://doi.org/10.1039/d0sm01706j>
- 33 Bunton, P. H., Tullier, M. P., Meiburg, E. & Pojman, J. A. The effect of a crosslinking chemical reaction on pattern formation in viscous fingering of miscible fluids in a Hele-Shaw cell. *Chaos: An Interdisciplinary Journal of Nonlinear Science* 27, 104614 (2017). <https://doi.org/10.1063/1.5001285>
- 34 Eriksen, F. K., Moura, M., Jankov, M., Turquet, A. L. & Måløy, K. J. Transition from viscous fingers to compact displacement during unstable drainage in porous media. *Physical Review Fluids* 7, 013901 (2022). <https://doi.org/10.1103/PhysRevFluids.7.013901>
- 35 Singh, A., Singh, Y. & Pandey, K. M. Viscous fingering instabilities in radial Hele-Shaw cell: A review. *Materials Today: Proceedings* 26, 760-762 (2020). <https://doi.org/https://doi.org/10.1016/j.matpr.2020.01.022>
- 36 Co, J. Y., Margalef-Català, M., Monack, D. M. & Amieva, M. R. Controlling the polarity of human gastrointestinal organoids to investigate epithelial biology and infectious diseases. *Nature Protocols* 16, 5171-5192 (2021). <https://doi.org/10.1038/s41596-021-00607-0>

- 37 Van Norman, G. A. Limitations of Animal Studies for Predicting Toxicity in Clinical Trials: Is it Time to Rethink Our Current Approach? *JACC Basic Transl Sci* 4, 845-854 (2019). <https://doi.org/10.1016/j.jacbts.2019.10.008>
- 38 Astashkina, A. I., Mann, B. K., Prestwich, G. D. & Grainger, D. W. Comparing predictive drug nephrotoxicity biomarkers in kidney 3-D primary organoid culture and immortalized cell lines. *Biomaterials* 33, 4712-4721 (2012). <https://doi.org/https://doi.org/10.1016/j.biomaterials.2012.03.001>
- 39 Davies, J. A. in *Organoids and Mini-Organs* (eds Jamie A. Davies & Melanie L. Lawrence) 3-23 (Academic Press, 2018).
- 40 Jenkinson, S. E. *et al.* The limitations of renal epithelial cell line HK-2 as a model of drug transporter expression and function in the proximal tubule. *Pflügers Archiv - European Journal of Physiology* 464, 601-611 (2012). <https://doi.org/10.1007/s00424-012-1163-2>
- 41 Bhattacharya, A. *et al.* Exploring the interaction between extracellular matrix components in a 3D organoid disease model to replicate the pathophysiology of breast cancer. *Journal of Experimental & Clinical Cancer Research* 42, 343 (2023). <https://doi.org/10.1186/s13046-023-02926-4>
- 42 Sato, T. *et al.* Single Lgr5 stem cells build crypt-villus structures in vitro without a mesenchymal niche. *Nature* (2009). <https://doi.org/10.1038/nature07935>
- 43 Clevers, H. Modeling Development and Disease with Organoids. *Cell* 165, 1586-1597 (2016). <https://doi.org/10.1016/j.cell.2016.05.082>
- 44 Lancaster, M. A. & Knoblich, J. A. Organogenesis in a dish: modeling development and disease using organoid technologies. *Science* 345, 1247125 (2014). <https://doi.org/10.1126/science.1247125>
- 45 Fatehullah, A., Tan, S. H. & Barker, N. Organoids as an in vitro model of human development and disease. *Nat Cell Biol* 18, 246-254 (2016). <https://doi.org/10.1038/ncb3312>
- 46 Andrews, M. G. & Kriegstein, A. R. Challenges of Organoid Research. *Annual Review of Neuroscience* 45, 23-39 (2022). <https://doi.org/https://doi.org/10.1146/annurev-neuro-111020-090812>

- 47 Ishihara, K. & Tanaka, E. M. Spontaneous symmetry breaking and pattern formation of organoids. *Current Opinion in Systems Biology* 11, 123-128 (2018).  
<https://doi.org/https://doi.org/10.1016/j.coisb.2018.06.002>
- 48 Hofer, M. & Lutolf, M. P. Engineering organoids. *Nat Rev Mater* 6, 402-420 (2021).  
<https://doi.org/10.1038/s41578-021-00279-y>
- 49 Tallapragada, N. P. *et al.* Inflation-collapse dynamics drive patterning and morphogenesis in intestinal organoids. *Cell Stem Cell* 28, 1516-1532.e1514 (2021).  
<https://doi.org/https://doi.org/10.1016/j.stem.2021.04.002>
- 50 Kane, K. I. W. *et al.* Determination of the rheological properties of Matrigel for optimum seeding conditions in microfluidic cell cultures. *AIP Advances* 8, 125332 (2018).  
<https://doi.org/10.1063/1.5067382>
- 51 Hofer, M., Duque-Correa, M. A. & Lutolf, M. P. A Bioengineered Platform for Enhanced Observability of Patterned Gastrointestinal Organoid Monolayers with Bilateral Access. *bioRxiv*, 2024.2001.2026.577381 (2024). <https://doi.org/10.1101/2024.01.26.577381>
- 52 Clevers, H., Loh, K. M. & Nusse, R. Stem cell signaling. An integral program for tissue renewal and regeneration: Wnt signaling and stem cell control. *Science* 346, 1248012 (2014). <https://doi.org/10.1126/science.1248012>
- 53 Sato, T. & Clevers, H. Growing self-organizing mini-guts from a single intestinal stem cell: mechanism and applications. *Science* 340, 1190-1194 (2013).  
<https://doi.org/10.1126/science.1234852>
- 54 Cherne, M. D. *et al.* A Synthetic Hydrogel, VitroGel® ORGANOID-3, Improves Immune Cell-Epithelial Interactions in a Tissue Chip Co-Culture Model of Human Gastric Organoids and Dendritic Cells. *Frontiers in Pharmacology* 12 (2021).  
<https://doi.org/10.3389/fphar.2021.707891>
- 55 Goodman, C. *et al.* A High-Throughput Metabolic Microarray Assay Reveals Antibacterial Effects of Black and Red Raspberries and Blackberries against *Helicobacter pylori* Infection. *Antibiotics* 10, 845-845 (2021).  
<https://doi.org/10.3390/antibiotics10070845>

- 56 Sebrell, T. A. *et al.* A Novel Gastric Spheroid Co-culture Model Reveals Chemokine-Dependent Recruitment of Human Dendritic Cells to the Gastric Epithelium. *Cellular and Molecular Gastroenterology and Hepatology* 8, 157-171.e153 (2019). <https://doi.org/10.1016/j.jcmgh.2019.02.010>
- 57 Ginga, N. J. & Slyman, R. Double-Barrel Perfusion System for Modification of Luminal Contents of Intestinal Organoids. *Methods Mol Biol* 2764, 205-224 (2024). [https://doi.org/10.1007/978-1-0716-3674-9\\_14](https://doi.org/10.1007/978-1-0716-3674-9_14)
- 58 Kopper, O. *et al.* An organoid platform for ovarian cancer captures intra- and interpatient heterogeneity. *Nat Med* 25, 838-849 (2019). <https://doi.org/10.1038/s41591-019-0422-6>
- 59 Vlachogiannis, G. *et al.* Patient-derived organoids model treatment response of metastatic gastrointestinal cancers. *Science* 359, 920-926 (2018). <https://doi.org/10.1126/science.aao2774>
- 60 Berkers, G. *et al.* Rectal Organoids Enable Personalized Treatment of Cystic Fibrosis. *Cell Rep* 26, 1701-1708.e1703 (2019). <https://doi.org/10.1016/j.celrep.2019.01.068>
- 61 Kim, J., Koo, B.-K. & Knoblich, J. A. Human organoids: model systems for human biology and medicine. *Nature Reviews Molecular Cell Biology* 21, 571-584 (2020). <https://doi.org/10.1038/s41580-020-0259-3>
- 62 Papaccio, F. *et al.* Will Organoids Fill the Gap towards Functional Precision Medicine? *J Pers Med* 12 (2022). <https://doi.org/10.3390/jpm12111939>
- 63 Co, J. Y., Klein, J. A., Kang, S. & Homan, K. A. Toward Inclusivity in Preclinical Drug Development: A Proposition to Start with Intestinal Organoids. *Advanced Biology* 7, 2200333 (2023). <https://doi.org/https://doi.org/10.1002/adbi.202200333>
- 64 Sebrell, T. A. *et al.* Live imaging analysis of human gastric epithelial spheroids reveals spontaneous rupture, rotation and fusion events. *Cell and tissue research* 371, 293-307 (2018). <https://doi.org/10.1007/s00441-017-2726-5>
- 65 Iijima, K. *et al.* Rebamipide, a cytoprotective drug, increases gastric mucus secretion in human: evaluations with endoscopic gastrin test. *Dig Dis Sci* 54, 1500-1507 (2009). <https://doi.org/10.1007/s10620-008-0507-4>

- 66 Yamasaki, K., Kanbe, T., Chijiwa, T., Ishiyama, H. & Morita, S. Gastric mucosal protection by OPC-12759, a novel antiulcer compound, in the rat. *Eur J Pharmacol* 142, 23-29 (1987). [https://doi.org/10.1016/0014-2999\(87\)90649-2](https://doi.org/10.1016/0014-2999(87)90649-2)
- 67 Seidler, U. & Sewing, K. F. Ca<sup>2+</sup>-dependent and -independent secretagogue action on gastric mucus secretion in rabbit mucosal explants. *Am J Physiol* 256, G739-746 (1989). <https://doi.org/10.1152/ajpgi.1989.256.4.G739>
- 68 Bersimbaev, R. I., Tairov, M. M. & Salganik, R. I. Biochemical mechanisms of regulation of mucus secretion by prostaglandin E<sub>2</sub> in rat gastric mucosa. *Eur J Pharmacol* 115, 259-266 (1985). [https://doi.org/10.1016/0014-2999\(85\)90698-3](https://doi.org/10.1016/0014-2999(85)90698-3)
- 69 Hewson, C. A., Edbrooke, M. R. & Johnston, S. L. PMA induces the MUC5AC respiratory mucin in human bronchial epithelial cells, via PKC, EGF/TGF- $\alpha$ , Ras/Raf, MEK, ERK and Sp1-dependent mechanisms. *J Mol Biol* 344, 683-695 (2004). <https://doi.org/10.1016/j.jmb.2004.09.059>
- 70 Zomer-van Ommen, D. D. *et al.* Comparison of ex vivo and in vitro intestinal cystic fibrosis models to measure CFTR-dependent ion channel activity. *J Cyst Fibros* 17, 316-324 (2018). <https://doi.org/10.1016/j.jcf.2018.02.007>
- 71 Jaworski, T. *et al.* Restorative impact of rabeprazole on gastric mucus and mucin production impairment during naproxen administration: its potential clinical significance. *Dig Dis Sci* 50, 357-365 (2005). <https://doi.org/10.1007/s10620-005-1611-3>
- 72 Cai, P. C. *et al.* Air–liquid intestinal cell culture allows in situ rheological characterization of intestinal mucus. *APL Bioengineering* 8, 026112 (2024). <https://doi.org/10.1063/5.0187974>
- 73 Zhang, J. *et al.* Rapid, autonomous high-throughput characterization of hydrogel rheological properties via automated sensing and physics-guided machine learning. *Applied Materials Today* 30, 101720 (2023). <https://doi.org/https://doi.org/10.1016/j.apmt.2022.101720>

CUMULATIVE REFERENCES CITED

- Abdullah, L. H., Coakley, R., Webster, M. J., Zhu, Y., Tarran, R., Radicioni, G., Kesimer, M., Boucher, R. C., Davis, C. W., & Ribeiro, C. M. P. (2018). Mucin Production and Hydration Responses to Mucopurulent Materials in Normal versus Cystic Fibrosis Airway Epithelia. *Am J Respir Crit Care Med*, 197(4), 481-491. <https://doi.org/10.1164/rccm.201706-1139OC>
- Abu Bakar, M. F., Ismail, N. A., Isha, A., & Mei Ling, A. L. (2016). Phytochemical Composition and Biological Activities of Selected Wild Berries (*Rubus moluccanus* L., *R. fraxinifolius* Poir., and *R. alpestris* Blume). *Evid Based Complement Alternat Med*, 2016, 2482930. <https://doi.org/10.1155/2016/2482930>
- Achberger, K., Probst, C., Haderspeck, J., Bolz, S., Rogal, J., Chuchuy, J., Nikolova, M., Cora, V., Antkowiak, L., Haq, W., Shen, N., Schenke-Layland, K., Ueffing, M., Liebau, S., & Loskill, P. (2019). Merging organoid and organ-on-a-chip technology to generate complex multi-layer tissue models in a human retina-on-a-chip platform. *Elife*, 8. <https://doi.org/10.7554/eLife.46188>
- Agarwal, K., Kaul, R., Garg, M., Shajahan, A., Jha, S. K., & Sampathkumar, S. G. (2013). Inhibition of mucin-type O-glycosylation through metabolic processing and incorporation of N-thioglycolyl-D-galactosamine peracetate (Ac5GalNTGc). *J Am Chem Soc*, 135(38), 14189-14197. <https://doi.org/10.1021/ja405189k>
- Ahmad, M., Ritzoulis, C., & Chen, J. (2018). Shear and extensional rheological characterisation of mucin solutions. *Colloids and Surfaces B: Biointerfaces*, 171, 614-621. <https://doi.org/https://doi.org/10.1016/j.colsurfb.2018.07.075>
- Aicher, S. M., Streicher, F., Chazal, M., Planas, D., Luo, D., Buchrieser, J., Nemcova, M., Seidlova, V., Zukal, J., Serra-Cobo, J., Pontier, D., Pain, B., Zimmer, G., Schwartz, O., Roingeard, P., Pikula, J., Dacheux, L., & Jouvenet, N. (2022). Species-Specific Molecular Barriers to SARS-CoV-2 Replication in Bat Cells. *J Virol*, 96(14), e0060822. <https://doi.org/10.1128/jvi.00608-22>
- Al-Eidan, F. A., McElnay, J. C., Scott, M. G., & McConnell, J. B. (2002). Management of *Helicobacter pylori* eradication--the influence of structured counselling and follow-up. *Br J Clin Pharmacol*, 53(2), 163-171. <https://doi.org/10.1046/j.0306-5251.2001.01531.x>
- Al-kaby, R. N., Jayaratne, J. S., Brox, T. I., Codd, S. L., Seymour, J. D., & Brown, J. R. (2018). Rheo-NMR of transient and steady state shear banding under shear startup. *Journal of Rheology*, 62(5), 1125-1134. <https://doi.org/10.1122/1.5037594>
- Allen, A., & Flemström, G. (2005a). Gastroduodenal mucus bicarbonate barrier: Protection against acid and pepsin. *American Journal of Physiology - Cell Physiology*. <https://doi.org/10.1152/ajpcell.00102.2004>

- Alqatari, S., Videbæk, T. E., Nagel, S. R., Hosoi, A., & Bischofberger, I. (2022). Confined Rayleigh-Taylor instability. *Physical Review Fluids*, 7(11), 110504. <https://doi.org/10.1103/PhysRevFluids.7.110504>
- Ambrosini, Y. M., Park, Y., Jergens, A. E., Shin, W., Min, S., Atherly, T., Borcharding, D. C., Jang, J., Allenspach, K., Mochel, J. P., & Kim, H. J. (2020). Recapitulation of the accessible interface of biopsy-derived canine intestinal organoids to study epithelial-luminal interactions. *PLoS ONE*, 15(4), e0231423. <https://doi.org/10.1371/journal.pone.0231423>
- Amieva, M., & Peek, R. M., Jr. (2016). Pathobiology of *Helicobacter pylori*-Induced Gastric Cancer. *Gastroenterology*, 150(1), 64-78. <https://doi.org/10.1053/j.gastro.2015.09.004>
- Andrews, M. G., & Kriegstein, A. R. (2022). Challenges of Organoid Research. *Annual Review of Neuroscience*, 45(Volume 45, 2022), 23-39. <https://doi.org/https://doi.org/10.1146/annurev-neuro-111020-090812>
- Arnold, I. C., Lee, J. Y., Amieva, M. R., Roers, A., Flavell, R. A., Sparwasser, T., & Muller, A. (2011). Tolerance rather than immunity protects from *Helicobacter pylori*-induced gastric preneoplasia. *Gastroenterology*, 140(1), 199-209. <https://doi.org/10.1053/j.gastro.2010.06.047>
- Arthur J. Atkinson Jr, J. B., Robert M. Craig, James C. Reynolds, Carol Donner. (1990). *Peptic Ulcer Disease: Mechanisms & Management* (P. B. Molinoff, Ed.). The Healthpress Publishing Group, Inc.
- Asaka M, S. A., Sugiyama T, Graham D. (2001). Gastric Cancer. In *Helicobacter pylori: Physiology and Genetics*. ASM Press. <https://www.ncbi.nlm.nih.gov/books/NBK2445/>
- Baggen, J., Persoons, L., Vanstreels, E., Jansen, S., Van Looveren, D., Boeckx, B., Geudens, V., De Man, J., Jochmans, D., Wauters, J., Wauters, E., Vanaudenaerde, B. M., Lambrechts, D., Neyts, J., Dallmeier, K., Thibaut, H. J., Jacquemyn, M., Maes, P., & Daelemans, D. (2021). Genome-wide CRISPR screening identifies TMEM106B as a proviral host factor for SARS-CoV-2. *Nat Genet*, 53(4), 435-444. <https://doi.org/10.1038/s41588-021-00805-2>
- Bahari, H. M., Ross, I. N., & Turnberg, L. A. (1982). Demonstration of a pH gradient across the mucus layer on the surface of human gastric mucosa in vitro. *Gut*, 23(6), 513-516. <https://doi.org/10.1136/gut.23.6.513>
- Bansil, R., Celli, J. P., Hardcastle, J. M., & Turner, B. S. (2013). The Influence of Mucus Microstructure and Rheology in *Helicobacter pylori* Infection. *Front Immunol*, 4, 310. <https://doi.org/10.3389/fimmu.2013.00310>



- Bansil, R., Hardcastle, J. M., & Constantino, M. A. (2015). Microrheology of Mucin: Tracking Particles and Helicobacter Pylori Bacteria. *Épitóanyag*, 67(4), 150-154. <https://doi.org/doi.org/10.14382/epitoanyag-jsbcm.2015.25>
- Bansil, R., Stanley, E., & LaMont, J. T. (1995). Mucin biophysics. *Annu Rev Physiol*, 57, 635-657. <https://doi.org/10.1146/annurev.ph.57.030195.003223>
- Bansil, R., & Turner, B. S. (2018). The biology of mucus: Composition, synthesis and organization. In *Advanced Drug Delivery Reviews* (Vol. 124, pp. 3-15): Elsevier B.V.
- Barker, N., Huch, M., Kujala, P., van de Wetering, M., Snippert, H. J., van Es, J. H., Sato, T., Stange, D. E., Begthel, H., van den Born, M., Danenberg, E., van den Brink, S., Korving, J., Abo, A., Peters, P. J., Wright, N., Poulsom, R., & Clevers, H. (2010). Lgr5(+ve) stem cells drive self-renewal in the stomach and build long-lived gastric units in vitro. *Cell Stem Cell*, 6(1), 25-36. <https://doi.org/10.1016/j.stem.2009.11.013>
- Barmapsalou, V., Rodler, A., Jacobson, M., Karlsson, E. M.-L., Pedersen, B. L., & Bergström, C. A. S. (2023). Development and validation of a porcine artificial colonic mucus model reflecting the properties of native colonic mucus in pigs. *European Journal of Pharmaceutical Sciences*, 181, 106361. <https://doi.org/https://doi.org/10.1016/j.ejps.2022.106361>
- Bartfeld, S., Bayram, T., Van De Wetering, M., Huch, M., Begthel, H., Kujala, P., Vries, R., Peters, P. J., & Clevers, H. (2015). In vitro expansion of human gastric epithelial stem cells and their responses to bacterial infection. *Gastroenterology*. <https://doi.org/10.1053/j.gastro.2014.09.042>
- Bej, R., & Haag, R. (2022). Mucus-Inspired Dynamic Hydrogels: Synthesis and Future Perspectives. *Journal of the American Chemical Society*, 144(44), 20137-20152. <https://doi.org/10.1021/jacs.1c13547>
- Berkers, G., van Mourik, P., Vonk, A. M., Kruisselbrink, E., Dekkers, J. F., de Winter-de Groot, K. M., Arets, H. G. M., Marck-van der Wilt, R. E. P., Dijkema, J. S., Vanderschuren, M. M., Houwen, R. H. J., Heijerman, H. G. M., van de Graaf, E. A., Elias, S. G., Majoor, C. J., Koppelman, G. H., Roukema, J., Bakker, M., Janssens, H. M.,... van der Ent, C. K. (2019). Rectal Organoids Enable Personalized Treatment of Cystic Fibrosis. *Cell Rep*, 26(7), 1701-1708.e1703. <https://doi.org/10.1016/j.celrep.2019.01.068>
- Bersimbaev, R. I., Tairov, M. M., & Salganik, R. I. (1985). Biochemical mechanisms of regulation of mucus secretion by prostaglandin E2 in rat gastric mucosa. *Eur J Pharmacol*, 115(2-3), 259-266. [https://doi.org/10.1016/0014-2999\(85\)90698-3](https://doi.org/10.1016/0014-2999(85)90698-3)
- Bertaux-Skeirik, N., Feng, R., Schumacher, M. A., Li, J., Mahe, M. M., Engevik, A. C., Javier, J. E., Peek, R. M., Jr., Ottemann, K., Orian-Rousseau, V., Boivin, G. P., Helmrath, M. A., & Zavros, Y. (2015). CD44 plays a functional role in Helicobacter pylori-induced epithelial

- cell proliferation. *PLoS Pathog*, 11(2), e1004663.  
<https://doi.org/10.1371/journal.ppat.1004663>
- Bhaskar, K. R., Garik, P., Turner, B. S., Bradley, J. D., Bansil, R., Stanley, H. E., & LaMont, J. T. (1992). Viscous fingering of HCl through gastric mucin. *Nature*, 360(6403), 458-461.  
<https://doi.org/10.1038/360458a0>
- Bhattacharya, A., Alam, K., Roy, N. S., Kaur, K., Kaity, S., Ravichandiran, V., & Roy, S. (2023). Exploring the interaction between extracellular matrix components in a 3D organoid disease model to replicate the pathophysiology of breast cancer. *Journal of Experimental & Clinical Cancer Research*, 42(1), 343. <https://doi.org/10.1186/s13046-023-02926-4>
- Biernat, M. M., Poniewierka, E., Blaszczyk, J., Czapla, L., Kempinski, R., Ksiadzyna, D., Grabinska, J., Binkowska, A., Megraud, F., & Gosciniak, G. (2014). Antimicrobial susceptibility of *Helicobacter pylori* isolates from Lower Silesia, Poland. *Arch Med Sci*, 10(3), 505-509. <https://doi.org/10.5114/aoms.2013.36917>
- Bimczok, D., Clements, R. H., Waites, K. B., Novak, L., Eckhoff, D. E., Mannon, P. J., Smith, P. D., & Smythies, L. E. (2010). Human primary gastric dendritic cells induce a Th1 response to *H. pylori*. *Mucosal Immunol*, 3(3), 260-269.  
<https://doi.org/10.1038/mi.2010.10>
- Bimczok, D. H., Marziah; Sebrell, Thomas; Hedges, Jodi; Snyder, Deann; Lyon, Katrina; et al. . (2023). *Antiviral responses in a Jamaican Fruit Bat intestinal organoid model of SARS-CoV-2 infection. Figshare Dataset*  
<https://doi.org/https://doi.org/10.6084/m9.figshare.23536797>
- Bischofberger, I., Ramachandran, R., & Nagel, S. R. (2015). An island of stability in a sea of fingers: emergent global features of the viscous-flow instability. *Soft Matter*, 11(37), 7428-7432. <https://doi.org/10.1039/c5sm00943j>
- Blanchard, T. G., & Czinn, S. J. (2015). Current Status and Prospects for a *Helicobacter pylori* Vaccine. *Gastroenterol Clin North Am*, 44(3), 677-689.  
<https://doi.org/10.1016/j.gtc.2015.05.013>
- Blutt, S. E., Crawford, S. E., Ramani, S., Zou, W. Y., & Estes, M. K. (2018). Engineered Human Gastrointestinal Cultures to Study the Microbiome and Infectious Diseases. *CMGH*.  
<https://doi.org/10.1016/j.jcmgh.2017.12.001>
- Boccellato, F., Woelffling, S., Imai-Matsushima, A., Sanchez, G., Goosmann, C., Schmid, M., Berger, H., Morey, P., Denecke, C., Ordemann, J., & Meyer, T. F. (2019). Polarised epithelial monolayers of the gastric mucosa reveal insights into mucosal homeostasis and defence against infection. *Gut*, 68(3), 400-413. <https://doi.org/10.1136/gutjnl-2017-314540>

- Bochner, B. R. (2009). Global phenotypic characterization of bacteria. *FEMS Microbiol Rev*, 33(1), 191-205. <https://doi.org/10.1111/j.1574-6976.2008.00149.x>
- Boegh, M., Foged, C., Müllertz, A., & Mørck Nielsen, H. (2013). Mucosal drug delivery: barriers, in vitro models and formulation strategies. *Journal of Drug Delivery Science and Technology*, 23(4), 383-391. [https://doi.org/10.1016/S1773-2247\(13\)50055-4](https://doi.org/10.1016/S1773-2247(13)50055-4)
- Boltin, D., & Niv, Y. (2013). Mucins in Gastric Cancer - An Update. *J Gastrointest Dig Syst*, 3(123), 15519. <https://doi.org/10.4172/2161-069x.1000123>
- Borten, M. A., Bajikar, S. S., Sasaki, N., Clevers, H., & Janes, K. A. (2018). Automated brightfield morphometry of 3D organoid populations by OrganoSeg. *Sci Rep*, 8(1), 5319. <https://doi.org/10.1038/s41598-017-18815-8>
- Bosco-Lauth, A. M., Porter, S. M., Fox, K. A., Wood, M. E., Neubaum, D., & Quilici, M. (2022). Experimental Infection of Brazilian Free-Tailed Bats (*Tadarida brasiliensis*) with Two Strains of SARS-CoV-2. *Viruses*, 14(8). <https://doi.org/10.3390/v14081809>
- Bouhaddou, M., Memon, D., Meyer, B., White, K. M., Rezelj, V. V., Correa Marrero, M., Polacco, B. J., Melnyk, J. E., Ulferts, S., Kaake, R. M., Batra, J., Richards, A. L., Stevenson, E., Gordon, D. E., Rojc, A., Obernier, K., Fabius, J. M., Soucheray, M., Miorin, L.,...Krogan, N. J. (2020). The Global Phosphorylation Landscape of SARS-CoV-2 Infection. *Cell*, 182(3), 685-712 e619. <https://doi.org/10.1016/j.cell.2020.06.034>
- Bravo, D., Hoare, A., Soto, C., Valenzuela, M. A., & Quest, A. F. (2018). *Helicobacter pylori* in human health and disease: Mechanisms for local gastric and systemic effects. *World J Gastroenterol*, 24(28), 3071-3089. <https://doi.org/10.3748/wjg.v24.i28.3071>
- Bray, F., Laversanne, M., Sung, H., Ferlay, J., Siegel, R. L., Soerjomataram, I., & Jemal, A. (2024). Global cancer statistics 2022: GLOBOCAN estimates of incidence and mortality worldwide for 36 cancers in 185 countries. *CA Cancer J Clin*, 74(3), 229-263. <https://doi.org/10.3322/caac.21834>
- Brook, C. E., Boots, M., Chandran, K., Dobson, A. P., Drosten, C., Graham, A. L., Grenfell, B. T., Muller, M. A., Ng, M., Wang, L. F., & van Leeuwen, A. (2020). Accelerated viral dynamics in bat cell lines, with implications for zoonotic emergence. *Elife*, 9. <https://doi.org/10.7554/eLife.48401>
- Brooks, E. L., Hussain, K. K., Kotecha, K., Abdalla, A., & Patel, B. A. (2023). Three-Dimensional-Printed Electrochemical Multiwell Plates for Monitoring Food Intolerance from Intestinal Organoids. *ACS Sens*, 8(2), 712-720. <https://doi.org/10.1021/acssensors.2c02245>

- Brown, J. S., Amend, S. R., Austin, R. H., Gatenby, R. A., Hammarlund, E. U., & Pienta, K. J. (2023). Updating the Definition of Cancer. *Molecular Cancer Research*, 21(11), 1142-1147. <https://doi.org/10.1158/1541-7786.MCR-23-0411>
- Bunton, P. H., Tullier, M. P., Meiburg, E., & Pojman, J. A. (2017). The effect of a crosslinking chemical reaction on pattern formation in viscous fingering of miscible fluids in a Hele-Shaw cell. *Chaos: An Interdisciplinary Journal of Nonlinear Science*, 27(10), 104614. <https://doi.org/10.1063/1.5001285>
- Burada, P. S., Hänggi, P., Marchesoni, F., Schmid, G., & Talkner, P. (2009). Diffusion in Confined Geometries. *ChemPhysChem*, 10(1), 45-54. <https://doi.org/https://doi.org/10.1002/cphc.200800526>
- Burke, B., Rocha, S. M., Zhan, S., Eckley, M., Reasoner, C., Addetia, A., Lewis, J., Fagre, A., Charley, P., Richt, J. A., Weiss, S. R., Tjalkens, R. B., Veesler, D., Aboellail, T., & Schountz, T. (2023). Regulatory T Cell-like Response to SARS-CoV-2 in Jamaican Fruit Bats (*Artibeus jamaicensis*) Transduced with Human ACE2. *bioRxiv*, 2023.2002.2013.528205. <https://doi.org/10.1101/2023.02.13.528205>
- Burucoa, C., & Axon, A. (2017). Epidemiology of Helicobacter pylori infection. *Helicobacter*, 22 Suppl 1. <https://doi.org/10.1111/hel.12403>
- Button, B., & Boucher, R. C. (2008). Role of mechanical stress in regulating airway surface hydration and mucus clearance rates. *Respir Physiol Neurobiol*, 163(1-3), 189-201. <https://doi.org/10.1016/j.resp.2008.04.020>
- Cai, P. C., Braunreuther, M., Shih, A., Spakowitz, A. J., Fuller, G. G., & Heilshorn, S. C. (2024). Air-liquid intestinal cell culture allows in situ rheological characterization of intestinal mucus. *APL Bioengineering*, 8(2), 026112. <https://doi.org/10.1063/5.0187974>
- Cai, Y., Liu, L., Xia, M., Tian, C., Wu, W., Dong, B., & Chu, X. (2022). SEDDS facilitate cinnamaldehyde crossing the mucus barrier: The perspective of mucus and Caco-2/HT29 co-culture models. *International Journal of Pharmaceutics*, 614, 121461. <https://doi.org/https://doi.org/10.1016/j.ijpharm.2022.121461>
- Ceci, C., Graziani, G., Faraoni, I., & Cacciotti, I. (2020). Strategies to improve ellagic acid bioavailability: from natural or semisynthetic derivatives to nanotechnological approaches based on innovative carriers. *Nanotechnology*, 31(38), 382001. <https://doi.org/10.1088/1361-6528/ab912c>
- Celli, J., Gregor, B., Turner, B., Afdhal, N. H., Bansil, R., & Erramilli, S. (2005). Viscoelastic Properties and Dynamics of Porcine Gastric Mucin. *Biomacromolecules*, 6(3), 1329-1333. <https://doi.org/10.1021/bm0493990>

- Celli, J. P., Turner, B. S., Afdhal, N. H., Ewoldt, R. H., McKinley, G. H., Bansil, R., & Erramilli, S. (2007). Rheology of Gastric Mucin Exhibits a pH-Dependent Sol–Gel Transition. *Biomacromolecules*, 8(5), 1580-1586. <https://doi.org/10.1021/bm0609691>
- Celli, J. P., Turner, B. S., Afdhal, N. H., Keates, S., Ghiran, I., Kelly, C. P., Ewoldt, R. H., McKinley, G. H., So, P., Erramilli, S., & Bansil, R. (2009). Helicobacter pylori moves through mucus by reducing mucin viscoelasticity. *Proc Natl Acad Sci U S A*, 106(34), 14321-14326. <https://doi.org/10.1073/pnas.0903438106>
- Cen, H., Mao, F., Aronchik, I., Fuentes, R. J., & Firestone, G. L. (2008). DEVD-NucView488: a novel class of enzyme substrates for real-time detection of caspase-3 activity in live cells. *22(7)*, 2243-2252. <https://doi.org/https://doi.org/10.1096/fj.07-099234>
- Cerezo, A. B., Catunescu, G. M., Gonzalez, M. M., Hornedo-Ortega, R., Pop, C. R., Rusu, C. C., Chirila, F., Rotar, A. M., Garcia-Parrilla, M. C., & Troncoso, A. M. (2020). Anthocyanins in Blueberries Grown in Hot Climate Exert Strong Antioxidant Activity and May Be Effective against Urinary Tract Bacteria. *Antioxidants (Basel)*, 9(6). <https://doi.org/10.3390/antiox9060478>
- Chan, L. L. Y., Gamage, A. M., Tan, C. W., Tan, K. S., Liu, J., Tay, D. J. W., Foo, R. J. H., Renia, L., Wang, Y., & Wang, L. F. (2023). Generation of self-replicating airway organoids from the cave nectar bat Eonycteris spelaea as a model system for studying host-pathogen interactions in the bat airway epithelium. *Emerg Microbes Infect*, 12(1), e2148561. <https://doi.org/10.1080/22221751.2022.2148561>
- Chatterjee, A., Yasmin, T., Bagchi, D., & Stohs, S. J. (2004). Inhibition of Helicobacter pylori in vitro by various berry extracts, with enhanced susceptibility to clarithromycin. *Mol Cell Biochem*, 265(1-2), 19-26. <https://doi.org/10.1023/b:mcbi.0000044310.92444.ec>
- Chen, E. Y., Tan, C. M., Kou, Y., Duan, Q., Wang, Z., Meirelles, G. V., Clark, N. R., & Ma'ayan, A. (2013). Enrichr: interactive and collaborative HTML5 gene list enrichment analysis tool. *BMC Bioinformatics*, 14, 128. <https://doi.org/10.1186/1471-2105-14-128>
- Chen, H., Yu, W., Chen, G., Meng, S., Xiang, Z., & He, N. (2017). Antinociceptive and Antibacterial Properties of Anthocyanins and Flavonols from Fruits of Black and Non-Black Mulberries. *Molecules*, 23(1). <https://doi.org/10.3390/molecules23010004>
- Chen, K. M., Guttenplan, J. B., Sun, Y. W., Cooper, T., Shalaby, N. A. E., Kosinska, W., Benitez, G., Aliaga, C., Zhu, J., Liao, J., Gowda, K., Amin, S., Stoner, G., & El-Bayoumy, K. (2018). Effects of Black Raspberry on Dibenzo[a,l]Pyrene Diol Epoxide Induced DNA Adducts, Mutagenesis, and Tumorigenesis in the Mouse Oral Cavity. *Cancer Prev Res (Phila)*, 11(3), 157-164. <https://doi.org/10.1158/1940-6207.CAPR-17-0278>
- Cherne, M. D., Sidar, B., Sebrell, T. A., Sanchez, H. S., Heaton, K., Kassama, F. J., Roe, M. M., Gentry, A. B., Chang, C. B., Walk, S. T., Jutila, M., Wilking, J. N., & Bimczok, D. (2021). A Synthetic Hydrogel, VitroGel® ORGANOID-3, Improves Immune Cell-

- Epithelial Interactions in a Tissue Chip Co-Culture Model of Human Gastric Organoids and Dendritic Cells. *Frontiers in Pharmacology*, 12. <https://doi.org/10.3389/fphar.2021.707891>
- Chey, W. D., Leontiadis, G. I., Howden, C. W., & Moss, S. F. (2017). ACG Clinical Guideline: Treatment of *Helicobacter pylori* Infection. *Am J Gastroenterol*, 112(2), 212-239. <https://doi.org/10.1038/ajg.2016.563>
- Clayton, E., & Munir, M. (2020). Fundamental Characteristics of Bat Interferon Systems. *Front Cell Infect Microbiol*, 10, 527921. <https://doi.org/10.3389/fcimb.2020.527921>
- Clevers, H. (2016). Modeling Development and Disease with Organoids. *Cell*, 165(7), 1586-1597. <https://doi.org/10.1016/j.cell.2016.05.082>
- Clevers, H., Loh, K. M., & Nusse, R. (2014). Stem cell signaling. An integral program for tissue renewal and regeneration: Wnt signaling and stem cell control. *Science*, 346(6205), 1248012. <https://doi.org/10.1126/science.1248012>
- Co, J. Y., Klein, J. A., Kang, S., & Homan, K. A. (2023). Toward Inclusivity in Preclinical Drug Development: A Proposition to Start with Intestinal Organoids. *Advanced Biology*, 7(12), 2200333. <https://doi.org/https://doi.org/10.1002/adbi.202200333>
- Co, J. Y., Margalef-Català, M., Monack, D. M., & Amieva, M. R. (2021). Controlling the polarity of human gastrointestinal organoids to investigate epithelial biology and infectious diseases. *Nature Protocols*, 16(11), 5171-5192. <https://doi.org/10.1038/s41596-021-00607-0>
- Cohen, L. E., Fagre, A. C., Chen, B., Carlson, C. J., & Becker, D. J. (2023). Coronavirus sampling and surveillance in bats from 1996-2019: a systematic review and meta-analysis. *Nat Microbiol*. <https://doi.org/10.1038/s41564-023-01375-1>
- Cornick, S., Tawiah, A., & Chadee, K. (2015). Roles and regulation of the mucus barrier in the gut. *Tissue Barriers*, 3(1-2), e982426. <https://doi.org/10.4161/21688370.2014.982426>
- Correa, P., & Piazzuelo, M. B. (2011). *Helicobacter pylori* Infection and Gastric Adenocarcinoma. *US Gastroenterol Hepatol Rev*, 7(1), 59-64. <https://www.ncbi.nlm.nih.gov/pubmed/21857882>
- Crowley, D., Becker, D., Washburne, A., & Plowright, R. (2020). Identifying Suspect Bat Reservoirs of Emerging Infections. *Vaccines (Basel)*, 8(2). <https://doi.org/10.3390/vaccines8020228>
- Cutler, A. F., & Schubert, T. T. (1993). Patient factors affecting *Helicobacter pylori* eradication with triple therapy. *Am J Gastroenterol*, 88(4), 505-509. <https://www.ncbi.nlm.nih.gov/pubmed/8470629>

- Cvetkovic, I., & Milicev, S. (2024). Pore-scale viscous fingering as a mechanism for pattern formation – a historical overview, application, and the ways of controlling it. *Advances in Physics: X*, 9(1), 2370838. <https://doi.org/10.1080/23746149.2024.2370838>
- Davies, J. A. (2018). Chapter 1 - Organoids and mini-organs: Introduction, history, and potential. In J. A. Davies & M. L. Lawrence (Eds.), *Organoids and Mini-Organs* (pp. 3-23). Academic Press. <https://doi.org/https://doi.org/10.1016/B978-0-12-812636-3.00001-8>
- Davies, J. A., & Lawrence, M. L. (2018). Chapter 14 - Four challenges for organoid engineers. In J. A. Davies & M. L. Lawrence (Eds.), *Organoids and Mini-Organs* (pp. 255-259). Academic Press. <https://doi.org/https://doi.org/10.1016/B978-0-12-812636-3.00014-6>
- De, R., Sarkar, A., Ghosh, P., Ganguly, M., Karmakar, B. C., Saha, D. R., Halder, A., Chowdhury, A., & Mukhopadhyay, A. K. (2018). Antimicrobial activity of ellagic acid against *Helicobacter pylori* isolates from India and during infections in mice. *J Antimicrob Chemother*, 73(6), 1595-1603. <https://doi.org/10.1093/jac/dky079>
- Dedhia, P. H., Bertaux-Skeirik, N., Zavros, Y., & Spence, J. R. (2016). Organoid Models of Human Gastrointestinal Development and Disease. *Gastroenterology*, 150(5), 1098-1112. <https://doi.org/10.1053/j.gastro.2015.12.042>
- DeDiego, M. L., Nieto-Torres, J. L., Jimenez-Guardeno, J. M., Regla-Nava, J. A., Alvarez, E., Oliveros, J. C., Zhao, J., Fett, C., Perlman, S., & Enjuanes, L. (2011). Severe acute respiratory syndrome coronavirus envelope protein regulates cell stress response and apoptosis. *PLoS Pathog*, 7(10), e1002315. <https://doi.org/10.1371/journal.ppat.1002315>
- Delon, L. C., Guo, Z., Oszmiana, A., Chien, C.-C., Gibson, R., Prestidge, C., & Thierry, B. (2019). A systematic investigation of the effect of the fluid shear stress on Caco-2 cells towards the optimization of epithelial organ-on-chip models. *Biomaterials*, 225, 119521. <https://doi.org/https://doi.org/10.1016/j.biomaterials.2019.119521>
- Derricott, H., Luu, L., Fong, W. Y., Hartley, C. S., Johnston, L. J., Armstrong, S. D., Randle, N., Duckworth, C. A., Campbell, B. J., Wastling, J. M., & Coombes, J. L. (2019). Developing a 3D intestinal epithelium model for livestock species. *Cell Tissue Res*. <https://doi.org/10.1007/s00441-018-2924-9>
- Dong, W., Matsuno, Y. K., & Kameyama, A. (2012). A procedure for Alcian blue staining of mucins on polyvinylidene difluoride membranes. *Anal Chem*, 84(20), 8461-8466. <https://doi.org/10.1021/ac301678z>
- Dubbelboer, I. R., Barmpatsalou, V., Rodler, A., Karlsson, E., Nunes, S. F., Holmberg, J., Haggstrom, J., & Bergstrom, C. A. S. (2022). Gastrointestinal mucus in dog: Physiological characteristics, composition, and structural properties. *Eur J Pharm Biopharm*, 173, 92-102. <https://doi.org/10.1016/j.ejpb.2022.02.019>

- Dutta, D., Heo, I., & Clevers, H. (2017). Disease Modeling in Stem Cell-Derived 3D Organoid Systems. *Trends Mol Med*, 23(5), 393-410. <https://doi.org/10.1016/j.molmed.2017.02.007>
- Dyer, V., Bruggemann, H., Sorensen, M., Kuhl, A. A., Hoffman, K., Brinkmann, V., Reines, M. D. M., Zimmerman, S., Meyer, T. F., & Koch, M. (2018). Genomic features of the *Helicobacter pylori* strain PMSS1 and its virulence attributes as deduced from its in vivo colonisation patterns. *Mol Microbiol*, 110(5), 761-776. <https://doi.org/10.1111/mmi.14123>
- Elbadawy, M., Kato, Y., Saito, N., Hayashi, K., Abugomaa, A., Kobayashi, M., Yoshida, T., Shibutani, M., Kaneda, M., Yamawaki, H., Mizutani, T., Lim, C. K., Saijo, M., Sasaki, K., Usui, T., & Omatsu, T. (2021). Establishment of Intestinal Organoid from *Rousettus leschenaultii* and the Susceptibility to Bat-Associated Viruses, SARS-CoV-2 and Pteropine Orthoreovirus. *Int J Mol Sci*, 22(19). <https://doi.org/10.3390/ijms221910763>
- Engevik, A. C., Kaji, I., & Goldenring, J. R. (2020). The Physiology of the Gastric Parietal Cell. *Physiol Rev*, 100(2), 573-602. <https://doi.org/10.1152/physrev.00016.2019>
- Eriksen, F. K., Moura, M., Jankov, M., Turquet, A. L., & Måløy, K. J. (2022). Transition from viscous fingers to compact displacement during unstable drainage in porous media. *Physical Review Fluids*, 7(1), 013901. <https://doi.org/10.1103/PhysRevFluids.7.013901>
- Fabricius, J., Manjate, S., & Wall, P. (2022). On pressure-driven Hele–Shaw flow of power-law fluids. *Applicable Analysis*, 101(14), 5107-5137. <https://doi.org/10.1080/00036811.2021.1880570>
- Fagerberg, L., Hallström, B. M., Oksvold, P., Kampf, C., Djureinovic, D., Odeberg, J., Habuka, M., Tahmasebpour, S., Danielsson, A., Edlund, K., Asplund, A., Sjöstedt, E., Lundberg, E., Szigartyo, C. A., Skogs, M., Takanen, J. O., Berling, H., Tegel, H., Mulder, J.,...Uhlén, M. (2014). Analysis of the human tissue-specific expression by genome-wide integration of transcriptomics and antibody-based proteomics. *Mol Cell Proteomics*, 13(2), 397-406. <https://doi.org/10.1074/mcp.M113.035600>
- Farran, A. J., Teller, S. S., Jha, A. K., Jiao, T., Hule, R. A., Clifton, R. J., Pochan, D. P., Duncan, R. L., & Jia, X. (2010). Effects of matrix composition, microstructure, and viscoelasticity on the behaviors of vocal fold fibroblasts cultured in three-dimensional hydrogel networks. *Tissue Eng Part A*, 16(4), 1247-1261. <https://doi.org/10.1089/ten.tea.2009.0344>
- Fatehullah, A., Tan, S. H., & Barker, N. (2016). Organoids as an in vitro model of human development and disease. *Nat Cell Biol*, 18(3), 246-254. <https://doi.org/10.1038/ncb3312>
- Fitzmaurice, C., Allen, C., Barber, R. M., Barregard, L., Bhutta, Z. A., Brenner, H., Dicker, D. J., Chimed-Orchir, O., Dandona, R., Dandona, L., Fleming, T., Forouzanfar, M. H., Hancock, J., Hay, R. J., Hunter-Merrill, R., Huynh, C., Hosgood, H. D., Johnson, C. O., Jonas, J. B.,...Naghavi, M. (2017). Global, regional, and national cancer incidence, mortality, years of life lost, years lived with disability, and disability-adjusted life-years for 32 cancer groups, 1990 to 2015: A Systematic Analysis for the Global Burden of



- Disease Study Global Burden. *JAMA Oncology*.  
<https://doi.org/10.1001/jamaoncol.2016.5688>
- Forssell, H. (1988). Gastric mucosal defence mechanisms: a brief review. *Scand J Gastroenterol Suppl*, 155, 23-28. <https://doi.org/10.3109/00365528809096277>
- Fruchart, M., Scheibner, C., & Vitelli, V. (2023). Odd Viscosity and Odd Elasticity. *Annual Review of Condensed Matter Physics*, 14(Volume 14, 2023), 471-510.  
<https://doi.org/https://doi.org/10.1146/annurev-conmatphys-040821-125506>
- Gamage, A. M., Tan, K. S., Chan, W. O. Y., Liu, J., Tan, C. W., Ong, Y. K., Thong, M., Andiappan, A. K., Anderson, D. E., Wang, Y., & Wang, L. F. (2020). Infection of human Nasal Epithelial Cells with SARS-CoV-2 and a 382-nt deletion isolate lacking ORF8 reveals similar viral kinetics and host transcriptional profiles. *PLoS Pathog*, 16(12), e1009130. <https://doi.org/10.1371/journal.ppat.1009130>
- Gatta, L., Vakil, N., Vaira, D., & Scarpignato, C. (2013). Global eradication rates for *Helicobacter pylori* infection: systematic review and meta-analysis of sequential therapy. *BMJ*, 347, f4587. <https://doi.org/10.1136/bmj.f4587>
- Gawenis, L. R., Greeb, J. M., Prasad, V., Grisham, C., Sanford, L. P., Doetschman, T., Andringa, A., Miller, M. L., & Shull, G. E. (2005). Impaired gastric acid secretion in mice with a targeted disruption of the NHE4 Na<sup>+</sup>/H<sup>+</sup> exchanger. *J Biol Chem*, 280(13), 12781-12789. <https://doi.org/10.1074/jbc.M414118200>
- Georgiades, P., Pudney, P. D. A., Thornton, D. J., & Waigh, T. A. (2014). Particle tracking microrheology of purified gastrointestinal mucins. *Biopolymers*, 101(4), 366-377. <https://doi.org/https://doi.org/10.1002/bip.22372>
- Gerrard, D. L., Hawkinson, A., Sherman, T., Modahl, C. M., Hume, G., Campbell, C. L., Schountz, T., & Fietze, S. (2017). Transcriptomic Signatures of Tacaribe Virus-Infected Jamaican Fruit Bats. *mSphere*, 2(5). <https://doi.org/10.1128/mSphere.00245-17>
- Gessulat, S., Schmidt, T., Zolg, D. P., Samaras, P., Schnatbaum, K., Zerweck, J., Knaute, T., Rechenberger, J., Delanghe, B., Huhmer, A., Reimer, U., Ehrlich, H. C., Aiche, S., Kuster, B., & Wilhelm, M. (2019). Prosit: proteome-wide prediction of peptide tandem mass spectra by deep learning. *Nat Methods*, 16(6), 509-518. <https://doi.org/10.1038/s41592-019-0426-7>
- Ginga, N. J., & Slyman, R. (2024). Double-Barrel Perfusion System for Modification of Luminal Contents of Intestinal Organoids. *Methods Mol Biol*, 2764, 205-224. [https://doi.org/10.1007/978-1-0716-3674-9\\_14](https://doi.org/10.1007/978-1-0716-3674-9_14)
- God, J., Tate, P. L., & Larcom, L. L. (2010). Red raspberries have antioxidant effects that play a minor role in the killing of stomach and colon cancer cells. *Nutr Res*, 30(11), 777-782. <https://doi.org/10.1016/j.nutres.2010.10.004>

- Gonçalves, I. C., Magalhães, A., Costa, A. M. S., Oliveira, J. R., Henriques, P. C., Gomes, P., Reis, C. A., & Martins, M. C. L. (2016). Bacteria-targeted biomaterials: Glycan-coated microspheres to bind *Helicobacter pylori*. *Acta Biomaterialia*, 33, 40-50. <https://doi.org/https://doi.org/10.1016/j.actbio.2016.01.029>
- Goodman, C., Lyon, K. N., Scotto, A., Smith, C., Sebrell, T. A., Gentry, A. B., Bala, G., Stoner, G. D., & Bimczok, D. (2021). A High-Throughput Metabolic Microarray Assay Reveals Antibacterial Effects of Black and Red Raspberries and Blackberries against *Helicobacter pylori* Infection. *Antibiotics*, 10(7), 845-845. <https://doi.org/10.3390/antibiotics10070845>
- Graham, D. Y. (2020). Transitioning of *Helicobacter pylori* Therapy from Trial and Error to Antimicrobial Stewardship. *Antibiotics (Basel)*, 9(10). <https://doi.org/10.3390/antibiotics9100671>
- Graw, S., Tang, J., Zafar, M. K., Byrd, A. K., Bolden, C., Peterson, E. C., & Byrum, S. D. (2020). proteiNorm - A User-Friendly Tool for Normalization and Analysis of TMT and Label-Free Protein Quantification. *ACS Omega*, 5(40), 25625-25633. <https://doi.org/10.1021/acsomega.0c02564>
- Gross, A., Torge, A., Schaefer, U. F., Schneider, M., Lehr, C. M., & Wagner, C. (2017). A foam model highlights the differences of the macro- and microrheology of respiratory horse mucus. *J Mech Behav Biomed Mater*, 71, 216-222. <https://doi.org/10.1016/j.jmbbm.2017.03.009>
- Gurbuz, I., Ozcelik, B., Gunbatan, T., Akkol, E. K., Sahinoz, M., & Akaydin, G. (2021). Antibacterial, antifungal and enzyme inhibitory effects of selected plants from Turkey. *Pak J Pharm Sci*, 34(3), 1011-1017. <https://www.ncbi.nlm.nih.gov/pubmed/34602426>
- Hager, T. J., Howard, L. R., & Prior, R. L. (2008). Processing and storage effects on monomeric anthocyanins, percent polymeric color, and antioxidant capacity of processed blackberry products. *J Agric Food Chem*, 56(3), 689-695. <https://doi.org/10.1021/jf071994g>
- Hall, J. S., Hofmeister, E., Ip, H. S., Nashold, S. W., Leon, A. E., Malavé, C. M., Falendysz, E. A., Rocke, T. E., Carossino, M., Balasuriya, U., & Knowles, S. (2023). Experimental Infection of Mexican Free-Tailed Bats (*Tadarida brasiliensis*) with SARS-CoV-2. *mSphere*, 8(1), e0026322. <https://doi.org/10.1128/msphere.00263-22>
- Hall, J. S., Knowles, S., Nashold, S. W., Ip, H. S., Leon, A. E., Rocke, T., Keller, S., Carossino, M., Balasuriya, U., & Hofmeister, E. (2021). Experimental challenge of a North American bat species, big brown bat (*Eptesicus fuscus*), with SARS-CoV-2. *Transbound Emerg Dis*, 68(6), 3443-3452. <https://doi.org/10.1111/tbed.13949>
- Harris, P. R., Mobley, H. L., Perez-Perez, G. I., Blaser, M. J., & Smith, P. D. (1996). *Helicobacter pylori* urease is a potent stimulus of mononuclear phagocyte activation and inflammatory cytokine production. *Gastroenterology*, 111(2), 419-425. <https://doi.org/10.1053/gast.1996.v111.pm8690207>

- He, H., Zhou, J., Xu, X., Zhou, P., Zhong, H., & Liu, M. (2024). Piezo channels in the intestinal tract [Review]. *Frontiers in Physiology*, 15. <https://doi.org/10.3389/fphys.2024.1356317>
- Hecht-Höger, A. M., Braun, B. C., Krause, E., Meschede, A., Krahe, R., Voigt, C. C., Greenwood, A. D., & Czirják, G. (2020). Plasma proteomic profiles differ between European and North American myotis bats colonized by *Pseudogymnoascus destructans*. *Mol Ecol*, 29(9), 1745-1755. <https://doi.org/10.1111/mec.15437>
- Heck, M., & Neely, B. A. (2020). Proteomics in Non-model Organisms: A New Analytical Frontier. *J Proteome Res*, 19(9), 3595-3606. <https://doi.org/10.1021/acs.jproteome.0c00448>
- Hedges, J. F., Snyder, D. T., Robison, A., Grifka-Walk, H. M., Blackwell, K., Shepardson, K., Kominsky, D., Rynda-Appl, A., Walcheck, B., & Jutila, M. A. (2022). An ADAM17-Neutralizing Antibody Reduces Inflammation and Mortality While Increasing Viral Burden in a COVID-19 Mouse Model. *Front Immunol*, 13, 918881. <https://doi.org/10.3389/fimmu.2022.918881>
- Hewson, C. A., Edbrooke, M. R., & Johnston, S. L. (2004). PMA induces the MUC5AC respiratory mucin in human bronchial epithelial cells, via PKC, EGF/TGF- $\alpha$ , Ras/Raf, MEK, ERK and Sp1-dependent mechanisms. *J Mol Biol*, 344(3), 683-695. <https://doi.org/10.1016/j.jmb.2004.09.059>
- Hill, D. R., & Spence, J. R. (2017). Gastrointestinal Organoids: Understanding the Molecular Basis of the Host-Microbe Interface. *Cell Mol Gastroenterol Hepatol*, 3(2), 138-149. <https://doi.org/10.1016/j.jcmgh.2016.11.007>
- Hirano, S., Nagatsu, Y., & Suzuki, R. X. (2022). Reversal of effects from gel production in a reacting flow dependent on gel strength. *Physical Review Fluids*, 7(2), 023201. <https://doi.org/10.1103/PhysRevFluids.7.023201>
- Ho, S. B., Takamura, K., Anway, R., Shekels, L. L., Toribara, N. W., & Ota, H. (2004). The adherent gastric mucous layer is composed of alternating layers of MUC5AC and MUC6 mucin proteins. *Digestive Diseases and Sciences*. <https://doi.org/10.1023/B:DDAS.0000043371.12671.98>
- Hof, L., Moreth, T., Koch, M., Liebisch, T., Kurtz, M., Tarnick, J., Lissek, S. M., Verstegen, M. M. A., van der Laan, L. J. W., Huch, M., Matthäus, F., Stelzer, E. H. K., & Pampaloni, F. (2021). Long-term live imaging and multiscale analysis identify heterogeneity and core principles of epithelial organoid morphogenesis. *BMC Biology*, 19(1), 37. <https://doi.org/10.1186/s12915-021-00958-w>
- Hofer, M., Duque-Correa, M. A., & Lutolf, M. P. (2024). A Bioengineered Platform for Enhanced Observability of Patterned Gastrointestinal Organoid Monolayers with Bilateral Access. *bioRxiv*, 2024.2001.2026.577381. <https://doi.org/10.1101/2024.01.26.577381>

- Hofer, M., & Lutolf, M. P. (2021). Engineering organoids. *Nat Rev Mater*, 6(5), 402-420. <https://doi.org/10.1038/s41578-021-00279-y>
- Hoffmann, W. (2021). Trefoil Factor Family (TFF) Peptides and their Different Roles in the Mucosal Innate Immune Defense and More: An Update. *Curr Med Chem*, 28(36), 7387-7399. <https://doi.org/10.2174/0929867328666210215114140>
- Hu, G. Y., Yu, B. P., Dong, W. G., Li, M. Q., Yu, J. P., Luo, H. S., & Rang, Z. X. (2003). Expression of TFF2 and Helicobacter pylori infection in carcinogenesis of gastric mucosa. *World J Gastroenterol*, 9(5), 910-914. <https://doi.org/10.3748/wjg.v9.i5.910>
- Huang, H., Huang, Y., Lau, W., Ou-Yang, H. D., Zhou, C., & El-Aasser, M. S. (2018). Integrating optical coherence tomography with gravimetric and video analysis (OCT-Gravimetry-Video method) for studying the drying process of polystyrene latex system. *Scientific Reports*, 8(1), 12962. <https://doi.org/10.1038/s41598-018-30914-8>
- Iijima, K., Ichikawa, T., Okada, S., Ogawa, M., Koike, T., Ohara, S., & Shimosegawa, T. (2009). Rebamipide, a cytoprotective drug, increases gastric mucus secretion in human: evaluations with endoscopic gastrin test. *Dig Dis Sci*, 54(7), 1500-1507. <https://doi.org/10.1007/s10620-008-0507-4>
- Ishihara, K., & Tanaka, E. M. (2018). Spontaneous symmetry breaking and pattern formation of organoids. *Current Opinion in Systems Biology*, 11, 123-128. <https://doi.org/https://doi.org/10.1016/j.coisb.2018.06.002>
- Ito, T., Kobayashi, D., Uchida, K., Takemura, T., Nagaoka, S., Kobayashi, I., Yokoyama, T., Ishige, I., Ishige, Y., Ishida, N., Furukawa, A., Muraoka, H., Ikeda, S., Sekine, M., Ando, N., Suzuki, Y., Yamada, T., Suzuki, T., & Eishi, Y. (2008). Helicobacter pylori invades the gastric mucosa and translocates to the gastric lymph nodes. *Lab Invest*, 88(6), 664-681. <https://doi.org/10.1038/labinvest.2008.33>
- Izadifar, Z., Sontheimer-Phelps, A., Lubamba, B. A., Bai, H., Fadel, C., Stejskalova, A., Ozkan, A., Dasgupta, Q., Bein, A., Junaid, A., Gulati, A., Mahajan, G., Kim, S., LoGrande, N. T., Naziripour, A., & Ingber, D. E. (2022). Modeling mucus physiology and pathophysiology in human organs-on-chips. *Adv Drug Deliv Rev*, 191, 114542. <https://doi.org/10.1016/j.addr.2022.114542>
- Jang, K. K., Kaczmarek, M. E., Dallari, S., Chen, Y. H., Tada, T., Axelrad, J., Landau, N. R., Stapleford, K. A., & Cadwell, K. (2022). Variable susceptibility of intestinal organoid-derived monolayers to SARS-CoV-2 infection. *PLoS Biol*, 20(3), e3001592. <https://doi.org/10.1371/journal.pbio.3001592>
- Jaworski, T., Sarosiek, I., Sostarich, S., Roeser, K., Connor, M., Brotze, S., Wallner, G., & Sarosiek, J. (2005). Restorative impact of rabeprazole on gastric mucus and mucin production impairment during naproxen administration: its potential clinical significance. *Dig Dis Sci*, 50(2), 357-365. <https://doi.org/10.1007/s10620-005-1611-3>

- Jenkinson, S. E., Chung, G. W., van Loon, E., Bakar, N. S., Dalzell, A. M., & Brown, C. D. A. (2012). The limitations of renal epithelial cell line HK-2 as a model of drug transporter expression and function in the proximal tubule. *Pflügers Archiv - European Journal of Physiology*, 464(6), 601-611. <https://doi.org/10.1007/s00424-012-1163-2>
- Jeong, H. J., Park, J. H., Kang, J. H., Sabaté Del Río, J., Kong, S. H., & Park, T. E. (2023). Organoid-Based Human Stomach Micro-Physiological System to Recapitulate the Dynamic Mucosal Defense Mechanism. *Adv Sci (Weinh)*, 10(27), e2300164. <https://doi.org/10.1002/advs.202300164>
- Jewell, M. P., Galyean, A. A., Kirk Harris, J., Zemanick, E. T., & Cash, K. J. (2019). Luminescent Nanosensors for Ratiometric Monitoring of Three-Dimensional Oxygen Gradients in Laboratory and Clinical *Pseudomonas aeruginosa* Biofilms. *Appl Environ Microbiol*, 85(20). <https://doi.org/10.1128/aem.01116-19>
- Johansson, M., Synnerstad, I., & Holm, L. (2000). Acid transport through channels in the mucous layer of rat stomach. *Gastroenterology*, 119(5), 1297-1304. <https://doi.org/https://doi.org/10.1053/gast.2000.19455>
- Johansson, M. E., Sjovall, H., & Hansson, G. C. (2013). The gastrointestinal mucus system in health and disease. *Nat Rev Gastroenterol Hepatol*, 10(6), 352-361. <https://doi.org/10.1038/nrgastro.2013.35>
- Johnson, B. A., Xie, X., Bailey, A. L., Kalveram, B., Lokugamage, K. G., Muruato, A., Zou, J., Zhang, X., Juelich, T., Smith, J. K., Zhang, L., Bopp, N., Schindewolf, C., Vu, M., Vanderheiden, A., Winkler, E. S., Swetnam, D., Plante, J. A., Aguilar, P.,...Menachery, V. D. (2021). Loss of furin cleavage site attenuates SARS-CoV-2 pathogenesis. *Nature*, 591(7849), 293-299. <https://doi.org/10.1038/s41586-021-03237-4>
- Jones, D. N., Ravelomanantsoa, N. A. F., Yeoman, C. J., Plowright, R. K., & Brook, C. E. (2022). Do gastrointestinal microbiomes play a role in bats' unique viral hosting capacity? *Trends Microbiol*, 30(7), 632-642. <https://doi.org/10.1016/j.tim.2021.12.009>
- Jory, M., Donnarumma, D., Blanc, C., Bellouma, K., Fort, A., Vachier, I., Casanellas, L., Bourdin, A., & Massiera, G. (2022). Mucus from human bronchial epithelial cultures: rheology and adhesion across length scales. *Interface Focus*, 12(6), 20220028. <https://doi.org/10.1098/rsfs.2022.0028>
- Josenhans, C., Eaton, K. A., Thevenot, T., & Suerbaum, S. (2000). Switching of flagellar motility in *Helicobacter pylori* by reversible length variation of a short homopolymeric sequence repeat in *fliP*, a gene encoding a basal body protein. *Infect Immun*, 68(8), 4598-4603. <https://doi.org/10.1128/IAI.68.8.4598-4603.2000>
- Jung, P., Sato, T., Merlos-Suarez, A., Barriga, F. M., Iglesias, M., Rossell, D., Auer, H., Gallardo, M., Blasco, M. A., Sancho, E., Clevers, H., & Batlle, E. (2011). Isolation and in vitro

- expansion of human colonic stem cells. *Nat Med*, 17(10), 1225-1227.  
<https://doi.org/10.1038/nm.2470>
- Kane, K. I. W., Lucumi Moreno, E., Lehr, C. M., Hachi, S., Dannert, R., Sanctuary, R., Wagner, C., Fleming, R. M. T., & Baller, J. (2018). Determination of the rheological properties of Matrigel for optimum seeding conditions in microfluidic cell cultures. *AIP Advances*, 8(12), 125332. <https://doi.org/10.1063/1.5067382>
- Kapanidis, A. N., Uphoff, S., & Stracy, M. (2018). Understanding Protein Mobility in Bacteria by Tracking Single Molecules. *J Mol Biol*, 430(22), 4443-4455.  
<https://doi.org/10.1016/j.jmb.2018.05.002>
- Karam, S. M., & Leblond, C. P. (1992). Identifying and counting epithelial cell types in the “corpus” of the mouse stomach. *The Anatomical Record*, 232(2), 231-246.  
<https://doi.org/https://doi.org/10.1002/ar.1092320208>
- Karam, S. M., & Leblond, C. P. (1993a). Dynamics of epithelial cells in the corpus of the mouse stomach. I. Identification of proliferative cell types and pinpointing of the stem cell. *Anat Rec*, 236(2), 259-279. <https://doi.org/10.1002/ar.1092360202>
- Karam, S. M., & Leblond, C. P. (1993b). Dynamics of epithelial cells in the corpus of the mouse stomach. III. Inward migration of neck cells followed by progressive transformation into zymogenic cells. *Anat Rec*, 236(2), 297-313. <https://doi.org/10.1002/ar.1092360204>
- Kauffman, G. L., Jr. (1981). Gastric mucus and bicarbonate secretion in relation to mucosal protection. *J Clin Gastroenterol*, 3(Suppl 2), 45-50.
- Kawakubo, M., Ito, Y., Okimura, Y., Kobayashi, M., Sakura, K., Kasama, S., Fukuda, M. N., Fukuda, M., Katsuyama, T., & Nakayama, J. (2004). Natural antibiotic function of a human gastric mucin against *Helicobacter pylori* infection. *Science*, 305(5686), 1003-1006. <https://doi.org/10.1126/science.1099250>
- Keilberg, D., & Ottemann, K. M. (2016a). How *Helicobacter pylori* senses, targets and interacts with the gastric epithelium. *Environmental Microbiology*, 18(3), 791-806.  
<https://doi.org/10.1111/1462-2920.13222>
- Khalifa, H. O., Kamimoto, M., Shimamoto, T., & Shimamoto, T. (2015). Antimicrobial Effects of Blueberry, Raspberry, and Strawberry Aqueous Extracts and their Effects on Virulence Gene Expression in *Vibrio cholerae*. *Phytother Res*, 29(11), 1791-1797.  
<https://doi.org/10.1002/ptr.5436>
- Khoo, H. E., Azlan, A., Tang, S. T., & Lim, S. M. (2017). Anthocyanidins and anthocyanins: colored pigments as food, pharmaceutical ingredients, and the potential health benefits. *Food Nutr Res*, 61(1), 1361779. <https://doi.org/10.1080/16546628.2017.1361779>

- Kim, J., Koo, B.-K., & Knoblich, J. A. (2020). Human organoids: model systems for human biology and medicine. *Nature Reviews Molecular Cell Biology*, 21(10), 571-584. <https://doi.org/10.1038/s41580-020-0259-3>
- Kim, J., Nguyen, T. T. H., Jin, J., Septiana, I., Son, G. M., Lee, G. H., Jung, Y. J., Qureshi, D., Mok, I. K., Pal, K., Yang, S. Y., Kim, S. B., & Kim, D. (2019). Anti-cariogenic Characteristics of Rubusoside. *Biotechnol Bioprocess Eng*, 24(2), 282-287. <https://doi.org/10.1007/s12257-018-0408-0>
- Kim, J. M., Kim, J. S., Jung, H. C., Kim, N., Kim, Y. J., & Song, I. S. (2004). Distribution of antibiotic MICs for *Helicobacter pylori* strains over a 16-year period in patients from Seoul, South Korea. *Antimicrob Agents Chemother*, 48(12), 4843-4847. <https://doi.org/10.1128/AAC.48.12.4843-4847.2004>
- Kim, S., Cassidy, J. J., Yang, B., Carthew, R. W., & Hilgenfeldt, S. (2016). Hexagonal Patterning of the Insect Compound Eye: Facet Area Variation, Defects, and Disorder. *Biophysical Journal*, 111(12), 2735-2746. <https://doi.org/10.1016/j.bpj.2016.11.004>
- Kim, S. H., Woo, H., Park, M., Rhee, K. J., Moon, C., Lee, D., Seo, W. D., & Kim, J. B. (2014). Cyanidin 3-O-glucoside reduces *Helicobacter pylori* VacA-induced cell death of gastric KATO III cells through inhibition of the SecA pathway. *Int J Med Sci*, 11(7), 742-747. <https://doi.org/10.7150/ijms.7167>
- Kim, T. H., & Shivdasani, R. A. (2016). Stomach development, stem cells and disease. *Development*, 143(4), 554-565. <https://doi.org/10.1242/dev.124891>
- Kip, A. M., Soons, Z., Mohren, R., Duivenvoorden, A. A. M., Roth, A. A. J., Cillero-Pastor, B., Neumann, U. P., Dejong, C. H. C., Heeren, R. M. A., Olde Damink, S. W. M., & Lenaerts, K. (2021). Proteomics analysis of human intestinal organoids during hypoxia and reoxygenation as a model to study ischemia-reperfusion injury. *Cell Death Dis*, 12(1), 95. <https://doi.org/10.1038/s41419-020-03379-9>
- Kirch, J., Schneider, A., Abou, B., Hopf, A., Schaefer, U. F., Schneider, M., Schall, C., Wagner, C., & Lehr, C. M. (2012). Optical tweezers reveal relationship between microstructure and nanoparticle penetration of pulmonary mucus. *Proc Natl Acad Sci U S A*, 109(45), 18355-18360. <https://doi.org/10.1073/pnas.1214066109>
- Klesk, K., Qian, M., & Martin, R. R. (2004). Aroma extract dilution analysis of cv. Meeker (*Rubus idaeus* L.) red raspberries from Oregon and Washington. *J Agric Food Chem*, 52(16), 5155-5161. <https://doi.org/10.1021/jf0498721>
- Kolpen, M., Kühl, M., Bjarnsholt, T., Moser, C., Hansen, C. R., Liengaard, L., Kharazmi, A., Pressler, T., Høiby, N., & Jensen, P. (2014). Nitrous oxide production in sputum from cystic fibrosis patients with chronic *Pseudomonas aeruginosa* lung infection. *PLoS ONE*, 9(1), e84353. <https://doi.org/10.1371/journal.pone.0084353>

- Kopper, O., de Witte, C. J., Löhmußaar, K., Valle-Inclan, J. E., Hami, N., Kester, L., Balgobind, A. V., Korving, J., Proost, N., Begthel, H., van Wijk, L. M., Revilla, S. A., Theeuwssen, R., van de Ven, M., van Roosmalen, M. J., Ponsioen, B., Ho, V. W. H., Neel, B. G., Bosse, T.,...Clevers, H. (2019). An organoid platform for ovarian cancer captures intra- and interpatient heterogeneity. *Nat Med*, 25(5), 838-849. <https://doi.org/10.1038/s41591-019-0422-6>
- Krajina, B. A., Tropini, C., Zhu, A., DiGiacomo, P., Sonnenburg, J. L., Heilshorn, S. C., & Spakowitz, A. J. (2017). Dynamic Light Scattering Microrheology Reveals Multiscale Viscoelasticity of Polymer Gels and Precious Biological Materials. *ACS Central Science*, 3(12), 1294-1303. <https://doi.org/10.1021/acscentsci.7b00449>
- Kramer, A., Green, J., Pollard, J., Jr., & Tugendreich, S. (2014). Causal analysis approaches in Ingenuity Pathway Analysis. *Bioinformatics*, 30(4), 523-530. <https://doi.org/10.1093/bioinformatics/btt703>
- Krauze-Baranowska, M., Majdan, M., Halasa, R., Glod, D., Kula, M., Fecka, I., & Orzel, A. (2014). The antimicrobial activity of fruits from some cultivar varieties of *Rubus idaeus* and *Rubus occidentalis*. *Food Funct*, 5(10), 2536-2541. <https://doi.org/10.1039/c4fo00129j>
- Kula, M., & Krauze-Baranowska, M. (2016). *Rubus occidentalis*: The black raspberry--its potential in the prevention of cancer. *Nutr Cancer*, 68(1), 18-28. <https://doi.org/10.1080/01635581.2016.1115095>
- Kuleshov, M. V., Stein, D. J., Clarke, D. J. B., Kropiwnicki, E., Jagodnik, K. M., Bartal, A., Evangelista, J. E., Hom, J., Cheng, M., Bailey, A., Zhou, A., Ferguson, L. B., Lachmann, A., & Ma'ayan, A. (2020). The COVID-19 Drug and Gene Set Library. *Patterns (N Y)*, 1(6), 100090. <https://doi.org/10.1016/j.patter.2020.100090>
- Kusters, J. G., Van Vliet, A. H. M., & Kuipers, E. J. (2006). Pathogenesis of *Helicobacter pylori* infection. *Clinical Microbiology Reviews*. <https://doi.org/10.1128/CMR.00054-05>
- Lai, S. K., Wang, Y. Y., Wirtz, D., & Hanes, J. (2009). Micro- and macrorheology of mucus. *Adv Drug Deliv Rev*, 61(2), 86-100. <https://doi.org/10.1016/j.addr.2008.09.012>
- Lamers, M. M., Beumer, J., van der Vaart, J., Knoops, K., Puschhof, J., Breugem, T. I., Ravelli, R. B. G., Paul van Schayck, J., Mykytyn, A. Z., Duimel, H. Q., van Donselaar, E., Riesebosch, S., Kuijpers, H. J. H., Schipper, D., van de Wetering, W. J., de Graaf, M., Koopmans, M., Cuppen, E., Peters, P. J.,...Clevers, H. (2020). SARS-CoV-2 productively infects human gut enterocytes. *Science*, 369(6499), 50-54. <https://doi.org/10.1126/science.abc1669>
- Lancaster, M. A., & Knoblich, J. A. (2014). Organogenesis in a dish: modeling development and disease using organoid technologies. *Science*, 345(6194), 1247125. <https://doi.org/10.1126/science.1247125>



- Larsen, M., Borisov, S. M., Grunwald, B., Klimant, I., & Glud, R. N. (2011). A simple and inexpensive high resolution color ratiometric planar optode imaging approach: application to oxygen and pH sensing. *Limnology and Oceanography: Methods*, 9(9), 348-360. <https://doi.org/10.4319/lom.2011.9.348>
- Lee, J. W., Kim, N., Nam, R. H., Lee, S. M., Kwon, Y. H., Sohn, S. D., Kim, J. M., Lee, D. H., & Jung, H. C. (2019). Favorable outcomes of culture-based *Helicobacter pylori* eradication therapy in a region with high antimicrobial resistance. *Helicobacter*, 24(2), e12561. <https://doi.org/10.1111/hel.12561>
- Lee, W. C., Goh, K. L., Loke, M. F., & Vadivelu, J. (2017). Elucidation of the Metabolic Network of *Helicobacter pylori* J99 and Malaysian Clinical Strains by Phenotype Microarray. *Helicobacter*, 22(1). <https://doi.org/10.1111/hel.12321>
- Lengsfeld, C., Deters, A., Faller, G., & Hensel, A. (2004). High molecular weight polysaccharides from black currant seeds inhibit adhesion of *Helicobacter pylori* to human gastric mucosa. *Planta Med*, 70(7), 620-626. <https://doi.org/10.1055/s-2004-827184>
- Leroy, E. M., Kumulungui, B., Pourrut, X., Rouquet, P., Hassanin, A., Yaba, P., Délicat, A., Paweska, J. T., Gonzalez, J.-P., & Swanepoel, R. (2005). Fruit bats as reservoirs of Ebola virus. *Nature*, 438(7068), 575-576. <https://doi.org/10.1038/438575a>
- Leushacke, M., Tan, S. H., Wong, A., Swathi, Y., Hajamohideen, A., Tan, L. T., Goh, J., Wong, E., Denil, S., Murakami, K., & Barker, N. (2017). Lgr5-expressing chief cells drive epithelial regeneration and cancer in the oxyntic stomach. *Nat Cell Biol*, 19(7), 774-786. <https://doi.org/10.1038/ncb3541>
- Levy, R., Okun, Z., & Shpigelman, A. (2019). The Influence of Chemical Structure and the Presence of Ascorbic Acid on Anthocyanins Stability and Spectral Properties in Purified Model Systems. *Foods*, 8(6). <https://doi.org/10.3390/foods8060207>
- Lewis, O. L., Keener, J. P., & Fogelson, A. L. (2017). A physics-based model for maintenance of the pH gradient in the gastric mucus layer. *Am J Physiol Gastrointest Liver Physiol*, 313(6), G599-G612. <https://doi.org/10.1152/ajpgi.00221.2017>
- Li, P.-S., Liang Lee, I., Yu, W.-L., Sun, J.-S., Jane, W.-N., & Shen, H.-H. (2014). A Novel Albumin-Based Tissue Scaffold for Autogenic Tissue Engineering Applications. *Scientific Reports*, 4(1), 5600. <https://doi.org/10.1038/srep05600>
- Liao, W., & Aranson, I. S. (2023). Viscoelasticity enhances collective motion of bacteria. *PNAS Nexus*, 2(9), pgad291. <https://doi.org/10.1093/pnasnexus/pgad291>
- Lieleg, O., Vladescu, I., & Ribbeck, K. (2010). Characterization of Particle Translocation through Mucin Hydrogels. *Biophysical Journal*, 98(9), 1782-1789. <https://doi.org/https://doi.org/10.1016/j.bpj.2010.01.012>

- Lila, M. A., Burton-Freeman, B., Grace, M., & Kalt, W. (2016). Unraveling Anthocyanin Bioavailability for Human Health. *Annu Rev Food Sci Technol*, 7, 375-393. <https://doi.org/10.1146/annurev-food-041715-033346>
- Lin, H., Li, H., Cho, H. J., Bian, S., Roh, H. J., Lee, M. K., Jung, S. K., Chung, S. J., Shim, C. K., & Kim, D. D. (2007). Air-Liquid Interface (ALI) culture of human bronchial epithelial cell monolayers as an in vitro model for airway drug transport studies. *Journal of Pharmaceutical Sciences*, 96(2). <https://doi.org/10.1002/jps.20803>
- Lin, W. W., Tsay, A. J., Lalime, E. N., Pekosz, A., & Griffin, D. E. (2021). Primary differentiated respiratory epithelial cells respond to apical measles virus infection by shedding multinucleated giant cells. *Proc Natl Acad Sci U S A*, 118(11). <https://doi.org/10.1073/pnas.2013264118>
- Linssen, R. S. N., Ma, J., Bem, R. A., & Rubin, B. K. (2020). Rational use of mucoactive medications to treat pediatric airway disease. *Paediatr Respir Rev*, 36, 8-14. <https://doi.org/10.1016/j.prrv.2020.06.007>
- Liou, J. M., Chang, C. Y., Chen, M. J., Chen, C. C., Fang, Y. J., Lee, J. Y., Wu, J. Y., Luo, J. C., Liou, T. C., Chang, W. H., Tseng, C. H., Wu, C. Y., Yang, T. H., Chang, C. C., Wang, H. P., Sheu, B. S., Lin, J. T., Bair, M. J., Wu, M. S.,...Helicobacter, C. (2015). The Primary Resistance of Helicobacter pylori in Taiwan after the National Policy to Restrict Antibiotic Consumption and Its Relation to Virulence Factors-A Nationwide Study. *PLoS ONE*, 10(5), e0124199. <https://doi.org/10.1371/journal.pone.0124199>
- Loveday, E. K., Hain, K. S., Kochetkova, I., Hedges, J. F., Robison, A., Snyder, D. T., Brumfield, S. K., Young, M. J., Jutila, M. A., Chang, C. B., & Taylor, M. P. (2021). Effect of Inactivation Methods on SARS-CoV-2 Virion Protein and Structure. *Viruses*, 13(4). <https://doi.org/10.3390/v13040562>
- Luna, N., Muñoz, M., Castillo-Castañeda, A., Hernandez, C., Urbano, P., Shaban, M., Paniz-Mondolfi, A., & Ramírez, J. D. (2023). Characterizing the blood microbiota of omnivorous and frugivorous bats (Chiroptera: Phyllostomidae) in Casanare, eastern Colombia. *PeerJ*, 11, e15169. <https://doi.org/10.7717/peerj.15169>
- Lyon, K., Bansil, R., & Bimczok, D. (2024). Profiling Luminal pH in Three-Dimensional Gastrointestinal Organoids Using Microelectrodes. *J Vis Exp*(209). <https://doi.org/10.3791/66900>
- MacAdam, A. (1993). The effect of gastro-intestinal mucus on drug absorption. *Advanced Drug Delivery Reviews*, 11(3), 201-220. [https://doi.org/10.1016/0169-409X\(93\)90010-2](https://doi.org/10.1016/0169-409X(93)90010-2)
- Magalhães, A., Rossez, Y., Robbe-Masselot, C., Maes, E., Gomes, J., Shevtsova, A., Bugaytsova, J., Borén, T., & Reis, C. A. (2016). Muc5ac gastric mucin glycosylation is shaped by

- FUT2 activity and functionally impacts *Helicobacter pylori* binding. *Scientific Reports*, 6(1), 25575. <https://doi.org/10.1038/srep25575>
- Mallah, S. I., Ghorab, O. K., Al-Salmi, S., Abdellatif, O. S., Tharmaratnam, T., Iskandar, M. A., Sefen, J. A. N., Sidhu, P., Atallah, B., El-Lababidi, R., & Al-Qahtani, M. (2021). COVID-19: breaking down a global health crisis. *Ann Clin Microbiol Antimicrob*, 20(1), 35. <https://doi.org/10.1186/s12941-021-00438-7>
- Malmlov, A., Bantle, C., Aboellail, T., Wagner, K., Campbell, C. L., Eckley, M., Chotiwan, N., Gullberg, R. C., Perera, R., Tjalkens, R., & Schountz, T. (2019). Experimental Zika virus infection of Jamaican fruit bats (*Artibeus jamaicensis*) and possible entry of virus into brain via activated microglial cells. *PLoS Negl Trop Dis*, 13(2), e0007071. <https://doi.org/10.1371/journal.pntd.0007071>
- Mao, Y., Nielsen, P., & Ali, J. (2022). Passive and Active Microrheology for Biomedical Systems [Review]. *Frontiers in Bioengineering and Biotechnology*, 10. <https://doi.org/10.3389/fbioe.2022.916354>
- Marczynski, M., Rickert, C. A., Fuhrmann, T., & Lieleg, O. (2022). An improved, filtration-based process to purify functional mucins from mucosal tissues with high yields. *Separation and Purification Technology*, 294, 121209. <https://doi.org/https://doi.org/10.1016/j.seppur.2022.121209>
- Marin, L., Miguelez, E. M., Villar, C. J., & Lombo, F. (2015). Bioavailability of dietary polyphenols and gut microbiota metabolism: antimicrobial properties. *Biomed Res Int*, 2015, 905215. <https://doi.org/10.1155/2015/905215>
- Markakis, P. (2012). *Anthocyanins as Food Colors* (1 ed.). Elsevier.
- Marques, T., David, L., Reis, C., & Nogueira, A. (2005). Topographic expression of MUC5AC and MUC6 in the gastric mucosa infected by *Helicobacter pylori* and in associated diseases. *Pathology - Research and Practice*, 201(10), 665-672. <https://doi.org/https://doi.org/10.1016/j.prp.2005.03.007>
- Marshall, B. J., & Warren, J. R. (1984). Unidentified curved bacilli in the stomach of patients with gastritis and peptic ulceration. *Lancet*, 1(8390), 1311-1315. [https://doi.org/10.1016/s0140-6736\(84\)91816-6](https://doi.org/10.1016/s0140-6736(84)91816-6)
- Martínez, L. E., Hardcastle, J. M., Wang, J., Pincus, Z., Tsang, J., Hoover, T. R., Bansil, R., & Salama, N. R. (2016). *Helicobacter pylori* strains vary cell shape and flagellum number to maintain robust motility in viscous environments. *Molecular Microbiology*. <https://doi.org/10.1111/mmi.13218>
- Mason, T. G. (2000). Estimating the viscoelastic moduli of complex fluids using the generalized Stokes–Einstein equation. *Rheologica Acta*, 39(4), 371-378. <https://doi.org/10.1007/s003970000094>

- Mason, T. G., Ganesan, K., van Zanten, J. H., Wirtz, D., & Kuo, S. C. (1997). Particle Tracking Microrheology of Complex Fluids. *Physical Review Letters*, 79(17), 3282-3285. <https://doi.org/10.1103/PhysRevLett.79.3282>
- McCracken, K. W., Aihara, E., Martin, B., Crawford, C. M., Broda, T., Treguier, J., Zhang, X., Shannon, J. M., Montrose, M. H., & Wells, J. M. (2017). Wnt/ $\beta$ -catenin promotes gastric fundus specification in mice and humans. *Nature*. <https://doi.org/10.1038/nature21021>
- McCracken, K. W., Cata, E. M., Crawford, C. M., Sinagoga, K. L., Schumacher, M., Rockich, B. E., Tsai, Y. H., Mayhew, C. N., Spence, J. R., Zavros, Y., & Wells, J. M. (2014). Modelling human development and disease in pluripotent stem-cell-derived gastric organoids. *Nature*, 516(7531), 400-404. <https://doi.org/10.1038/nature13863>
- McShane, A., Bath, J., Jaramillo, A. M., Ridley, C., Walsh, A. A., Evans, C. M., Thornton, D. J., & Ribbeck, K. (2021). Mucus. *Curr Biol*, 31(15), R938-R945. <https://doi.org/10.1016/j.cub.2021.06.093>
- Megraud, F., Neman-Simha, V., & Brugmann, D. (1992). Further evidence of the toxic effect of ammonia produced by *Helicobacter pylori* urease on human epithelial cells. *Infect Immun*, 60(5), 1858-1863. <https://doi.org/10.1128/iai.60.5.1858-1863.1992>
- Meldrum, O. W., Yakubov, G. E., Bonilla, M. R., Deshmukh, O., McGuckin, M. A., & Gidley, M. J. (2018). Mucin gel assembly is controlled by a collective action of non-mucin proteins, disulfide bridges, Ca<sup>2+</sup>-mediated links, and hydrogen bonding. *Scientific Reports*, 8(1), 5802. <https://doi.org/10.1038/s41598-018-24223-3>
- Meziu, E., Koch, M., Fleddermann, J., Schwarzkopf, K., Schneider, M., & Kraegeloh, A. (2021). Visualization of the structure of native human pulmonary mucus. *Int J Pharm*, 597, 120238. <https://doi.org/10.1016/j.ijpharm.2021.120238>
- Miyoshi, H., & Stappenbeck, T. S. (2013). In vitro expansion and genetic modification of gastrointestinal stem cells in spheroid culture. *Nature Protocols*. <https://doi.org/10.1038/nprot.2013.153>
- Mohammadi, S., Morell-Perez, C., Wright, C. W., Wyche, T. P., White, C. H., Sana, T. R., & Lieberman, L. A. (2021). Assessing donor-to-donor variability in human intestinal organoid cultures. *Stem Cell Reports*, 16(9), 2364-2378. <https://doi.org/10.1016/j.stemcr.2021.07.016>
- Morgan, E., Arnold, M., Camargo, M. C., Gini, A., Kunzmann, A. T., Matsuda, T., Meheus, F., Verhoeven, R. H. A., Vignat, J., Laversanne, M., Ferlay, J., & Soerjomataram, I. (2022). The current and future incidence and mortality of gastric cancer in 185 countries, 2020-40: A population-based modelling study. *EClinicalMedicine*, 47, 101404. <https://doi.org/10.1016/j.eclinm.2022.101404>

- Mosbauer, K., Fritsch, V. N., Adrian, L., Bernhardt, J., Gruhlke, M. C. H., Slusarenko, A. J., Niemeyer, D., & Antelmann, H. (2021). The Effect of Allicin on the Proteome of SARS-CoV-2 Infected Calu-3 Cells. *Front Microbiol*, 12, 746795. <https://doi.org/10.3389/fmicb.2021.746795>
- Moschakis, T. (2013). Microrheology and particle tracking in food gels and emulsions. *Current Opinion in Colloid & Interface Science*, 18(4), 311-323. <https://doi.org/https://doi.org/10.1016/j.cocis.2013.04.011>
- Munster, V. J., Adney, D. R., van Doremalen, N., Brown, V. R., Miazgowicz, K. L., Milne-Price, S., Bushmaker, T., Rosenke, R., Scott, D., Hawkinson, A., de Wit, E., Schountz, T., & Bowen, R. A. (2016). Replication and shedding of MERS-CoV in Jamaican fruit bats (*Artibeus jamaicensis*). *Sci Rep*, 6, 21878. <https://doi.org/10.1038/srep21878>
- Murphy, K. C., Hung, B. P., Browne-Bourne, S., Zhou, D., Yeung, J., Genetos, D. C., & Leach, J. K. (2017). Measurement of oxygen tension within mesenchymal stem cell spheroids. *Journal of The Royal Society Interface*, 14(127), 20160851. <https://doi.org/10.1098/rsif.2016.0851>
- Nakamura, H., Yoshiyama, H., Takeuchi, H., Mizote, T., Okita, K., & Nakazawa, T. (1998). Urease plays an important role in the chemotactic motility of *Helicobacter pylori* in a viscous environment. *Infect Immun*, 66(10), 4832-4837. <https://doi.org/10.1128/IAI.66.10.4832-4837.1998>
- Nazende, G. T., Akif, E. T., & Marc, S. (2014). Inhalable Antibiotic Nanoformulations for the Treatment of *Pseudomonas Aeruginosa* Infection in Cystic Fibrosis – A Review. *Drug Delivery Letters*, 4(3), 193-207. <https://doi.org/http://dx.doi.org/10.2174/2210303104666140222002101>
- Neely, B. A., Janech, M. G., Fenton, M. B., Simmons, N. B., Bland, A. M., & Becker, D. J. (2021). Surveying the Vampire Bat (*Desmodus rotundus*) Serum Proteome: A Resource for Identifying Immunological Proteins and Detecting Pathogens. *J Proteome Res*, 20(5), 2547-2559. <https://doi.org/10.1021/acs.jproteome.0c00995>
- Niv, Y. (2015). *Helicobacter pylori* and gastric mucin expression: A systematic review and meta-analysis. *World J Gastroenterol*, 21(31), 9430-9436. <https://doi.org/10.3748/wjg.v21.i31.9430>
- Nnyigide, O. S., & Hyun, K. (2023). A comprehensive review of food rheology: analysis of experimental, computational, and machine learning techniques. *Korea-Australia Rheology Journal*, 35(4), 279-306. <https://doi.org/10.1007/s13367-023-00075-w>
- Nordman, H., Davies, J. R., Lindell, G., de Bolós, C., Real, F., & Carlstedt, I. (2002). Gastric MUC5AC and MUC6 are large oligomeric mucins that differ in size, glycosylation and tissue distribution. *Biochem J*, 364(Pt 1), 191-200. <https://doi.org/10.1042/bj3640191>

- O'Connor, A., Liou, J. M., Gisbert, J. P., & O'Morain, C. (2019). Review: Treatment of *Helicobacter pylori* Infection 2019. *Helicobacter*, 24 Suppl 1, e12640. <https://doi.org/10.1111/hel.12640>
- O'Farrell, C., Stamatopoulos, K., Simmons, M., & Batchelor, H. (2021). In vitro models to evaluate ingestible devices: Present status and current trends. *Advanced Drug Delivery Reviews*, 178, 113924. <https://doi.org/10.1016/j.addr.2021.113924>
- OhAinle, M., Helms, L., Vermeire, J., Roesch, F., Humes, D., Basom, R., Delrow, J. J., Overbaugh, J., & Emerman, M. (2018). A virus-packageable CRISPR screen identifies host factors mediating interferon inhibition of HIV. *Elife*, 7. <https://doi.org/10.7554/eLife.39823>
- Okkelman, I. A., Neto, N., Papkovsky, D. B., Monaghan, M. G., & Dmitriev, R. I. (2020). A deeper understanding of intestinal organoid metabolism revealed by combining fluorescence lifetime imaging microscopy (FLIM) and extracellular flux analyses. *Redox Biol*, 30, 101420. <https://doi.org/10.1016/j.redox.2019.101420>
- Pabst, B., Pitts, B., Lauchnor, E., & Stewart, P. S. (2016). Gel-Entrapped *Staphylococcus aureus* Bacteria as Models of Biofilm Infection Exhibit Growth in Dense Aggregates, Oxygen Limitation, Antibiotic Tolerance, and Heterogeneous Gene Expression. *Antimicrob Agents Chemother*, 60(10), 6294-6301. <https://doi.org/10.1128/aac.01336-16>
- Panda, S. K., Padhi, L., Leyssen, P., Liu, M., Neyts, J., & Luyten, W. (2017). Antimicrobial, Anthelmintic, and Antiviral Activity of Plants Traditionally Used for Treating Infectious Disease in the Similipal Biosphere Reserve, Odisha, India. *Front Pharmacol*, 8, 658. <https://doi.org/10.3389/fphar.2017.00658>
- Papaccio, F., Cabeza-Segura, M., Garcia-Micò, B., Tarazona, N., Roda, D., Castillo, J., & Cervantes, A. (2022). Will Organoids Fill the Gap towards Functional Precision Medicine? *J Pers Med*, 12(11). <https://doi.org/10.3390/jpm12111939>
- Parente, I. A., Chiara, L., & Bertoni, S. (2024). Exploring the potential of human intestinal organoids: Applications, challenges, and future directions. *Life Sciences*, 352, 122875. <https://doi.org/10.1016/j.lfs.2024.122875>
- Park, J. U., Cho, J. S., Kim, J. S., Kim, H. K., Jo, Y. H., Rahman, M. A. A., & Lee, Y. I. (2020). Synergistic Effect of *Rubus crataegifolius* and *Ulmus macrocarpa* Against *Helicobacter pylori* Clinical Isolates and Gastritis. *Front Pharmacol*, 11, 4. <https://doi.org/10.3389/fphar.2020.00004>
- Pastukh, N., Peretz, A., Brodsky, D., Isakovich, N., Azrad, M., & On, A. (2018). Antimicrobial susceptibility of *Helicobacter pylori* strains isolated from children in Israel. *J Glob Antimicrob Resist*, 12, 175-178. <https://doi.org/10.1016/j.jgar.2017.10.004>

- Patwa, A., Thiéry, A., Lombard, F., Lilley, M. K. S., Boisset, C., Bramard, J.-F., Bottero, J.-Y., & Barthélémy, P. (2015). Accumulation of nanoparticles in “jellyfish” mucus: a bio-inspired route to decontamination of nano-waste. *Scientific Reports*, 5(1), 11387. <https://doi.org/10.1038/srep11387>
- Peek, R. M., Jr., Blaser, M. J., Mays, D. J., Forsyth, M. H., Cover, T. L., Song, S. Y., Krishna, U., & Pietenpol, J. A. (1999). Helicobacter pylori strain-specific genotypes and modulation of the gastric epithelial cell cycle. *Cancer Res*, 59(24), 6124-6131. <https://www.ncbi.nlm.nih.gov/pubmed/10626802>
- Peiffer, D. S., Wang, L. S., Zimmerman, N. P., Ransom, B. W., Carmella, S. G., Kuo, C. T., Chen, J. H., Oshima, K., Huang, Y. W., Hecht, S. S., & Stoner, G. D. (2016). Dietary Consumption of Black Raspberries or Their Anthocyanin Constituents Alters Innate Immune Cell Trafficking in Esophageal Cancer. *Cancer Immunol Res*, 4(1), 72-82. <https://doi.org/10.1158/2326-6066.CIR-15-0091>
- Peiffer, D. S., Zimmerman, N. P., Wang, L. S., Ransom, B. W., Carmella, S. G., Kuo, C. T., Siddiqui, J., Chen, J. H., Oshima, K., Huang, Y. W., Hecht, S. S., & Stoner, G. D. (2014). Chemoprevention of esophageal cancer with black raspberries, their component anthocyanins, and a major anthocyanin metabolite, protocatechuic acid. *Cancer Prev Res (Phila)*, 7(6), 574-584. <https://doi.org/10.1158/1940-6207.CAPR-14-0003>
- Perez-Riverol, Y., Csordas, A., Bai, J., Bernal-Llinares, M., Hewapathirana, S., Kundu, D. J., Inuganti, A., Griss, J., Mayer, G., Eisenacher, M., Perez, E., Uszkoreit, J., Pfeuffer, J., Sachsenberg, T., Yilmaz, S., Tiwary, S., Cox, J., Audain, E., Walzer, M.,... Vizcaino, J. A. (2019). The PRIDE database and related tools and resources in 2019: improving support for quantification data. *Nucleic Acids Res*, 47(D1), D442-D450. <https://doi.org/10.1093/nar/gky1106>
- Peterson, A. J., Menheniott, T. R., O'Connor, L., Walduck, A. K., Fox, J. G., Kawakami, K., Minamoto, T., Ong, E. K., Wang, T. C., Judd, L. M., & Giraud, A. S. (2010). Helicobacter pylori infection promotes methylation and silencing of trefoil factor 2, leading to gastric tumor development in mice and humans. *Gastroenterology*, 139(6), 2005-2017. <https://doi.org/10.1053/j.gastro.2010.08.043>
- Phillips, G. J., James, S. L., & Lethem, M. I. (1997). Rheological Properties and Hydration of Airway Mucus. In D. F. Rogers & M. I. Lethem (Eds.), *Airway Mucus: Basic Mechanisms and Clinical Perspectives* (pp. 117-147). Birkhäuser Basel. [https://doi.org/10.1007/978-3-0348-8874-5\\_6](https://doi.org/10.1007/978-3-0348-8874-5_6)
- Pieper, M., Schulz-Hildebrandt, H., Schmutde, I., Quell, K. M., Laumonnier, Y., Hüttmann, G., & König, P. (2022). Intravital imaging of mucus transport in asthmatic mice using microscopic optical coherence tomography. *Am J Physiol Lung Cell Mol Physiol*, 323(4), L423-L430. <https://doi.org/10.1152/ajplung.00455.2021>

- Pleguezuelos-Manzano, C., Puschhof, J., van den Brink, S., Geurts, V., Beumer, J., & Clevers, H. (2020). Establishment and Culture of Human Intestinal Organoids Derived from Adult Stem Cells. *Curr Protoc Immunol*, 130(1), e106. <https://doi.org/10.1002/cpim.106>
- Ploug, H., Stolte, W., Epping, E. H. G., & Jørgensen, B. B. (1999). Diffusive boundary layers, photosynthesis, and respiration of the colony-forming plankton algae, *Phaeocystis* sp. *Limnology and Oceanography*, 44(8), 1949-1958. <https://doi.org/https://doi.org/10.4319/lo.1999.44.8.1949>
- Pojer, E., Mattivi, F., Johnson, D., & Stockley, C. S. (2013). The Case for Anthocyanin Consumption to Promote Human Health: A Review. *Compr Rev Food Sci Food Saf*, 12(5), 483-508. <https://doi.org/10.1111/1541-4337.12024>
- Powell, R. H., & Behnke, M. S. (2017). WRN conditioned media is sufficient for in vitro propagation of intestinal organoids from large farm and small companion animals. *Biol Open*, 6(5), 698-705. <https://doi.org/10.1242/bio.021717>
- Pruitt, K. D., Brown, G. R., Hiatt, S. M., Thibaud-Nissen, F., Astashyn, A., Ermolaeva, O., Farrell, C. M., Hart, J., Landrum, M. J., McGarvey, K. M., Murphy, M. R., O'Leary, N. A., Pujar, S., Rajput, B., Rangwala, S. H., Riddick, L. D., Shkeda, A., Sun, H., Tamez, P.,...Ostell, J. M. (2014). RefSeq: an update on mammalian reference sequences. *Nucleic Acids Res*, 42(Database issue), D756-763. <https://doi.org/10.1093/nar/gkt1114>
- Puupponen-Pimia, R., Nohynek, L., Alakomi, H. L., & Oksman-Caldentey, K. M. (2005). Bioactive berry compounds-novel tools against human pathogens. *Appl Microbiol Biotechnol*, 67(1), 8-18. <https://doi.org/10.1007/s00253-004-1817-x>
- Puupponen-Pimia, R., Nohynek, L., Meier, C., Kahkonen, M., Heinonen, M., Hopia, A., & Oksman-Caldentey, K. M. (2001). Antimicrobial properties of phenolic compounds from berries. *J Appl Microbiol*, 90(4), 494-507. <https://doi.org/10.1046/j.1365-2672.2001.01271.x>
- Räz, T. (2017). The silent hexagon: explaining comb structures. *Synthese*, 194(5), 1703-1724. <https://doi.org/10.1007/s11229-016-1014-3>
- Reid, J. E., & Jackson, A. C. (2001). Experimental rabies virus infection in *Artibeus jamaicensis* bats with CVS-24 variants. *J Neurovirol*, 7(6), 511-517. <https://doi.org/10.1080/135502801753248097>
- Reily, C., Stewart, T. J., Renfrow, M. B., & Novak, J. (2019). Glycosylation in health and disease. *Nat Rev Nephrol*, 15(6), 346-366. <https://doi.org/10.1038/s41581-019-0129-4>
- Ridley, R. G. (1989). *Antibodies: A Laboratory Manual* (E. H. a. D. Lane, Ed. 2009/04/14 ed., Vol. 54). Cambridge University Press. <https://doi.org/10.1017/S0016672300028548>



- Ritchie, M. E., Phipson, B., Wu, D., Hu, Y., Law, C. W., Shi, W., & Smyth, G. K. (2015). limma powers differential expression analyses for RNA-sequencing and microarray studies. *Nucleic Acids Res*, 43(7), e47. <https://doi.org/10.1093/nar/gkv007>
- Riva, L., Yuan, S., Yin, X., Martin-Sancho, L., Matsunaga, N., Pache, L., Burgstaller-Muehlbacher, S., De Jesus, P. D., Teriete, P., Hull, M. V., Chang, M. W., Chan, J. F., Cao, J., Poon, V. K., Herbert, K. M., Cheng, K., Nguyen, T. H., Rubanov, A., Pu, Y.,...Chanda, S. K. (2020). Discovery of SARS-CoV-2 antiviral drugs through large-scale compound repurposing. *Nature*, 586(7827), 113-119. <https://doi.org/10.1038/s41586-020-2577-1>
- Roesler, B. M., Rabelo-Goncalves, E. M., & Zeitune, J. M. (2014). Virulence Factors of *Helicobacter pylori*: A Review. *Clin Med Insights Gastroenterol*, 7, 9-17. <https://doi.org/10.4137/CGast.S13760>
- Rogers, S. S., Waigh, T. A., Zhao, X., & Lu, J. R. (2007). Precise particle tracking against a complicated background: polynomial fitting with Gaussian weight. *Phys Biol*, 4(3), 220-227. <https://doi.org/10.1088/1478-3975/4/3/008>
- Rossez, Y., Maes, E., Lefebvre Darroman, T., Gosset, P., Ecobichon, C., Joncquel Chevalier Curt, M., Boneca, I. G., Michalski, J.-C., & Robbe-Masselot, C. (2012). Almost all human gastric mucin O-glycans harbor blood group A, B or H antigens and are potential binding sites for *Helicobacter pylori*. *Glycobiology*, 22(9), 1193-1206. <https://doi.org/10.1093/glycob/cws072>
- Rubin, B. K. (2010). Mucus and Mucins. *Otolaryngologic Clinics of North America*, 43(1), 27-34. <https://doi.org/10.1016/j.otc.2009.11.002>
- Samad, M. A., Hashim, S. H., Simarani, K., & Yaacob, J. S. (2016). Antibacterial Properties and Effects of Fruit Chilling and Extract Storage on Antioxidant Activity, Total Phenolic and Anthocyanin Content of Four Date Palm (*Phoenix dactylifera*) Cultivars. *Molecules*, 21(4), 419. <https://doi.org/10.3390/molecules21040419>
- Sato, T., & Clevers, H. (2013). Growing self-organizing mini-guts from a single intestinal stem cell: mechanism and applications. *Science*, 340(6137), 1190-1194. <https://doi.org/10.1126/science.1234852>
- Sato, T., Stange, D. E., Ferrante, M., Vries, R. G., Van Es, J. H., Van den Brink, S., Van Houdt, W. J., Pronk, A., Van Gorp, J., Siersema, P. D., & Clevers, H. (2011). Long-term expansion of epithelial organoids from human colon, adenoma, adenocarcinoma, and Barrett's epithelium. *Gastroenterology*, 141(5), 1762-1772. <https://doi.org/10.1053/j.gastro.2011.07.050>
- Sato, T., Vries, R. G., Snippert, H. J., Van De Wetering, M., Barker, N., Stange, D. E., Van Es, J. H., Abo, A., Kujala, P., Peters, P. J., & Clevers, H. (2009). Single Lgr5 stem cells build crypt-villus structures in vitro without a mesenchymal niche. *Nature*. <https://doi.org/10.1038/nature07935>

- Schlottau, K., Rissmann, M., Graaf, A., Schon, J., Sehl, J., Wylezich, C., Hoper, D., Mettenleiter, T. C., Balkema-Buschmann, A., Harder, T., Grund, C., Hoffmann, D., Breithaupt, A., & Beer, M. (2020). SARS-CoV-2 in fruit bats, ferrets, pigs, and chickens: an experimental transmission study. *Lancet Microbe*, 1(5), e218-e225. [https://doi.org/10.1016/S2666-5247\(20\)30089-6](https://doi.org/10.1016/S2666-5247(20)30089-6)
- Schountz, T., Baker, M. L., Butler, J., & Munster, V. (2017). Immunological Control of Viral Infections in Bats and the Emergence of Viruses Highly Pathogenic to Humans. *Front Immunol*, 8, 1098. <https://doi.org/10.3389/fimmu.2017.01098>
- Schreiber, S., Garten, D., Nguyen, T. H., Konradt, M., Bucker, R., & Scheid, P. (2007). In situ measurement of pH in the secreting canaliculus of the gastric parietal cell and adjacent structures. *Cell and Tissue Research*, 329(2), 313-320. <https://doi.org/10.1007/s00441-007-0427-1>
- Schubert, M. L. (2004). Gastric secretion. *Curr Opin Gastroenterol*, 20(6), 519-525. <https://doi.org/10.1097/00001574-200411000-00003>
- Schumacher, M. A., Aihara, E., Feng, R., Engevik, A., Shroyer, N. F., Ottemann, K. M., Worrell, R. T., Montrose, M. H., Shivdasani, R. A., & Zavros, Y. (2015). The use of murine-derived fundic organoids in studies of gastric physiology. *J Physiol*, 593(8), 1809-1827. <https://doi.org/10.1113/jphysiol.2014.283028>
- Searle, B. C., Pino, L. K., Egertson, J. D., Ting, Y. S., Lawrence, R. T., MacLean, B. X., Villen, J., & MacCoss, M. J. (2018). Chromatogram libraries improve peptide detection and quantification by data independent acquisition mass spectrometry. *Nat Commun*, 9(1), 5128. <https://doi.org/10.1038/s41467-018-07454-w>
- Sebrell, T. A., Hashimi, M., Sidar, B., Wilkinson, R. A., Kirpotina, L., Quinn, M. T., Malkoc, Z., Taylor, P. J., Wilking, J. N., & Bimczok, D. (2019). A Novel Gastric Spheroid Co-culture Model Reveals Chemokine-Dependent Recruitment of Human Dendritic Cells to the Gastric Epithelium. *Cell Mol Gastroenterol Hepatol*, 8(1), 157-171 e153. <https://doi.org/10.1016/j.jcmgh.2019.02.010>
- Sebrell, T. A., Sidar, B., Bruns, R., Wilkinson, R. A., Wiedenheft, B., Taylor, P. J., Perrino, B. A., Samuelson, L. C., Wilking, J. N., & Bimczok, D. (2018). Live imaging analysis of human gastric epithelial spheroids reveals spontaneous rupture, rotation and fusion events. *Cell Tissue Res*, 371(2), 293-307. <https://doi.org/10.1007/s00441-017-2726-5>
- Seidler, U., & Sewing, K. F. (1989). Ca<sup>2+</sup>-dependent and -independent secretagogue action on gastric mucus secretion in rabbit mucosal explants. *Am J Physiol*, 256(4 Pt 1), G739-746. <https://doi.org/10.1152/ajpgi.1989.256.4.G739>
- Seidlitz, T., Koo, B.-K., & Stange, D. E. (2021). Gastric organoids—an in vitro model system for the study of gastric development and road to personalized medicine. *Cell Death & Differentiation*, 28(1), 68-83. <https://doi.org/10.1038/s41418-020-00662-2>

- Seidlitz, T., Merker, S. R., Rothe, A., Zakrzewski, F., von Neubeck, C., Grützmann, K., Sommer, U., Schweitzer, C., Schölch, S., Uhlemann, H., Gaebler, A. M., Werner, K., Krause, M., Baretton, G. B., Welsch, T., Koo, B. K., Aust, D. E., Klink, B., Weitz, J., & Stange, D. E. (2019). Human gastric cancer modelling using organoids. *Gut*, 68(2), 207-217. <https://doi.org/10.1136/gutjnl-2017-314549>
- Serrano, C., Harris, P. R., Smith, P. D., & Bimczok, D. (2021). Interactions between *H. pylori* and the Gastric Microbiome: Impact on Gastric Homeostasis and Disease. *Curr Opin Physiol*, 21, 57-64. <https://doi.org/10.1016/j.cophys.2021.04.003>
- Serrano, C. A., Leon, M. A., Palma, C., Vera, M., Hernandez, C., & Harris, P. R. (2017). Helicobacter pylori-Clarithromycin Resistance in Symptomatic Pediatric Patients in a High Prevalence Country. *J Pediatr Gastroenterol Nutr*, 64(3), e56-e60. <https://doi.org/10.1097/MPG.0000000000001257>
- Shaw, T. I., Srivastava, A., Chou, W. C., Liu, L., Hawkinson, A., Glenn, T. C., Adams, R., & Schountz, T. (2012). Transcriptome sequencing and annotation for the Jamaican fruit bat (*Artibeus jamaicensis*). *PLoS ONE*, 7(11), e48472. <https://doi.org/10.1371/journal.pone.0048472>
- Sierra, J. C., Asim, M., Verriere, T. G., Piazuolo, M. B., Suarez, G., Romero-Gallo, J., Delgado, A. G., Wroblewski, L. E., Barry, D. P., Peek, R. M., Gobert, A. P., & Wilson, K. T. (2018). Epidermal growth factor receptor inhibition downregulates Helicobacter pylori-induced epithelial inflammatory responses, DNA damage and gastric carcinogenesis. *Gut*. <https://doi.org/10.1136/gutjnl-2016-312888>
- Simian, M., & Bissell, M. J. (2017). Organoids: A historical perspective of thinking in three dimensions. *J Cell Biol*, 216(1), 31-40. <https://doi.org/10.1083/jcb.201610056>
- Singh, A., Singh, Y., & Pandey, K. M. (2020). Viscous fingering instabilities in radial Hele-Shaw cell: A review. *Materials Today: Proceedings*, 26, 760-762. <https://doi.org/https://doi.org/10.1016/j.matpr.2020.01.022>
- Smith, S. I., & Yamaoka, Y. (2023). Antibiotic Resistance and Therapy for Helicobacter pylori Infection. *Antibiotics (Basel)*, 12(12). <https://doi.org/10.3390/antibiotics12121669>
- Soll, A. H., & Walsh, J. H. (1979). Regulation of gastric acid secretion. *Annu Rev Physiol*, 41, 35-53. <https://doi.org/10.1146/annurev.ph.41.030179.000343>
- Stamos, J. L., Chu, M. L., Enos, M. D., Shah, N., & Weis, W. I. (2014). Structural basis of GSK-3 inhibition by N-terminal phosphorylation and by the Wnt receptor LRP6. *Elife*, 3, e01998. <https://doi.org/10.7554/eLife.01998>
- Stanifer, M. L., Guo, C., Doldan, P., & Boulant, S. (2020). Importance of Type I and III Interferons at Respiratory and Intestinal Barrier Surfaces. *Front Immunol*, 11, 608645. <https://doi.org/10.3389/fimmu.2020.608645>

- Stanifer, M. L., Kee, C., Cortese, M., Zumaran, C. M., Triana, S., Mukenhirn, M., Kraeusslich, H. G., Alexandrov, T., Bartenschlager, R., & Boulant, S. (2020). Critical Role of Type III Interferon in Controlling SARS-CoV-2 Infection in Human Intestinal Epithelial Cells. *Cell Rep*, 32(1), 107863. <https://doi.org/10.1016/j.celrep.2020.107863>
- Stoner, G. D., Wang, L. S., & Casto, B. C. (2008). Laboratory and clinical studies of cancer chemoprevention by antioxidants in berries. *Carcinogenesis*, 29(9), 1665-1674. <https://doi.org/10.1093/carcin/bgn142>
- Støvring Mortensen, J., Saaby, L., Harloff-Helleberg, S., & Mørck Nielsen, H. (2022). Barrier properties of ex vivo porcine intestinal mucus are highly independent of isolation and storage conditions. *Eur J Pharm Biopharm*, 174, 106-110. <https://doi.org/10.1016/j.ejpb.2022.03.015>
- Strugala, P., Dudra, A., Kucharska, A. Z., Sokol-Letowska, A., Wojnicz, D., Cisowska, A., Walkowski, S., Sroka, Z., Gabrielska, J., & Hendrich, A. B. (2015). Biological activity of the methanol and water extracts of the fruits of anthocyanin-rich plants grown in south-west Poland. *Nat Prod Commun*, 10(3), 467-474. <https://www.ncbi.nlm.nih.gov/pubmed/25924531>
- Su, C., Padra, M., Constantino, M. A., Sharba, S., Thorell, A., Lindén, S. K., & Bansil, R. (2018). Influence of the viscosity of healthy and diseased human mucins on the motility of *Helicobacter pylori*. *Scientific Reports*, 8(1). <https://doi.org/10.1038/s41598-018-27732-3>
- Su-Arcaro, C., Liao, W., Bieniek, K., Constantino, M. A., Decker, S. M., Turner, B. S., & Bansil, R. (2023). Unraveling the Intertwined Effect of pH on *Helicobacter pylori* Motility and the Microrheology of the Mucin-Based Medium It Swims in. *Microorganisms*, 11(11). <https://doi.org/10.3390/microorganisms11112745>
- Subudhi, S., Rapin, N., Bollinger, T. K., Hill, J. E., Donaldson, M. E., Davy, C. M., Warnecke, L., Turner, J. M., Kyle, C. J., Willis, C. K. R., & Misra, V. (2017). A persistently infecting coronavirus in hibernating *Myotis lucifugus*, the North American little brown bat. *J Gen Virol*, 98(9), 2297-2309. <https://doi.org/10.1099/jgv.0.000898>
- Tabarki, S., Aouadhi, C., Mechergui, K., Hammi, K. M., Ksouri, R., Raies, A., & Toumi, L. (2017). Comparison of Phytochemical Composition and Biological Activities of *Rubus ulmifolius* Extracts Originating from Four Regions of Tunisia. *Chem Biodivers*, 14(1). <https://doi.org/10.1002/cbdv.201600168>
- Tacconelli, E., Carrara, E., Savoldi, A., Harbarth, S., Mendelson, M., Monnet, D. L., Pulcini, C., Kahlmeter, G., Kluytmans, J., Carmeli, Y., Ouellette, M., Outtersson, K., Patel, J., Cavaleri, M., Cox, E. M., Houchens, C. R., Grayson, M. L., Hansen, P., Singh, N.,... Group, W. H. O. P. P. L. W. (2018). Discovery, research, and development of new antibiotics: the WHO priority list of antibiotic-resistant bacteria and tuberculosis. *Lancet Infect Dis*, 18(3), 318-327. [https://doi.org/10.1016/S1473-3099\(17\)30753-3](https://doi.org/10.1016/S1473-3099(17)30753-3)

- Takafumi, I. T., Kazuhiko, I. (2011). Protective Effects of Gastric Mucus. *Gastritis and Gastric Cancer*. <https://doi.org/10.5772/23951>
- Takase, Y., Fujishima, K., & Takahashi, T. (2023). The 3D Culturing of Organoids from Murine Intestinal Crypts and a Single Stem Cell for Organoid Research. *J Vis Exp*(194). <https://doi.org/10.3791/65219>
- Takeshita, Y., Johnson, K. S., Coletti, L. J., Jannasch, H. W., Walz, P. M., & Warren, J. K. (2020). Assessment of pH dependent errors in spectrophotometric pH measurements of seawater. *Marine Chemistry*, 223, 103801. <https://doi.org/https://doi.org/10.1016/j.marchem.2020.103801>
- Tallapragada, N. P., Cambra, H. M., Wald, T., Keough Jalbert, S., Abraham, D. M., Klein, O. D., & Klein, A. M. (2021). Inflation-collapse dynamics drive patterning and morphogenesis in intestinal organoids. *Cell Stem Cell*, 28(9), 1516-1532.e1514. <https://doi.org/https://doi.org/10.1016/j.stem.2021.04.002>
- Tan, B., Yang, J. C., Young, C. L., Bishu, S., Owyang, S. Y., El-Zaatari, M., Zhang, M., Grasberger, H., Qian, J. M., & Kao, J. Y. (2018). Helicobacter pylori Antimicrobial Susceptibility Testing-Guided Salvage Therapy in the USA: A Real Life Experience. *Dig Dis Sci*, 63(2), 437-445. <https://doi.org/10.1007/s10620-017-4880-8>
- Tan, S., & Berg, D. E. (2004). Motility of urease-deficient derivatives of Helicobacter pylori. *J Bacteriol*, 186(3), 885-888. <https://doi.org/10.1128/JB.186.3.885-888.2004>
- Thim, L., Madsen, F., & Poulsen, S. S. (2002). Effect of trefoil factors on the viscoelastic properties of mucus gels. *European Journal of Clinical Investigation*, 32(7), 519-527. <https://doi.org/https://doi.org/10.1046/j.1365-2362.2002.01014.x>
- Tian, L., Tan, Y., Chen, G., Wang, G., Sun, J., Ou, S., Chen, W., & Bai, W. (2019). Metabolism of anthocyanins and consequent effects on the gut microbiota. *Crit Rev Food Sci Nutr*, 59(6), 982-991. <https://doi.org/10.1080/10408398.2018.1533517>
- Tong, J., & Gu, Q. (2020). Expression and Clinical Significance of Mucin Gene in Chronic Rhinosinusitis. *Curr Allergy Asthma Rep*, 20(11), 63. <https://doi.org/10.1007/s11882-020-00958-w>
- Tong, S., Zhu, X., Li, Y., Shi, M., Zhang, J., Bourgeois, M., Yang, H., Chen, X., Recuenco, S., Gomez, J., Chen, L. M., Johnson, A., Tao, Y., Dreyfus, C., Yu, W., McBride, R., Carney, P. J., Gilbert, A. T., Chang, J.,...Donis, R. O. (2013). New world bats harbor diverse influenza A viruses. *PLoS Pathog*, 9(10), e1003657. <https://doi.org/10.1371/journal.ppat.1003657>
- Triana, S., Metz-Zumaran, C., Ramirez, C., Kee, C., Doldan, P., Shahraz, M., Schraivogel, D., Gschwind, A. R., Sharma, A. K., Steinmetz, L. M., Herrmann, C., Alexandrov, T., Boulant, S., & Stanifer, M. L. (2021). Single-cell analyses reveal SARS-CoV-2

- interference with intrinsic immune response in the human gut. *Mol Syst Biol*, 17(4), e10232. <https://doi.org/10.15252/msb.202110232>
- Tsai, Y. H., Czerwinski, M., Wu, A., Dame, M. K., Attili, D., Hill, E., Colacino, J. A., Nowacki, L. M., Shroyer, N. F., Higgins, P. D. R., Kao, J. Y., & Spence, J. R. (2018). A Method for Cryogenic Preservation of Human Biopsy Specimens and Subsequent Organoid Culture. *Cell Mol Gastroenterol Hepatol*, 6(2), 218-222 e217. <https://doi.org/10.1016/j.jcmgh.2018.04.008>
- Tshibangu-Kabamba, E., & Yamaoka, Y. (2021). Helicobacter pylori infection and antibiotic resistance - from biology to clinical implications. *Nat Rev Gastroenterol Hepatol*, 18(9), 613-629. <https://doi.org/10.1038/s41575-021-00449-x>
- Tulio, A. Z., Jr., Reese, R. N., Wyzgoski, F. J., Rinaldi, P. L., Fu, R., Scheerens, J. C., & Miller, A. R. (2008). Cyanidin 3-rutinoside and cyanidin 3-xylosylrutinoside as primary phenolic antioxidants in black raspberry. *J Agric Food Chem*, 56(6), 1880-1888. <https://doi.org/10.1021/jf072313k>
- Unisense. (2023a). *Microprofiling system user manual*. <https://unisense.com/wp-content/uploads/2021/09/2023.11-MicroProfiling-System-2.pdf>
- Unisense. (2023b). *pH and reference electrode manual*. <https://unisense.com/wp-content/uploads/2023/05/2023.05-pH-and-ref-sensor-manual.pdf>
- Unisense. (2023c). *Sensortrace suite user manual*. <https://unisense.com/wp-content/uploads/2021/10/SensorTrace-Suite-Manual.pdf>
- Unisense. (2024). <https://unisense.com/products/ph-microelectrode/>
- VanDussen, K. L., Marinshaw, J. M., Shaikh, N., Miyoshi, H., Moon, C., Tarr, P. I., Ciorba, M. A., & Stappenbeck, T. S. (2015). Development of an enhanced human gastrointestinal epithelial culture system to facilitate patient-based assays. *Gut*, 64(6), 911-920. <https://doi.org/10.1136/gutjnl-2013-306651>
- Venerito, M., Vasapolli, R., Rokkas, T., & Malfertheiner, P. (2018). Gastric cancer: epidemiology, prevention, and therapy. *Helicobacter*, 23 Suppl 1, e12518. <https://doi.org/10.1111/hel.12518>
- Vicsek, T., Czirók, A., Ben-Jacob, E., Cohen, I. I., & Shochet, O. (1995). Novel type of phase transition in a system of self-driven particles. *Phys Rev Lett*, 75(6), 1226-1229. <https://doi.org/10.1103/PhysRevLett.75.1226>
- Vidova, V., & Spacil, Z. (2017). A review on mass spectrometry-based quantitative proteomics: Targeted and data independent acquisition. *Anal Chim Acta*, 964, 7-23. <https://doi.org/10.1016/j.aca.2017.01.059>

- Villahermosa, D., Corzo, A., Garcia-Robledo, E., González, J. M., & Papaspyrou, S. (2016). Kinetics of Indigenous Nitrate Reducing Sulfide Oxidizing Activity in Microaerophilic Wastewater Biofilms. *PLoS ONE*, *11*(2), e0149096. <https://doi.org/10.1371/journal.pone.0149096>
- Vlachogiannis, G., Hedayat, S., Vatsiou, A., Jamin, Y., Fernández-Mateos, J., Khan, K., Lampis, A., Eason, K., Huntingford, I., Burke, R., Rata, M., Koh, D. M., Tunariu, N., Collins, D., Hulkki-Wilson, S., Ragulan, C., Spiteri, I., Moorcraft, S. Y., Chau, I.,...Valeri, N. (2018). Patient-derived organoids model treatment response of metastatic gastrointestinal cancers. *Science*, *359*(6378), 920-926. <https://doi.org/10.1126/science.aao2774>
- Vukosavljevic, B., Murgia, X., Schwarzkopf, K., Schaefer, U. F., Lehr, C. M., & Windbergs, M. (2017). Tracing molecular and structural changes upon mucolysis with N-acetyl cysteine in human airway mucus. *Int J Pharm*, *533*(2), 373-376. <https://doi.org/10.1016/j.ijpharm.2017.07.022>
- Wagner, C. E., Krupkin, M., Smith-Dupont, K. B., Wu, C. M., Bustos, N. A., Witten, J., & Ribbeck, K. (2023). Comparison of Physicochemical Properties of Native Mucus and Reconstituted Mucin Gels. *Biomacromolecules*, *24*(2), 628-639. <https://doi.org/10.1021/acs.biomac.2c01016>
- Wang, K., Tian, S., Galindo-Gonzalez, J., Davalos, L. M., Zhang, Y., & Zhao, H. (2020). Molecular adaptation and convergent evolution of frugivory in Old World and neotropical fruit bats. *Mol Ecol*, *29*(22), 4366-4381. <https://doi.org/10.1111/mec.15542>
- Wang, L. S., Hecht, S. S., Carmella, S. G., Yu, N., Larue, B., Henry, C., McIntyre, C., Rocha, C., Lechner, J. F., & Stoner, G. D. (2009). Anthocyanins in black raspberries prevent esophageal tumors in rats. *Cancer Prev Res (Phila)*, *2*(1), 84-93. <https://doi.org/10.1158/1940-6207.CAPR-08-0155>
- Wang, L. S., & Stoner, G. D. (2008). Anthocyanins and their role in cancer prevention. *Cancer Lett*, *269*(2), 281-290. <https://doi.org/10.1016/j.canlet.2008.05.020>
- Wang, X., Zhang, L., Li, P., Zheng, Y., Yang, Y., & Ji, S. (2022). Apelin/APJ system in inflammation. *Int Immunopharmacol*, *109*, 108822. <https://doi.org/10.1016/j.intimp.2022.108822>
- Wang, Y., Kim, R., Sims, C. E., & Allbritton, N. L. (2019). Building a Thick Mucus Hydrogel Layer to Improve the Physiological Relevance of In Vitro Primary Colonic Epithelial Models. *Cellular and Molecular Gastroenterology and Hepatology*, *8*(4), 653-655.e655. <https://doi.org/10.1016/j.jcmgh.2019.07.009>
- Watanabe, S., Masangkay, J. S., Nagata, N., Morikawa, S., Mizutani, T., Fukushi, S., Alviola, P., Omatsu, T., Ueda, N., Iha, K., Taniguchi, S., Fujii, H., Tsuda, S., Endoh, M., Kato, K., Tohya, Y., Kyuwa, S., Yoshikawa, Y., & Akashi, H. (2010). Bat coronaviruses and

- experimental infection of bats, the Philippines. *Emerg Infect Dis*, 16(8), 1217-1223. <https://doi.org/10.3201/eid1608.100208>
- Weihs, D., Mason, T. G., & Teitell, M. A. (2006). Bio-microrheology: a frontier in microrheology. *Biophys J*, 91(11), 4296-4305. <https://doi.org/10.1529/biophysj.106.081109>
- Wen, R. (2015). Polymorphisms in mucin genes in the development of gastric cancer. *World Journal of Gastrointestinal Oncology*. <https://doi.org/10.4251/wjgo.v7.i11.328>
- Wheeler, K. M., Cárcamo-Oyarce, G., Turner, B. S., Dellos-Nolan, S., Co, J. Y., Lehoux, S., Cummings, R. D., Wozniak, D. J., & Ribbeck, K. (2019). Mucin glycans attenuate the virulence of *Pseudomonas aeruginosa* in infection. *Nature Microbiology*, 4(12), 2146-2154. <https://doi.org/10.1038/s41564-019-0581-8>
- Williams, S. E., & Turnberg, L. A. (1981). Demonstration of a pH gradient across mucus adherent to rabbit gastric mucosa: evidence for a 'mucus-bicarbonate' barrier. *Gut*, 22(2), 94-96. <https://doi.org/10.1136/gut.22.2.94>
- Winter, H. H., & Jackson, J. (1995). Linear Viscoelasticity. In J. A. Covas, J. F. Agassant, A. C. Diogo, J. Vlachopoulos, & K. Walters (Eds.), *Rheological Fundamentals of Polymer Processing* (pp. 61-92). Springer Netherlands. [https://doi.org/10.1007/978-94-015-8571-2\\_3](https://doi.org/10.1007/978-94-015-8571-2_3)
- Wolfel, R., Corman, V. M., Guggemos, W., Seilmaier, M., Zange, S., Muller, M. A., Niemeyer, D., Jones, T. C., Vollmar, P., Rothe, C., Hoelscher, M., Bleicker, T., Brunink, S., Schneider, J., Ehmann, R., Zwirgmaier, K., Drosten, C., & Wendtner, C. (2020). Virological assessment of hospitalized patients with COVID-2019. *Nature*, 581(7809), 465-469. <https://doi.org/10.1038/s41586-020-2196-x>
- Wolffling, S., Daddi, A. A., Imai-Matsushima, A., Fritsche, K., Goosmann, C., Traulsen, J., Lisle, R., Schmid, M., Reines-Benassar, M. D. M., Pfannkuch, L., Brinkmann, V., Bornschein, J., Malfertheiner, P., Ordemann, J., Link, A., Meyer, T. F., & Boccellato, F. (2021). EGF and BMPs Govern Differentiation and Patterning in Human Gastric Glands. *Gastroenterology*, 161(2), 623-636 e616. <https://doi.org/10.1053/j.gastro.2021.04.062>
- Wykoff, J. A., Shaffer, K. M., Araba, K. C., Markovetz, M. R., Patarin, J., Robert de Saint Vincent, M., Donaldson, S. H., & Ehre, C. (2022). Rapid Viscoelastic Characterization of Airway Mucus Using a Benchtop Rheometer. *J Vis Exp*(182). <https://doi.org/10.3791/63876>
- Xiao, S., & Zhou, L. (2020). Gastric Stem Cells: Physiological and Pathological Perspectives. *Front Cell Dev Biol*, 8, 571536. <https://doi.org/10.3389/fcell.2020.571536>



- Xu, H., Li, J., Chen, H., Wang, C., & Ghishan, F. K. (2013). NHE8 plays important roles in gastric mucosal protection. *Am J Physiol Gastrointest Liver Physiol*, 304(3), G257-261. <https://doi.org/10.1152/ajpgi.00433.2012>
- Yamasaki, K., Kanbe, T., Chijiwa, T., Ishiyama, H., & Morita, S. (1987). Gastric mucosal protection by OPC-12759, a novel antiulcer compound, in the rat. *Eur J Pharmacol*, 142(1), 23-29. [https://doi.org/10.1016/0014-2999\(87\)90649-2](https://doi.org/10.1016/0014-2999(87)90649-2)
- Yan, H., Jiao, H., Liu, Q., Zhang, Z., Xiong, Q., Wang, B. J., Wang, X., Guo, M., Wang, L. F., Lan, K., Chen, Y., & Zhao, H. (2021). ACE2 receptor usage reveals variation in susceptibility to SARS-CoV and SARS-CoV-2 infection among bat species. *Nat Ecol Evol*, 5(5), 600-608. <https://doi.org/10.1038/s41559-021-01407-1>
- Yoshiyama, H., & Nakazawa, T. (2000). Unique mechanism of *Helicobacter pylori* for colonizing the gastric mucus. *Microbes and Infection*, 2(1), 55-60. [https://doi.org/https://doi.org/10.1016/S1286-4579\(00\)00285-9](https://doi.org/https://doi.org/10.1016/S1286-4579(00)00285-9)
- Zamani, M., Ebrahimitabar, F., Zamani, V., Miller, W. H., Alizadeh-Navaei, R., Shokri-Shirvani, J., & Derakhshan, M. H. (2018). Systematic review with meta-analysis: the worldwide prevalence of *Helicobacter pylori* infection. *Aliment Pharmacol Ther*, 47(7), 868-876. <https://doi.org/10.1111/apt.14561>
- Zang, R., Gomez Castro, M. F., McCune, B. T., Zeng, Q., Rothlauf, P. W., Sonnek, N. M., Liu, Z., Brulois, K. F., Wang, X., Greenberg, H. B., Diamond, M. S., Ciorba, M. A., Whelan, S. P. J., & Ding, S. (2020). TMPRSS2 and TMPRSS4 promote SARS-CoV-2 infection of human small intestinal enterocytes. *Sci Immunol*, 5(47). <https://doi.org/10.1126/sciimmunol.abc3582>
- Zhang, J., Liu, Y., Chandra Sekhar, P. D., Singh, M., Tong, Y., Kucukdeger, E., Yoon, H. Y., Haring, A. P., Roman, M., Kong, Z., & Johnson, B. N. (2023). Rapid, autonomous high-throughput characterization of hydrogel rheological properties via automated sensing and physics-guided machine learning. *Applied Materials Today*, 30, 101720. <https://doi.org/https://doi.org/10.1016/j.apmt.2022.101720>
- Zhang, N., Ohlstrom, D., Pang, S., Bharadwaj, N. S., Qu, A., Grossniklaus, H., & Coskun, A. F. (2023). Tissue Spatial Omics Dissects Organoid Biomimicry. *GEN Biotechnology*, 2(5), 372-383. <https://doi.org/10.1089/genbio.2023.0039>
- Zhang, Q., Amooie, A., Bazant, M. Z., & Bischofberger, I. (2021). Growth morphology and symmetry selection of interfacial instabilities in anisotropic environments. *Soft Matter*, 17(5), 1202-1209. <https://doi.org/10.1039/d0sm01706j>
- Zhang, Q., Yang, X., Li, P., Huang, G., Feng, S., Shen, C., Han, B., Zhang, X., Jin, F., Xu, F., & Lu, T. J. (2015). Bioinspired engineering of honeycomb structure – Using nature to inspire human innovation. *Progress in Materials Science*, 74, 332-400. <https://doi.org/https://doi.org/10.1016/j.pmatsci.2015.05.001>

- Zhong, C., & Langrish, T. (2020). A comparison of different physical stomach models and an analysis of shear stresses and strains in these system. *Food Research International*, 135, 109296. <https://doi.org/https://doi.org/10.1016/j.foodres.2020.109296>
- Zhou, H., Ji, J., Chen, X., Bi, Y., Li, J., Wang, Q., Hu, T., Song, H., Zhao, R., Chen, Y., Cui, M., Zhang, Y., Hughes, A. C., Holmes, E. C., & Shi, W. (2021). Identification of novel bat coronaviruses sheds light on the evolutionary origins of SARS-CoV-2 and related viruses. *Cell*, 184(17), 4380-4391 e4314. <https://doi.org/10.1016/j.cell.2021.06.008>
- Zhou, J., Li, C., Liu, X., Chiu, M. C., Zhao, X., Wang, D., Wei, Y., Lee, A., Zhang, A. J., Chu, H., Cai, J.-P., Yip, C. C.-Y., Chan, I. H.-Y., Wong, K. K.-Y., Tsang, O. T.-Y., Chan, K.-H., Chan, J. F.-W., To, K. K.-W., Chen, H., & Yuen, K. Y. (2020). Infection of bat and human intestinal organoids by SARS-CoV-2. *Nature Medicine*, 26(7), 1077-1083. <https://doi.org/10.1038/s41591-020-0912-6>
- Zhou, P., Cowled, C., Todd, S., Crameri, G., Virtue, E. R., Marsh, G. A., Klein, R., Shi, Z., Wang, L. F., & Baker, M. L. (2011). Type III IFNs in pteropid bats: differential expression patterns provide evidence for distinct roles in antiviral immunity. *J Immunol*, 186(5), 3138-3147. <https://doi.org/10.4049/jimmunol.1003115>
- Zhou, P., Yang, X. L., Wang, X. G., Hu, B., Zhang, L., Zhang, W., Si, H. R., Zhu, Y., Li, B., Huang, C. L., Chen, H. D., Chen, J., Luo, Y., Guo, H., Jiang, R. D., Liu, M. Q., Chen, Y., Shen, X. R., Wang, X.,...Shi, Z. L. (2020). A pneumonia outbreak associated with a new coronavirus of probable bat origin. *Nature*, 579(7798), 270-273. <https://doi.org/10.1038/s41586-020-2012-7>
- Zomer-van Ommen, D. D., de Poel, E., Kruisselbrink, E., Oppelaar, H., Vonk, A. M., Janssens, H. M., van der Ent, C. K., Hagemeijer, M. C., & Beekman, J. M. (2018). Comparison of ex vivo and in vitro intestinal cystic fibrosis models to measure CFTR-dependent ion channel activity. *J Cyst Fibros*, 17(3), 316-324. <https://doi.org/10.1016/j.jcf.2018.02.007>

## APPENDICES

APPENDIX A

ORGANOID LINES AND TISSUE DONORS

Table A1. All human gastric organoid lines used in Chapter 2. F: female; M: male; B: Black; C: Caucasian; H: Hispanic.

Figure	Organoid		Tissue Donor		
	Line	Passage	Sex	Age	Ethnicity
2.2A	35	6	F	40	B
2.2B	7	4/15	F	26	B
	1	16	F	45	C
	34	3	F	44	Unknown
	35	6	F	40	B
2.2C	7	15	F	26	B
2.2D	36	1	-	Unknown	-
	7	4/5/9	F	26	B
	37	1	-	Unknown	-
	31	3	F	45	H
2.2E	10	15	F	43	Unknown
2.2F	34	3	F	33	C
2.2G	7	5	F	26	B

Table A2. All human gastric organoid lines used in Chapter 3. F: female; M: male; B: Black; C: Caucasian; H: Hispanic.

Figure	Organoid		Tissue Donor		
	Line	Passage	Sex	Age	Ethnicity
3.1	35	8	F	40	B
3.2	7	7	F	26	B
3.3	35	5	F	40	B
3.4	35	5	F	40	B
3.5	7	7	F	26	B

Table A3. All human gastric organoid lines used in Chapter 4. F: female; M: male; B: Black; C: Caucasian; H: Hispanic. All 5 digit numbers correspond to a tissue identification number.

Figure	Organoid		Tissue Donor		
	Line	Passage	Sex	Age	Ethnicity
4.1A	19138	-	M	56	C
	20	5	F	50	H
4.1C	7	8	F	26	B
4.1E	31	8	F	45	H
4.1F	5	8	F	38	C
	7	4	F	26	B
4.1G	5	8	F	38	C
	7	4	F	26	B
	01314	-	M	30	H
	02650	-	M	47	H
	07457	-	F	17	C
	04942	-	M	16	C
	06292	-	F	58	C
	06471	-	F	31	C
4.1H/I and 4.2A-E	7	9	F	26	B
	19138		M	56	C
	17196		M	51	C
	07457		F	17	C
	05774		F	39	B
4.3A	28	3	F	45	Unknown
	04702	-	M	51	Unknown
	7	4/9	F	26	B
	5	9	F	38	C
	07457	-	F	17	C
4.3A-B	5	9	F	38	B
	7	9	F	26	B
	28	3	F	45	Unknown
	04702		M	51	Unknown
	07457		F	17	Unknown
4.4A	5	9	F	38	B
	7	9	F	26	B
	05774	-	F	39	B
	04702	-	M	51	Unknown
	06471	-	F	31	C
4.4B	7	9	F	26	B
	06471	-	F	31	C

Table A3 Continued.

Figure	Organoid		Tissue Donor		
	Line	Passage	Sex	Age	Ethnicity
4.4C	5	9	F	38	B
	7	4/9	F	26	B
	06292	-	F	58	C
	06471	-	F	31	C
	07457	-	F	17	C
4.5C	7	9	F	26	B
4.5E	31	8	F	45	H
4.5F	06471	-	F	31	C

APPENDIX B

CULTURE MEDIA



Table B1. Human gastric organoid expansion media components.

L-WRN Conditioned Medium	50%
Advanced DMEM/F12	37%
Fetal bovine serum	10%
Penicillin/streptomycin	1%
L-glutamine	1%
Gentamycin	0.10%
Amphotericin B	0.10%
HEPES Buffer	0.40%
Y-27632	0.10%
SB-431542	0.10%